# Neural Mechanisms Underlying the Action Sequence of an Escape Response in *Drosophila* Larvae

**Jiayi Zhu**

Integrated Program in Neuroscience

McGill University, Montreal

March 2024

A thesis submitted to McGill University in partial fulfillment of the requirements of the degree of

Doctor of Philosophy

## Table of Contents

List of Figures and Tables ..... 3
List of Abbreviations ..... 5
Abstract ..... 6
Résumé ..... 8
Acknowledgments ..... 10
Contribution of Authors ..... 11
CHAPTER 1 Introduction ..... 13
1. Action sequences ..... 13
1.1. Action sequences are crucial in all aspects of animal survival ..... 13
1.2. Theories of action sequences ..... 13
1.2.1. Synfire chain model ..... 14
1.2.2. Ramp-to-threshold theory ..... 15
1.2.3. Hierarchical suppression theory ..... 15
1.3. Stereotyped and learned action sequences ..... 17
2. *Drosophila* larval escape behavior ..... 18
2.1. *Drosophila* is an advantageous animal model in neuroscience ..... 18
2.1.1. Neurogenetic tools in *Drosophila* ..... 19
2.1.2. The whole-CNS connectome promotes circuit studies ..... 20
2.2. *Drosophila* larvae deploy various defense mechanisms when triggered by parasitic wasps, including escape behaviors ..... 21
2.3. The escape behaviors are displayed in sequences ..... 22
3. The mechanism of *Drosophila* larval escape behavior ..... 23
3.1. Various sensory modalities are involved in the escape sequence ..... 23
3.2. The core circuitry of rolling has been mapped out ..... 24
3.3. Inhibitory mechanisms play an essential role in the escape circuitry ..... 26
4. Evolution of the *Drosophila* behaviors ..... 29
4.1. Evolution of behaviors and circuits in metazoans ..... 29
4.2. Comparative studies in *Drosophilid* species reveal the neural mechanisms underlying conserved behaviors ..... 31
4.3. Evolution in *Drosophila* larval escape strategies ..... 33

CHAPTER 2 Feedback inhibition by a descending GABAergic neuron regulates timing of escape behavior in *Drosophila* larvae ..... 46
CHAPTER 3 Comparative connectomics and escape behavior in larvae of closely related *Drosophila* species ..... 132
CHAPTER 4 Discussion ..... 190
1. Subtypes of Basin neurons have different functions in escape-rolling ..... 190
2. *Drosophila* larvae as an animal model for elucidating the neural bases of the hierarchical suppression model of behavioral sequences ..... 191
3. *Drosophila* larval escape behavior serves as a model for action selection ..... 193
4. Descending neurons play various roles in *Drosophila* behaviors ..... 194
5. Motor motifs are involved in the escape rolling sequence ..... 195
6. Evolutionary studies shine a light on the encoding of escape sequences ..... 196
7. Action sequences are likely compatible with several mechanisms ..... 197
8. Limitations ..... 198
9. Concluding remarks ..... 199

## List of Figures and Tables

CHAPTER 1

Figure 1. The *Drosophila* larval escape sequence ..... 22

Figure 2. *Drosophila* larval nociceptive circuit ..... 24

CHAPTER 2

Figure 1. Activation of SS04185 inhibits rolling evoked by activation of Basin neurons ..... 86

Figure 2. SS04185-DN, but not SS04185-MB, inhibits rolling when co-activated with Basins .. 89

Figure 3. SS04185-DN is identical to SeIN128 ..... 92

Figure 4. SeIN128 receives input from Basin and A00c neurons ..... 95

Figure 5. SeIN128 is GABAergic and negatively controls rolling ..... 97

Figure 6. Inhibition of SeIN128 prolongs rolling and delays initiation of crawling ..... 99

Figure 7. SeIN128 sends feedback inhibition to Basins ..... 101

Figure 8. SeIN128 inhibits rolling elicited by both Basin-2 and Basin-4 activation ..... 103

Figure S1-1. SS04185 inhibits rolling ..... 105

Figure S1-2. SS04185 inhibits rolling ..... 107

Figure S2. SS04185-DN inhibits rolling ..... 110

Figure S4-1. SeIN128 is downstream of Basin and A00c neurons ..... 113

Figure S4-2. Synapses from SeIN128 to Basin-2 are located near Basin-2 outputs ..... 115

Figure S5. SeIN128 is GABAergic ..... 117

Figure S6. SeIN128 inhibition enhances rolling ..... 119

Figure S7. SeIN128 sends feedback inhibition to Basins ..... 121

Figure S8. SeIN128 inhibits rolling elicited by both Basin-2 and Basin-4 activation ..... 124

CHAPTER 3

Figure 1. *Drosophila* species show a wide range of escape responses to noxious stimulation ... 153

Figure 2. Anatomy of *D. santomea, D. melanogaster, D. biarmipes, D. persimilis, and D. virilis* sensory neurons in the peripheral nervous system ..... 156

Figure 3. Structure of mdIV and chordotonal neuron terminals in *D. santomea* ..... 158

Figure 4. Morphology and properties of second-order nociceptive local interneurons ..... 160

Figure 5. Basin-1, Basin-2, and Basin-4 receive inputs from mdIV neurons and chordotonal neurons in *D. santomea* ..... 162

Figure S1. *Drosophila* species show a wide range of escape responses to noxious heat stimulation …….. 181
Table S1. *Drosophilid* species used in this study …… 183
Table S2. Number of sensory neurons in *D. melanogaster*, *D. santomea*, *D. biampes*, *D. virilis* and *D. persimilis* …… 184
Table S3. Strong partners (>10 synapses from downstream of mdIV neurons) of mdIV neurons and synapse number with each mdIV neurons …….. 186
Table S4. Connectivity between Basins and mdIV or chordotonal neurons in *D. santomea* and *D. melanogaster* …….. 188

## List of Abbreviations

| | |
|---|---|
| 5-HT | 5-hydroxytryptamine |
| ABLK | Abdominal leucokinin neuron |
| AITC | Allyl isothiocyanate |
| C4da | Class IV dendrite arborization neuron |
| CATMAID | Collaborative annotation toolkit for massive amounts of image data |
| ChAT | Choline acetyltransferase |
| ChR2 | Channelrhodopsin-2 |
| CNS | Central nervous system |
| DEET | N, N-diethyl-meta-toluamide |
| DN | Descending neuron |
| DnB | Down-and-Back neuron |
| Dp-ilp7 | Dorsal pair insulin-like-peptide-7-producing neuron |
| EM | Electron microscope |
| Fas2 | Fasciclin2 |
| FIB–SEM | Focused ion beam–scanning electron microscope |
| GABA | Gamma-aminobutyric acid |
| GEVI | Genetically encoded fluorescent voltage indicator |
| GtACR | *Guillardia theta* anion-conducting channelrhodopsin |
| Kir | Inwardly rectifying potassium channels |
| $KZip^{+}$ | Killer zipper |
| MB | Mushroom body |
| mCSI | Medial clusters of C4da second-order interneuron |
| mdIV | Multidendritic class IV neuron |
| MYA | Million years ago |
| NMDA | N-methyl-D-aspartate |
| SEZ | Subesophageal zone |
| SNa | Segmental nerve a motor neuron |
| TEM | Transmission electron microscopy |
| VNC | Ventral nerve cord |

**Abstract**

Action sequences are a common phenomenon in the animal kingdom. They encompass daily activities like feeding and less frequent but critical behaviors, such as escape behaviors. Operating an action sequence in the correct order enables animals to survive and thrive. Despite the variability of the actions in the action sequences, they share common features such as selection at transition and overall stereotyped sequencing. With these shared features, it is plausible that most action sequences share general encoding principles to coordinate the different actions in a certain order. Currently, there are several popular theories explaining the encoding principles, but the issue of how nervous systems generate action sequences remains unsolved. In this thesis, I focused on *Drosophila* larval escape behavior to investigate the encoding mechanism and examine several different theories for action sequences.

The larval escape behavior displays a stereotyped action sequence: larvae curl up and slide perpendicularly, termed as rolling, and subsequently crawl at a pace faster than their normal locomotion. In addition, the larval brain connectome has been reported, including the core circuit of this action sequence, allowing a more in-depth study of its circuit mechanism. Combining the strength of behavior tests and circuit examination, I identified a pair of descending neurons – SeIN128 – in the subesophageal zone (SEZ) that inhibits rolling through feedback on Basin-2, a key neuron in the rolling circuit, which also shortened the delay of the first crawling event after the initial rolling. Due to the proximity of their output to Basin-2 to Basin-2 outputs, SeIN128 might modulate the information flow from Basin-2 to shorten the overall duration of rolling and promote the subsequent fast crawling.

To further explore how action sequences may be altered by small variations of the neural circuit, we can alternatively approach the problem from the perspective of evolutionary

developmental biology, focusing on closely related species. Indeed, nuances in behaviors can be traced back to the differences in connectomes during evolution. Therefore, comparative studies at both layers can facilitate the research of neural mechanisms underlying behaviors. Chapter 3 of this thesis discusses the conservation of the escape rolling in 12 *Drosophilid* species. As a result, *D. santomea* has been targeted because of its hypersensitive rolling responses, and this has resulted in the improvement of our understanding of several connections in the circuitry, elucidating their significance in encoding escape rolling.

Through exploring the circuit of *Drosophila* larval escape behavior, I identified a feedback inhibitory motif to facilitate the termination of rolling and thus enable the execution of fast crawling, as well as the motifs that enhance the escape rolling response. These findings not only offer insights into the encoding mechanism of this specific escape sequence but also provide shreds of evidence to examine the varied theories in action sequences.

**Résumé**

Les séquences d'action sont un phénomène courant dans le règne animal. Elles englobent à la fois des activités quotidiennes, telles que l'alimentation, et des comportements moins fréquents mais essentiels, tels que les comportements de fuite. L'exécution d'une séquence d'actions dans le bon ordre permet aux animaux de survivre et de prospérer. Malgré la grande variabilité des comportements impliqués dans les séquences d'action, celles-ci partagent des caractéristiques communes, telles que la sélection lors de la transition et l'enchaînement stéréotypé global. Compte tenu de ces caractéristiques communes, il est plausible que la plupart des séquences d'action partagent des principes d'encodage généraux permettant de coordonner les différentes actions dans un certain ordre. Il existe actuellement plusieurs théories expliquant les principes d'encodage, mais la façon dont les systèmes nerveux génèrent des séquences d'action n'est toujours pas élucidée. Dans cette thèse, je me concentre sur le comportement de fuite des larves de drosophile pour étudier les mécanismes d'encodage, examinant la plausibilité de plusieurs théories différentes au sein de ces séquences d'action.

Le comportement de fuite des larves présente une séquence d'action stéréotypée : les larves se recroquevillent et glissent perpendiculairement à leur axe longitudinal, un comportement dénommé “roulade”, puis rampent à un rythme plus rapide que leur locomotion normale. De plus, le connectome du circuit neural qui permettent les comportements de fuite chez la larve a été décrit, permettant une étude plus approfondie de son mécanisme. En combinant la force des expériences comportementales et l'examen du circuit, j'ai identifié une paire de neurones descendants - SeIN128 - dans la zone sous-œsophagienne (SEZ) qui inhibe la roulade par rétro-inhibition sur Basin-2, un neurone clé dans le circuit de roulade, ce qui a également raccourci le délai du premier événement de reptation après la roulade initiale. En raison de la proximité de leur sortie avec les

sorties de Basin-2, SeIN128 pourrait moduler le flux d'informations provenant de Basin-2 afin de raccourcir la durée globale du roulement et de favoriser la rapidité de la reptation qui s'ensuit.

Pour approfondir l'étude de la manière dont les séquences d'action peuvent être modifiées par de petites variations du circuit neuronal, nous pouvons également aborder le problème sous l'angle de la biologie évolutive, en nous concentrant sur des espèces étroitement apparentées. En effet, sous cet angle, les nuances dans les comportements peuvent être attribuées aux différences dans les connectomes au cours de l'évolution. Par conséquent, les études comparatives au niveau du comportement et du connectome peuvent faciliter la recherche des mécanismes neuronaux qui sous-tendent les séquences d'actions. Le chapitre 3 de cette thèse traite de la préservation de la roulade chez 12 espèces de drosophiles. En conséquence, D. santomea a été ciblé en raison de ses réponses hypersensibles aux stimuli nocifs qui induisent à la roulade, ce qui a entraîné l'amélioration de notre compréhension de plusieurs connexions dans le circuit, élucidant leur importance dans l'encodage de la roulade de fuite.

En explorant le circuit du comportement de fuite des larves de drosophile, j'ai identifié un motif de rétro-inhibition qui facilite la fin de la roulade et permet ainsi l'exécution d'une reptation rapide, ainsi que les motifs qui renforcent la réponse de roulade de fuite. Ces résultats permettent non seulement de mieux comprendre le mécanisme d'encodage de cette séquence d'évasion spécifique, mais fournissent également des éléments de preuve permettant d'examiner les diverses théories relatives aux séquences d'action.

**Acknowledgments**

First, I would like to thank all current and former members of the Ohyama lab for their support and assistance. I learned so much from Dr. Tomoko Ohyama throughout my degree. Without her insightful guidance and mentorship, I could not have published and become a better researcher. I cannot express my gratitude enough to Jean-Christophe Boivin for his companionship and our numerous treasured discussions. I am grateful for Alastair Garner, who provided many pieces of training and valuable ideas for initiating my projects. I appreciate Jing Ning's assistance with my experiments and many delightful lunch hours. I would love to thank Yi Qing Zhao for her fellowship and generous support. I am also grateful to Fei Huang for her friendship and discussions. In addition, many thanks to our undergraduate research students.

Second, I sincerely thank my advisory committee members, Dr. Donald van Meyel and Dr. Arjun Krishnaswamy, for their dedication to overseeing my academic performance and offering precious suggestions.

Most importantly, I thank my family and friends for their encouragement and moral support, without which I would not appreciate this graduate experience as much as I have done. I am deeply grateful to all of you.

**Contribution of Authors**

Jiayi Zhu and Dr. Tomoko Ohyama conceptualized the thesis and designed the experiments. Jiayi Zhu conducted most of the experiments with the help of Dr. Tomoko Ohyama and other co-authors as described below. Jiayi Zhu trained the rolling classifier with the Janelia Automatic Animal Behavior Annotator (JAABA), and Dr. Jean-Baptiste Masson provided the pipeline for detecting all other *Drosophila* larval behaviors. Jiayi Zhu analyzed all data and generated figures under the guidance of Dr. Tomoko Ohyama.

This thesis was drafted by Jiayi Zhu and edited by Jiayi Zhu and Dr. Tomoko Ohyama.

Following is the description of other authors' contributions:

Chapter 2:

Jean-Christophe Boivin conducted part of the behavior experiments for Figure 5B-5D and Figure 1-supplement 2 and assisted in the calcium imaging shown for Figure 7 and Figure 4-supplement 1B-1C.

Alastair Garner provided training and discussed in-depth data analysis.

Jing Ning helped with the behavior experiment for Figure 6-supplement 1 and the immunostaining for Figure 5-supplement 1C-1D.

Sophia Zhao assisted in the behavior experiment for Figure 5B-5D and the immunostaining for Figure 5-supplement 1C-1D.

Chapter 3:

Jean-Christophe Boivin repeated the behavior experiments for Figure 1F-1J and participated in the neuron reconstruction for Figures 3 and 4.

Dr. Tomoko Ohyama conducted the behavior experiment for Figure 1B-1E and generated the immunostaining data for Figure 2.

Song Pang, Dr. Zhiyuan Lu, Dr. C. Shan Xu, and Dr. Harald Hess prepared the sample, performed FIB-SEM imaging and provided the FIB-SEM data.

Dr. Stephan Saalfeld registered the FIB-SEM images and uploaded the data to CATMAID software for neuron reconstruction.

Remy Tabano, Melissa Pestemalciyan, Diane Nguyen, Angelica Le, Xinbei Wan, Shua Noh, Ally Shin, Aliona Fezoua, Dr. Cécile Tissot, Yiran Fan, Abby woods, Alice Luo, and Dan Huy Tran participated in the neuron reconstruction for Figures 3 and 4.

# CHAPTER 1 Introduction

## 1. Action sequences

### 1.1. Action sequences are crucial in all aspects of animal survival

An action sequence refers to a set of movements that occur in a particular order. They are prevalent in every aspect of any animal's life cycle, including but not limited to behavioral sequences seen in feeding, fighting, escaping, and mating (Herberholz et al., 2001; Liu et al., 2023; Manning, 1960; Ohyama et al., 2015; Seeds et al., 2014). The actions involved can be distinct, ranging from tail-flip responses in crayfish to keystrokes made by a human on a keyboard (Herberholz et al., 2001; Houghton & Hartley, 1995; Lashley, 1951). Regardless of the differences in animal models, sensory stimuli, and behaviors, action sequences are similar in how they are organized in the central nervous system (CNS). Given the variety of action sequences throughout the animal kingdom, each sequence is unlikely to require a distinct set of rules to encode the behaviors. Instead, many action sequences likely share a similar logic of encoding. Given the possibility that the underlying neural mechanisms of action sequences may be consistent, a wide range of techniques in different animal models have been used to explore the action sequence encoding principles (Averbeck et al., 2002; Herberholz et al., 2001; Kaplan et al., 2020; Liu et al., 2023; Seeds et al., 2014). Efforts have also been made to examine these principles in humans in a non-invasive manner to circumvent the technical and ethical difficulties of directly studying human neural circuits (Adams, 1984; Kachergis et al., 2014).

### 1.2. Theories of action sequences

Over more than 70 years of dedicated study, researchers have hypothesized several theories to explain action sequences (Abeles, 1991; Dawkins, 1976; Lashley, 1951; Manning, 1960; Mazzucato, 2022). To test these theories, numerous research groups around the world have

examined them in many animal models. Here, I discuss three well-studied hypotheses—synfire chain, ramp-to-threshold, and hierarchical suppression hypotheses—and the lines of evidence supporting each.

### 1.2.1. Synfire chain model

Synfire chain theory is one of the most popular hypotheses for action sequences. The premise for this theory is that the initiation and prosecution of the action responses require the firing of the corresponding neurons sequentially. In other words, neurons responsible for actions early in an action sequence will activate neurons responsible for actions later in an action sequence. Neurons are activated sequentially to result in a reflex chain of behaviors. The chains of neurons activating one another result in the chains of relevant behaviors.

This theory, also known as the reflex chain hypothesis, originated in the early 20$^{th}$ century, and the term 'synfire chain' was first introduced in 1982 (Abeles, 1982; Abeles, 1991; Sherrington, 1906). To understand neural circuits of the central nervous system, monkey cerebral cortical neural activities were recorded. Analysis of the activities not only discovered the synchronous spiking pattern of the cortical neurons but also revealed the temporal propagation of such synchronous firing activities (Abeles, 1982). This temporal propagation of synchronous spiking was then termed synfire chains. A strong association was driven between synfire chains and specific behaviors, leading to the official birth of synfire chain theory. Following this study, more evidence has been reported in other animal models, such as the birdsong sequence in zebra finches and spatial navigation behavior in rats (Ikegaya et al., 2004; Long et al., 2010; Pastalkova et al., 2008). An *in vivo* study showed that disrupting the correlations of neural activities in a synfire chain caused an interruption of the corresponding action sequence, further supporting the synfire chain theory (Ikegaya et al., 2004).

### 1.2.2. Ramp-to-threshold theory

The ramp-to-threshold theory is a general neural encoding principle found in various behaviors, positing that membrane depolarization accumulate over time and neurons fire when the accumulation reaches the threshold (Murakami & Mainen, 2015). In action selections, the ramp-to-threshold model means that the integrating neuron accumulates the evidence to make the corresponding decisions (Manning, 1960; Vijayan et al., 2023). Regarding action sequences where several actions occur in order, these actions are triggered at different thresholds by the same integrating neuron. The lower the threshold is, the earlier the action is shown in the sequence. Although this model is less explored in action sequences, a recent study of *Drosophila* adult courtship behavior provided solid evidence of such an integrating neuron controlling three consecutive behaviors (McKellar et al., 2019). Adding this to the evidence in action selection, the ramp-to-threshold model might attract more attention and provide another perspective for explaining the encoding of action sequences.

### 1.2.3. Hierarchical suppression theory

In a study of human typing behavior, Lashley and his colleagues reported the hierarchical suppression hypothesis in 1951 (Lashley, 1951). It posits that in an action sequence, the sensory stimuli activate all of the actions, and these actions suppress each other in competition. The suppression hierarchy translates into an action sequence. In this pioneering work, analysis of the spontaneous typos showed that these typos were usually letters that closely followed the correct letter, such as ‘aplhabet’ instead of ‘alphabet’. This pattern raised the possibility that these typos were not random. Instead, because typists preprocessed the letters that were to be typed next, the action modules for typing the subsequent letters were already preactivated, increasing their probabilities of being mistakenly sequenced. This finding refuted the domino-like synfire chain

theory and suggested that mutual inhibition is involved in this behavior to ensure accuracy in typing.

Following this pioneering work, more reports support hierarchical organization over the chain-like organization of behaviors. For example, advanced planning in sequential behaviors was observed. This planning explains why the delay in the start of action sequences varies based on the complexity of the sequences, which further supports the preactivation of the action modules instead of the sequential activation suggested by the synfire chain theory (Henry & Rogers, 1960; Rosenbaum, 1988; Sternberg et al., 1978). In addition, features of preceding behaviors enable the prediction of the subsequent behavior, implying that the actions are planned and preactivated, and they do not wait until all of the preceding actions are executed to be activated (Averbeck et al., 2002; Cohen & Rosenbaum, 2004; Kent, 1983; Rosenbaum et al., 2007; van der Wel & Rosenbaum, 2007).

Through years of collaborative hard work, hierarchical suppression model has been examined in various organisms and behaviors (Geddes et al., 2018; Houghton & Hartley, 1995; Kaplan et al., 2020; Seeds et al., 2014). For instance, swimming and body shortening in leeches mutually inhibit each other (Brian & William, 1997). Similarly, in *Pleurobranchaea*, feeding and withdrawal behavior compete (Jing & Gillette, 1995). Hierarchical organization has also been reported in learned behavior sequences in mouse basal ganglia pathways (Geddes et al., 2018). Recently, adult *Drosophila* was observed to perform a strict grooming sequence. The activation of specific grooming behaviors inhibited other behaviors in the action sequence (Seeds et al., 2014). Moreover, researchers reported the neural circuit underlying such mutual inhibition of grooming actions, providing strengthened evidence for hierarchical suppression model in this animal model (Guo et al., 2022).

These three theories above have all been examined in various animal models. They could be supported by evidence at both behavior and neural circuit levels, suggesting that these coding principles are conserved throughout evolution. We can generate valuable insights into the neural mechanisms encoding action sequences by studying them in laboratory settings.

### 1.3. Stereotyped and learned action sequences

Action sequences can be divided into two general categories. Some action sequences are stereotyped, such as the well-known egg-retrieval behavior of the gray goose and the mating behavior of the stickleback (Lorenz & Tinbergen, 1938; Tinbergen, 1952). These so-called fixed action patterns are innate and are not acquired through learning. Such behavioral sequences continue until complete, even if the stimuli that trigger the sequences are prematurely removed (Lorenz & Tinbergen, 1938; Tinbergen, 1952). In contrast to fixed action patterns, whose lengths tend to be modifiable, learned action sequences, such as birdsong, are more flexible and modifiable at the beginning and are consolidated only later (Anthony & Fernando, 2000; Marler, 1970).

Both categories of action sequences are investigated intensively. They are likely encoded by similar principles (e.g., the hierarchical order of a learned mouse action sequence and a stereotyped *Drosophila* grooming sequence) (Geddes et al., 2018; Seeds et al., 2014). Learned action sequences provide a comparatively more complex animal model involving action sequences and learning. When dealt with improperly, the learning process can become a confounding factor in studying the action sequences. However, stereotyped action sequences are generally more straightforward to isolate from other behaviors. More importantly, they are more consistent without the involvement of a learning process. For example, in stickleback mating, females complete their genetically pre-determined rigid courtship behavior similarly without learning (Tinbergen, 1952).

In short, the simplicity of stereotyped action sequences allows researchers to control for external cues, internal cues, and neural responses to explore their roles in action sequences. Due to the neat isolation from other behaviors and brain processes, the roles of these factors in stereotyped action sequences are independent of other neural mechanisms (e.g., cognitive processing). Taking advantage of the relative simplicity of stereotyped action sequences, this thesis will focus on one such action sequence—the *Drosophila* larval rolling-crawling sequence.

## 2. *Drosophila* larval escape behavior

### 2.1. *Drosophila* is an advantageous animal model in neuroscience

Since the first white-eyed *Drosophila* was observed, *D. melanogaster* has been one of the most significant animal models in genetics due to its ease of rearing and maintenance, short lifespan, and well-studied genetic background. Numerous tools have been developed in *Drosophila*, especially binary systems (i.e., the gal4/UAS system, lexA/lexAop system, and the QF/QUAS system), which enable the manipulation of genetic expression with high spatial-temporal specificity (Brand & Perrimon, 1993; Lai & Lee, 2006; Potter et al., 2010).

With a relatively small central nervous system (~10,000 neurons in larvae and ~100,000 neurons in adults), *Drosophila* is also frequently used as an experimental model in neuroscience. The holistic gal4 strains expressed in CNS neurons allowed bottom-up investigation, while recent progress in tomics, such as the whole CNS connectome and transcriptome in *Drosophila,* made top-down studies possible (Eichler et al., 2017; Gerhard et al., 2017; Karaiskos et al., 2017; Luan et al., 2006; Pfeiffer et al., 2010; Winding et al., 2023). In addition, the second generation of gal4 provides more precise spatial control in smaller subsets of neurons, and the recent development in genetic tools enables various specific manipulations or examinations in *Drosophila* simultaneously (Cao et al., 2013; Klapoetke et al., 2014; Luan et al., 2020; Nakai et al., 2001; Siegel & Isacoff,

1997). With the progress in both the genetic handles to target neurons and the tools to manipulate or monitor these neurons to investigate their functions combined, it has become much easier and more straightforward to study the central nervous system (CNS) of *Drosophila*, encouraging the expansion of *Drosophila* neuroscience studies.

### 2.1.1. Neurogenetic tools in *Drosophila*

The genetic tools in *Drosophila* help manipulate and monitor neural activities, allowing the in-depth study of the CNS. Neuronal manipulation consists of both activation and suppression of neural activities. On the one hand, to activate neurons, cation channels gated by heat (e.g., TrpA1), chemicals (e.g., ATP for $P2X_2$), and light (e.g., channelrhodopsins) were discovered and developed (Khakh et al., 2003; Neely et al., 2011; Sineshchekov et al., 2002). The recent progress of optogenetics has further broadened its future. In addition to the original blue light-elicited ChR2, other light-sensitive channels activated by a spectrum of light wavelengths were found or engineered (Klapoetke et al., 2014). For example, we utilized CsChrimson, a red-light-shifted channelrhodopsin, in this thesis. On the other hand, innate inhibitors (e.g., inwardly rectifying potassium [Kir] channels and tetanus toxin), heat-sensitive inhibitors (e.g., $Shibire^{ts1}$), and light-gated anion channels can inhibit neurons (e.g., Halorhodopsins, GtACR) (Dolan et al., 2017; Doring et al., 2002; Govorunova et al., 2016; Li et al., 2005; Sweeney et al., 1995; van de Goor et al., 1995).

Aside from manipulating neural activities, monitoring how neurons respond to stimuli is equally essential. In mammalian studies, electrophysiology recordings such as patch clamps are helpful methods to monitor neural activities. Still, such recordings are much more challenging to conduct in *Drosophila* due to the size of its CNS. Instead, in *Drosophila* studies, fluorescent proteins are engineered to visualize neural activities, including calcium signals (e.g., GCaMP),

voltage signals (e.g., genetically encoded fluorescent voltage indicator proteins [GEVIs]), and neurotransmitter releases (e.g., R-iGluSnFR1) (Cao et al., 2013; Nakai et al., 2001; Siegel & Isacoff, 1997; Wu et al., 2018).

2.1.2. The whole-CNS connectome promotes circuit studies

Despite the technical difficulty in electrophysiological recording that originates in the small size of the *Drosophila* CNS, the relevant smaller CNS size makes it possible to map all connectivity. A thorough understanding of connectivity could offer valuable insights into neural functions and cross-correlations among groups of neurons. Therefore, since the first publication of a connectome study in *Drosophila* larvae in 2015, partial CNS connectomes have been reported to elucidate local neural circuits (Berck et al., 2016; Eichler et al., 2017; Gerhard et al., 2017; Huckesfeld et al., 2021; Ohyama et al., 2015; Scheffer et al., 2020; Winding et al., 2023; Zheng et al., 2018).

These studies provided insights into how the CNS is wired to some extent and enhanced research on specific behaviors or brain regions. For example, the larval mushroom body has recurrent feedback and feed-across compartment motifs that could play a role in memory reinforcement or conflicting memory formation (Eichler et al., 2017). Additionally, the comparison of the nociceptive circuit connectivity of first-instar larvae and third-instar larvae showed that while the lengths of neurites and the numbers of synapses increased fivefold during development, the morphology and connectivity profiles remained the same (Gerhard et al., 2017). This finding suggests that during development, the sensation of danger rooted in nociception remains consistent, and similar comparative studies could unveil rewiring and conservation in CNS development. The connectome dataset was consulted in discovering several integrating neurons in the escape circuit that this thesis focuses on to confirm their synaptic connections with the core circuitry (Burgos et al., 2018; Hu et al., 2017; Takagi et al., 2017). In 2023, the whole-brain connectome was reported,

enabling more in-depth research into local circuits and connections across different brain regions to illustrate how these regions wire together to function in harmony (Winding et al., 2023). The ongoing progress in the *Drosophila* connectome encourages computational analysis and functional study of CNS circuits.

### 2.2. *Drosophila* larvae deploy various defense mechanisms when triggered by parasitic wasps, including escape behaviors

With all of the strengths of *Drosophila* larvae as an animal model, the specific escape behaviors they exhibit make them the focus of this thesis. All animals are faced with dangers in the wild. To survive, they have developed various strategies to escape such threats.

One of the major threats to *Drosophila* larvae is their predator, parasitoid wasps (Hwang et al., 2007). Female wasps lay eggs in *Drosophila* larvae after penetrating their cuticles with ovipositors. The eggs feed on *Drosophila* larvae to grow, leading to the death of *Drosophila* larvae. To avoid this, *Drosophila* larvae have evolved with several solutions. They exhibit several immune responses through various signaling pathways (e.g., Toll and immune deficiency signaling pathways and JAK/STAT signaling pathways) to kill or inhibit the growth of the parasitoid after infection (Bertet et al., 2009; Louradour et al., 2017; Rizki & Rizki, 1992; Yang & Hultmark, 2017). Their other effort aims at infection prevention. During attempts of wasps to pierce through *Drosophila* larval cuticles, *Drosophila* larvae display several escape responses to reduce the possibility of being parasitized, which are categorized as nocifensive behaviors (i.e., the nociceptive responses to defend against injury) and other behaviors (Hwang et al., 2007). The nocifensive responses include escape rolling, the perpendicular movement driven by rotations around the rostrocaudal axis, and writhing, featuring head and tail waving (Hwang et al., 2007; Tracey et al., 2003). Both nocifensive responses effectively remove the ovipositor and block wasps

from parasitizing. *Drosophila* larvae also display less intense responses, such as turning, stopping, and hunching (i.e., head withdrawal).

2.3. The escape behaviors are displayed in sequences

Given this repertoire of escape behaviors, *Drosophila* larvae select the most appropriate responses based on several factors. One of these factors is the exact location of the stimulation (Takagi et al., 2017). When larvae are attacked from the posterior end, they tend to crawl forward with their regular locomotion pattern and then turn. When the attacks approach from the anterior side, larvae hunch, writhe, and turn. However, if they are attacked on the middle part of their body, their decision on escape responses also depends on the timing. Upon attack, they mostly curl their bodies in a C-shape and slide perpendicularly to the body axis to perform escape rolling (Figure 1) (Ohyama et al., 2015). Subsequently, they crawl faster than the regular locomotion speed to outrun the predators (Figure 1).

This escape sequence is an outstanding model for investigating the encoding mechanism of the action sequence. First, escape rolling behavior is unique from other escape behaviors because it does not initiate without nociceptive stimuli. Perpendicular sliding and rapid locomotion are both easy to detect among escape behaviors. Most importantly, the combination of rolling followed by fast crawling is a rigid action sequence. In other words, this response order is always conserved whenever nocifensive escape behavior is observed.

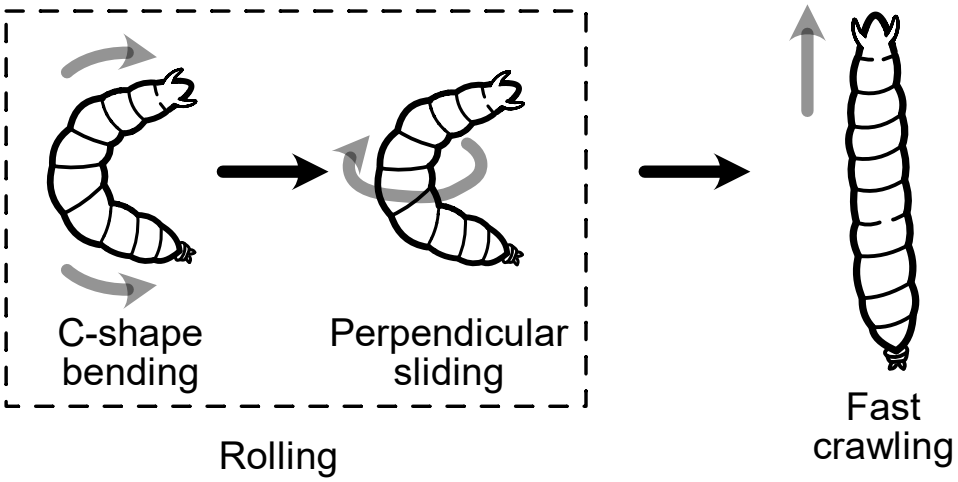


Figure 1. The *Drosophila* larval escape sequence.

## 3. The mechanism of *Drosophila* larval escape behavior

### 3.1. Various sensory modalities are involved in the escape sequence

To study the neural mechanism of this action sequence, the underlying circuit and the sensory stimuli activating the circuit are targeted. As mentioned before, escape rolling can only be activated with nociceptive stimuli. Since intense heat, coldness, chemicals, and mechanosensory stimulations all trigger nociception, these various modalities of nociception have all been examined to determine their ability to trigger escape rolling (Himmel et al., 2019; Hwang et al., 2007; Im & Galko, 2012; Tracey et al., 2003).

In the seminal work on rolling behavior, noxious heat (above 38°C) elicited this sideways roll in a corkscrew-like motion (Tracey et al., 2003). However, the other form of thermal nociception, noxious cold (below 15°C), was later found to trigger the contraction of larvae as well as head and tail lifting behaviors but not escape rolling (Himmel et al., 2021). In addition, both mechanical (i.e., von Frey filament stimuli) and chemical (e.g., acids and menthol) nociception activate escape rolling responses, indicating that rolling is not bound to any modality but is evoked by nociceptive signals (Himmel et al., 2019; Im & Galko, 2012; Tracey et al., 2003). In particular,

moderate mechanical stimuli (i.e., vibration) cannot initiate escape rolling but facilitate it when delivered with nociceptive stimuli, suggesting that different modalities might accumulate sensory inputs for the *Drosophila* CNS to integrate and command the motor system to conduct rolling (Ohyama et al., 2015).

### 3.2. The core circuitry of rolling has been mapped out

Examining various nociceptive stimuli was accompanied by investigating the sensory neurons encoding the response. Multidendritic class IV (mdIV) neurons are activated by all nociceptive modalities, and their activation triggers rolling (Tracey et al., 2003). In addition, mechanosensory neurons (e.g., chordotonal, mdIII, and mdII neurons) facilitate escape rolling by encoding mechanical vibration (Hu et al., 2017; Ohyama et al., 2015).

All of these sensory inputs are integrated at the second-order sensory neurons (i.e., Basin, A08n, Dp-ilp7, DnB, mCSI, Wave, pr1 neurons) (Burgos et al., 2018; Dason et al., 2020; Hu et al., 2017; Hu et al., 2020; Imambocus et al., 2022; Ohyama et al., 2015; Takagi et al., 2017; Yoshino et al., 2017). These neurons are all postsynaptic to mdIV, and except for A08n, they all receive inputs from mechanosensory neurons. Activating most of these second-order sensory neurons triggers rolling except the Dp-ilp7 neuron, which facilitates rolling. The information these second-order sensory neurons integrate is processed locally or delivered to the higher-order processing centers. Then, it converges at motor motifs in the ventral nerve cord (VNC) to execute rolling.

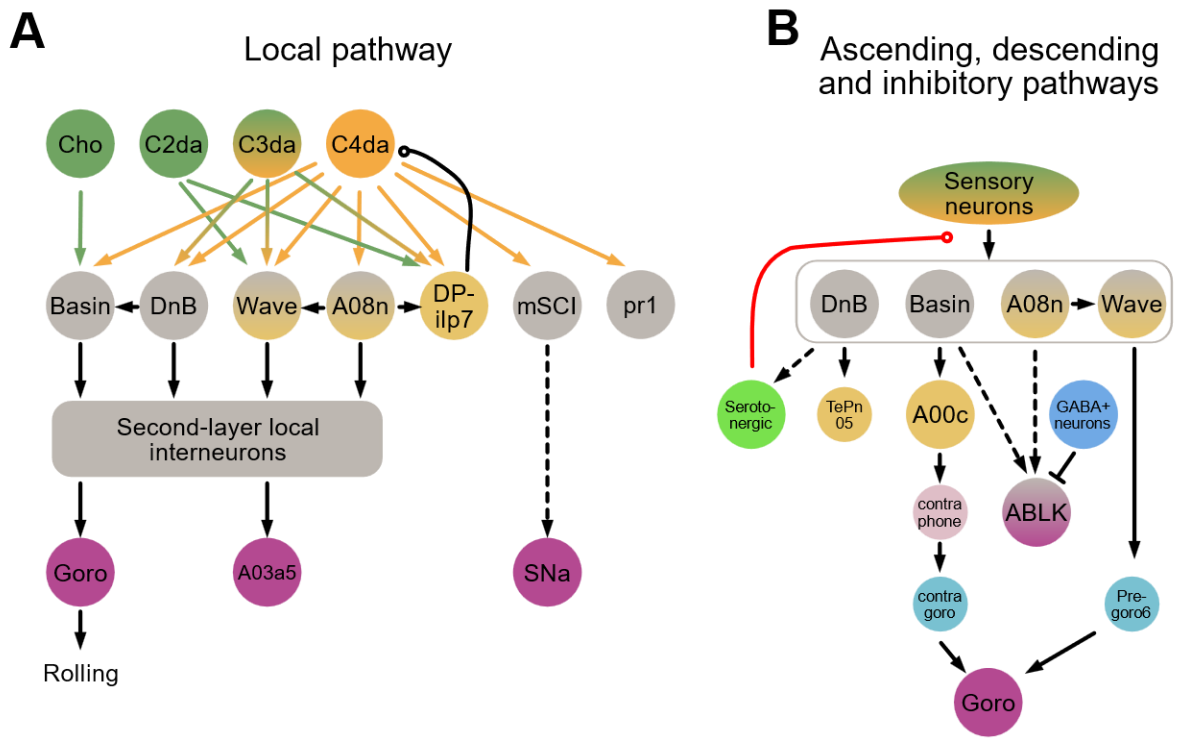


Figure 2. *Drosophila* larval nociceptive circuit. (Adapted) (Boivin et al., 2023)

(A) A detailed diagram of local excitatory pathways in the *Drosophila* larval nociceptive circuit. Mechanosensory and nociceptive neurons are shown in green and orange, respectively. Local interneurons are shown in gray, and second-layer local interneurons (e.g., A23g, A05q, A02g, T05u, Swallowtail, and A09o) are represented collectively by a gray bracket. The command-like neuron Goro, the premotor neuron A03a5, and the motor neuron SNa are shown in purple; these neurons comprise a motor module. (B) A diagram showing critical neurons comprising the ascending, descending, and inhibitory/modulatory pathways of the *Drosophila* larval nocifensive rolling circuit. Ascending neurons are shown in yellow; neurons in the brain and subesophageal zone (SEZ) are in pink; descending neurons are in cyan, and inhibitory neurons are in blue. In both (A, B), bi-colored neurons (e.g., Wave, A08n) send projections locally within the ventral nerve cord (VNC) as well as ascending projections to the brain or SEZ. (Whether ABLK neurons are local

interneurons or part of the motor module remains unclear.) Solid and dotted lines indicate direct and indirect connections, respectively. A line terminating in an arrowhead, open circle, or filled square denotes a connection with an excitatory, modulatory, or inhibitory influence, respectively, on the target neuron. In (B), smaller neurons represent those identified morphologically from EM reconstruction data but whose biological functions remain unclear. The modulatory influence of serotonergic neurons (light green) has thus far only been reported in experience-dependent plasticity during development.

Puzzles remain partially unsolved at the motor layer of this circuit. One command-like neuron for rolling has been reported as Goro (Ohyama et al., 2015). Goro elicits rolling only but not fast crawling, while second-order sensory neurons such as Basin trigger other escape responses, such as fast crawling, tying Goro to solely rolling. Regardless of its role in rolling, Goro is downstream of most of the second-order sensory neurons (i.e., Basin, A08n, Dp-ilp7, Wave, DnB) in the rolling circuit but not all of them, implying that parallel motor circuits might exist for rolling (Burgos et al., 2018; Kaneko et al., 2017; Ohyama et al., 2015; Takagi et al., 2017). For example, as a second-order sensory neuron that elicits rolling responses, mCSI is not upstream of Goro but instead activates the motor neuron SNa to encode rolling (Yoshino et al., 2017). Although their direct postsynaptic partner remains unclear, mCSI is expected to excite an unknown motif independent of Goro to initiate rolling. Shortly, the premotor neurons downstream of Goro and mSCI will be further investigated to illustrate how they coordinate the motor neurons and the corresponding muscles to conduct rolling.

### 3.3. Inhibitory mechanisms play an essential role in the escape circuitry

Aside from excitatory neural pathways, inhibitory motifs are also significant in various neural circuits to modulate outputs, inhibit competing motifs, and gate baseline activities (Hu et

al., 2020; Jovanic et al., 2016; Oikawa et al., 2023). In this larval escape circuit, inhibition mechanisms are also reported to play several roles, including conversion from linear signals to categorical signals, competition between action motifs, and developmental modulation (Hu et al., 2020; Jovanic et al., 2016; Nakamizo-Dojo et al., 2023; Oikawa et al., 2023).

3.3.1. Linear sensory inputs transform into a categorical go-no-go signal through inhibitory thresholding

In the seminal work on escape-rolling behavior, nociceptive inputs are reported to be perceived in a graded manner (Tracey et al., 2003). The higher the temperature is, the more frequent the mdIV spikes are. Such a graded trend of nociceptive input encoding was also observed in other modalities, such as mechano-nociceptive von Frey stimuli and HCl concentrations (Im & Galko, 2012; Tracey et al., 2003). A whole CNS imaging study revealed the regions encoding nociceptive information and those integrating sensory inputs (Hu et al., 2020). The neural activities in the sensory region were linear, while the signals in the integrating region were binary. This linear-to-binary conversion is carried out by GABA signaling onto the ABLK neurons in the integration region. This GABA signal inhibits ABLK neural activities at the subthreshold sensory stimulation, enabling the categorical coding for escape rolling. This GABAergic inhibition prevents escape rolling in response to subthreshold stimulation and ensures precise decision-making with a clear threshold.

3.3.2. Basin-1 and Basin-2, the second-order sensory neurons in the core circuitry, are shown to inhibit each other

While Basin neurons are second-order sensory neurons sharing similar morphologies, the four pairs of Basin neurons recurrent in each abdominal segment trigger different escape patterns (Ohyama et al., 2015). For example, when given mechanosensory input, Basin-1 promotes

hunching, and Basin-2 promotes bending, both of which are nonnocifensive escape responses (Jovanic et al., 2016). Since the same mechanosensory stimuli (e.g., air puff) activate both Basin-1 and Basin-2, and their corresponding behaviors (i.e., hunching and bending) are mutually exclusive, the larval CNS has to avoid the ambiguity between the encoding of hunching and bending. This clarifying neural mechanism is dependent on various layers and motifs of inhibition. In addition to the intuitive mutual inhibition and feedforward inhibition between the two parallel pathways, there is also lateral disinhibition to facilitate transitions and feedback disinhibition to assist in the maintenance of actions. The multiple layers and structures of inhibition enable behavioral competition, maintenance, and transition.

### 3.3.3. Inhibition mediates the competition between feeding and escape behaviors

Aside from the mutual inhibition between hunching and turning, a recent report discussed inhibition at a higher level of behavior (Nakamizo-Dojo et al., 2023). Instead of deciding which escape responses to exhibit, inhibition encrypts whether to escape in this scenario. When larvae are exposed to food deprivation, sugar intake promotes their secretion of insulin-like peptide 2, which excites GABAergic descending neurons to inhibit mdIV neurons, targeting their presynaptic regions. With this pathway, feeding signals after starvation do not reduce the sensation of nociceptive inputs but modulate the transmission of the sensory inputs to neurons in the integrating layer to shift the behavior choice. This delicate mechanism showcases the integration of external and internal cues through inhibition to encode the appropriate responses under the given context.

### 3.3.4. Developmental desensitization involves 5-HT inhibition

Experience shapes behavior. In the animal kingdom, long-term activation could cause feedback-inhibition-induced desensitization, such as the accumulation of neurotransmitters in rod cells in the retina due to overexcitation inhibiting the activity of rhodopsins (Kang Derwent et al.,

2002; Pepperberg, 2003). This feedback mechanism is also proper in *Drosophila* larval escape behavior. When given chronic nociceptive stimuli (e.g., AITC, optogenetic activation of mdIV neurons) during development, *Drosophila* larvae display desensitization phenotypes (i.e., a decreased level of rolling) (Kaneko et al., 2017). The decreased rolling response resulted from the reduced level of nociception integration into the second-order sensory neurons (e.g., Basin, A08n) but not from downregulated nociception. The signals from mdIV neurons to second-order sensory neurons are tempered by feedback inhibition from second-order sensory neurons via 5-HT. Here, the inhibition motif contributes to plasticity and prevents overexcitation of the escape circuit.

These inhibition motifs reported in the escape circuit in *Drosophila* larvae suggest the significance of inhibition in encoding escape behaviors. Thus, studying inhibition motifs offers potential insights into the escape sequence of interest. Additionally, among the three theories of action sequences discussed previously, hierarchical suppression model is emphasizes the role of inhibition the most, hinting that it might explain this escape sequence better than the other theories.

## 4. Evolution of the *Drosophila* behaviors

### 4.1. Evolution of behaviors and circuits in metazoans

Evolutionary development is a field that strives to understand the origins of evolutionary differences through the development of species. Conversely, the study of evolution also contributes to developmental studies. Historically, most research on evolutionary development has been conducted in genetics and morphology since these are the significant features applied in taxonomy. The most well-known example is the fetal development of *Homo sapiens,* which involves the development of gill slits that develop into gills in fish embryos, providing solid evidence of common ancestry (Cartmill et al., 1987).

Similar to general morphologies, CNS are also conservatively evolved, enabling them to be studied in evolutionary development. For instance, vertebrates all similarly have a forebrain, a midbrain, and a hindbrain. The similarities in closely related species allow detailed exploration in the CNS to target the neural or motif modulations for their corresponding behaviors (Tosches et al., 2018). With species slightly distant from each other from the perspective of evolution, the emergence of simple yet crucial motifs, neurons, or molecules would be conveniently isolated (Auer et al., 2020; Prieto-Godino et al., 2017).

Behavior evolution is trickier to research due to the complexity of any given behavior. In addition, different evolution pathways complicate the situation. They may diverge from common primitive behaviors, converge from distinct origins, or parallelly develop. However, such evolution is still successfully isolated in some animal models to examine how different species encode and perform similar behaviors with minor deviations (Katz, 2011; Katz & Harris-Warrick, 1999). These studies involving, but not limited to, sea slugs, crickets, and songbirds demonstrate numerous behavioral models to study the behavioral differences and their mechanisms in closely related species (Colquitt et al., 2021; Hoy et al., 1977; Sakurai & Katz, 2017). For example, cross-comparing the swimming patterns in various sea slug species demonstrated categorizations of the motor patterns and led to a detailed comparison of relevant neural circuits (Newcomb et al., 2012).

Typical mechanisms driving such behavior evolution could be the enhancement or loss of sensory structures, variabilities in the information processing in the CNS, or motor systems decoding the command differently (Auer et al., 2020; Lim et al., 2004; Newcomb et al., 2012). These studies not only elucidated the evolution of the specific behavior but also facilitated the research of those behaviors by providing a naturally controlled scenario where small amounts of

variables were altered. Therefore, comparative studies have been conducted in neuroscience more frequently to shed light on neural circuits and behaviors.

### 4.2. Comparative studies in *Drosophilid* species reveal the neural mechanisms underlying conserved behaviors

*Drosophilid* species have been studied in detail thanks to their relatively smaller genome and CNS and less complex behaviors. The *Drosophila* genus has eight subgenera, and the species mainly come from these two subgenera: the *Drosophila* subgenus and the *Sophophora* subgenus. *Drosophila melanogaster* is a member of the *Sophophora* subgenus, along with *D. simulans*, *D. sechelia*, and several other well-known species. Comparative studies using these species have offered valuable insights into the circuit structure and the varied functions of neurons (Ding et al., 2019; Himmel et al., 2021; Manning, 1960).

Various aspects of evolution in *Drosophila* have been explored and investigated. Most straightforwardly, the genomes for several *Drosophilid* species are sequenced and reported, allowing comparison at the molecular level (Drosophila 12 Genomes et al., 2007; Lin et al., 2007; Stark et al., 2007). Similarly, behaviors such as escape, feeding, and courtship are contrasted among species (Ding et al., 2019; Himmel et al., 2021; Kim et al., 2017). For instance, in a recent report, larval nociceptive behaviors stimulated by cold plates (0-10°C) were studied in 11 *Drosophilid* species (Himmel et al., 2021). They all exhibited bilateral contraction behavior, where larvae lifted their anterior and posterior ends toward the midline, perhaps to avoid coldness. Interestingly, the *repleta* group shared a distinct subsequent nociceptive behavior where their rear end was raised, and the posterior spiracles expanded when exposed to coldness, which was not observed in other *Drosophilid* species. Further investigation into such variations in cold

nociceptive behaviors could lead to the discovery of neural circuits underlying this unique spiracle expansion.

Comparative studies focused on stereotyped *Drosophilid* behaviors similar to this cold nociceptive behavior could contribute to the knowledge of evolution and enhance the understanding of circuits and behaviors. The phenotypic differences could be traced back to the connectomes, thus drawing an association or even a causal relationship between circuits and behaviors. Although the precise neural mechanism for the abovementioned cold nociceptive behavior is still unknown, the behavior difference might have originated in circuit-level variabilities or differential genetic expression, which would be intriguing to investigate.

In addition, the power of comparative study in circuit research has been showcased in courtship behavior in *Drosophila,* where circuit research and evolution comparison assisted each other (Ding et al., 2019). As one of the most investigated behaviors among the *Drosophilid* species, courtship consists of chasing the female, dancing, singing, waving wings, licking, and so on. Singing is conserved in *Drosophila* species among these courtship behaviors since they all vibrate their wings to signal the females. However, the details differ for each species. For example, out of the two basic song types, sine-form and pulse-form song, most species have pulse-form songs executed by unilateral wing vibration. Nevertheless, not all species exhibit sine-form songs, indicating that this unilateral pulse-form song is an ancestral behavior. *D. melanogaster*, for instance, displays a unilateral pulse-form song and a sine-form song. However, *D. yakuba* and *D. santomea* perform an additional bilateral wing vibration termed as a clack song.

pIP10 neurons in *D. yakuba* activated this clack song. They also evoked a unilateral pulse song in both *D. yakuba* and *D. melanogaster*, suggesting the fundamental role of pIP10 neurons in courtship singing circuits. Further investigation showed that activating pIP10 in *D.*

*melanogaster* with very low intensity triggered a less-reported song pattern resembling the clack song, implying that *D. melanogaster* has primitive wiring for the clack song. Even though both *D. melanogaster* and *D. yakuba* could sing clack songs, the shift in the threshold to trigger clack songs accounted for the differential courtship behaviors. This threshold change was not caused by the morphologies or the electrophysiological properties of pIP10 neurons in these species. Still, it was possibly attributed to different connectome diagrams in *Drosophilid* species, supporting the idea that evolutionary comparison studies in closely related species can promote neural circuit research.

### 4.3. Evolution in *Drosophila* larval escape strategies

Ecologically, *Drosophila* species survive in various geographical regions and thus consume varied food, endure different climates, and encounter distinct predator wasps, which could result in the evolution of their escape responses while confronting wasps. Aside from *D. melanogaster*, other species have developed various versions of escape strategies. *D. sechellia*, for example, lacks the immune responses that *D. melanogaster* and *D. simulans* display to inhibit the growth of wasp eggs (Salazar-Jaramillo & Wertheim, 2021). This absence of specific immune strategies originated from food choices. Due to their specific niche on the Seychelles Islands, *D. sechellia* feed on the fruit *Morinda citrifolia* (noni), which might be harmful to parasitic wasps, reducing their selective pressure from parasitoid wasps and the necessity of immune responses specific to wasp parasitization (Salazar-Jaramillo & Wertheim, 2021). In addition, *Drosophila* species escape when given aversive odors (e.g., geosmin, DEET [N, N-diethyl-meta-toluamide]). A comparative study showed that *D. melanogaster* and *D. suzukii* larvae both escape from aversive odors, but *D. suzukii* displayed a more intense escape behavior, which is absent in *D. melanogaster* (Fleury et al., 2004). Even though the underlying mechanism remains unclear, combining this with other studies reporting how genetic variances contribute to varied levels of susceptibility, it is plausible that

*Drosophilid* species exhibit deviation in their larval escape rolling behaviors, enabling a more detailed dissection of the escape rolling circuits as well as the mechanisms of their escape sequences.

**References**


Abeles, M. (1982). *Local Cortical Circuits: An Electrophysiological Study*. Springer-Verlag. https://books.google.ca/books?id=s25lwwEACAAJ

Abeles, M. (1991). *Corticonics : neural circuits of the cerebral cortex*. Cambridge University Press. https://books.google.ca/books?id=v46SDOLJrLcC

Adams, J. A. (1984). Learning of movement sequences. *Psychological Bulletin*, *96*(1), 3-28. https://doi.org/10.1037/0033-2909.96.1.3

Anthony, J. L., & Fernando, N. (2000). Age at Deafening Affects the Stability of Learned Song in Adult Male Zebra Finches. *The Journal of Neuroscience*, *20*(13), 5054. https://doi.org/10.1523/JNEUROSCI.20-13-05054.2000

Averbeck, B. B., Chafee, M. V., Crowe, D. A., & Georgopoulos, A. P. (2002). Parallel processing of serial movements in prefrontal cortex. *Proc Natl Acad Sci U S A*, *99*(20), 13172-13177. https://doi.org/10.1073/pnas.162485599

Bahn, J. H., Lee, G., & Park, J. H. (2009). Comparative analysis of Pdf-mediated circadian behaviors between Drosophila melanogaster and D. virilis. *Genetics*, *181*(3), 965-975. https://doi.org/10.1534/genetics.108.099069

Bertet, C., Rauzi, M., & Lecuit, T. (2009). Repression of Wasp by JAK/STAT signalling inhibits medial actomyosin network assembly and apical cell constriction in intercalating epithelial cells. *Development*, *136*(24), 4199-4212. https://doi.org/10.1242/dev.040402

Bidaye, S. S., Machacek, C., Wu, Y., & Dickson, B. J. (2014). Neuronal control of Drosophila walking direction. *Science*, *344*(6179), 97-101. https://doi.org/10.1126/science.1249964

Boivin, J. C., Zhu, J., & Ohyama, T. (2023). Nociception in fruit fly larvae. *Front Pain Res (Lausanne)*, *4*, 1076017. https://doi.org/10.3389/fpain.2023.1076017

Brand, A. H., & Perrimon, N. (1993). Targeted gene expression as a means of altering cell fates and generating dominant phenotypes. *Development*, *118*(2), 401-415. https://doi.org/10.1242/dev.118.2.401

Brian, K. S., & William, B. K., Jr. (1997). The Neuronal Basis of the Behavioral Choice between Swimming and Shortening in the Leech: Control Is Not Selectively Exercised at Higher Circuit Levels. *The Journal of Neuroscience*, *17*(2), 786. https://doi.org/10.1523/JNEUROSCI.17-02-00786.1997

Burgos, A., Honjo, K., Ohyama, T., Qian, C. S., Shin, G. J., Gohl, D. M., Silies, M., Tracey, W. D., Zlatic, M., Cardona, A., & Grueber, W. B. (2018). Nociceptive interneurons control modular motor pathways to promote escape behavior in Drosophila. *Elife*, *7*. https://doi.org/10.7554/eLife.26016

Cao, G., Platisa, J., Pieribone, V. A., Raccuglia, D., Kunst, M., & Nitabach, M. N. (2013). Genetically targeted optical electrophysiology in intact neural circuits. *Cell*, *154*(4), 904-913. https://doi.org/10.1016/j.cell.2013.07.027

Capelli, P., Pivetta, C., Soledad Esposito, M., & Arber, S. (2017). Locomotor speed control circuits in the caudal brainstem. *Nature*, *551*(7680), 373-377. https://doi.org/10.1038/nature24064

Cartmill, M., Hylander, W. L., & Shafland, J. (1987). *Human structure*. Harvard University Press.

Cohen, R. G., & Rosenbaum, D. A. (2004). Where grasps are made reveals how grasps are planned: generation and recall of motor plans. *Experimental Brain Research*, *157*(4), 486-495. https://doi.org/10.1007/s00221-004-1862-9

Cregg, J. M., Leiras, R., Montalant, A., Wanken, P., Wickersham, I. R., & Kiehn, O. (2020). Brainstem neurons that command mammalian locomotor asymmetries. *Nat Neurosci*, *23*(6), 730-740. https://doi.org/10.1038/s41593-020-0633-7

Dason, J. S., Cheung, A., Anreiter, I., Montemurri, V. A., Allen, A. M., & Sokolowski, M. B. (2020). Drosophila melanogaster foraging regulates a nociceptive-like escape behavior through a developmentally plastic sensory circuit. *Proc Natl Acad Sci U S A*, *117*(38), 23286-23291. https://doi.org/10.1073/pnas.1820840116

Dawkins, R. (1976). Hierarchical organisation: A candidate principle for ethology. In *Growing points in ethology.* Cambridge U Press.

Diesmann, M., Gewaltig, M. O., & Aertsen, A. (1999). Stable propagation of synchronous spiking in cortical neural networks. *Nature*, *402*(6761), 529-533. https://doi.org/10.1038/990101

Ding, Y., Lillvis, J. L., Cande, J., Berman, G. J., Arthur, B. J., Long, X., Xu, M., Dickson, B. J., & Stern, D. L. (2019). Neural Evolution of Context-Dependent Fly Song. *Curr Biol*, *29*(7), 1089-1099 e1087. https://doi.org/10.1016/j.cub.2019.02.019

Dolan, M. J., Luan, H., Shropshire, W. C., Sutcliffe, B., Cocanougher, B., Scott, R. L., Frechter, S., Zlatic, M., Jefferis, G., & White, B. H. (2017). Facilitating Neuron-Specific Genetic Manipulations in Drosophila melanogaster Using a Split GAL4 Repressor. *Genetics*, *206*(2), 775-784. https://doi.org/10.1534/genetics.116.199687

Doring, F., Wischmeyer, E., Kuhnlein, R. P., Jackle, H., & Karschin, A. (2002). Inwardly rectifying K+ (Kir) channels in Drosophila. A crucial role of cellular milieu factors Kir channel function. *J Biol Chem*, *277*(28), 25554-25561. https://doi.org/10.1074/jbc.M202385200

Eichler, K., Li, F., Litwin-Kumar, A., Park, Y., Andrade, I., Schneider-Mizell, C. M., Saumweber, T., Huser, A., Eschbach, C., Gerber, B., Fetter, R. D., Truman, J. W., Priebe, C. E., Abbott, L. F., Thum, A. S., Zlatic, M., & Cardona, A. (2017). The complete connectome of a learning and memory centre in an insect brain. *Nature*, *548*(7666), 175-182. https://doi.org/10.1038/nature23455

Fleury, F., Ris, N., Allemand, R., Fouillet, P., Carton, Y., & Boulétreau, M. (2004). Ecological and Genetic Interactions in Drosophila–parasitoids Communities: A Case Study with D. Melanogaster, D. Simulans and their Common Leptopilina Parasitoids in South-eastern France. *Genetica*, *120*(1), 181-194. https://doi.org/10.1023/B:GENE.0000017640.78087.9e

Geddes, C. E., Li, H., & Jin, X. (2018). Optogenetic Editing Reveals the Hierarchical Organization of Learned Action Sequences. *Cell*, *174*(1), 32-43 e15. https://doi.org/10.1016/j.cell.2018.06.012

Gerhard, S., Andrade, I., Fetter, R. D., Cardona, A., & Schneider-Mizell, C. M. (2017). Conserved neural circuit structure across Drosophila larval development revealed by comparative connectomics. *Elife*, *6*. https://doi.org/10.7554/eLife.29089

Govorunova, E. G., Cunha, S. R., Sineshchekov, O. A., & Spudich, J. L. (2016). Anion channelrhodopsins for inhibitory cardiac optogenetics. *Sci Rep*, *6*, 33530. https://doi.org/10.1038/srep33530

Guo, L., Zhang, N., & Simpson, J. H. (2022). Descending neurons coordinate anterior grooming behavior in Drosophila. *Curr Biol*, *32*(4), 823-833 e824. https://doi.org/10.1016/j.cub.2021.12.055

Henry, F. M., & Rogers, D. E. (1960). Increased response latency for complicated movements and a "memory drum" theory of neuromotor reaction. *Research Quarterly of the American Association for Health, Physical Education, & Recreation*, *31*, 448-458. https://doi.org/10.1080/10671188.1960.10762052

Herberholz, J., Issa, F. A., & Edwards, D. H. (2001). Patterns of neural circuit activation and behavior during dominance hierarchy formation in freely behaving crayfish. *J Neurosci*, *21*(8), 2759-2767. https://doi.org/10.1523/jneurosci.21-08-02759.2001

Himmel, N. J., Letcher, J. M., Sakurai, A., Gray, T. R., Benson, M. N., & Cox, D. N. (2019). Drosophila menthol sensitivity and the Precambrian origins of transient receptor potential-

dependent chemosensation. *Philos Trans R Soc Lond B Biol Sci*, *374*(1785), 20190369. https://doi.org/10.1098/rstb.2019.0369

Himmel, N. J., Letcher, J. M., Sakurai, A., Gray, T. R., Benson, M. N., Donaldson, K. J., & Cox, D. N. (2021). Identification of a neural basis for cold acclimation in Drosophila larvae. *iScience*, *24*(6), 102657. https://doi.org/10.1016/j.isci.2021.102657

Houghton, G., & Hartley, T. (1995). Parallel models of serial behavior: Lashley revisited. *Psyche*, *2*(25), 1-25.

Hu, C., Petersen, M., Hoyer, N., Spitzweck, B., Tenedini, F., Wang, D., Gruschka, A., Burchardt, L. S., Szpotowicz, E., Schweizer, M., Guntur, A. R., Yang, C. H., & Soba, P. (2017). Sensory integration and neuromodulatory feedback facilitate Drosophila mechanonociceptive behavior. *Nat Neurosci*, *20*(8), 1085-1095. https://doi.org/10.1038/nn.4580

Hu, Y., Wang, C., Yang, L., Pan, G., Liu, H., Yu, G., & Ye, B. (2020). A Neural Basis for Categorizing Sensory Stimuli to Enhance Decision Accuracy. *Curr Biol*, *30*(24), 4896-4909 e4896. https://doi.org/10.1016/j.cub.2020.09.045

Hwang, R. Y., Zhong, L., Xu, Y., Johnson, T., Zhang, F., Deisseroth, K., & Tracey, W. D. (2007). Nociceptive neurons protect Drosophila larvae from parasitoid wasps. *Curr Biol*, *17*(24), 2105-2116. https://doi.org/10.1016/j.cub.2007.11.029

Ikegaya, Y., Aaron, G., Cossart, R., Aronov, D., Lampl, I., Ferster, D., & Yuste, R. (2004). Synfire chains and cortical songs: temporal modules of cortical activity. *Science*, *304*(5670), 559-564. https://doi.org/10.1126/science.1093173

Im, S. H., & Galko, M. J. (2012). Pokes, sunburn, and hot sauce: Drosophila as an emerging model for the biology of nociception. *Dev Dyn*, *241*(1), 16-26. https://doi.org/10.1002/dvdy.22737

Imambocus, B. N., Zhou, F., Formozov, A., Wittich, A., Tenedini, F. M., Hu, C., Sauter, K., Macarenhas Varela, E., Heredia, F., Casimiro, A. P., Macedo, A., Schlegel, P., Yang, C. H., Miguel-Aliaga, I., Wiegert, J. S., Pankratz, M. J., Gontijo, A. M., Cardona, A., & Soba, P. (2022). A neuropeptidergic circuit gates selective escape behavior of Drosophila larvae. *Curr Biol*, *32*(1), 149-163 e148. https://doi.org/10.1016/j.cub.2021.10.069

Jing, J., & Gillette, R. (1995). Neuronal elements that mediate escape swimming and suppress feeding behavior in the predatory sea slug Pleurobranchaea. *Journal of Neurophysiology*, *74*(5), 1900-1910. https://doi.org/10.1152/jn.1995.74.5.1900

Jovanic, T., Schneider-Mizell, C. M., Shao, M., Masson, J. B., Denisov, G., Fetter, R. D., Mensh, B. D., Truman, J. W., Cardona, A., & Zlatic, M. (2016). Competitive Disinhibition Mediates Behavioral Choice and Sequences in Drosophila. *Cell*, *167*(3), 858-870 e819. https://doi.org/10.1016/j.cell.2016.09.009

Kachergis, G., Wyatte, D., O'Reilly, R. C., de Kleijn, R., & Hommel, B. (2014). A continuous-time neural model for sequential action. *Philos Trans R Soc Lond B Biol Sci*, *369*(1655). https://doi.org/10.1098/rstb.2013.0623

Kaneko, T., Macara, A. M., Li, R., Hu, Y., Iwasaki, K., Dunnings, Z., Firestone, E., Horvatic, S., Guntur, A., Shafer, O. T., Yang, C. H., Zhou, J., & Ye, B. (2017). Serotonergic Modulation Enables Pathway-Specific Plasticity in a Developing Sensory Circuit in Drosophila. *Neuron*, *95*(3), 722. https://doi.org/10.1016/j.neuron.2017.07.023

Kang Derwent, J. J., Qtaishat, N. M., & Pepperberg, D. R. (2002). Excitation and desensitization of mouse rod photoreceptors in vivo following bright adapting light. *J Physiol*, *541*(Pt 1), 201-218. https://doi.org/10.1113/jphysiol.2001.013227

Kaplan, H. S., Salazar Thula, O., Khoss, N., & Zimmer, M. (2020). Nested Neuronal Dynamics Orchestrate a Behavioral Hierarchy across Timescales. *Neuron*, *105*(3), 562-576.e569. https://doi.org/https://doi.org/10.1016/j.neuron.2019.10.037

Karaiskos, N., Wahle, P., Alles, J., Boltengagen, A., Ayoub, S., Kipar, C., Kocks, C., Rajewsky, N., & Zinzen, R. P. (2017). The Drosophila embryo at single-cell transcriptome resolution. *Science*, *358*(6360), 194-199. https://doi.org/10.1126/science.aan3235

Katz, P. S. (2011). Neural mechanisms underlying the evolvability of behaviour. *Philos Trans R Soc Lond B Biol Sci*, *366*(1574), 2086-2099. https://doi.org/10.1098/rstb.2010.0336

Katz, P. S., & Harris-Warrick, R. M. (1999). The evolution of neuronal circuits underlying species-specific behavior. *Curr Opin Neurobiol*, *9*(5), 628-633. https://doi.org/10.1016/S0959-4388(99)00012-4

Kent, R. D. (1983). The Segmental Organization of Speech. In P. F. MacNeilage (Ed.), *The Production of Speech* (pp. 57-89). Springer New York. https://doi.org/10.1007/978-1-4613-8202-7_4

Khakh, B. S., Gittermann, D., Cockayne, D. A., & Jones, A. (2003). ATP modulation of excitatory synapses onto interneurons. *J Neurosci*, *23*(19), 7426-7437. https://doi.org/10.1523/JNEUROSCI.23-19-07426.2003

Kim, D., Alvarez, M., Lechuga, L. M., & Louis, M. (2017). Species-specific modulation of food-search behavior by respiration and chemosensation in Drosophila larvae. *Elife*, *6*. https://doi.org/10.7554/eLife.27057

Kim, M. D., Wen, Y., & Jan, Y. N. (2009). Patterning and organization of motor neuron dendrites in the Drosophila larva. *Dev Biol*, *336*(2), 213-221. https://doi.org/10.1016/j.ydbio.2009.09.041

Klapoetke, N. C., Murata, Y., Kim, S. S., Pulver, S. R., Birdsey-Benson, A., Cho, Y. K., Morimoto, T. K., Chuong, A. S., Carpenter, E. J., Tian, Z., Wang, J., Xie, Y., Yan, Z., Zhang, Y., Chow, B. Y., Surek, B., Melkonian, M., Jayaraman, V., Constantine-Paton, M., . . . Boyden, E. S. (2014). Independent optical excitation of distinct neural populations. *Nat Methods*, *11*(3), 338-346. https://doi.org/10.1038/nmeth.2836

Lai, S. L., & Lee, T. (2006). Genetic mosaic with dual binary transcriptional systems in Drosophila. *Nat Neurosci*, *9*(5), 703-709. https://doi.org/10.1038/nn1681

Lashley, K. S. (1951). The problem of serial order in behavior. In *Cerebral mechanisms in behavior; the Hixon Symposium.* (pp. 112-146). Wiley.

Lewis, E. B. (1978). A gene complex controlling segmentation in Drosophila. *Nature*, *276*(5688), 565-570. https://doi.org/10.1038/276565a0

Li, X., Gutierrez, D. V., Hanson, M. G., Han, J., Mark, M. D., Chiel, H., Hegemann, P., Landmesser, L. T., & Herlitze, S. (2005). Fast noninvasive activation and inhibition of neural and network activity by vertebrate rhodopsin and green algae channelrhodopsin. *Proc Natl Acad Sci U S A*, *102*(49), 17816-17821. https://doi.org/10.1073/pnas.0509030102

Liu, Q., Yang, X., Luo, M., Su, J., Zhong, J., Li, X., Chan, R. H. M., & Wang, L. (2023). An iterative neural processing sequence orchestrates feeding. *Neuron*, *111*(10), 1651-1665 e1655. https://doi.org/10.1016/j.neuron.2023.02.025

Long, M. A., Jin, D. Z., & Fee, M. S. (2010). Support for a synaptic chain model of neuronal sequence generation. *Nature*, *468*(7322), 394-399. https://doi.org/10.1038/nature09514

Lorenz, K., & Tinbergen, N. (1938). Taxis und Instinkthandlung in der Eirollbewegung der Graugans. [Directed and instinctive behavior in the egg rolling movements of the gray goose.]. *Zeitschrift für Tierpsychologie*, *2*, 1-29. https://doi.org/10.1111/j.1439-0310.1939.tb01558.x

Louradour, I., Sharma, A., Morin-Poulard, I., Letourneau, M., Vincent, A., Crozatier, M., & Vanzo, N. (2017). Reactive oxygen species-dependent Toll/NF-kappaB activation in the

Drosophila hematopoietic niche confers resistance to wasp parasitism. *Elife*, *6*. https://doi.org/10.7554/eLife.25496

Luan, H., Diao, F., Scott, R. L., & White, B. H. (2020). The Drosophila Split Gal4 System for Neural Circuit Mapping. *Front Neural Circuits*, *14*, 603397. https://doi.org/10.3389/fncir.2020.603397

Luan, H., Peabody, N. C., Vinson, C. R., & White, B. H. (2006). Refined spatial manipulation of neuronal function by combinatorial restriction of transgene expression. *Neuron*, *52*(3), 425-436. https://doi.org/10.1016/j.neuron.2006.08.028

Manning, A. (1960). The Sexual Behaviour of Two Sibling Drosophila Species. *Behaviour*, *15*(1-2), 123-145. https://doi.org/https://doi.org/10.1163/156853960X00133

Marler, P. (1970). A comparative approach to vocal learning: Song development in white-crowned sparrows. *Journal of Comparative and Physiological Psychology*, *71*(2, Pt.2), 1-25. https://doi.org/10.1037/h0029144

Masson, J. B., Laurent, F., Cardona, A., Barre, C., Skatchkovsky, N., Zlatic, M., & Jovanic, T. (2020). Identifying neural substrates of competitive interactions and sequence transitions during mechanosensory responses in Drosophila. *PLoS Genet*, *16*(2), e1008589. https://doi.org/10.1371/journal.pgen.1008589

Mazzucato, L. (2022). Neural mechanisms underlying the temporal organization of naturalistic animal behavior. *Elife*, *11*. https://doi.org/10.7554/eLife.76577

McGinnis, W., Garber, R. L., Wirz, J., Kuroiwa, A., & Gehring, W. J. (1984). A homologous protein-coding sequence in Drosophila homeotic genes and its conservation in other metazoans. *Cell*, *37*(2), 403-408. https://doi.org/10.1016/0092-8674(84)90370-2

McKellar, C. E., Lillvis, J. L., Bath, D. E., Fitzgerald, J. E., Cannon, J. G., Simpson, J. H., & Dickson, B. J. (2019). Threshold-Based Ordering of Sequential Actions during Drosophila Courtship. *Curr Biol*, *29*(3), 426-434 e426. https://doi.org/10.1016/j.cub.2018.12.019

Murakami, M., & Mainen, Z. F. (2015). Preparing and selecting actions with neural populations: toward cortical circuit mechanisms. *Curr Opin Neurobiol*, *33*, 40-46. https://doi.org/10.1016/j.conb.2015.01.005

Nakai, J., Ohkura, M., & Imoto, K. (2001). A high signal-to-noise Ca(2+) probe composed of a single green fluorescent protein. *Nat Biotechnol*, *19*(2), 137-141. https://doi.org/10.1038/84397

Nakamizo-Dojo, M., Ishii, K., Yoshino, J., Tsuji, M., & Emoto, K. (2023). Descending GABAergic pathway links brain sugar-sensing to peripheral nociceptive gating in Drosophila. *Nat Commun*, *14*(1), 6515. https://doi.org/10.1038/s41467-023-42202-9

Naniwa, K., & Aonuma, H. (2021). Descending and Ascending Signals That Maintain Rhythmic Walking Pattern in Crickets. *Front Robot AI*, *8*, 625094. https://doi.org/10.3389/frobt.2021.625094

Neely, G. G., Keene, A. C., Duchek, P., Chang, E. C., Wang, Q. P., Aksoy, Y. A., Rosenzweig, M., Costigan, M., Woolf, C. J., Garrity, P. A., & Penninger, J. M. (2011). TrpA1 regulates thermal nociception in Drosophila. *PLoS One*, *6*(8), e24343. https://doi.org/10.1371/journal.pone.0024343

Ohyama, T., Schneider-Mizell, C. M., Fetter, R. D., Aleman, J. V., Franconville, R., Rivera-Alba, M., Mensh, B. D., Branson, K. M., Simpson, J. H., Truman, J. W., Cardona, A., & Zlatic, M. (2015). A multilevel multimodal circuit enhances action selection in Drosophila. *Nature*, *520*(7549), 633-639. https://doi.org/10.1038/nature14297

Oikawa, I., Kondo, S., Hashimoto, K., Yoshida, A., Hamajima, M., Tanimoto, H., Furukubo-Tokunaga, K., & Honjo, K. (2023). A descending inhibitory mechanism of nociception mediated by an evolutionarily conserved neuropeptide system in Drosophila. *Elife*, *12*. https://doi.org/10.7554/eLife.85760

Pastalkova, E., Itskov, V., Amarasingham, A., & Buzsaki, G. (2008). Internally generated cell assembly sequences in the rat hippocampus. *Science*, *321*(5894), 1322-1327. https://doi.org/10.1126/science.1159775

Pepperberg, D. R. (2003). Bleaching desensitization: background and current challenges. *Vision Res*, *43*(28), 3011-3019. https://doi.org/10.1016/s0042-6989(03)00484-x

Pfeiffer, B. D., Ngo, T. T., Hibbard, K. L., Murphy, C., Jenett, A., Truman, J. W., & Rubin, G. M. (2010). Refinement of tools for targeted gene expression in Drosophila. *Genetics*, *186*(2), 735-755. https://doi.org/10.1534/genetics.110.119917

Potter, C. J., Tasic, B., Russler, E. V., Liang, L., & Luo, L. (2010). The Q system: a repressible binary system for transgene expression, lineage tracing, and mosaic analysis. *Cell*, *141*(3), 536-548. https://doi.org/10.1016/j.cell.2010.02.025

Rizki, T. M., & Rizki, R. M. (1992). Lamellocyte differentiation in Drosophila larvae parasitized by Leptopilina. *Dev Comp Immunol*, *16*(2-3), 103-110. https://doi.org/10.1016/0145-305x(92)90011-z

Rosenbaum, D. A. (1988). Successive Approximations to a Model of Human Motor Programming. In G. H. Bower (Ed.), *Psychology of Learning and Motivation* (Vol. 21, pp. 153-182). Academic Press. https://doi.org/https://doi.org/10.1016/S0079-7421(08)60028-6

Rosenbaum, D. A., Cohen, R. G., Jax, S. A., Weiss, D. J., & van der Wel, R. (2007). The problem of serial order in behavior: Lashley's legacy. *Hum Mov Sci*, *26*(4), 525-554. https://doi.org/10.1016/j.humov.2007.04.001

Salazar-Jaramillo, L., & Wertheim, B. (2021). Does Drosophila sechellia escape parasitoid attack by feeding on a toxic resource? *PeerJ*, *9*, e10528.

Schnell, B., Ros, I. G., & Dickinson, M. H. (2017). A Descending Neuron Correlated with the Rapid Steering Maneuvers of Flying Drosophila. *Curr Biol*, *27*(8), 1200-1205. https://doi.org/10.1016/j.cub.2017.03.004

Seeds, A. M., Ravbar, P., Chung, P., Hampel, S., Midgley, F. M., Jr., Mensh, B. D., & Simpson, J. H. (2014). A suppression hierarchy among competing motor programs drives sequential grooming in Drosophila. *Elife*, *3*, e02951. https://doi.org/10.7554/eLife.02951

Severi, K. E., Portugues, R., Marques, J. C., O'Malley, D. M., Orger, M. B., & Engert, F. (2014). Neural control and modulation of swimming speed in the larval zebrafish. *Neuron*, *83*(3), 692-707. https://doi.org/10.1016/j.neuron.2014.06.032

Sherrington, C. S. (1906). *The Integrative Action of the Nervous System*. Yale University Press. https://books.google.ca/books?id=f69LAAAAMAAJ

Siegel, M. S., & Isacoff, E. Y. (1997). A genetically encoded optical probe of membrane voltage. *Neuron*, *19*(4), 735-741. https://doi.org/10.1016/s0896-6273(00)80955-1

Sineshchekov, O. A., Jung, K. H., & Spudich, J. L. (2002). Two rhodopsins mediate phototaxis to low- and high-intensity light in Chlamydomonas reinhardtii. *Proc Natl Acad Sci U S A*, *99*(13), 8689-8694. https://doi.org/10.1073/pnas.122243399

Sternberg, S., Monsell, S., Knoll, R. L., & Wright, C. E. (1978). 6 - The Latency and Duration of Rapid Movement Sequences: Comparisons of Speech and Typewriting. In G. E. Stelmach (Ed.), *Information Processing in Motor Control and Learning* (pp. 117-152). Academic Press. https://doi.org/https://doi.org/10.1016/B978-0-12-665960-3.50011-6

Sweeney, S. T., Broadie, K., Keane, J., Niemann, H., & O'Kane, C. J. (1995). Targeted expression of tetanus toxin light chain in Drosophila specifically eliminates synaptic transmission and causes behavioral defects. *Neuron*, *14*(2), 341-351. https://doi.org/10.1016/0896-6273(95)90290-2

Takagi, S., Cocanougher, B. T., Niki, S., Miyamoto, D., Kohsaka, H., Kazama, H., Fetter, R. D., Truman, J. W., Zlatic, M., Cardona, A., & Nose, A. (2017). Divergent Connectivity of Homologous Command-like Neurons Mediates Segment-Specific Touch Responses in Drosophila. *Neuron*, *96*(6), 1373-1387 e1376. https://doi.org/10.1016/j.neuron.2017.10.030

Tinbergen, N. (1952). The Curious Behavior of the Stickleback. *Scientific American*, *187*(6), 22-27. http://www.jstor.org.proxy3.library.mcgill.ca/stable/24944080

Tracey, W. D., Jr., Wilson, R. I., Laurent, G., & Benzer, S. (2003). painless, a Drosophila gene essential for nociception. *Cell*, *113*(2), 261-273. https://doi.org/10.1016/s0092-8674(03)00272-1

van de Goor, J., Ramaswami, M., & Kelly, R. (1995). Redistribution of synaptic vesicles and their proteins in temperature-sensitive shibire(ts1) mutant Drosophila. *Proc Natl Acad Sci U S A*, *92*(12), 5739-5743. https://doi.org/10.1073/pnas.92.12.5739

van der Wel, R. P. R. D., & Rosenbaum, D. A. (2007). Coordination of locomotion and prehension. *Experimental Brain Research*, *176*(2), 281-287. https://doi.org/10.1007/s00221-006-0618-0

Vijayan, V., Wang, F., Wang, K., Chakravorty, A., Adachi, A., Akhlaghpour, H., Dickson, B. J., & Maimon, G. (2023). A rise-to-threshold process for a relative-value decision. *Nature*, *619*(7970), 563-571. https://doi.org/10.1038/s41586-023-06271-6

Winding, M., Pedigo, B. D., Barnes, C. L., Patsolic, H. G., Park, Y., Kazimiers, T., Fushiki, A., Andrade, I. V., Khandelwal, A., Valdes-Aleman, J., Li, F., Randel, N., Barsotti, E., Correia, A., Fetter, R. D., Hartenstein, V., Priebe, C. E., Vogelstein, J. T., Cardona, A., & Zlatic, M. (2023). The connectome of an insect brain. *Science*, *379*(6636), eadd9330. https://doi.org/10.1126/science.add9330

Wu, J., Abdelfattah, A. S., Zhou, H., Ruangkittisakul, A., Qian, Y., Ballanyi, K., & Campbell, R. E. (2018). Genetically Encoded Glutamate Indicators with Altered Color and Topology. *ACS Chem Biol*, *13*(7), 1832-1837. https://doi.org/10.1021/acschembio.7b01085

Yang, H., & Hultmark, D. (2017). Drosophila muscles regulate the immune response against wasp infection via carbohydrate metabolism. *Sci Rep*, *7*(1), 15713. https://doi.org/10.1038/s41598-017-15940-2

Yoshino, J., Morikawa, R. K., Hasegawa, E., & Emoto, K. (2017). Neural Circuitry that Evokes Escape Behavior upon Activation of Nociceptive Sensory Neurons in Drosophila Larvae. *Curr Biol*, *27*(16), 2499-2504 e2493. https://doi.org/10.1016/j.cub.2017.06.068

Zarin, A. A., Mark, B., Cardona, A., Litwin-Kumar, A., & Doe, C. Q. (2019). A multilayer circuit architecture for the generation of distinct locomotor behaviors in Drosophila. *Elife*, *8*. https://doi.org/10.7554/eLife.51781

## CHAPTER 2 Feedback inhibition by a descending GABAergic neuron regulates timing of escape behavior in *Drosophila* larvae

This manuscript discussed how a feedback inhibition motif facilitates rolling termination and fast crawling initiation. With the behavior and circuit level evidence, we identified a pair of descending neurons, SeIN128, that received excitatory inputs from Basin-2 and sent inhibitory outputs to Basin-2 to inhibit rolling and allow fast crawling execution. This finding supports the hierarchical suppression model in encoding this escape sequence and rejects ramp-to-threshold or synfire chain theories in this scenario.

**Feedback inhibition by a descending GABAergic neuron regulates timing of escape behavior in *Drosophila* larvae**

Jiayi Zhu[1,2], Jean-Christophe Boivin[1,2], Alastair Garner[1,2], Jing Ning[1], Yi Qing Zhao[1], Tomoko Ohyama[1,2,3*]

[1] Department of Biology, McGill University, Docteur Penfield Ave., Montreal, QC, H3A 1B1, Canada

[2] Integrated Program of Neuroscience, Pine Ave. W., McGill University, Montreal, QC, H3A 1A1, Canada

[3] Alan Edwards Center for Research on Pain, McGill University, University St., Montreal, QC, H3A 2B4, Canada

*Correspondence: tomoko.ohyama@mcgill.ca

Keywords: escape behavior, nociceptive circuit, descending neuron, GABA, *Drosophila*

**Abstract**

Escape behaviors help animals avoid harm from predators and other threats in the environment. Successful escape relies on integrating information from multiple stimulus modalities (of external or internal origin) to compute trajectories toward safe locations, choose between actions that

satisfy competing motivations, and execute other strategies that ensure survival. To this end, escape behaviors must be adaptive. When a *Drosophila melanogaster* larva encounters a noxious stimulus, such as the focal pressure a parasitic wasp applies to the larval cuticle via its ovipositor, it initiates a characteristic escape response. The escape sequence consists of an initial abrupt bending, a corkscrew-like rolling, and finally rapid crawling. Previous work has shown that the detection of noxious stimuli primarily relies on class IV multi dendritic arborization neurons (Class IV neurons ) located beneath the body wall, and more recent studies have identified several important components in the nociceptive neural circuitry involved in rolling. However, the neural mechanisms that underlie the rolling-escape sequence remain unclear. Here we present both functional and anatomical evidence suggesting that bilateral descending neurons within the subesophageal zone of *D. melanogaster* larva play a crucial role in regulating the termination of rolling and subsequent transition to escape crawling. We demonstrate that these descending neurons (designated SeIN128) are inhibitory and receive inputs from a second-order interneuron upstream (Basin-2) and an ascending neuron downstream of Basin-2 (A00c). Together with optogenetic experiments showing that joint stimulation of SeIN128 neurons and Basin-2 influence the temporal dynamics of rolling, our findings collectively suggest that the ensemble of SeIN128, Basin-2, and A00c neurons forms a GABAergic feedback loop onto Basin-2, which inhibits rolling and thereby facilitates the shift to escape crawling.

## Introduction

Virtually all organisms on earth face the threat of being maimed or killed by one or more predatory organisms. Not surprisingly, when organisms encounter threat-associated stimuli, they exhibit a

wide variety of escape responses appropriate to their biological construction and the specific predators within their ecological niche (Burrell, 2017; Campagner et al., 2023; Chin & Tracey, 2017; Im & Galko, 2012; Peirs & Seal, 2016). Typically, these escape responses consist of a sequence of simple actions. The roundworm *C. elegans*, for example, in response to a touch to its head, exhibits rapid backward locomotion coupled with a suppression of head movements, followed by a deep ventral bend (omega turn) and a 180-degree reversal in the direction of locomotion. This sequence allows the roundworm to escape from nematophagal fungi that cohabitate with it in organic debris (Chalfie & Sulston, 1981; Chalfie et al., 1985).

When *Drosophila melanogaster* larvae encounter noxious stimuli, such as the stimulation that accompanies an attempt by a parasitic wasp to penetrate the larval cuticle with its ovipositor, they exhibit an escape response consisting of an initial abrupt bending, followed by corkscrew-like rolling, and finally, rapid crawling (Hwang et al., 2007; Ohyama et al., 2015; Onodera et al., 2017; Tracey et al., 2003). Previous work has shown that noxious stimuli are primarily detected by class IV dendritic arborization neurons (Class IV neurons) located beneath the body wall (Tracey et al., 2003). More recent studies have identified several important components in the downstream nociceptive neural circuitry, particularly those involved rolling (Burgos et al., 2018; Dason et al., 2020; Hu et al., 2017; Hu et al., 2020; Imambocus et al., 2022; Kaneko et al., 2017; Ohyama et al., 2015; Takagi et al., 2017; Yoshino et al., 2017). To date, however, the neural mechanisms that underlie the rolling-escape sequence, notably, the transition from rolling to crawling, have remained unclear.

In this study, we provide both functional and anatomical evidence that, bilateral descending neurons in the subesophageal zone (SEZ) of *D. melanogaster* larva, which comprise part of a neural circuit underlying rolling, a characteristic nocifensive escape response, potentially regulates

the termination of rolling and subsequent transition to escape crawling. We show that these descending neurons, which we designate as SeIN128, are identical to those denoted previously as SS04185 (Ohyama et al., 2015), are inhibitory neurons that receive inputs from Basin-2 (a second-order interneuron upstream) and A00c (an ascending neuron downstream of Basin-2), and provide GABAergic feedback onto Basin-2. Together with behavioral analyses of rolling during systematic optogenetic manipulation of SeIN128 and Basin-2 activity, our findings suggest that an ensemble of neurons—SeIN128, Basin-2, and A00c—forms an inhibitory feedback circuit that inhibits rolling, which in turn facilitates the shift to escape crawling.

**SS04185 facilitates rolling termination and shortens the latency of crawling behavior in the escape responses**

In a previous study, we showed that activation of all Basin neurons (Basin-1, -2, -3, and -4) induced rolling followed by fast crawling (Figure 1A) (Ohyama et al., 2015). Here, we first examined whether optogenetic activation of all four Basins expressing the red-shifted opsin CsChrimson (using Basin-1-4 Gal4, i.e., R72F11-Gal4) could elicit the same behavior. Upon activation of all Basins, we observed rolling mostly within the first 5 s, followed by crawling (Figure 1B (top panel), C and D). Crawling speed during the activation of all Basins following rolling was ~1.5 times that of the crawling speed at baseline (Figure 1D) (Ohyama et al., 2015).

To identify the neurons responsible for escape behavior (rolling and/or fast crawling), we conducted a behavioral screening of ~250 split Gal4 lines that were labeled in the central nervous system (CNS) when co-activated with all Basins. With respect to rolling, we found that activation of the split-Gal4 line, SS04185 (i.e., $w^{1118}$; *R54B01-Gal4*$^{AD}$; *R46E07-Gal4*$^{DBD}$), significantly

reduced the probability of rolling when compared to activating only the Basins however does not affect the crawling speed (Figure 1B–E, supplementary video 1-2).

The likelihood of rolling upon joint activation of SS04185 neurons and Basins might decrease because activation of SS04185 neurons trigger other actions, such as crawling, head casting, hunching, or stopping, and not because they solely inhibit rolling evoked by Basins. To investigate this possibility, we examined the effect of SS04185 activation in isolation and found that this did not induce any extra actions such as turning, hunching, or stopping (Figure 1–figure supplement 1A-D). These data suggest that joint activation of Basins and SS04185 neurons reduces rolling because SS04185 activation inhibits the Basin circuit.

Next, we explored how the quality of rolling changed during joint activation of SS04185 and Basin neurons. First, we examined the amount of time animals spent rolling during Basin activation. The average time spent rolling (percentage of the 30-s stimulation period) was 23.9% (7.2 s out of 30 s) following activation of Basins alone, whereas it was only 5.9% following joint activation of Basins with SS04185 (1.8 s out of 30 s) (Figure 1–figure supplement 1E). Additionally, the duration of each rolling bout was significantly shorter when SS04185 neurons were co-activated with Basins (Mann-Whitney U test, $p < 0.001$; Figure 1F).

The duration of a rolling bouts could decrease because of changes in the latency to initiate rolling, latency to terminate rolling, or both. To investigate how SS04185 activation affects these temporal parameters of rolling, we analyzed the latencies for the initiation and termination of the first rolling bout. Compared to activating Basins alone, co-activating the Basins and SS04185-expressing neurons only marginally increased latency to onset of the first rolling bout (Figure 1G), whereas it markedly reduced the latency for the termination of rolling (Mann-Whitney U test, $p < 0.001$;

Figure 1H). These data strongly suggest that SS04185-expressing neurons are involved in terminating rolling.

If the rolling module inhibits crawling, then premature termination of rolling might allow crawling to commence sooner than normal. Joint activation of SS04185 and Basins resulted in the initiation of the first crawling bout occurring earlier than when only Basins were activated (Mann Whitney U test, $p < 0.001$; Figure 1I, Figure 1–figure supplement 1F). The time from the end of rolling to the start of crawling remained similar between the groups in which the Basins were activated alone and in which the Basins and SS04185 were co-activated (Figure 1–figure supplement 1G). This is consistent with the higher probability of crawling during activation of SS04185 and Basin neurons (Figure 1–figure supplement 1H). Lastly, activation of SS04185 neurons in conjunction with Basins did not change the crawling speed compared to activation of Basins alone (Figure 1–figure supplement 1I). These results collectively indicate that SS04185 activation terminates rolling and facilitates the shift to fast crawling.

**A pair of descending neurons in SS04185 contributes to termination of rolling**

To identify the neurons that express SS04185 upon CsChrimson activation, we examined the localization of SS04185-labeled neurons. We found that SS04185 split-Gal4 strongly labeled a pair of descending neurons located within the subesophageal zone (SEZ) and mushroom body (MB) neurons within the brain (Figure 2A). To pinpoint which of these neurons are involved in reducing the probability of rolling (Figure 1B,C and E), we varied the level of SS04185 expression among the pair of SS04185-expressing descending neurons (SS04185-DN) and the SS04185-expressing MB (SS04185-MB) neurons (jointly with the Basins as in Figure 1). These manipulations allowed us to assess the resultant behavioral outcomes.

If SS04185-MB neurons are involved in the modulation of rolling, then reducing SS04185-MB expression should reduce the extent to which activation of both SS04185-DN neurons and SS04185-MB neurons decreases the probability of rolling. To test this conjecture, we expressed Killer Zipper ($KZip^{+}$), which interferes with the binding of $Gal4^{AD}$ and $Gal4^{DBD}$ in SS04185-MB neurons with MB LexA line (R13F02-LexA), consequently leading to a significant reduction in CsChrimson expression in SS04185-MB neurons (Figure 2B, Figure 2–figure supplement 1A) (Dolan et al., 2017; Vogt et al., 2016). When compared to $KZip^{+}$ controls, which do not express SS04185 (Figure 2C, black bars), however, activation of SS04185 neurons with reduced SS04185-MB expression (Figure 2C, red bars on the right; Figure 2–figure supplement 1B) still reduced rolling probability (as well as the total duration of rolling [Figure 2–figure supplement 1C]) to a level no different from that of $KZip^{-}$ controls expressing SS04185 fully in both SS04185-MB and SS04185-DN neurons (Figure 2C, dark red bars in the middle). Additionally, co-activation of MB Gal4 lines (MB247-Gal4) with Basins (without activation of SS04185-DN neurons) did not reduce the probability of rolling (Figure 2–figure supplement 1D-E) (Pauls et al., 2010). These data indicate that SS04185-DN neurons inhibit rolling.

To further test the role of SS04185-DN neurons, we investigated whether these neurons were involved in reducing the duration of each rolling bout (Figure 1A, D, F). However, knockdown of SS04185-MB neurons did not increase the duration of rolling bouts (Figure 2D). Furthermore, the earlier onset of crawling triggered by the activation of SS04185 neurons remained the same with knockdown of SS04185-MB neurons (Figure 2E). Collectively, these results strongly suggest that the behavioral effects on both rolling and crawling, as illustrated in figure 1, are primarily mediated by SS04185-DN neurons.

To further ascertain the role of SS04185-DN neurons in the regulation of rolling, we employed the heat shock FlpOut mosaic expression approach. This technique allowed for controlled and sporadic expression of CsChrimson in SS04185 neurons thorough random induction of Flippase by manipulating the timing and duration of heat shock (Golic and Lindquist, 1989; Nern et al., 2015). We compared larvae subjected to activation of both SS04185-MB and SS04185-DN neurons (red, Figure 2–figure supplement 1F) with those subjected only to activation of SS04185-MB neurons (black, Figure 2–figure supplement 1G), to assess the degree to which the former showed behavioral effects. Remarkably, activation of both SS04185-MB and SS04185-DN neurons resulted in a reduction in both the probability and duration of rolling when compared to activation of SS04185-MB neurons alone (Figure 2F and G, Figure 2–figure supplement 1H-I). Furthermore, activation of both SS04185-MB and SS04185-DN neurons reduced the latency to the end of the first rolling bout and the initiation of the first crawling bout (Figure 2H, Figure 2–figure supplement 1J). These findings provide compelling evidence that SS04185-DN neurons, but not SS04185-MB neurons, play an important role in the termination of rolling.

In addition, the off response of turning caused by SS04185 stimulation was recapitulated by SS04185-MB neurons activation alone (Figure 1B, Figure 2–figure supplement 1K). This indicates that this off response is independent of the rolling inhibition triggered by SS04185-DN and is not further explored here.

**Descending neurons identified by SS04185 correspond to SeIN128 neurons**

In a previous EM study, we identified a set of neurons designated as SeIN128, whose cell bodies in the SEZ send axonal projections throughout the thoracic and abdominal segments (Figure 3A) (Ohyama et al., 2015). Our immunostaining data also showed that the cell bodies of SS04185-DN

neurons are located in the SEZ, with axons bilaterally innervating the medial regions of the ventral nerve cord (VNC) from the thoracic to abdominal segments A8/9 (Figure 2A), suggesting that SS04185-DN and SeIN128 neurons are one and the same.

To verify this possibility, we examined the detailed anatomy of SS04185-DN neurons by immunostaining them with several markers and compared our immunostaining images with the corresponding images obtained via EM reconstruction of the entire CNS of a 1$^{st}$ instar *Drosophila* larva (Ohyama et al., 2015; Winding et al., 2023). We confirmed that the projections of SeIN128 neurons are distributed within the ventromedial neural tract (one of the six major neural tracts) in *Drosophila* larvae (Figure 3A, B, and C) in EM reconstruction data. We also confirmed that the cell bodies of SS04185-DN neurons were again located in the SEZ region, where the most anterior of the three neuropils in the thoracic region was marked by N-cadherin (Figure 3D). Viewed from the side (i.e., in the longitudinal or sagittal plane), both the cell bodies and axonal arbor were located ventrally (Figure 3D, far right). Immunostaining with Fasciclin2 (Fas2), which labels various neural tracts in the VNC (Grenningloh et al., 1991; Santos et al., 2007), showed colocalization of the axonal projections of SS04185-DN neurons and the Fas2-labeled ventromedial tract (Figure 3C and E). The similarity of the locations of their cell bodies and the distributions of their axonal processes suggests the identity of the SS04185-DN and SeIN128 neurons.

A previous EM study showed that SeIN128 neurons were located downstream of Basin neurons (Ohyama et al., 2015). To further confirm the identity of SS04185-DN and SeIN128 neurons, we compared the distributions of the axonal projections of SS04185-DN neurons in relation to those of several key neurons within the rolling circuit: the Basins, A00c neurons (a group of ascending neurons downstream of the Basins, and which facilitate rolling), and mdIV neurons (nociceptive

sensory neurons upstream of the Basins). Immunostaining revealed that Basin projections colocalize with those of SS04185-DN neurons in both the horizontal and transverse planes (Figure 3F, top and lower panels, respectively), with the horizontal view showing that SS04185-DN projections are distributed slightly medial to those of Basins within the ventromedial tract (Figure 3F, top panels), which resembles their colocalization pattern reported in EM (Figure 3B, C and G). Similarly, we compared the distributions of SS04185-DN projections with those of A00c or mdIV projections. We found that the projections of A00c colocalize with those of SS04185-DN in a similar fashion along the rostrocaudal axis within the ventromedial tract (Figure 3H and I), with A00c projections distributed more medially than SS04185-DN projections, consistent with the distribution patterns of SeIN128 projections and A00c projections in the EM reconstruction dataset (Figure 3B, H and I). In contrast, the distributions of mdIV projections did not colocalize with those of SS04185-DN projections, as the mdIV projections were displaced more laterally relative to the SS04185-DN projections in the horizontal and transverse planes (Figure 3J, top and lower panels, respectively), consistent with the distribution patterns of SeIN128 and mdIV projections in the EM reconstruction dataset (Figure 3K). In the transverse plane, the projections of SS04185-DN neurons were also distributed dorsomedial to those of mdIV (Figure 3J, lower panel), consistent with the corresponding distribution patterns in the EM reconstruction dataset (Figure 3B, C and K).

We conclude that the morphological findings for SS04185-DN neurons, together with data on the distribution of their axonal projections in relation to that of Basin, A00c, and mdIV neurons, strongly suggest the identity of SS04185-DN and SeIN128 neurons.

**Connectome and functional connectivity analyses: SeIN128 neurons receive inputs from Basin-2 and A00c**

A previous study that reconstructed larval neurons involved in the rolling circuit showed that Basin-2 and A00c neurons (in the VNC) make excitatory synaptic contacts onto SeIN128 neurons (in the CNS), which in turn make reciprocal inhibitory synaptic contacts onto Basin-2 and A00c neurons (Figure 4A, Figure 4–figure supplement 1A) (Ohyama et al., 2015). These data suggest that SeIN128 neurons are directly activated by Basin-2 and A00c (which also receives inputs from Basin-1, Basin-2, and Basin-4).

To assess the functional significance of these synaptic connections between SeIN128 neurons and Basins or A00c, we activated either Basins or A00c neurons and examined the resultant GCaMP signaling in SeIN128 neurons. Specifically, after expressing CsChrimson in Basins and A00c neurons and GCaMP in SeIN128 neurons, we used a two-photon microscope (920-nm laser) and monitored GCaMP signaling in SeIN128 neurons during illumination of a specimen with a 620-nm LED for 1 s (0.04–1.4 $\mu W/mm^2$), which activated either Basins or A00c neurons. GCaMP signals in SeIN128 neurons increased in an intensity-dependent manner when either Basins and A00c were activated (Figure 4B and C). Peak activity occurred at around 3 s after the onset of LED stimulation, which was similar to the results when Basins or A00c neurons were stimulated (Figure 4B and C). Finally, both Basin and A00c stimulation resulted in linear dose-dependent increases in SeIN128 firing (Figure 4–figure supplement 1B). These results are consistent with the notion that SeIN128 neurons are downstream of Basins or A00c neurons.

To compare the neural responses between Basins and SeIN128 or A00c neurons, we recorded neural activity in A00c neurons with GCaMP while stimulating Basin neurons in the same experimental setting. Although A00c neurons displayed a similar dose-dependent increase in peak

axonal firing as the intensity of optogenetic stimulation of Basin neurons increased, unlike SeIN128 neurons they showed no delay in peak firing activity (Figure 4D and E, Figure 4—figure supplement 1B), suggesting that A00c and SeIN128 neurons function differently in the rolling circuit.

We then investigated the anatomical locations of the synaptic outputs and inputs of SeIN128 neurons, and found that, whereas their outgoing projections primarily make synaptic contacts along the anterior-posterior nerve axis, the inputs coming from other neurons are mainly located in the SEZ (Figure 3A). These data suggest that the main synaptic inputs onto SeIN128 neurons in the SEZ mediate the slow responses upon activation of Basins or A00c neurons. On the other hand, SeIN128 neurons make axo-axonal contacts onto Basin-2 neurons (Figure 4–figure supplement 2A-G): that is, their axons make synaptic contacts with the dorsal and medial processes of Basin-2, which correspond to their axonal compartments (Figure 4–figure supplement 2E-G). These data suggest that the multiple synaptic inputs onto SeIN128 neurons mediate their neural responses. .

**SeIN128 neurons are GABAergic and inhibitory**

The results thus far indicate that activation of SeIN128 neurons inhibits rolling (Figure 1A–C) and that SeIN128 neurons provide inputs onto Basin-2 and A00c (Figure 4A). These findings suggest that SeIN128 neurons might be inhibitory. To test this possibility, we performed immunostaining experiments and found that SeIN128 neurons colocalized with glutamic acid decarboxylase (Gad)-positive neurons but not with acetylcholine- or glutamate-positive neurons, suggesting that SeIN128 neurons are GABAergic inhibitory neurons (Figure 5A, Figure 5–figure supplement 1A, and B).

We reasoned that if GABA in SeIN128 neurons is necessary for inhibiting rolling, then selectively knocking down GABA secretion in SeIN128 neurons should enhance rolling. When we expressed RNAi *HMS02355* in SeIN128 neurons to knock down vesicular GABA transporter (VGAT) expression and suppress the release of GABA, the population-level rolling probability increased from 23.6% to 45.2% (Figure 5B and C) (Kallman et al., 2015; Zhao et al., 2019). We confirmed *HMS02355* expression by immunostaining: pan neural *HMS02355* expression decreased the GABA and VGAT expression in the neuropil (Figure 5–figure supplement 1C, and D). Although the control (only Basins neurons expressed CsChrimson with RNAi HMS02355) showed lower probability of rolling probability (23.6%) comparing to similar genotype without RNAi HMS02355 such as Figure 2C or 2F. This indicate that RNAi HMS02355 background reduces the probability of rolling. Furthermore, the duration of each bout of rolling increased from 0.8 s to 1.4 s (Figure 5D). These data support the idea that SeIN128 neurons inhibit rolling via GABAergic transmission.

**Inhibition of SeIN128 increases probability and duration of rolling**

To further test whether the release of GABA upon activating SeIN128 neurons is necessary for inhibiting rolling, we expressed tetanus toxin (TNT) in SeIN128 neurons to block synaptic transmission. Silencing SeIN128 neurons via TNT while triggering rolling by optogenetically activating Basin neurons via *R72F11-LexA>LexAop-CsChrimson* significantly increased the probability of rolling compared to controls (Figure 6A and B). Silencing SeIN128 neurons via TNT extended the duration of each rolling bout, as well as the total rolling duration, in each larva (Figure 6C and D). We also examined the rolling-escape crawling sequence upon silencing

SeIN128 neurons, and found that the time to offset of rolling and the time onset of crawling were both delayed relative to controls (Figure 6E and F).

Given that TNT is expressed constitutively during development, long-term compensatory changes in the nervous system could have contributed to alterations in the parameters of rolling and crawling. To test whether similar results could be replicated with the use of a temporally specific intervention, we expressed *shibire*$^{ts1}$ (*shi*$^{ts1}$) in SeIN128 neurons to block synaptic transmission at temperatures above 30°C (van de Goor et al., 1995; Kitamoto, 2001). Silencing SeIN128 neurons via *shibire*$^{ts1}$ increased the probability of rolling from 60.4% to 79.7% (Figure 6–figure supplement 1A and B). The total duration of rolling per animal during stimulation increased from 10 to 12 s (Figure 6–figure supplement 1C). Although the duration of each rolling bout, the time to onset of the first rolling bout and time to onset of the first crawling bout did not differ from those of controls (Figure 6–figure supplement 1D, E and G), the time to offset of the first rolling bout delayed relative to controls ($p = 0.013$ for Figure 6–figure supplement 1F). Together with the results showing that activation of SeIN128 neurons inhibits rolling, these findings suggest that the activity of SeIN128 neurons is important in controlling the duration of rolling and the shift to crawling.

**Basins receive GABAergic inputs that inhibit rolling**

Given that Basins receive axo-axonal inputs from SeIN128 neurons and GABA signaling in SeIN128 neurons inhibits rolling, we next used RNA interference (RNAi) to test whether Basins receive GABAergic signals from SeIN128. We hypothesized that knockdown of GABA receptors in Basin neurons would increase the probability and duration of rolling at the population level. To knock down ionotropic GABA-A receptors (GABA-A-R) and G-protein-coupled GABA-B receptors (GABA-B-R1 and GABA-B-R2), we tested Basin neurons with GABA-A-R, GABA-B-

R1, and GABA-B-R2 RNAi lines (i.e., *HMC03643* for GABA-A-R, *HMC03388* for GABA-B-R1[1], *JF02989* for GABA-B-R1[2] and *HMC02975* for GABA-B-R2, respectively). For all RNAi lines, the rolling probability at the population level increased from 80% to 90% or even higher (Figure 7A), while the total rolling duration at the individual level increased for each larva throughout the stimulation window (Figure 7–figure supplement 1A). All GABA receptor knockdown groups showed significant increases in rolling duration across multiple bouts (Figure 7B); all groups except for GABA-B-R1[1] showed a reduced time to onset of the first rolling bout (Figure 7–figure supplement 1B); and only the GABA-B-R2 and GABA-A-R groups showed a delayed offset of the first rolling bout (Figure 7–figure supplement 1C). None of the groups differed from controls in the time to onset of the first crawling bout (Figure 7–figure supplement 1D). The greatest increase in the probability and duration of rolling was seen during knockdown of ionotropic GABA-A-R (*Rdl*), suggesting that Rdl contributes most to the inhibition of Basin neurons (Figure 7A and B).

To investigate whether SeIN128 neurons actually inhibit Basins, we recorded the activity of all Basins during activation of SeIN128 neurons. We compared GCaMP signaling in the Basins when they were co-activated with SeIN128 neurons (experimental treatment) or when they were activated alone (control treatment), with the intensity of optogenetic stimulation varied from 0.04 to 1.4 $\mu W/mm^2$. We found that Basins in the experimental group showed reductions in GCaMP signaling by 11% to 36% compared to those in the control group (Figure 7C, Figure 7–figure supplement 1E and F). The reductions were observed at all stimulation intensities when contrasting peak GCaMP responses, and statistically significant at intensities of 0.3 and 0.5 $\mu W/mm^2$ (Figure 7C, Figure 7–figure supplement 1E and F). Collectively, these data support the idea that SeIN128 neurons directly inhibit the activity of Basins via GABA.

**Effects of SeIN128 activation on rolling elicited by activating individual Basins**

In the studies above, we measured the activity of all Basins while manipulating the activity of SeIN128 neurons. Connectome and behavioral analyses indicate, however, that of the four types of Basins, only Basin-2 and Basin-4 receive nociceptive input from mdIV and trigger rolling (Ohyama et al., 2015). Moreover, as noted above, an examination of the larval connectome (Ohyama et al., 2015; Winding et al., 2023) revealed that Basin-2 both receives axo-axonal inputs from SeIN128 neurons and sends excitatory projections to the same SeIN128 neurons, whereas a similar examination revealed that Basin-4 neither receives inputs from, nor sends any outputs to, SeiN128 neurons. Therefore, we hypothesized that activation of SeIN128 neurons would inhibit rolling elicited by Basin-2 activation and modify the temporal parameters of rolling, but not affect rolling elicited by Basin-4 activation.

We first examined the pattern of rolling evoked by optogenetically activating Basin-2. Basin-2 activation induced multiple bouts of rolling throughout the stimulation window (Figure8–figure supplement 1A). Furthermore, the rolling elicited by Basin-2 activation tended to be sustained (Figure8–figure supplement 1A). Next, to determine how SeIN128 activation affects the pattern of rolling elicited by Basin-2 activation, we optogenetically activated SeIN128 neurons and Basin-2 simultaneously. As expected, compared to the probability of rolling in control animals in which only Basin-2 was activated, the probability of rolling in experimental animals in which Basin-2 and SeIN128 neurons were simultaneously activated was significantly lower (66.7% vs 24.4%; Figure 8A, Figure 8–figure supplement 1D). We also examined other parameters of rolling, including the time from the start (onset) of stimulation to the onset of the first rolling bout, termination (offset) of the first rolling bout, and onset of the first crawling bout, as well as the

duration of the rolling bout (i.e., the time from its onset to its offset). Consistent with the hypothesis that SeIN128 activation inhibits Basin-2 activity, the duration of the rolling bout significantly decreased (Figure 8B, Mann-Whitney test, $p = 0.0034$, *Cohen's d* = 0.351) and the time to onset of the first rolling bout significantly increased in experimental animals compared to controls (Figure 8–figure supplement 1E; Mann-Whitney test, $p < 0.001$). In addition, as expected, the time to offset of the first rolling bout (Figure 8C; Mann-Whitney test, $p = 0.0047$, *Cohen's d* = 0.607) and time to onset of the first crawling bout (Figure 8D; Mann-Whitney test, $p = 0.0074$, *Cohen's d* = 0.548) both significantly decreased in experimental animals compared to controls. Collectively, these findings suggest that Basin-2 neurons play a major role in mediating the effects of SeIN128 activation on rolling induced by optogenetic activation of all Basin neurons.

To ascertain our expectation that SeIN128 activation would have little if any effect on the pattern of rolling elicited by Basin-4 activation, given the absence of any identifiable synaptic contacts between Basin-4 neurons and SeIN128 neurons based on available information on the larval connectome, we also carried out the same analyses as those described above for rolling elicited by Basin-2 activation. We examined the pattern of rolling evoked by optogenetically activating Basin-4, and found that this manipulation induced rolling mostly within the first 5 s of stimulation (Figure 8–figure supplement 1B and F). Consequently, at the population level, rolling elicited by Basin-4 activation was transient compared to the rolling elicited by Basin-2 activation (compare Figure 8–figure supplement 1A vs 1B) (Figure 8–figure supplement 1C).

We then assessed whether SeIN128 activation would affect rolling elicited by Basin-4 activation. Surprisingly, compared to control animals, the probability of rolling in experimental animals was significantly lower (66.7% vs 26.8%; Figure 8E), much as was the case for rolling elicited by Basin-2 activation. We also examined the other rolling parameters, and found that the duration of

the rolling bouts (Figure 8F; Mann-Whitney test, $p = 0.032$, Cohen's $d = 0.248$), time to offset of the first rolling bout (Figure 8G; Mann-Whitney test, $p < 0.0047$, Cohen's $d = 0.427$), and time to onset of the first crawling bout (Figure 8H; Mann-Whitney test, $p < 0.001$, Cohen's $d = 1.039$) all significantly decreased in experimental animals compared to controls, although the effect sizes were smaller compared to those observed for rolling elicited by Basin-2 activation. The time to onset of the first rolling bout, however, did not significantly differ between experimental animals and controls (Figure 8–figure supplement 1G). These findings suggest the possibility that sites further downstream of Basin-4 neurons may be involved in inhibitory processes that affect rolling elicited by Basin-4 activation.

**Discussion**

In this study, we provide both anatomical and functional evidence that, bilateral descending neurons in the brain of *D. melanogaster* larva, which comprise part of a neural circuit underlying a characteristic rolling response that larvae exhibit when evading parasitization by wasps, potentially regulates the termination of rolling and the subsequent transition to escape crawling. We showed that these descending neurons, which we designated as SeIN128, were identical to those previously identified as a component of the nociceptive circuit; were inhibitory neurons that receive excitatory inputs from Basin-2, a second-order interneuron upstream, and A00c, an ascending neuron downstream of Basin-2; and provided GABAergic feedback onto Basin-2, presumably via the axo-axonal synaptic contacts made by the axon terminal endings of SeIN128 neurons onto the axons of Basin-2. Optogenetic activation studies further showed that joint stimulation of SeIN128 and Basin-2 neurons systematically altered the temporal dynamics of rolling and subsequent escape crawling. Collectively, the evidence suggests that the ensemble of

SeIN128, Basin-2, and A00c neurons constitutes a novel inhibitory feedback circuit that provides reduces Basin-2 activity, which in turn, here influence the activity of a key interneuron of the rolling circuit via a novel inhibitory mechanism.

**Feedback inhibition in a nociceptive circuit**

Feedback inhibition occurs when an excitatory neuron sends projections to an inhibitory neuron, which in turn sends projections back onto the same excitatory neuron, often at its presynaptic terminals (Isaacson & Scanziani, 2011; Kapfer et al., 2007; Ray et al., 2020; Stokes & Isaacson, 2010; Yoshimura & Callaway, 2005). The hallmark of feedback inhibition lies in its ability to modulate the duration and magnitude of incoming excitatory signals, thereby fine-tuning neural responses and maintaining homeostasis (Kapfer et al., 2007; Papadopoulou et al., 2011; Stokes & Isaacson, 2010; Yoshimura & Callaway, 2005). Compared to the fast temporal dynamics of feedforward inhibition, in which an inhibitory neuron directly inhibits an excitatory neuron downstream of it, the temporal dynamics of feedback inhibition are slower, primarily due to the added synaptic delays (two or more) following activation of an excitatory neuron (Papadopoulou et al., 2011; Ray et al., 2020; Stokes & Isaacson, 2010). The slow temporal dynamics serve to inhibit the sustained neural activity and magnitude of incoming excitatory signals (Papadopoulou et al., 2011; Ray et al., 2020; Stokes & Isaacson, 2010).

In this study, we showed that SeIN128 neurons are descending neurons whose main inputs arrive in the brain and SEZ regions, and whose outputs target the VNC. We also found that SeIN128 neurons receive excitatory inputs from Basin-2 as well as its downstream neuron A00c, and in turn send inhibitory projections back to these neurons in the VNC, potentially establishing a feedback inhibition motif that modulates the nociceptive rolling circuit. The interplay we observed among SeIN128 neurons, Basin-2, and A00c are consistent with this view. Our findings revealed that

activation of SeIN128 neurons has a suppressive effect on Basin-2 activity and, notably, on the duration of rolling. These observations support the idea that feedback inhibition is critical in regulating the temporal aspects of nociceptive responses.

**Inhibition of Basin-2 by SeIN128 neurons is mediated by axo-axonal synapses**

Neurons form a wide variety of neural networks that perform various computations in the brain. Typically, a neuron receives inputs via axo-dendritic synapses (i.e., contacts made by the axon terminals of an upstream neuron with its dendrites), which play a role in the spatial and temporal computations that lead to the firing of action potentials. Less commonly, the axon terminals of an upstream neuron may contact the soma (i.e., via axo-somatic synapses) or axon (i.e., via axo-axonal synapses) of a downstream neuron (Palay, 1956; Pinault et al., 1997; Zheng et al., 2018). Axo-axonal synapses have a subtle effect on neurotransmission at the network level because the activity in presynaptic neurons does not alter the membrane potential (Cattaert & El Manira, 1999; Guo & Hu, 2014; McGann, 2013). Axo-axonal synapses mainly affect the release probability of neurotransmitter vesicles in response to an action potential triggered in the postsynaptic neuron (McGann, 2013; Oleson et al., 2012).

Recent studies suggest that the activity of axo-axonal synapses can prevent the transmission of action potentials. For example, it has been reported that, neurotransmission mediated by type-B muscarinic receptors at lateral axo-axonal connections between *Drosophila* Kenyon Cells is critical for stimulus specificity learning in *Drosophila* (Manoim et al., 2022); inhibitory axo-axonal connections between Chandelier cells and CA1 pyramidal cells are important for activity-dependent plasticity (Pan-Vazquez et al., 2020; Schneider-Mizell et al., 2021); and GABAergic axo-axonal interneurons in the amygdala are crucial for generating action potentials in the principal output cells (Veres et al., 2023). Furthermore, EM connectome analyses of the entire larval brain

reveal that ~70% of all synapses in *Drosophila* larvae are axo-dendritic whereas ~30% are axo-axonal, suggesting that the latter may have considerable influence over network function (Winding et al., 2023).

In this study, we found a feedback connection between SeIN128 and Basin-2 mediated by axon-axonal synapses (Figure4 – supplementary 2E-G). The slow increase of SeIN128 activity in response to Basin-2 or A00c activation could potentially occur because of these axo-axonal connections. This delayed activity may play an important role in the feedback inhibition of Basin-2 activity, and in turn, the termination of rolling.

**Roles of Basin-2 and Basin-4 in escape behavior**

Previous studies have shown that, Basin-2 and Basin-4 receive both chordotonal sensory and nociceptive sensory inputs, and in addition, play a critical role in escape behavior (Ohyama et al., 2015). Here we investigated the differences between rolling induced by activation of Basin-2 or Basin-4. We found that activation of Basin-2 induced rolling that was sustained. Furthermore, activation of SeIN128 neurons reduced the duration of rolling induced by joint activation of Basin-2, which resulted in a delay in the onset of rolling and an earlier termination of rolling. These data indicate that activation of Basin-2 serves to maintain rolling. Connectome data indicate that SeIN128 neurons provide inhibitory input onto Basin-2, which is consistent with the finding that SeIN128 activation reduces the duration of rolling.

On the other hand, activation of Basin-4 induced rolling that was transient, which was then followed by rapid crawling. Furthermore, activation of SeIN128 neurons reduced the probability of rolling but did not affect the duration of rolling (Figure 8F). This suggests that activation of Basin-4 is important for the induction of rolling, but not its maintenance. The behavioral effects of coactivating SeIN128 and Basin-4, together with connectome data indicating the lack of any

connections between SeIN128 neurons and Basin-4, suggest that these descending neurons target neurons downstream of Basin-4 neurons.

**Other inputs onto SeIN128 neurons modify escape behavior**

The dendritic regions of SeIN128 neurons are located in the SEZ and brain, suggesting that SeIN128 neurons receive other inputs from SEZ and brain neurons. In this study, we did not examine these inputs. Connectome data indicate that MB output neurons project onto SeIN128 neurons (Ohyama et al., 2015). Given the well-established role of MB neurons in learning, this finding suggests that SeIN128 neurons could play a role in experience-dependent modulation of rolling. Two recent studies have shown that descending neurons inhibit nociceptive neurons (Nakamizo-Dojo et al., 2023; Oikawa et al., 2023). Specifically, one study showed that insulin signaling modulates escape behavior by activating GABAergic descending neurons that inhibit nociceptive sensory neurons (Nakamizo-Dojo et al., 2023), whereas the other demonstrated an inhibitory mechanism mediated by the neuropeptide Drosulfakinin, a homologue of cholecystokinin in mammals (Oikawa et al., 2023). Whether SeIN128 neurons are also influenced by insulin signaling or Drusulfakinin, however, remains to be seen.

In summary, our study delineates a neuronal ensemble consisting of a set of descending inhibitory neurons, a first-order interneuron (Basin-2), and an ascending neuron (A00c) in fruit fly larvae, which functions as an inhibitory feedback circuit that regulates the probability and duration of rolling, and thereby facilitates the transition from rolling to crawling. This work represents another example of how detailed analyses of connectomes and functional analyses of neural and behavioral activity can identify mechanistic explanations of behavioral phenomena at the level of neural circuits—in this case, how neuronal ensembles generate behavioral sequences.

## Materials and Methods:

## Key resources table

| Reagent or resource | Source or reference | Identifiers |
|---|---|---|
| **Antibodies** | | |
| Mouse anti-Brp monoclonal antibody, clone nc82 | Developmental Studies Hybridoma Bank | Cat# nc82, RRID:AB_2314866 |
| Mouse 1D4 anti-fasciclin II antibody | Developmental Studies Hybridoma Bank | Cat# 1D4 anti-Fasciclin II, RRID:AB_528235 |
| Rat anti-cadherin, DN- (extracellular domain) antibody | Developmental Studies Hybridoma Bank | Cat# DN-Ex #8, RRID:AB_528121 |
| Chicken anti-GFP antibody | Abcam | Cat# ab13970, RRID:AB_300798 |
| Rabbit anti-GFP polyclonal antibody, unconjugated | Thermo Fisher Scientific | Cat# A-6455, RRID:AB_221570 |
| Rabbit anti-DsRed polyclonal antibody | Takara Bio | Cat# 632496, RRID:AB_10013483 |
| Mouse anti-Drosophila choline acetyltransferase monoclonal antibody, unconjugated | Developmental Studies Hybridoma Bank | Cat# chat4b1, RRID:AB_528122 |
| Rabbit anti-GABA antibody | Millipore Sigma | Cat # A2052 |
| Rabbit anti-GLUT1 antibody | Gift from Aberbe lab | |
| Rabbit anti-VGAT antibody | Gift from Krantz lab | |
| Goat anti-chicken IgY (H+L) secondary antibody, Alexa Fluor™ 488 | Thermo Fisher Scientific | Cat# A-11039, RRID:AB_2534096 |
| Goat anti-rabbit IgG (H+L) highly cross-adsorbed secondary antibody, Alexa Fluor™ 488 | Thermo Fisher Scientific | Cat# A-11034, RRID:AB_ 2576217 |
| Goat anti-rabbit IgG (H+L) cross-adsorbed secondary antibody, Alexa Fluor™ 568 | Thermo Fisher Scientific | Cat# A-11011, RRID:AB_143157 |
| Goat anti-mouse IgG (H+L) cross-adsorbed secondary antibody, Alexa Fluor™ 568 | Thermo Fisher Scientific | Cat# A-11004, RRID:AB_2534072 |
| Goat anti-rat IgG (H+L) Alexa Fluor™ 568 | Thermo Fisher Scientific | Cat# A-11077, RRID:AB_2534121 |
| Goat anti-rat IgG (H+L) Alexa Fluor™ 647 | Thermo Fisher Scientific | Cat# A-21247, RRID:AB_141778 |
| **Chemicals** | | |
| PBS, Phosphate Buffered Saline, 10x solution | Fisher Scientific | Cat# BP399-1 |
| Triton X-100 | Millipore Sigma | Cat# X100-100ML |
| Paraformaldehyde 20% aqueous solution | Electron Microscopy Sciences | Cat# 15713 |
| Normal goat serum | Gibco | PCN5000 |
| VECTASHIELD antifade mounting medium | Vector Laboratories | Cat# H-1000-10 |
| Drosophila Agar | Diamed | Cat# GEN66-103 |
| All Trans Retinal | Toronto Research Chemicals Inc. | Cat# R24000 |
| Poly-L-lysine | Sigma-Aldrich | Cat# P1524 |
| **Fly strains** | | |
| R72F11-Gal4 (attp2) | Bloomington Drosophila Stock Center | RRID: BDRC_39786 |
| R71A10-Gal4 (attp2) | Bloomington Drosophila Stock Center | RRID: BDRC_39562 |
| w; R54B01-Gal4$^{AD}$;R46E07-Gal4$^{DBD}$ (SS04185) | Gift from Zlatic lab | N/A |
| w; R72F11-Gal4$^{AD}$;R38H09-Gal4$^{DBD}$ (SS00739) | Gift from Zlatic lab | N/A |

| | | |
|---|---|---|
| w; R72F11-Gal4$^{AD}$;R57F07-Gal4$^{DBD}$ (SS00740) | Gift from Zlatic lab | N/A |
| MB247-Gal4, mef2-Gal4 | Bloomington Drosophila Stock Center | RRID: BDRC_50742 |
| R13F02-LexA (attp40) | Bloomington Drosophila Stock Center | RRID: BDRC_52460 |
| R72F11-LexA (attp40) | Bloomington Drosophila Stock Center | RRID: BDRC_94661 |
| R71A10-LexA (attp40) | Gift from Zlatic lab | N/A |
| Mi{Trojan-LexA-QFAD.2}Gad1 | Bloomington Drosophila Stock Center | RRID: BDRC_60324 |
| 20xUAS-IVS-CsChrimson::mVenus (attp2) | Bloomington Drosophila Stock Center | RRID: BDRC_55134 |
| 20xUAS-IVS-CsChrimson::mVenus (attP18) | Bloomington Drosophila Stock Center | RRID: BDRC_55136 |
| 20xUAS-IVS-CsChrimson::mVenus (attP18);;R72F11-Gal4 (attp2) | Bloomington Drosophila Stock Center | RRID: BDRC_79599 |
| 13xLexAop2-IVS-CsChrimson::mVenus (attP18) | Bloomington Drosophila Stock Center | RRID: BDRC_55137 |
| 13xLexAop2-IVS-CsChrimson::tdTomato (attP18) | Gift from Rubin lab | N/A |
| 13xLexAop2-IVS-CsChrimson::tdTomato (vk000005) | Bloomington Drosophila Stock Center | RRID: BDRC_82183 |
| 20xUAS(FRT.stop)CsChrimson.mVenus(attP18), pBPhsFlp2::Pest (AttP3) | Gift from Rubin lab | N/A |
| hs(KDRT.stop)FLP (attP18) | Bloomington Drosophila Stock Center | RRID: BDRC_67091 |
| 20xUAS(FRT.stop)-CsChrimson::mVenus | Gift from Rubin lab | N/A |
| UAS-TeTxLC.tnt | Bloomington Drosophila Stock Center | RRID: BDRC_28838 |
| 20xUAS-TTS-Shibire$^{ts1}$-p10(vk00005) | Bloomington Drosophila Stock Center | PRID: BDRC_66600 |
| 10xUAS-IVS-myr::GFP (attP18) | Gift from Rubin lab | N/A |
| 13xLexAop-dsRed (attP2) | Gift from Rubin lab | N/A |
| 20xUAS-IVS-GCaMP6s (vk00005) | Bloomington Drosophila Stock Center | RRID: BDRC_4279 |
| 20xLexAop-IVS-Syn21-GCaMP6s (su(HW)attP8) | Gift from Rubin lab | N/A |
| 20xUAS-Syn21-opGCaMP6s (su(Hw)attP8) | Gift from Rubin lab | N/A |
| 10xUAS-Syn21-CsChrimson88::tdTomato(attP18) | Gift from Rubin lab | N/A |
| HMS02355 | Bloomington Drosophila Stock Center | RRID: BDRC_41958 |
| HMC03388 | Bloomington Drosophila Stock Center | RRID: BDRC_51817 |
| JF02989 | Bloomington Drosophila Stock Center | RRID: BDRC_28353 |
| HMC02975 | Bloomington Drosophila Stock Center | RRID: BDRC_50608 |
| HMC03643 | Bloomington Drosophila Stock Center | RRID: BDRC_52903 |
| **Software and algorithms** | | |
| FIJI | https://fiji.sc/ | RRID: SCR_002285 |
| MATLAB | MathWorks | RRID: SCR_001622 |
| CATMAID | https://catmaid.readthedocs.org/ | RRID: SCR_006278 |
| Multi Worm Tracker | http://sourceforge.net/projects/mwt | N/A |

| | | |
|---|---|---|
| ZEN | Carl Zeiss Microscopy | Version 2.1 (blue edition) |
| Affinity Designer | Affinity | Version 1.10.5 |
| ScanImage | MBF Bioscience | N/A |

## Fly stocks and maintenance

All *D. melanogaster* stock lines used in this study were raised on Bloomington Drosophila Stock Center cornmeal food. Flies were maintained in a humidity- and temperature-controlled chamber kept at 18°C or 25°C, 40% humidity, and set to a 12-hour light/dark cycle. All crosses for experiments were reared at 25°C and 40% humidity.

## Fly genotypes used in experiments

### -Main figures

| Fig. | Panel | Labels | Genotypes |
|---|---|---|---|
| 1 | B | Basins>Chrimson | *20xUAS-IVS-CsChrimson::mVenus/+;+; R72F11-Gal4/+* |
| 1 | B | Basins + SS04185>Chrimson | *20xUAS-IVS-CsChrimson::mVenus/+; R54B01-Gal4.AD/+; R46E07-Gal4.DBD/ R72F11-Gal4* |
| 1 | C-D, F | control | *20xUAS-IVS-CsChrimson::mVenus/+; +; R72F11-Gal4/+* |
| 1 | C-D, F | SS04185 | *20xUAS-IVS-CsChrimson::mVenus/+; R54B01-Gal4.AD/+; R46E07-Gal4.DBD/R72F11-Gal4* |
| 1 | E | ctrl / attp2>Chrimson | *20xUAS-IVS-CsChrimson::mVenus/+;;* |
| 1 | E | SS04185 / attp2>Chrimson | *20xUAS-IVS-CsChrimson::mVenus/+; R54B01-Gal4.AD/+; R46E07-Gal4.DBD/+* |
| 1 | E | ctrl / Basins>Chrimson | *20xUAS-IVS-CsChrimson::mVenus/+; +; R72F11-Gal4/+* |
| 1 | E | SS04185 / Basins>Chrimson | *20xUAS-IVS-CsChrimson::mVenus/+; R54B01-Gal4.AD/+; R46E07-Gal4.DBD/R72F11-Gal4* |
| 1 | G-I | ctrl | *20xUAS-IVS-CsChrimson::mVenus/+; +; R72F11-Gal4/+* |
| 1 | G-I | SS04185 | *20xUAS-IVS-CsChrimson::mVenus/+; R54B01-Gal4.AD/+; R46E07-Gal4.DBD/R72F11-Gal4* |
| 2 | A | | *10xUAS-IVS-myr::GFP/+; R54B01-Gal4.AD/+; R46E07-Gal4.DBD/+* |
| 2 | B | control | *20xUAS-IVS-CsChrimson::mVenus/+; R54B01-Gal4.AD/+; R46E07-Gal4.DBD/R72F11-Gal4* |
| 2 | B | MB>KZip+ | *20xUAS-IVS-CsChrimson::mVenus/+; R13F02-LexA,LexAop-KZip$^{+}$/R54B01-Gal4.AD; R72F11-Gal4/R46E07-Gal4.DBD* |
| 2 | C, E | MB>KZip+ / ctrl | *20xUAS-IVS-CsChrimson::mVenus/+; R13F02-LexA,LexAop-KZip$^{+}$/+; R72F11-Gal4/+* |
| 2 | C, E | - / SS04185 | *20xUAS-IVS-CsChrimson::mVenus/+; R54B01-Gal4.AD/+; R46E07-Gal4.DBD/R72F11-Gal4* |
| 2 | C, E | MB>KZip+ / SS04185 | *20xUAS-IVS-CsChrimson::mVenus/+; R13F02-LexA,LexAop-KZip$^{+}$/R54B01-Gal4.AD; R72F11-Gal4/R46E07-Gal4.DBD* |

| | | | |
|---|---|---|---|
| 2 | D | MB>KZip+ | *20xUAS-IVS-CsChrimson::mVenus/+; R13F02-LexA,LexAop-KZip$^{+}$/+; R72F11-Gal4/+* |
| 2 | D | SS04185 | *20xUAS-IVS-CsChrimson::mVenus/+; R54B01-Gal4.AD/+; R46E07-Gal4.DBD/R72F11-Gal4* |
| 2 | D | MB>KZip+, SS04185 | *20xUAS-IVS-CsChrimson::mVenus/+; R13F02-LexA,LexAop-KZip$^{+}$/R54B01-Gal4.AD; R72F11-Gal4/R46E07-Gal4.DBD* |
| 2 | F, H | ctrl | *w+, hs(KDRT.stop)FLP/13xLexAop2-IVS-CsChrimson::tdTomato; R54B01-Gal4.AD/72F11-LexA;20xUAS-(FRT.stop)-CsChrimson::mVenus/R46E07-Gal4.DBD* |
| 2 | F, H | SS04185-DN | *w+, hs(KDRT.stop)FLP/13xLexAop2-IVS-CsChrimson::tdTomato; R54B01-Gal4.AD/72F11-LexA;20xUAS-(FRT.stop)-CsChrimson::mVenus/R46E07-Gal4.DBD* |
| 2 | G | control | *w+, hs(KDRT.stop)FLP/13xLexAop2-IVS-CsChrimson::tdTomato; R54B01-Gal4.AD/72F11-LexA;20xUAS-(FRT.stop)-CsChrimson::mVenus/R46E07-Gal4.DBD* |
| 2 | G | SS04185-DN | *w+, hs(KDRT.stop)FLP/13xLexAop2-IVS-CsChrimson::tdTomato; R54B01-Gal4.AD/72F11-LexA;20xUAS-(FRT.stop)-CsChrimson::mVenus/R46E07-Gal4.DBD* |
| 3 | D, E | | *10xUAS-IVS-myr::GFP/+; R54B01-Gal4.AD/+; R46E07-Gal4.DBD/+* |
| 3 | F | | *w; R54B01-Gal4.AD/R72F11-LexA; R46E07-Gal4.DBD/13xLexAop2-IVS-CsChrimson::tdTomata, 20xUAS-IVS-GCaMP6s* |
| 3 | H | | *w; R54B01-Gal4.AD/R71A10-LexA; R46E07-Gal4.DBD/13xLexAop2-IVS-CsChrimson::tdTomata, 20xUAS-IVS-GCaMP6s* |
| 3 | J | | *w; R54B01-Gal4.AD/ppk1.9-LexA; R46E07-Gal4.DBD/13xLexAop2-IVS-CsChrimson::tdTomata, 20xUAS-IVS-GCaMP6s* |
| 4 | B | | *w; R72F11-LexA/R54B01-Gal4.AD; 13xLexAop-CsChrimson, 20xUAS-IVS-UAS-GCaMP6s/R46E07-Gal4.DBD* |
| 4 | C | | *w; R71A10-LexA/R54B01-Gal4.AD; 13xLexAop-CsChrimson, 20xUAS-IVS-UAS-GCaMP6s/R46E07-Gal4.DBD* |
| 4 | D | | *w; R72F11-LexA/+; 13xLexAop2-IVS -CsChrimson::tdTomato, 20xUAS-IVS-UAS-GCaMP6s/R71A10-Gal4* |
| 4 | E | A00c | *w; R72F11-LexA/+; 13xLexAop2-IVS -CsChrimson::tdTomato, 20xUAS-IVS-UAS-GCaMP6s/R71A10-Gal4* |
| 4 | E | SS04185 | *w; R72F11-LexA/R54B01-Gal4.AD; 13xLexAop2-IVS -CsChrimson::tdTomato, 20xUAS-IVS-UAS-GCaMP6s/R46E07-Gal4.DBD* |
| 5 | A | | *10xUAS-myr::GFP; R54B01-Gal4.AD/13x-LexAop-dsRed; R46E07-Gal4.DBD/ Mi{Trojan-LexA-QFAD.2}Gad1* |
| 5 | B, D | control | *13xLexAop2-IVS-CsChrimson::mVenus;R72F11-lexA/+; HMS02355/+* |
| 5 | B, D | SS04185 | *13xLexAop2-IVS-CsChrimson::mVenus; R72F11-lexA/R54B01-Gal4.AD; HMS02355/R46E07-Gal4.DBD* |
| 5 | C | ctrl | *13xLexAop2-IVS-CsChrimson::mVenus;R72F11-lexA/+; HMS02355/+* |
| 5 | C | SS04185 | *13xLexAop2-IVS-CsChrimson::mVenus; R72F11-lexA/R54B01-Gal4.AD; HMS02355/R46E07-Gal4.DBD* |
| 6 | A | control>TNT | *13xLexAop2-IVS-CsChrimson::mVenus; R72F11-LexA/+; UAS-TeTxLC.tnt /+* |
| 6 | A | SS04185>TNT | *13xLexAop2-IVS-CsChrimson::mVenus; R72F11-LexA/R54B01-Gal4.AD; UAS-TeTxLC.tnt/R46E07-Gal4.DBD* |
| 6 | B, D-F | ctrl | *13xLexAop2-IVS-CsChrimson::mVenus; R72F11-LexA/+; UAS-TeTxLC.tnt /+* |
| 6 | B, D-F | SS04185 | *13xLexAop2-IVS-CsChrimson::mVenus; R72F11-LexA/R54B01-Gal4.AD; UAS-TeTxLC.tnt/R46E07-Gal4.DBD* |

| | | | |
|---|---|---|---|
| 6 | C | control | *13xLexAop2-IVS-CsChrimson::mVenus; R72F11-LexA/+; UAS-TeTxLC.tnt /+* |
| 6 | C | SS04185 | *13xLexAop2-IVS-CsChrimson::mVenus; R72F11-LexA/R54B01-Gal4.AD; UAS-TeTxLC.tnt/R46E07-Gal4.DBD* |
| 7 | A, B | control | *20xUAS-IVS-CsChrimson::mVenus/+; ; R72F11-Gal4/+* |
| 7 | A, B | GABA-B-R1[1] | *20xUAS-IVS-CsChrimson::mVenus/+; ; R72F11-Gal4/UAS-HMC03388* |
| 7 | A, B | GABA-B-R1[2] | *20xUAS-IVS-CsChrimson::mVenus/+; ; R72F11-Gal4/UAS-JF02989* |
| 7 | A, B | GABA-B-R2 | *20xUAS-IVS-CsChrimson::mVenus/+; ; R72F11-Gal4/UAS-HMC02975* |
| 7 | A, B | GABA-A-R | *20xUAS-IVS-CsChrimson::mVenus/+; ; R72F11-Gal4/UAS-HMC03643* |
| 7 | C | control | *20xUAS-Syn21-opGCaMP6s,10XUAS-Syn21-CsChrimson88::tdTomato/+;CyO/+;TM6/R72F11-Gal4* |
| 7 | C | SS04185 | *20xUAS-Syn21-opGCaMP6s,10XUAS-Syn21-CsChrimson88::tdTomato/+;CyO/R54B01-Gal4.AD;R72F11-Gal4/R46E07-Gal4.DBD* |
| 8 | A, C-D | ctrl | *20xUAS-IVS-CsChrimson::mVenus/+; R72F11-Gal4.AD/+; R38H09-Gal4.DBD/+* |
| 8 | A, C-D | SS04185 | *20xUAS-IVS-CsChrimson::mVenus/+; R72F11-Gal4.AD/R54B01-Gal4.AD; R38H09-Gal4.DBD/R46E07-Gal4.DBD* |
| 8 | B | control | *20xUAS-IVS-CsChrimson::mVenus/+; R72F11-Gal4.AD/+; R38H09-Gal4.DBD/+* |
| 8 | B | SS04185 | *20xUAS-IVS-CsChrimson::mVenus/+; R72F11-Gal4.AD/R54B01-Gal4.AD; R38H09-Gal4.DBD/R46E07-Gal4.DBD* |
| 8 | E, G-H | ctrl | *20xUAS-IVS-CsChrimson::mVenus/+; R72F11-Gal4.AD/+; R57F07-Gal4.DBD/+* |
| 8 | E, G-H | SS04185 | *20xUAS-IVS-CsChrimson::mVenus/+; R72F11-Gal4.AD/R54B01-Gal4.AD; R57F07-Gal4.DBD/R46E07-Gal4.DBD* |
| 8 | F | control | *20xUAS-IVS-CsChrimson::mVenus/+; R72F11-Gal4.AD/+; R57F07-Gal4.DBD/+* |
| 8 | F | SS04185 | *20xUAS-IVS-CsChrimson::mVenus/+; R72F11-Gal4.AD/R54B01-Gal4.AD; R57F07-Gal4.DBD/R46E07-Gal4.DBD* |

## -Supplementary figures

| Fig. | Panel | Labels | Genotypes |
|---|---|---|---|
| 1-1 | A-D | ctrl | *20xUAS-IVS-CsChrimson::mVenus/+;;* |
| 1-1 | A-D | SS04185 | *20xUAS-IVS-CsChrimson::mVenus/+; R54B01-Gal4.AD/+; R46E07-Gal4.DBD/+* |
| 1-1 | E, G-H | ctrl | *20xUAS-IVS-CsChrimson::mVenus/+; +; R72F11-Gal4/+* |
| 1-1 | E, G-H | SS04185 | *20xUAS-IVS-CsChrimson::mVenus/+; R54B01-Gal4.AD/+; R46E07-Gal4.DBD/R72F11-Gal4* |
| 1-1 | F | control | *20xUAS-IVS-CsChrimson::mVenus/+; +; R72F11-Gal4/+* |
| 1-1 | F | SS04185 | *20xUAS-IVS-CsChrimson::mVenus/+; R54B01-Gal4.AD/+; R46E07-Gal4.DBD/R72F11-Gal4* |
| 1-1 | I | ctrl / attp2>Chrimson | *20xUAS-IVS-CsChrimson::mVenus/+;;* |
| 1-1 | I | SS04185 / attp2>Chrimson | *20xUAS-IVS-CsChrimson::mVenus/+; R54B01-Gal4.AD/+; R46E07-Gal4.DBD/+* |
| 1-1 | I | ctrl / Basins>Chrimson | *20xUAS-IVS-CsChrimson::mVenus/+; +; R72F11-Gal4/+* |
| 1-1 | I | SS04185 / Basins>Chrimson | *20xUAS-IVS-CsChrimson::mVenus/+; R54B01-Gal4.AD/+; R46E07-Gal4.DBD/R72F11-Gal4* |
| 1-2 | A-C | control | *20xUAS-IVS-CsChrimson::mVenus/+;; R72F11-Gal4/+* |

| | | | |
|---|---|---|---|
| 1-2 | A-C | 54B01-AD | *20xUAS-IVS-CsChrimson::mVenus/+; R54B01-Gal4.AD/+; R72F11-Gal4/+* |
| 1-2 | A-C | 46E07-DBD | *20xUAS-IVS-CsChrimson::mVenus/+; +; R72F11-Gal4/ R46E07-Gal4.DBD* |
| 1-2 | A-C | SS04185 | *20xUAS-IVS-CsChrimson::mVenus/+; R54B01-Gal4.AD/+; R46E07-Gal4.DBD/R72F11-Gal4* |
| 2 | A | | *20xUAS-IVS-CsChrimson::mVenus/+; R13F02-LexA,LexAop-KZip$^{+}$/R54B01-Gal4.AD; R72F11-Gal4/R46E07-Gal4.DBD* |
| 2 | B | MB>Kzip+ | *20xUAS-IVS-CsChrimson::mVenus/+; R13F02-LexA,LexAop-Kzip$^{+}$/+; R72F11-Gal4/+* |
| 2 | B | SS04185 | *20xUAS-IVS-CsChrimson::mVenus/+; R54B01-Gal4.AD/+; R46E07-Gal4.DBD/R72F11-Gal4* |
| 2 | B | MB>Kzip+, SS04185 | *20xUAS-IVS-CsChrimson::mVenus/+; R13F02-LexA,LexAop-Kzip$^{+}$/R54B01-Gal4.AD; R72F11-Gal4/R46E07-Gal4.DBD* |
| 2 | C | MB>Kzip+ / ctrl | *20xUAS-IVS-CsChrimson::mVenus/+; R13F02-LexA,LexAop-Kzip$^{+}$/+; R72F11-Gal4/+* |
| 2 | C | - / SS04185 | *20xUAS-IVS-CsChrimson::mVenus/+; R54B01-Gal4.AD/+; R46E07-Gal4.DBD/R72F11-Gal4* |
| 2 | C | MB>Kzip+ / SS04185 | *20xUAS-IVS-CsChrimson::mVenus/+; R13F02-LexA,LexAop-Kzip$^{+}$/R54B01-Gal4.AD; R72F11-Gal4/R46E07-Gal4.DBD* |
| 2 | D | control | *20xUAS-IVS-CsChrimson::mVenus/+; +; R72F11-Gal4/+* |
| 2 | D | MB247 | *20xUAS-IVS-CsChrimson::mVenus/+; R54B01-Gal4.AD/+; R46E07-Gal4.DBD/R72F11-Gal4* |
| 2 | E | ctrl | *20xUAS-IVS-CsChrimson::mVenus/+; +; R72F11-Gal4/+* |
| 2 | E | MB247 | *20xUAS-IVS-CsChrimson::mVenus/+; R54B01-Gal4.AD/+; R46E07-Gal4.DBD/R72F11-Gal4* |
| 2 | F, G | | *w+, hs(KDRT.stop)FLP/13xLexAop-CsChrimson::tdTomato; R54B01-Gal4.AD/72F11-LexA;20xUAS-(FRT.stop)-CsChrimson::mVenus/R46E07-Gal4.DBD* |
| 2 | H | control | *w+, hs(KDRT.stop)FLP/13xLexAop-CsChrimson::tdTomato; R54B01-Gal4.AD/72F11-LexA; 20xUAS-(FRT.stop)-CsChrimson::mVenus/R46E07-Gal4.DBD* |
| 2 | H | SS04185-DN | *w+, hs(KDRT.stop)FLP/13xLexAop-CsChrimson::tdTomato; R54B01-Gal4.AD/72F11-LexA; 20xUAS-(FRT.stop)-CsChrimson::mVenus/R46E07-Gal4.DBD* |
| 2 | I-J | ctrl | *w+, hs(KDRT.stop)FLP/13xLexAop-CsChrimson::tdTomato; R54B01-Gal4.AD/72F11-LexA; 20xUAS-(FRT.stop)-CsChrimson::mVenus/R46E07-Gal4.DBD* |
| 2 | I-J | SS04185-DN | *w+, hs(KDRT.stop)FLP/13xLexAop-CsChrimson::tdTomato; R54B01-Gal4.AD/72F11-LexA; 20xUAS-(FRT.stop)-CsChrimson::mVenus/R46E07-Gal4.DBD* |
| 4 | B | Basins>Chrimson | *w; R72F11-LexA/R54B01-Gal4.AD; 13xLexAop2-IVS -CsChrimson::tdTomato, 20xUAS-IVS- GCaMP6s/R46E07-Gal4.DBD* |
| 4 | B | A00c>Chrimson | *w; R71A10-LexA/R54B01-Gal4.AD; 13xLexAop2-IVS -CsChrimson::tdTomato, 20xUAS-IVS-GCaMP6s/R46E07-Gal4.DBD* |
| 4 | C | SeIN128 (Basins>Chrimson) | *w; R72F11-LexA/R54B01-Gal4.AD; 13xLexAop2-IVS -CsChrimson::tdTomato, 20xUAS-IVS- GCaMP6s/R46E07-Gal4.DBD* |

| | | | |
|---|---|---|---|
| 4 | C | SeIN128 (A00c>Chrimson) | *w; R71A10-LexA/R54B01-Gal4.AD; 13xLexAop2-IVS -CsChrimson::tdTomato, 20xUAS-IVS-GCaMP6s/R46E07-Gal4.DBD* |
| 4 | C | A00c (Basins>Chrimson) | *w; R72F11-LexA/+; 13xLexAop2-IVS -CsChrimson::tdTomato, 20xUAS-IVS-GCaMP6s/R71A10-Gal4* |
| 5 | A, B | | *10xUAS-IVS-myr::GFP/+; R54B01-Gal4.AD/+; R46E07-Gal4.DBD/+* |
| 5 | C, D | ctrl | *w; ; R57C10-Gal4/+* |
| 5 | C, D | VGAT-RNAi | *w; ; R57C10-Gal4/UAS-HMS02355* |
| 6 | A, D | control | *13xLexAop2-IVS-CsChrimson::mVenus; R72F11-LexA/+; 20xUAS-TTS-Shibire$^{ts1}$/+* |
| 6 | A, D | SS04185 | *13xLexAop2-IVS-CsChrimson::mVenus; R72F11-LexA/R54B01-Gal4.AD; 20xUAS-TTS-Shibire$^{ts1}$/R46E07-Gal4.DBD* |
| 6 | B-C, E-G | ctrl | *13xLexAop2-IVS-CsChrimson::mVenus; R72F11-LexA/+; 20xUAS-TTS-Shibire$^{ts1}$/+* |
| 6 | B-C, E-G | SS04185 | *13xLexAop2-IVS-CsChrimson::mVenus; R72F11-LexA/R54B01-Gal4.AD; 20xUAS-TTS-Shibire$^{ts1}$/R46E07-Gal4.DBD* |
| 7 | A-D | control | *20xUAS-IVS-CsChrimson::mVenus/+; ; R72F11-Gal4/+* |
| 7 | A-D | GABA-B-R1[1] | *20xUAS-IVS-CsChrimson::mVenus/+; ; R72F11-Gal4/UAS-HMC03388* |
| 7 | A-D | GABA-B-R1[2] | *20xUAS-IVS-CsChrimson::mVenus/+; ; R72F11-Gal4/UAS-JF02989* |
| 7 | A-D | GABA-B-R2 | *20xUAS-IVS-CsChrimson::mVenus/+; ; R72F11-Gal4/UAS-HMC02975* |
| 7 | A-D | GABA-A-R | *20xUAS-IVS-CsChrimson::mVenus/+; ; R72F11-Gal4/UAS-HMC03643* |
| 7 | E | Basins>Chrimson | *20xUAS-Syn21-opGCaMP6s,10XUAS-Syn21-CsChrimson88::tdTomato/+;CyO/+;TM6/R72F11-Gal4* |
| 7 | F | Basins + SeIN128>Chrimson | *20xUAS-Syn21-opGCaMP6s,10XUAS-Syn21-CsChrimson88::tdTomato/+;CyO/R54B01-Gal4.AD;R72F11-Gal4/R46E07-Gal4.DBD* |
| 8 | A | Basin2>Chrimson | *20xUAS-IVS-CsChrimson::mVenus/+; R72F11-Gal4.AD/+; R38H09-Gal4.DBD/+* |
| 8 | B | Basin4>Chrimson | *20xUAS-IVS-CsChrimson::mVenus/+; R72F11-Gal4.AD/+; R57F07-Gal4.DBD/+* |
| 8 | C | Basin-2 | *20xUAS-IVS-CsChrimson::mVenus/+; R72F11-Gal4.AD/+; R38H09-Gal4.DBD/+* |
| 8 | C | Basin-4 | *20xUAS-IVS-CsChrimson::mVenus/+; R72F11-Gal4.AD/+; R57F07-Gal4.DBD/+* |
| 8 | D | control | *20xUAS-IVS-CsChrimson::mVenus/+; R72F11-Gal4.AD/+; R38H09-Gal4.DBD/+* |
| 8 | D | SS04185 | *20xUAS-IVS-CsChrimson::mVenus/+; R72F11-Gal4.AD/R54B01-Gal4.AD; R38H09-Gal4.DBD/R46E07-Gal4.DBD* |
| 8 | E | ctrl | *20xUAS-IVS-CsChrimson::mVenus/+; R72F11-Gal4.AD/+; R38H09-Gal4.DBD/+* |
| 8 | E | SS04185 | *20xUAS-IVS-CsChrimson::mVenus/+; R72F11-Gal4.AD/R54B01-Gal4.AD; R38H09-Gal4.DBD/R46E07-Gal4.DBD* |
| 8 | F | control | *20xUAS-IVS-CsChrimson::mVenus/+; R72F11-Gal4.AD/+; R57F07-Gal4.DBD/+* |
| 8 | F | SS04185 | *20xUAS-IVS-CsChrimson::mVenus/+; R72F11-Gal4.AD/R54B01-Gal4.AD; R57F07-Gal4.DBD/R46E07-Gal4.DBD* |
| 8 | G | ctrl | *20xUAS-IVS-CsChrimson::mVenus/+; R72F11-Gal4.AD/+; R57F07-Gal4.DBD/+* |
| 8 | G | SS04185 | *20xUAS-IVS-CsChrimson::mVenus/+; R72F11-Gal4.AD/R54B01-Gal4.AD; R57F07-Gal4.DBD/R46E07-Gal4.DBD* |

## Behavior assay

To optogenetically stimulate neurons, embryos were collected for 24 hours and larvae were raised on fly food plates with 0.2 mM trans-retinal (Toronto Research Chemicals, R240000). The larvae were kept in the dark at 25°C for four days to grow to the 3$^{rd}$ instar stage. Before the experiment, food plates with larvae were rinsed with a 15% sucrose solution to separate the larvae from the food. Larvae were then moved to a sieve, washed with water, dried, and placed evenly on 2% agar plates. The agar plate with animals were placed under a camera in the arena of the behavior rig.

- **Behavior apparatus**

The behavior rig consisted of several apparatuses (see Ohyama et al., 2013 for details and modified by following), including a C-MOS camera (Grasshopper Camera USB3, GS3-U3-41C6M-C, FLIR), infrared 850 nm light-emitting diode (LED) illumination (Waveform Lighting Co.), a 624 nm (LED, Waveform Lighting Co.), for optogenetic manipulations, a computer, and a heating panel. Both the camera and LED source were controlled by the computer. LED stimuli were controlled by customized software while larval behaviors were recorded using the Multi-Worm Tracker (MWT) software, a real-time image-analysis software (Swierczek et al., 2011). These two pieces of software were synchronized in the behavior assay to precisely deliver the stimulation during specified time windows.

- **Optogenetic stimulation**

Before delivering optogenetic stimulation, larvae were placed in the arena for 45 seconds. Subsequently, two 30secons 624 nm LED stimuli were presented successively with a 30-s interval between them. The LED intensity used in each experiment is shown below.

| **Figure number** | **Optogenetic stimulation irradiance** ($\mu W/mm^2$) |
|---|---|
| Figure 1 | 0.84 |
| Figure 1 – supplementary figure-1 | 0.84 |
| Figure 1 – supplementary figure-2 | 0.48 |

| | |
|---|---|
| Figure 2C-E | 5.9 |
| Figure 2F-H | 1.8 |
| Figure 2 – supplementary figure-1B-C | 5.9 |
| Figure 2 – supplementary figure-1D-E | 0.84 |
| Figure 2 – supplementary figure-1H-J | 1.8 |
| Figure 5B-D | 1.8 |
| Figure 6 | 1.8 |
| Figure 6 – supplementary figure-1 | 1.8 |
| Figure 7A-B | 0.84 |
| Figure 7 – supplementary figure-1A-D | 0.84 |
| Figure 8A-D | 3.9 |
| Figure 8E-H | 1.8 |
| Figure 8 – supplementary figure-1A-C | 1.8 |
| Figure 8 – supplementary figure-1D-E | 3.9 |
| Figure 8 – supplementary figure-1F-G | 1.8 |

**Heat shock FlpOut mosaic expression**

First instar *Drosophila* larvae were heat shocked in water bath at 37°C for 12 min as previously reported (Nern et al., 2015). With the precise temporal and temperature control of heat shock, larvae with the genotype of *w+, hs(KDRT.stop)FLP/13xLexAop2-IVS-CsChrimson::tdTomato; R54B01-Gal4.AD/72F11-LexA;20xUAS-(FRT.stop)-CsChrimson::mVenus/R46E07-Gal4.DBD* had sporadic CsChrimson::mVenus expression driven by SS04185 split GAL4. As a result, the ratio of the larvae with SS04185-DN and SS04185-MB expression to those with only SS04185-MB expression was 1:1. Each individual larva was individually examined with optogenetic stimulation and behavior analysis. After behavioral experiments, larval mVenus expression was confirmed.

**Thermal stimulation**

To provide heat stimulation, we built thermal control systems with a proportional-integral-derivative (PID) temperature controller (ITC-106VH, Inkbird), a solid-state relay for temperature controllers (SSR-25A, Inkbird), a K-Type thermocouple to detect temperature, and a heat panel. The thermal control system was connected to a custom-built incubator designed to maintain a steady temperature inside the behavior rig at 32°C and warm the agar plates. The temperature of the agar plates was monitored by a thermometer gun (62 MAX+ Compact Infrared Thermometer, Fluke) before and after the experiment to verify the appropriate temperature for *shibire*$^{ts1}$ to be functional. Larvae were sealed in a plastic sieve and pre-heated in a water bath for 10 min to reach 32°C before the test. In order to maintain the temperature above 30°C during the test, a replica of the thermal control system mentioned above was installed in the behavior rig, and the behavior rig was pre-heated overnight before any thermal experiment.

For *shibire*$^{ts1}$ experiments with heat stimulation, during the first 5 s of the test, larvae were left on the agar plates without LED stimulation. Subsequently, the larvae were optogenetically stimulated with a 624-nm LED for 30 s.

**Behavior analysis**

Larvae were tracked in real-time using MWT software (https://github.com/Ichoran/choreography). Videos were not recorded. Instead, the contour, spine, and center of mass for each larva were generated and recorded by MWT as a function of time. From these tracking data, the key parameters of larval motion were computed using Choreography software (a component of the MWT software package which measured the behavioral parameters offline) as described previously (Ohyama et al., 2013; Ohyama et al., 2015). The behavioral parameters generated by Choreography algorithm included speed, crabspeed (*i.e.*, the speed perpendicular to the body axis),

curve (*i.e.,* body curvature), cast (*i.e.,* head bending angle), midline (*i.e.,* body length), morpwidth (*i.e.,* body width), area (*i.e.,* area of larvae from the dorsal view), and bias (*i.e.,* fractional excess of time spent moving one way). In this offline process, objects that were tracked for less than 5 s or moved less than one body length of a larva were rejected. We refer readers to the open-source package for further details of the software implementations for the above calculations.

- **Behavior detection**

After extracting behavioral parameters from Choreography, we used an unsupervised machine learning behavior classification algorithm to detect and quantify the following behaviors: hunching (Hunch), head-bending (Turn), stopping (Stop), and peristaltic crawling (Crawl) as previously reported (Masson et al., 2020). Escape rolling (Roll) was detected with a classifier developed with Janelia Automatic Animal Behavior Annotator (JAABA) (Kabra et al., 2013; Ohyama et al., 2015). JAABA transformed the MWT tracking data into a collection of 'per-frame' behavioral parameters s and regenerated 2D dorsal-view videos of the tracked larvae. Behaviors were then labeled manually frame-by-frame with these regenerated videos. In real-life, rolling is a rotation surround larval body axis with a C-chape body curvature, resulting in a movement perpendicular to the body axis. With these regenerated 2D dorsal-view videos, we defined roll as a movement perpendicular to larval body axis while curling in C-shape (Supplementary video -1 and -2). Based on this definition, we labeled roll, non-roll, and unknown frames in the randomly chosen ~10,000 frames to train the algorithm to correctly classify larval rolling behavior. If a larva did not curl up in C-shape or move sideways, they were labeled as non-rolling. This refusion of false positives especially as the beginning and the end of each rolling bout enhanced accuracy. This algorithm integrated these training labels and parameters generated with Choreography in a time series, such as speed, crabspeed, and body curvature, to generate a score for rolling detection. Above a certain

threshold, the classifier labeled the frame as rolling. This classifier, which has false negative and false positive rates of 7.4% and 7.8%, respectively (n=102), was utilized to detect rolling in this paper.

- **Behavior quantification**

The outputs of these behavior detection pipelines served as the input to a customized follow-up MATLAB-based analysis. Only the larvae being tracked fully during the stimulation window were selected for analysis. The percentages of animals performing given behaviors as well as their crawling speed in time series at a frame rate of 10 fps were plotted to depict the behavioral responses. To quantify the behavioral phenotype at the population level, the proportions of larvae that performed given behaviors at least once in the first 5 s after the onset of the stimulation were calculated in percentages. A collection of individual-level parameters (e.g., aggregated durations of rolling throughout the stimulation window, starts and ends of the first rolling event after stimulus onset, starts of the first crawling event after the first rolling event in the stimulation window) were generated and analyzed to describe the effects of stimulation on escape behaviors. Specifically, the starts of the first crawling events after the first rolling events were recorded as 30 s by default if larvae rolled but never initiated crawling during the stimulation window. Furthermore, the cumulative plots of the durations of each rolling event were contrasted to describe the event-level differences.

**Larval dissections and immunohistochemistry**

Standard immunocytochemical procedures were followed (Patel, 1994) Briefly the CNSs of *Drosophila* larvae were dissected in phosphate-buffered saline (PBS). After dissection, tissues were fixed with 4% paraformaldehyde for 20 min, washed with PBS 3 times and then washed with 0.4% Triton X-100 in PBS (PBST) twice. Samples were incubated at room temperature with a

blocking solution (5% normal goat serum [NGS]) for 1 h. Next, the samples were incubated with the primary antibody solutions at 4°C overnight and washed 15 minutes for 6 times. Specially, anti-VGAT was incubated for 48h to compensate for the permeability, The primary antibodies were diluted at concentrations of 1:3000 for chicken anti-GFP; 1:1000 for rabbit anti-GFP, rabbit anti-GABA and rabbit anti-dsRed; 1:200 for rabbit anti-VGAT; 1:50 for mouse nc82; and 1:20 for rat anti-DN-Cadherin, mouse anti-Fas2, mouse anti-choline acetyltransferase (ChAT), and rabbit anti-GLUT1 in 5% NGS. CNS samples were then incubated with a secondary antibody solution at 4°C overnight and washed 15 minutes for 6 times. The secondary antibodies, including anti-chicken Alexa488, anti-rabbit Alexa488, anti-mouse Alexa568, anti-rabbit Alexa568, and anti-rat Alexa568, were all diluted at the concentration of 1:500. These samples were mounted in VECTASHIELD antifade mounting medium and imaged by a Zeiss LSM 710 confocal microscope with a 20x/NA0.8 objective lens (Zeiss) and Zen digital imaging software (Zeiss). All images were processed using Fiji software (https://imagej.new/Fiji, ImageJ, NIH Bethesda).

**Immunohistochemistry image analysis**

Larval CNS image stacks were processed with FIJI. For figure 5-supplementary 1C and D, 4-6 slices on the z dimension were averaged. The neuropil at A4-A6 segments was manually selected as ROI. The intensity was measured per CNS and compared with student's t test.

**Two-photon calcium imaging assay**

The CNSs of third instar larvae were dissected out in cold Baines external physiological saline (135 mM NaCl, 5 mM KCl, 5 mM TES, 36 mM sucrose, 2 mM $CaCl_2$-$2H_2O$, 4 mM $MgCl_2$-$6H_2O$, pH 7.15), and secured on a poly-L-lysine coated cover glass placed in a small Sylgard plate.

Functional calcium imaging experiments were performed on a customized two-photon microscope equipped with a Galvo-Resonant Scanner (Cambridge) controlled by Scanimage software (mbf

BIOSCIENCE) using a 40x/0.80NA water immersion objective (LUMPlanFL, Olympus). A Mai Tai®, Ti:Sapphire Ultrafast Laser (Spectra Physics) tuned to 925 nm was used for excitation of GCaMP protein. Fluorescence signals were collected with photomultiplier tubes (Hamamatsu) after bandpass filtering. Images were acquired by the Galvo-Resonant Scanner for a single plane of the CNS.

Each larva was stimulated by a 620-nm LED (Thorlabs) through the objective three times with a 30-s interval between periods of stimulation. Every stimulus consisted of a 30-ms pulse given every 100 ms for a total of 1 s. Light intensity was measured to be 0.8-1.4 mW/mm2. Images were acquired at a resolution of 512 x 512 pixels with a frame rate of 30 fps. Fluorescence intensities were averaged to 6 fps and processed in FIJI, and analyzed in MATLAB with customized scripts. Regions of interest (ROI) were determined by the standard deviation of the full recording. $\Delta F=(F-F_0)/F_0$. $F_0$ is the average of images taken 10 frames (i.e., 1.7 s) before stimulation. $F$ is the mean value of the fluorescence in the ROI averaged every 5 frames from the start of the 5-s period before stimulation to end of the 15-s period after the onset of each stimulation. For each larva, $\Delta F$ is obtained through averaging the $\Delta F$ during the three stimulation periods. The peak $\Delta F$s were the maximal values selected from the onset of stimulation to 15 s after stimulus onset.

**Statistics**

The probabilities for each response were analyzed by Chi-square tests. For the other parameters, when multiple groups were tested, their normality was examined first. If the normality assumption was rejected, Kruskal-Wallis tests were performed for multiple group variance comparisons, followed by multiple-comparison-corrected Wilcoxon–Mann–Whitney tests as post hoc pairwise comparisons. If normality was met, analysis of variance (ANOVA) was performed for variance comparisons and multiple-comparison-corrected student's t-tests were utilized for pairwise

comparisons. For two group comparisons, the Wilcoxon–Mann–Whitney test was conducted if the normality assumption was offended, and the student's t-test was applied if normality was met. All analyses were conducted with MATLAB.

**Data availability statement**

The original contributions presented in this study are included in the article/supplemental material; further inquiries may be directed to the corresponding author.

**Conflict of interests**

The authors declare that the research was conducted in the absence of any commercial or financial relationships that could be construed as a potential conflict of interests.

**Author contributions**

Conceptualization, J.Z. and T.O. Writing – Original Draft, J.Z. and T.O; Writing – Review & Editing, J.Z., J-C.B., and T.O. Formal Analysis, J.Z., J-C.B., and T.O. Performing experiments, J.Z., J-C.B., J.N., Y.Q.Z., and T.O. Supervision, T.O.

**Funding**

This work was funded by McGill University, the National Sciences and Engineering Research Council (NSERC, RGPIN/04781-2017), the Canadian Institute of Health Research (CIHR, PTJ-376836), the Fonds de recherche du Quebéc – Nature et technologies (FRQNT, 2019-N-25523), and the Canada Foundation for Innovation (CFI, CFI365333). J-C.B was supported by Fonds de recherche du Quebéc-Santé (FRQS) graduate training award.

**Acknowledgements**

We thank J.W. Truman, A. Cardona and M. Zlatic for generating and sharing the split Gal4 lines. J. Truman and M. Zlatic for constructive inputs on the project. Confocal images were collected at

the McGill University Advanced Bio Imaging Facility (ABIF), RRID:SCR_017697. We also thank the Bloomington stock center for providing fly stocks. We thank members of Ohyama lab for critical comments on the manuscript.

**Inclusion and diversity**

One or more of authors of this paper self-identifies as a member of the LGBTYQ+ community.

**Figure legends:**

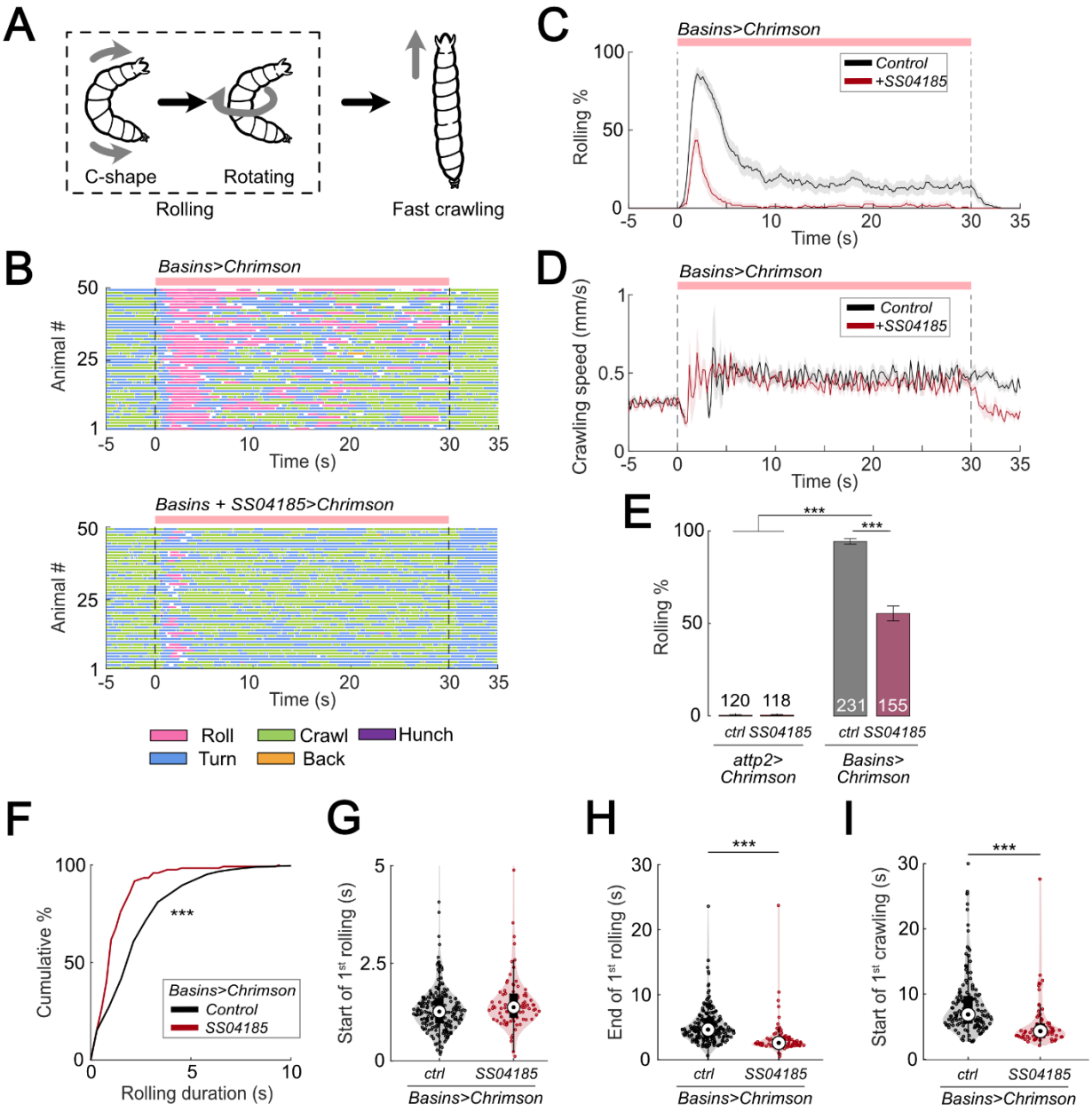


**Figure 1. Activation of SS04185 inhibits rolling evoked by activation of Basin neurons**

(A) Cartoon of *Drosophila* larval escape sequence.

(B) Ethograms of Basin activation (top panel) and co-activation of SS04185 and Basins (bottom panel). Each row represents an individual larva. Pink, blue, green, orange, and purple lines represent bouts of rolling, turning, crawling, backward crawling, and hunching. The red bar and

dashed lines indicate the time window during which neural activation was present. Genotypes: *20xUAS-IVS-CsChrimson::mVenus/+;+; R72F11-Gal4/+* (top); *20xUAS-IVS-CsChrimson::mVenus/+; R54B01-Gal4.AD/+; R46E07-Gal4.DBD/ R72F11-Gal4* (bottom). Genotypes in (C-D, F-I) are the same as those mentioned here.

(C) Time series of larval crawling speed during co-activation of SS04185 and Basins (red) and activation of Basins alone (black). Shaded areas represent the standard error. The red bar and dashed lines denote the optogenetic stimulation window.

(D) Time series of rolling probabilities of larvae during co-activation of SS04185 and Basins (red) and activation of Basins alone (black). Shaded areas represent 95% confidential intervals for rolling probabilities. The red bar and dashed lines denote the optogenetic stimulation window.

(E) Rolling probabilities of larvae with activation of different neurons. Error bars represent the 95% confidence interval. Genotypes from left to right: 1) *20xUAS-IVS-CsChrimson::mVenus/+; ; ,* 2) *20xUAS-IVS-CsChrimson::mVenus/+; R54B01-Gal4.AD/+; R46E07-Gal4.DBD/+*, 3) *20xUAS-IVS-CsChrimson::mVenus/+; ; R72F11-Gal4/+*, 4) *20xUAS-IVS-CsChrimson::mVenus/+; R54B01-Gal4.AD/+; R46E07-Gal4.DBD/ R72F11-Gal4.* n = 120, 118, 231, 155 from left to right. Statistics: Chi-square test, $\chi^2 = 0$, $p > 0.05$ for the first two groups; $\chi^2 = 83.85$, $p < 0.001$ for the last two groups; and $\chi^2 = 365.51$, $p < 0.001$ for the comparison between the first two groups and the last two groups.

(F) Cumulative plot of rolling duration. Statistics: Mann-Whitney test, $p < 0.001$, n = 652, 120.

(G) A violin plot showing start of first rolling bout for each larva during stimulation. Statistics: Mann-Whitney test, $p = 0.027$, n = 225, 89.

(H) A violin plot displaying end of first rolling bout for each larva during stimulation. Statistics: Mann-Whitney test, $p < 0.001$, n = 225, 89.

(I) A violin plot presenting start of first crawling bout for each larva during stimulation. Statistics: Mann-Whitney test, $p < 0.001$, n = 214, 70.

$^{**}p < 0.01$, $^{***}p < 0.001$.

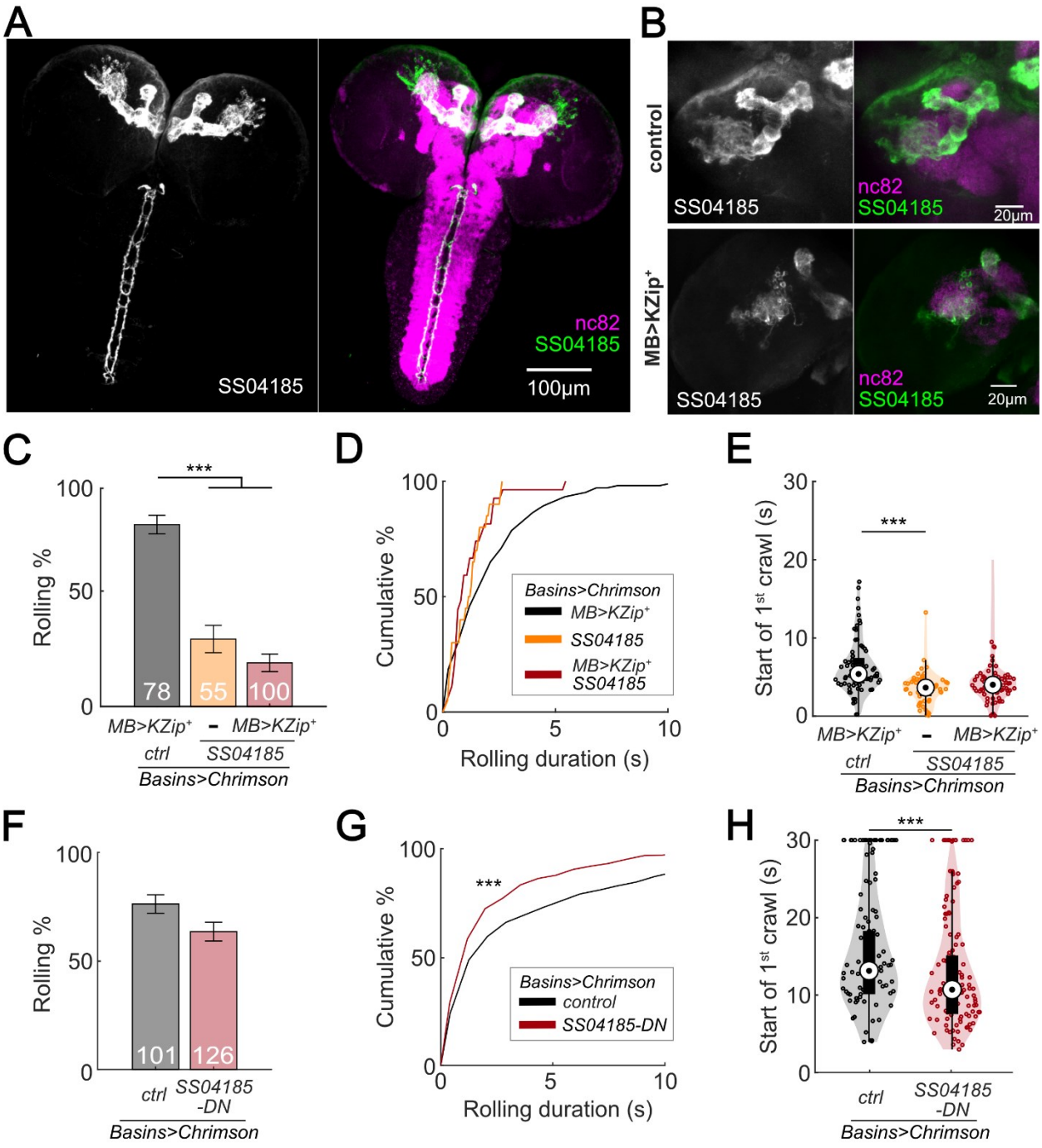


**Figure 2. SS04185-DN, but not SS04185-MB, inhibits rolling when co-activated with Basins**

(A) Morphology of SS04185 neurons. GFP, grey (left), green (right); nc82, magenta. Anterior, up; dorsal view; scale bar, 100 µm. Genotype: 10x*UAS-IVS-myr::GFP/+; R54B01-Gal4.AD/+; R46E07-Gal4.DBD/+*.

(B) Kenyon cells are less labeled in SS04185 with MB>Killer Zipper. CsChrimson::mVenus expression in Kenyon cells of SS04185 in Control and SS04185 with Killer Zipper in mushroom body (MB). mVenus, grey (left), green (right); nc82, magenta. Anterior, up; dorsal view; scale bar, 20 µm. Genotype: *20xUAS-IVS-CsChrimson::mVenus/+; R54B01-Gal4.AD/+; R46E07-Gal4.DBD/+* (control); *20xUAS-IVS-CsChrimson::mVenus/+; R13F02-LexA,LexAop-KZip$^{+}$/R54B01-Gal4.AD; R72F11-Gal4/R46E07-Gal4.DBD* (MB>KZip$^{+}$).

(C) Rolling probabilities of larvae with activation of SS04185 reduce the expression of CsChrimson in mushroom body (MB) neurons. Error bars, 95% confidence interval. n = 78, 55, 100 from left to right. Statistics: Chi-square test, $\chi^2 = 2.32$, $p > 0.05$ for the two groups with SS04185 expression; $\chi^2 = 37.50$, $p < 0.001$ for the comparison between the two groups on the left; $\chi^2 = 70.45$, $p < 0.001$ for the comparison between the groups with *MB>KZip$^{+}$* expression which reduce expression of CsChrimson in MB. Genotypes: *20xUAS-IVS-CsChrimson::mVenus/+; R13F02-LexA,LexAop-KZip$^{+}$/+; R72F11-Gal4/+* (black); *20xUAS-IVS-CsChrimson::mVenusR54B01-Gal4.AD/+; R46E07-Gal4.DBD/R72F11-Gal4* (orange); *20xUAS-IVS-CsChrimson::mVenus/+; R13F02-LexA,LexAop-KZip$^{+}$/R54B01-Gal4.AD; R72F11-Gal4/R46E07-Gal4.DBD* (red). Genotypes in (D-E) are the same as mentioned here.

(D) Cumulative plot of rolling duration. Statistics: Kruskal-Wallis test: H = 8.28, $p = 0.016$; Bonferroni-corrected Mann-Whitney test, $p > 0.05$ for all pairwise post-hoc tests, n = 103, 20, 27 from left to right.

(E) A violin plot of start of first crawling bout for each larva during stimulation. Statistics: Kruskal-Wallis test: H = 15.02, $p < 0.001$; Bonferroni-corrected Mann-Whitney test, $p > 0.05$ for the two groups with SS04185 expression; $p < 0.001$ for the comparison between the group without SS04185 expression and the groups with full SS04185 expression, n = 65, 20, 7 from left to right.

(F) The probabilities of larval rolling during first 5 s of stimulation. Error bars, 95% confidence interval. n = 101, 126. Statistics: Chi-square test, $\chi^2 = 4.27$, $p = 0.039$. Genotype: *13xLexAop2-IVS-CsChrimson::tdTomato/w*$^{+}$*, hs-FLP; R54B01-Gal4.AD/72F11-LexA; 20xUAS-(FRT.stop)-CsChrimson::mVenus/R46E07-Gal4.DBD.* Genotypes in (G-H) are the same as mentioned here.

(G) Cumulative plot of rolling duration. Statistics: Mann-Whitney test, $p < 0.001$, n = 350, 473.

(H) A violin plot of start of first crawling bout for each larva during stimulation. Statistics: Mann-Whitney test, $p < 0.001$, n = 97, 120.

$^{**}p < 0.01$, $^{***}p < 0.001$.

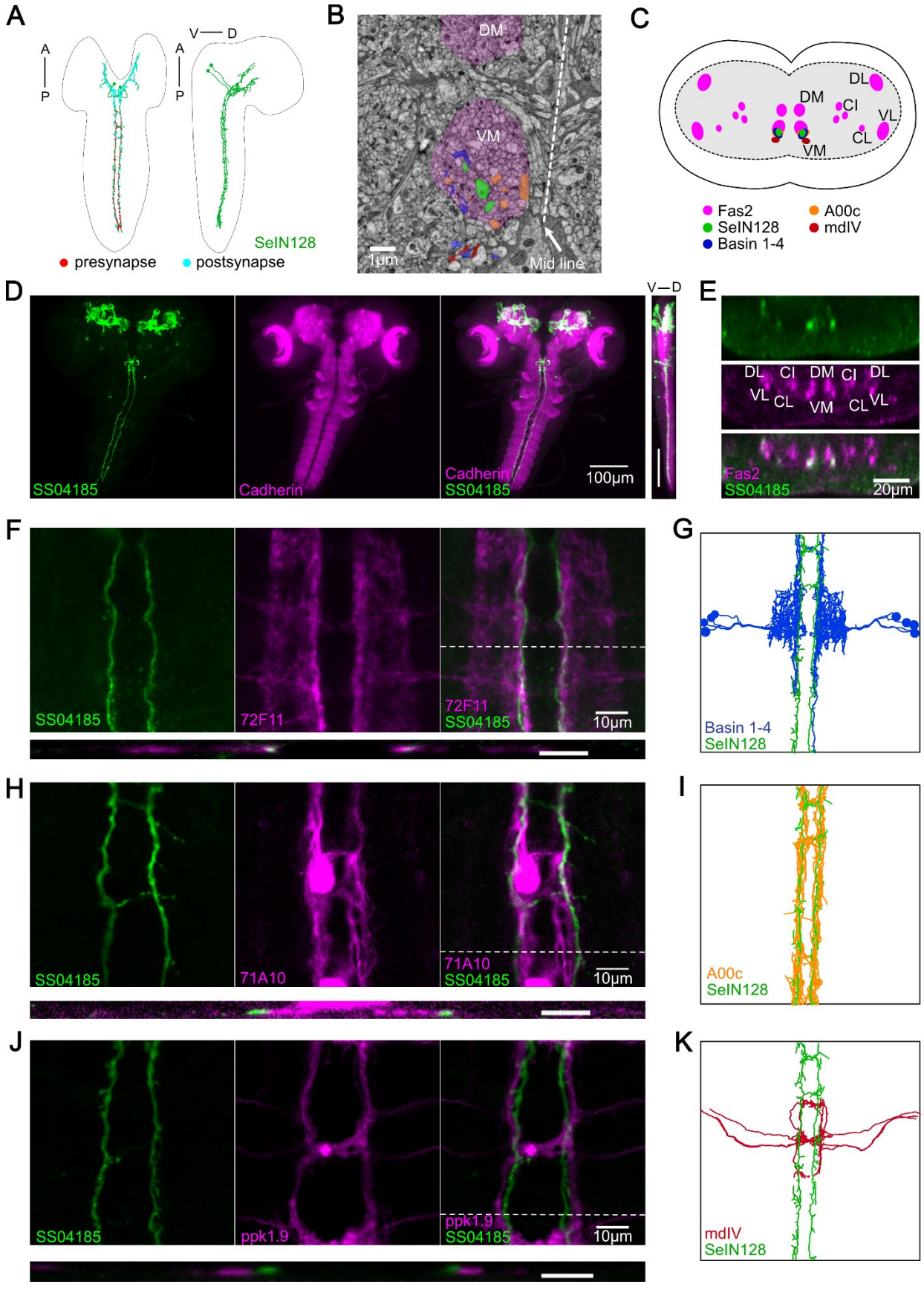
A
A
P
V — D
A
P
SeIN128
presynapse
postsynapse
B
DM
VM
1μm
Mid line
C
DL
DM
CI
VL
CL
VM
Fas2
SeIN128
Basin 1-4
A00c
mdIV
D
V — D
SS04185
Cadherin
Cadherin
SS04185
100μm
E
DL
CI
DM
CI
DL
VL
CL
VM
CL
VL
Fas2
SS04185
20μm
F
SS04185
72F11
72F11
SS04185
10μm
G
Basin 1-4
SeIN128
H
SS04185
71A10
71A10
SS04185
10μm
I
A00c
SeIN128
J
SS04185
ppk1.9
ppk1.9
SS04185
10μm
K
mdIV
SeIN128

**Figure 3. SS04185-DN is identical to SeIN128**

(A) TEM neuron reconstruction of SeIN128 neurons. Left panel: anterior, up; dorsal view. Right panel: anterior, up; dorsal, right; lateral view. Red dots, presynaptic sites. Cyan dots, postsynaptic sites.

(B) A transverse section of larval CNS from EM reconstruction data. SeIN128 (green), Basins (blue), and A00c (orange) are located in ventromedial tract (VM). mdIV, red; magenta, neural tracts. DM, dorsomedial tract; VM, ventromedial tract. Dorsal, up; anterior view; scale bar, 1 μm.

(C) Cartoon generated based on transverse section of SeIN128, Basin-1 to Basin-4, A00c, and mdIV from EM neuron reconstruction data and (D). Nerve tracts are shown in magenta. Dorsal, up; posterior view. DM, dorsomedial tract; VM, ventromedial tract; CI, central-intermediate tract; CL, central-lateral tract; DL, dorsolateral tract; VL, ventrolateral tract. SeIN128, green; Basin-1 to Basin-4, blue; A00c, orange; mdIV, red.

(D) SS04185-expressing neurons co-stained with N-Cadherin. A cell body of SS04185-Descending neuron located in ventral part of the subesophageal zone (SEZ). SS04185, Green; N-Cadherin, magenta. Anterior, up; left, dorsal view; right, longitudinal section; scale bar, 100 μm. Genotype: *10xUAS-IVS-myr::GFP/+; R54B01-Gal4.AD/+; R46E07-Gal4.DBD/+*. SS04185, Green; Cadherin, magenta. Anterior, left, dorsal, up; lateral view; scale bar, 100 μm.

(E) Transverse section of SS04185-DN co-stained with Fas2. SS04185-DN located at ventromedial tract (VM). SS04185, Green; Fas2, magenta. Dorsal, up; posterior view; scale bar, 20 μm. DM, dorsomedial tract; VM, ventromedial tract; CI, central-intermediate tract; CL, central-lateral tract; DL, dorsolateral tract; VL, ventrolateral tract. Genotype: *10xUAS-IVS-myr::GFP/+; R54B01-Gal4.AD/+; R46E07-Gal4.DBD/+*.

(F, H, J) SS04185-DN co-localized with Basins or A00C neuron tract but not MdIV. SS04185, Green; Basins (F), A00c (H) or mdIV (J), magenta;. Genotype: *w; R54B01-Gal4.AD/R72F11-LexA(F) 71A10-LexA(H) or ppk1.9-LexA(J); R46E07-Gal4.DBD/13xLexAop2-IVS-CsChrimson::tdTomato,20xUAS-IVS-GCaMP6s.* Top panel: anterior, up; dorsal view; scale bar, 10 μm. Bottom panel: dorsal, up; posterior view; scale bar, 5 μm.

(G, I, K) SeIN128, Basin-2, A00c or mdIV morphologies from the TEM neural reconstruction. Anterior, up; dorsal view. SS04185, green; Basin-2, blue; A00C, orange; mdIV, red.

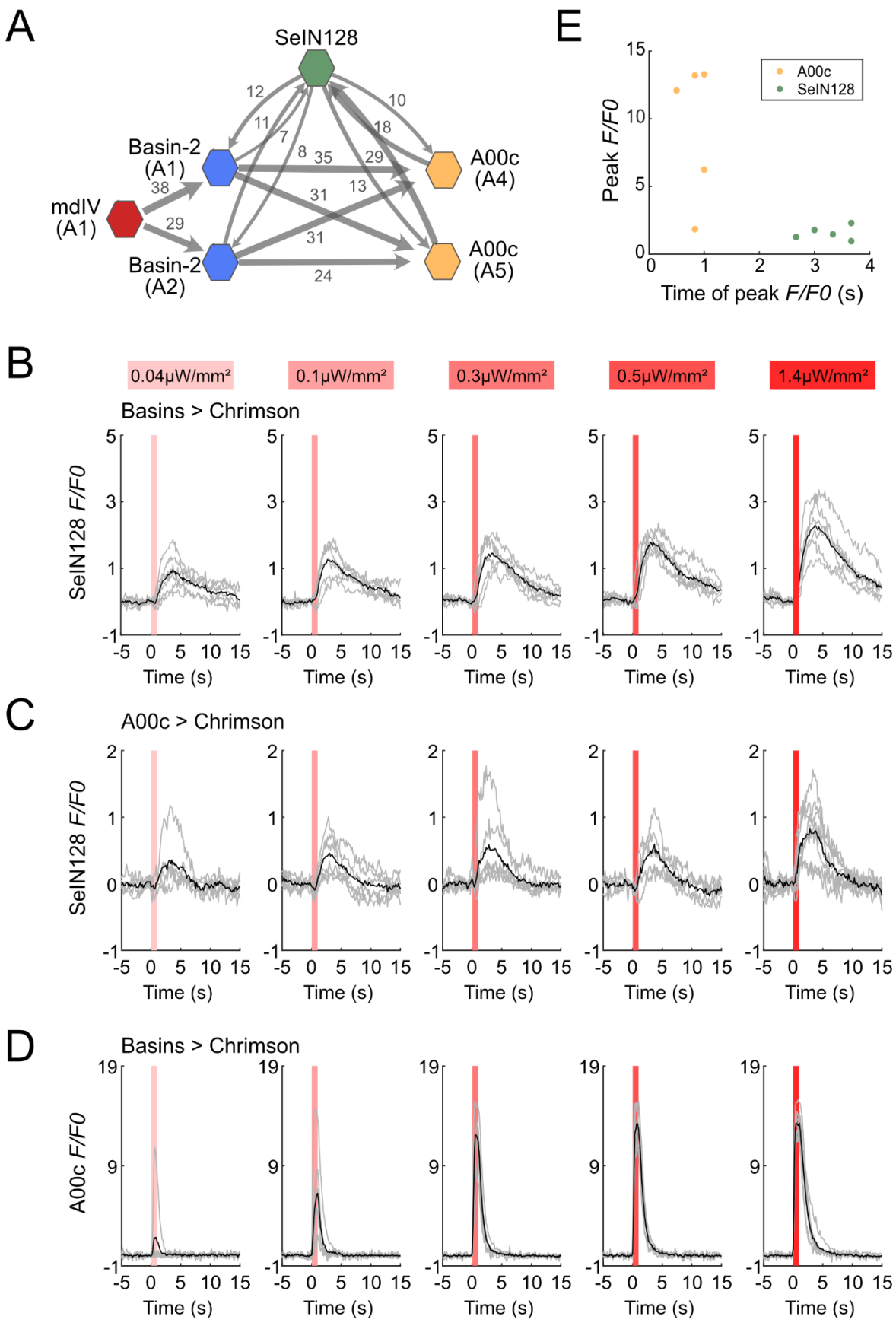
A
SeIN128
Basin-2
(A1)
mdIV
(A1)
Basin-2
(A2)
A00c
(A4)
A00c
(A5)
12
11
7
8
35
29
10
18
38
31
13
29
31
24
E
A00c
SeIN128
Peak F/F0
Time of peak F/F0 (s)
B
0.04µW/mm²
0.1µW/mm²
0.3µW/mm²
0.5µW/mm²
1.4µW/mm²
Basins > Chrimson
SeIN128 F/F0
Time (s)
C
A00c > Chrimson
SeIN128 F/F0
Time (s)
D
Basins > Chrimson
A00c F/F0
Time (s)

**Figure 4. SeIN128 receives input from Basin and A00c neurons**

(A) Summary of the connectivity between SeIN128 and the escape circuit. SeIN128 receives inputs from Basin-2 and A00c and provide feedback to Basin-2 and A00c. Synapse number shown next to connection arrows, where line width is proportional to synapse number. All connections in the ventral nerve cord are shown except unilateral synapses, <5 synapses, between neurons. Each polygon represents a pair of the indicated neuron and segment (segment number is shown under the neuron name). SeIN128, green; Basin-2, blue; A00c, orange; mdIV, red.

(B, C) SeIN128 is functionally downstream of Basins (B) or A00c (C). Calcium transients, $\Delta F/F_0$ traces of GCaMP6s in SeIN128 axons (black line, mean; gray line, single larva) during 610-nm optogenetic activation of Basins at various intensities. Vertical gray line represents optogenetic activation. Genotype: *w; R72F11-LexA (B) or R71A10-LexA (C) /R54B01-Gal4.AD; 13xLexAop2-IVS—CsChrimson::tdTomato, 20xUAS-IVS-GCaMP6s/R46E07-Gal4.DBD.*

(D) A00c responses are faster and stronger than SeIN128 responses during activation of Basins. Calcium transients (black line, mean; gray line, single larva) represented by $\Delta F/F_0$ in A00c by of 610-nm optogenetic activation of Basins at various intensities. Genotype: *w; R72F11-LexA/+; 13xLexAop2-IVS-CsChrimson::tdTomato, 20xUAS-IVS-GCaMP6s/R71A10-Gal4.*

For (B) to (D), irradiances from left to right are 0.04, 0.1, 0.3, 0.5, and 1.4 $\mu W/mm^2$. For each irradiance (n = 6), individual traces are shown with gray lines whereas the average of individuals is shown in black. The shaded gray area indicates the period of optogenetic activation (0 to 1 s).

(E) The timing of the peak $\Delta F/F_0$ correlated with the identity of the neurons but not the peak $\Delta F/F_0$ value. SeIN128 neurons are shown as orange dots, whereas A00c is shown as a green dot.

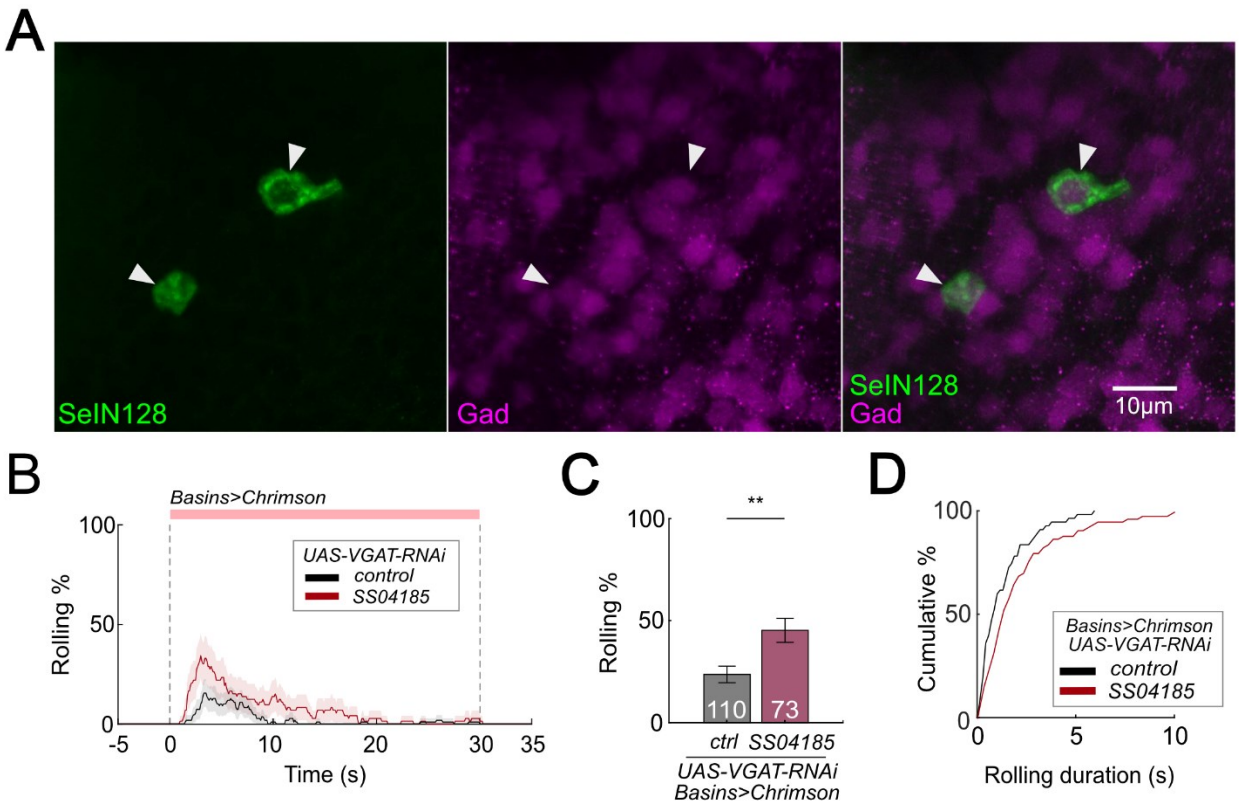


**Figure 5. SeIN128 is GABAergic and negatively controls rolling**

(A) Immunostaining of SeIN128 cell body (green) and GABAergic neuron (magenta). Genotype: *10xUAS-IVS-myr::GFP; R54B01-Gal4.AD/13xLexAop-dsRed; R46E07-Gal4.DBD/Trojan-GAD-T2A-LexA.* White triangles indicate locations of SeIN128 cell bodies. Anterior, up; dorsal view; scale bar, 10 μm.

(B) Time series of rolling probabilities of larvae with Basin activation (black), or VGAT RNAi in SS04185 and Basin activation (red). The red bar and dashed lines display the window of optogenetic stimulation eliciting larval escape responses. Shaded areas show 95% confidential intervals of rolling probabilities. Genotypes: *13xLexAop2-IVS-CsChrimson::mVenus; R72F11-LexA/+; HMS02355/+* (black); *13xLexAop2-IVS-CsChrimson::mVenus; R72F11-LexA/R54B01-Gal4.AD; HMS02355/R46E07-Gal4.DBD* (red). Genotypes in (C, D) are the same as mentioned here.

(C) Binned larval rolling probabilities during first 5 s of stimulation in (A). Error bars, 95% confidence interval. n = 110, 73. Statistics: Chi-square test, $\chi^2 = 9.34$, $p < 0.001$.

(D) Cumulative plot of rolling duration. Statistics: Mann-Whitney test, $p = 0.015$, n = 55, 73.

$^{**}p < 0.01$, $^{***}p < 0.001$.

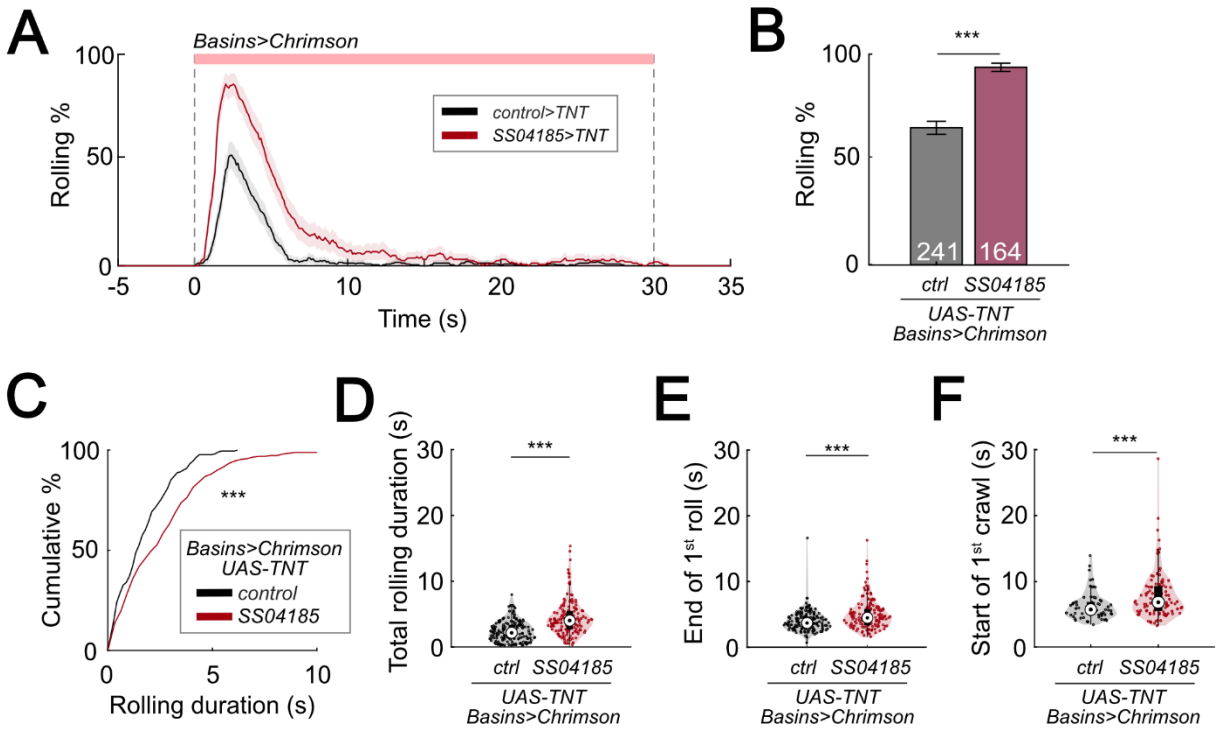


**Figure 6. Inhibition of SeIN128 prolongs rolling and delays initiation of crawling**

(A) Time series of rolling probabilities of larvae with Basin activation (black), or SS04185 inhibition and Basin activation (red). Shaded regions show 95% confidential intervals of rolling probabilities. Genotypes: *13xLexAop2-IVS-CsChrimson::mVenus; R72F11-LexA/+; UAS-TeTxLC.tnt/+* (black); *13xLexAop2-IVS-CsChrimson::mVenus; R72F11-LexA/R54B01-Gal4.AD; UAS-TeTxLC.tnt/R46E07-Gal4.DBD* (red). Genotypes in (B-F) are the same as mentioned here.

(B) Rolling probabilities during first 5 s of stimulation in (A). Error bars, 95% confidence interval. n = 241, 164. Statistics: Chi-square test, $\chi^2 = 44.02$, $p < 0.001$.

(C) A violin plot of total time spent rolling for each individual larva during stimulation. Statistics: Mann-Whitney test, $p < 0.001$, n = 221, 258.

(D) Cumulative plot of rolling duration. Statistics: Mann-Whitney test, $p < 0.001$, n = 160, 154.

(E) A violin plot of end of first rolling bout for each larva during stimulation. Statistics: Mann-Whitney test, $p < 0.001$, n = 160, 154.

(F) A violin plot of start of first crawling bout for each larva during stimulation. Statistics: Mann-Whitney test, $p < 0.001$, n = 65, 105.

$^{**}p < 0.01$, $^{***}p < 0.001$.

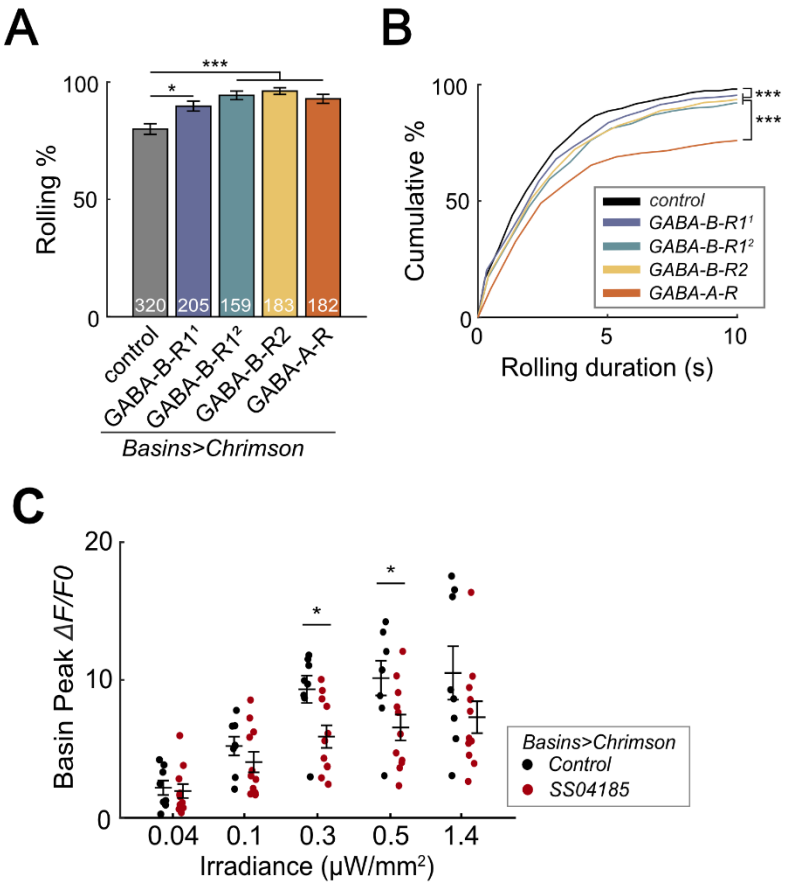


**Figure 7. SeIN128 sends feedback inhibition to Basins**

(A) Rolling probabilities for larvae with GABAR-RNAi in their Basin neurons. From left to right, the genotypes are *20xUAS-IVS-CsChrimson::mVenus/+; ; R72F11-Gal4/+* (black*), 20xUAS—IVS-CsChrimson::mVenus/+; ; R72F11-Gal4/UAS-HMC03388* (blue), *20xUAS-IVS-CsChrimson::mVenus/+; ; R72F11-Gal4/UAS-JF02989* (green), *20xUAS-IVS-CsChrimson::mVenus/+; ; R72F11-Gal4/UAS-HMC02975* (yellow), and *20xUAS-IVS-CsChrimson::mVenus/+; ; R72F11-Gal4/UAS-HMC03643* (orange). Genotypes in (B) are the same as mentioned here. N = 320, 205, 159, 183, 182 from left to right. Statistics: Chi-square test, Bonferroni correction. GABA-B-R1[1] group: $\chi^2 = 8.76$, $p = 0.012$. GABA-B-R1[2] group: $\chi^2 = 24.70$, $p < 0.001$. GABA-B-R2 group: $\chi^2 = 25.77$, $p < 0.001$. GABA-A-R group: $\chi^2 = 16.29$, $p < 0.001$.

(B) Cumulative plot of rolling duration. Statistics: Kruskal-Wallis test: H = 69.52, $p < 0.001$; Bonferroni-corrected Mann-Whitney test, $p < 0.001$ for GABA-B-R1$^2$, GABA-B-R2, and GABA-A-R RNAi groups, n = 520, 488, 387, 582, 306 from left to right.

(C) Summary of peak $\Delta F/F_0$ in Basin axons with or without SeIN128 activation under various irradiances. Control groups shown in black are without SeIN128 activation while experimental groups shown in red are with SeIN128 activation. Statistics: Mann-Whitney test, $p > 0.05$ for irradiances of 0.04, 0.1, 1.4 μW/mm$^2$; $p = 0.016$ for irradiance of 0.3 μW/mm$^2$; $p = 0.032$ for irradiance of 0.5 μW/mm$^2$. Genotype: *20xUAS-Syn21-opGCaMP6s, 10xUAS-Syn21-CsChrimson88::tdTomato/+; CyO/+;R72F11-Gal4/TM6* (black); *20xUAS-Syn21-opGCaMP6s,10xUAS-Syn21-CsChrimson88::tdTomato/+;CyO/R54B01-Gal4.AD;R72F11-Gal4/R46E07-Gal4.DBD* (red).

$^{**}p < 0.01$, $^{***}p < 0.001$.

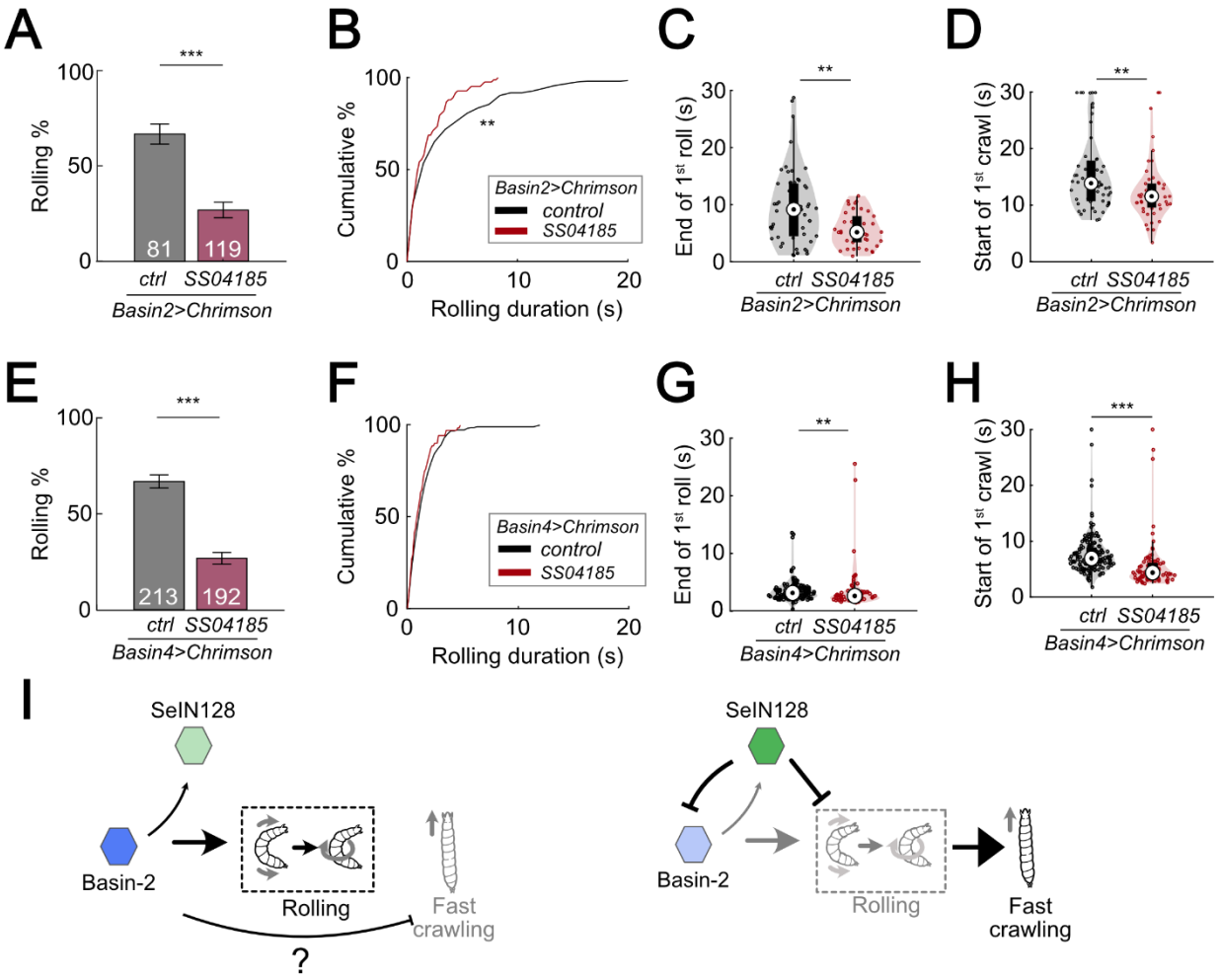


**Figure 8. SeIN128 inhibits rolling elicited by both Basin-2 and Basin-4 activation**

(A) Binned larval rolling probabilities during the first 5 s of stimulation. Error bars, 95% confidence interval. n = 81, 119. Statistics: Chi-square test, $\chi^2 = 35.51$, $p < 0.001$. Genotypes: *20xUAS-IVS-CsChrimson::mVenus/+; R72F11-Gal4.AD/+; R38H09-Gal4.DBD/+* (black); *20xUAS-IVS-CsChrimson::mVenus/+; R72F11-Gal4.AD/R54B01-Gal4.AD; R38H09-Gal4.DBD/R46E07-Gal4.DBD* (red). Genotypes in (B-D) are the same as mentioned here.

(B) Cumulative plot of rolling duration. Statistics: Mann-Whitney test, $p = 0.0034$, n = 206, 83.

(C) A violin plot of end of first rolling bout for each larva during stimulation. Statistics: Mann-Whitney test, $p = 0.0047$, n = 57, 38.

(D) A violin plot of start of first crawling bout for each larva during stimulation. Statistics: Mann-Whitney test, $p = 0.045$, n = 107, 38.

(E) Binned larval rolling probabilities during first 5 s of stimulation. Error bars, 95% confidence interval. n = 192, 213. Statistics: Chi-square test, $\chi^2 = 64.81$, $p < 0.001$. Genotypes: *20xUAS-IVS-CsChrimson::mVenus/+; R72F11-Gal4.AD/+; R57F07-Gal4.DBD/+* (black); *20xUAS-IVS-CsChrimson::mVenus/+; R72F11-Gal4.AD/R54B01-Gal4.AD; R57F07-Gal4.DBD/R46E07-Gal4.DBD* (red). Genotypes in (F-H) are the same as mentioned here.

(F) Cumulative plot of rolling duration. Statistics: Mann-Whitney test, $p = 0.032$, n = 231, 71.

(G) A violin plot of end of first rolling bout for each larva during stimulation. Statistics: Mann-Whitney test, $p = 0.0047$, n = 129, 61.

(H) A violin plot of start of first crawling bout for each larva during stimulation. Statistics: Mann-Whitney test, $p < 0.001$, n = 159, 71.

(I) A summarizing illustration. Basin-2 activates rolling and supresses fast crawling, while SeIN128 decreases Basin-2 activities to inhibit rolling and disinhibit fast crawling. Arrows show activation and blunt ends represent inhibition.

$^{**}p < 0.01$, $^{***}p < 0.001$.

**Legends for Supplementary figures**

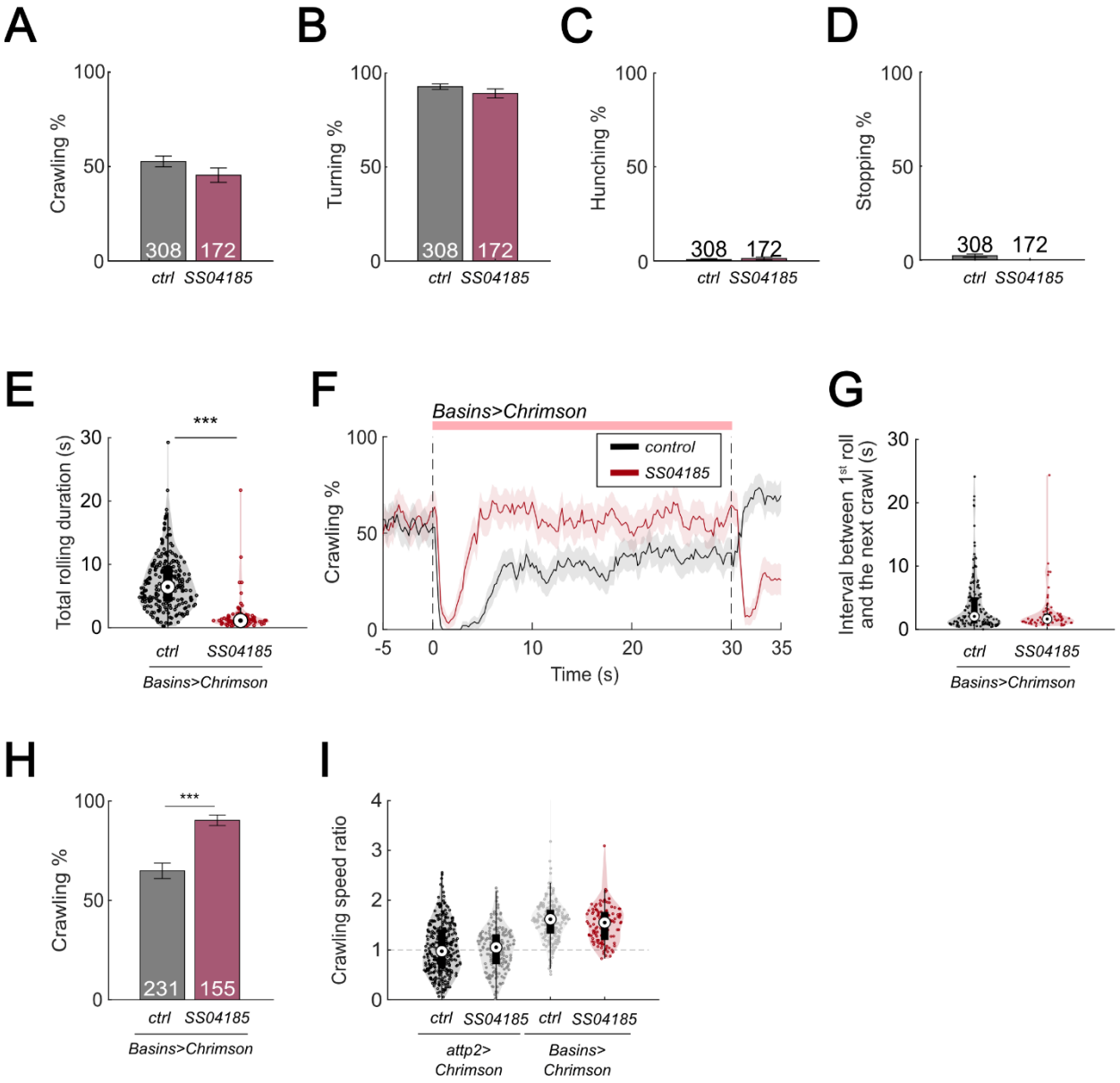


**Figure S1-1. SS04185 inhibits rolling**

(A) Crawling probabilities of larvae with the activation of SS04185-expressing neurons. Error bars, 95% confidence interval. Genotypes: *20xUAS-IVS-CsChrimson::mVenus/+;;* (black); *20xUAS-IVS-CsChrimson::mVenus/+; R54B01-Gal4.AD/+; R46E07-Gal4.DBD/+* (red). Genotypes in (B-D) are the same as shown here. n = 308, 172. Statistics: Chi-square test, $\chi^2 = 2.32$, $p > 0.05$.

(B) Turning probabilities of larvae with activation of SS04185-expressing neurons. Error bars, 95% confidence interval. n = 308, 172. Statistics: Chi-square test, $\chi^2 = 1.77$, $p > 0.05$.

(C) Hunching probabilities of larvae with activation of SS04185-expressing neurons. Error bars, 95% confidence interval. n = 308, 172. Statistics: Chi-square test, $\chi^2 = 0.35$, $p > 0.05$.

(D) Stopping probabilities of larvae with activation of SS04185-expressing neurons. Error bars, 95% confidence interval. n = 308, 172. Statistics: Chi-square test, $\chi^2 = 3.97$, $p = 0.046$.

(E) A violin plot of total time spent rolling for each individual larva during stimulation. Statistics: Mann-Whitney test, $p < 0.001$, n = 225, 89.

(F) Time series of crawling probabilities of SS04185 and Basin coactivation larvae (green) and Basin activation only larvae (black). Shaded areas show 95% confidential intervals of the crawling probabilities. Dashed lines display the window of optogenetic stimulation. Genotypes: *20xUAS-IVS-CsChrimson::mVenus/+; +; R72F11-Gal4/+* (control); *20xUAS-IVS-CsChrimson::mVenus/+; R54B01-Gal4.AD/+; R46E07-Gal4.DBD/R72F11-Gal4* (SS04185). Genotypes in (G-H) are the same as mentioned here. n = 228, 124.

(G) A violin plot of interval between first roll and next crawl. Statistics: Mann-Whitney test, $p > 0.05$, n = 151, 74.

(H) Crawling probabilities of SS04185 and Basin coactivation larvae (red) and Basin activation only larvae (black). Error bars, 95% confidence interval. n = 228, 124. Statistics: Chi-square test, $\chi^2 = 28.36$, $p < 0.001$.

(I) A violin plot of crawling speed ratio of larvae with null, SS04185 neuron, Basin, SS04185 neuron and Basin activation (from left to right). Crawling speed ratio = crawling speed 5 to 10 s after stimulation onset / crawling speed 0 to 5 s before stimulation onset. Statistics: Kruskal-Wallis test: H = 144, $p < 0.001$; Bonferroni corrected Mann-Whitney test: $p > 0.05$ for two groups on the

left and two groups on the right. n = 308, 172, 227, 124. Genotypes from left to right: 1) *20xUAS-IVS-CsChrimson::mVenus/+;;* ; 2) *20xUAS-IVS-CsChrimson::mVenus/+; R54B01-Gal4.AD/+; R46E07-Gal4.DBD/+*; 3) *20xUAS-IVS-CsChrimson::mVenus/+;; R72F11-Gal4/+*; 4) *20xUAS-IVS-CsChrimson::mVenus/+; R54B01-Gal4.AD/+; R46E07-Gal4.DBD/R72F11-Gal4.*

$^{**}p < 0.01$, $^{***}p < 0.001$.

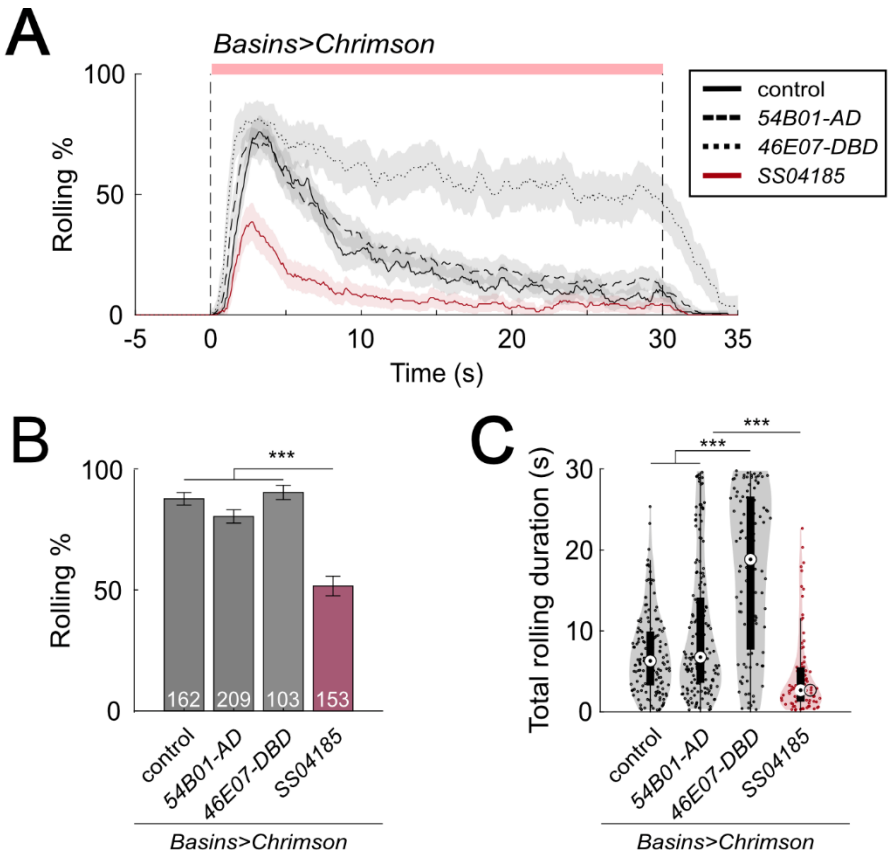


**Figure S1-2. SS04185 inhibits rolling**

(A) Time series of rolling probabilities of larvae during co-activation of SS04185 and Basins (red) and activation of Basins alone (black). Shaded areas represent 95% confidential intervals for rolling probabilities. The red bar and vertical dashed lines denote the optogenetic stimulation window. Genotypes: 1) *20xUAS-IVS-CsChrimson::mVenus/+; ; R72F11-Gal4/+* (control), 2) *20xUAS-IVS-CsChrimson::mVenus/+; R54B01-Gal4.AD/+; R72F11-Gal4/+* (54B01-AD), 3) *20xUAS-IVS-CsChrimson::mVenus/+; ; R72F11-Gal4/ R46E07-Gal4.DBD* (46E07-DBD), 4) *20xUAS-IVS-CsChrimson::mVenus/+; R54B01-Gal4.AD/+; R46E07-Gal4.DBD/ R72F11-Gal4* (SS04185). Genotypes in (B)-(C) are the same as mentioned here. n = 162, 209, 103, 153.

(B) Rolling probabilities of larvae plotted in (A) in the first 5s of stimulation. Error bars represent the 95% confidence interval. n = 162, 209, 103, 153 from left to right. Statistics: Chi-square test,

$\chi^2 = 6.66$, $p > 0.05$ for the left three groups and $\chi^2 = 72.52$, $p < 0.001$ for the comparison between the left three groups and the SS04185 group.

(C) A violin plot of total time spent rolling for each individual larva during stimulation. Statistics: Kruskal-Wallis test: H = 105.99, $p < 0.001$; Bonferroni-corrected Mann-Whitney test, $p > 0.05$ for the comparison between control and 54B01-AD; $p < 0.001$ for all other pair-wise comparisons, n = 151, 172, 100, 86.

$^{**}p < 0.01$, $^{***}p < 0.001$.

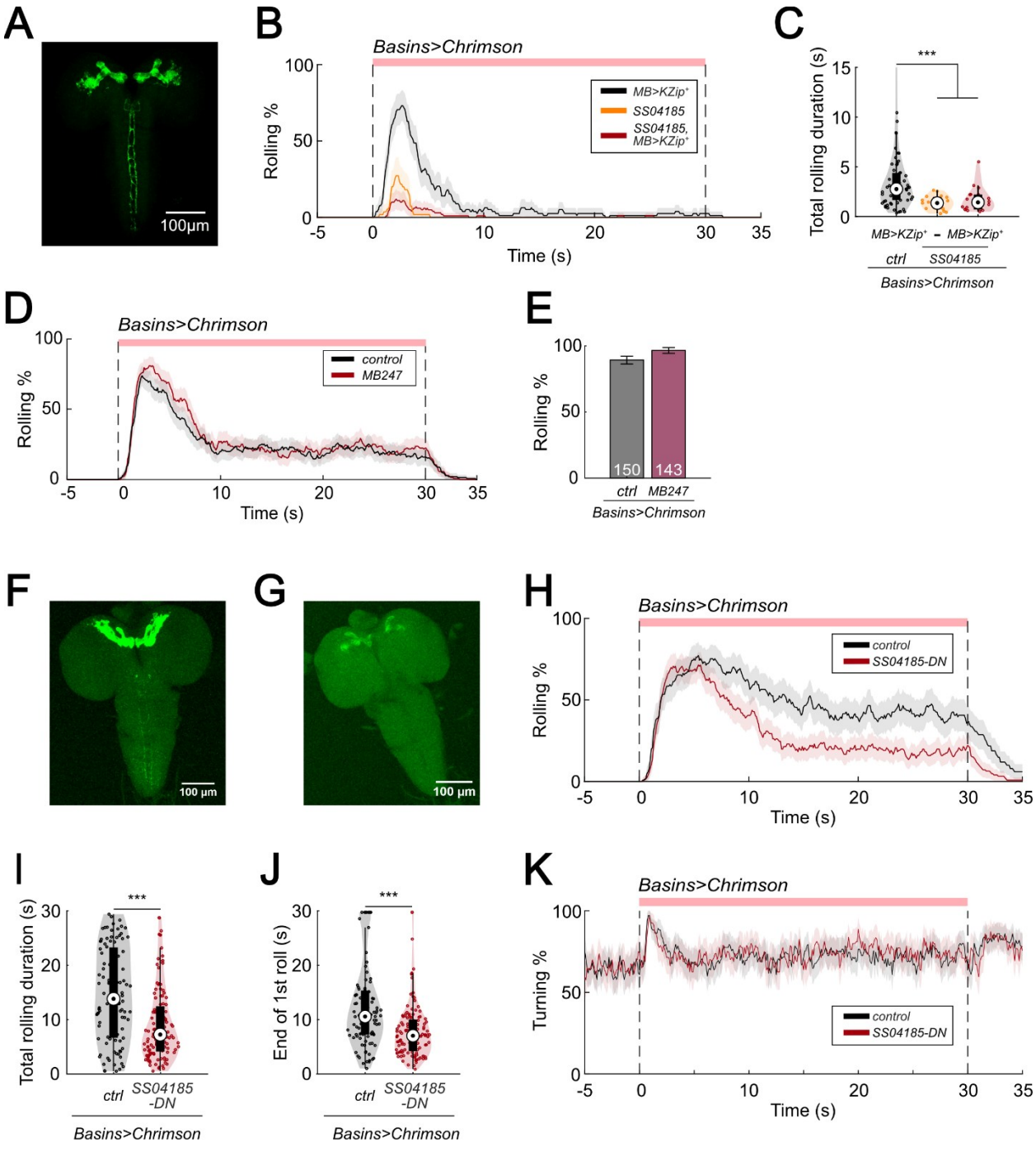


**Figure S2. SS04185-DN inhibits rolling**

(A) Morphology of SS04185 neurons with split Gal4 inhibition in mushroom body (MB). GFP, Green. Anterior, up; dorsal view; scale bar, 100 μm. Genotype: *20xUAS-IVS-*

*CsChrimson::mVenus/+; R13F02-LexA,LexAop-KZip$^{+}$/R54B01-Gal4.AD; R72F11-Gal4/R46E07-Gal4.DBD.*

(B) Time series of rolling probabilities of larvae with split Gal4 inhibition in MB (black), SS04185 activation (orange), and both SS04185 activation and split Gal4 inhibition in MB (red). Shaded areas show 95% confidential intervals of rolling probabilities. The red bar and dashed lines display the window of optogenetic stimulation. Genotypes: *20xUAS-IVS-CsChrimson::mVenus/+; R13F02-LexA,LexAop-KZip$^{+}$/+; R72F11-Gal4/+* (black); *20xUAS-IVS-CsChrimson::mVenus/+; R54B01-Gal4.AD/+; R46E07-Gal4.DBD/R72F11-Gal4* (orange); *20xUAS-IVS-CsChrimson::mVenus/+; R13F02-LexA,LexAop-KZip$^{+}$/R54B01-Gal4.AD; R72F11-Gal4/R46E07-Gal4.DBD* (red). Genotypes in (C) are the same as mentioned here.

(C) A violin plot of total time spent rolling for each individual larva during stimulation. Statistics: Kruskal-Wallis test: H = 21.05, $p < 0.001$; Bonferroni-corrected Mann-Whitney test, $p > 0.05$ for the two groups with SS04185 expression; $p < 0.001$ for the comparison between the group without SS04185 expression and the two groups with SS04185 expression, n = 66, 17, 21 from left to right.

(D) Time series of rolling probabilities of larvae with Basin activation (black), or Basin and MB coactivation (red). The red bar and dashed lines display the window of optogenetic stimulation eliciting larval escape responses. Shaded areas show 95% confidential intervals of rolling probabilities. n = 150, 143. Genotype: *20xUAS-IVS-CsChrimson::mVenus/+; +; R72F11-Gal4/+* (control); *20xUAS-IVS-CsChrimson::mVenus/+;+; MB247-Gal4/R72F11-Gal4* (MB247). Genotypes in (E) are the same as mentioned here.

(E) Binned larval rolling probabilities during the first 5 s of stimulation in (D). Error bars, 95% confidence interval. n = 150, 143. Statistics: Chi-square test, $\chi^2 = 3.80$, $p > 0.05$.

(F) and (G) show immunostaining of SS04185-expressing neurons. SS04185, Green. Anterior, up; dorsal view; scale bar, 100 μm Genotype: *w+, hs(KDRT.stop)FLP/13xLexAop2-IVS-CsChrimson::tdTomato; R54B01-Gal4.AD/72F11-LexA; 20xUAS-FRT(stop)-CsChrimson::mVenus/R46E07-Gal4.DB.* Genotypes in (H-K) are the same as mentioned here. (F) has both SS04185-DN and SS04185-MB expression only, and (G) has SS04185-MB expression.

(H) Time series of rolling probabilities of larvae with SS04185-MB activation (black), or SS04185-MB and SS04185-DN coactivation (red). The red bar and dashed lines display the window of optogenetic stimulation eliciting larval escape responses. Shaded areas show 95% confidential intervals of rolling probabilities.

(I) A violin plot of total time spent rolling for each individual larva during stimulation. Statistics: Mann-Whitney test, $p < 0.001$, n = 99, 124.

(J) A violin plot of end of first rolling bout for each larva during stimulation. Statistics: Mann-Whitney test, $p < 0.001$, n = 99, 124.

(K) Time series of turning probabilities of larvae with SS04185-MB activation (black), or SS04185-MB and SS04185-DN coactivation (red). The red bar and dashed lines display the window of optogenetic stimulation eliciting larval escape responses. Shaded areas show 95% confidential intervals of turning probabilities.

$^{**}p < 0.01$, $^{***}p < 0.001$.

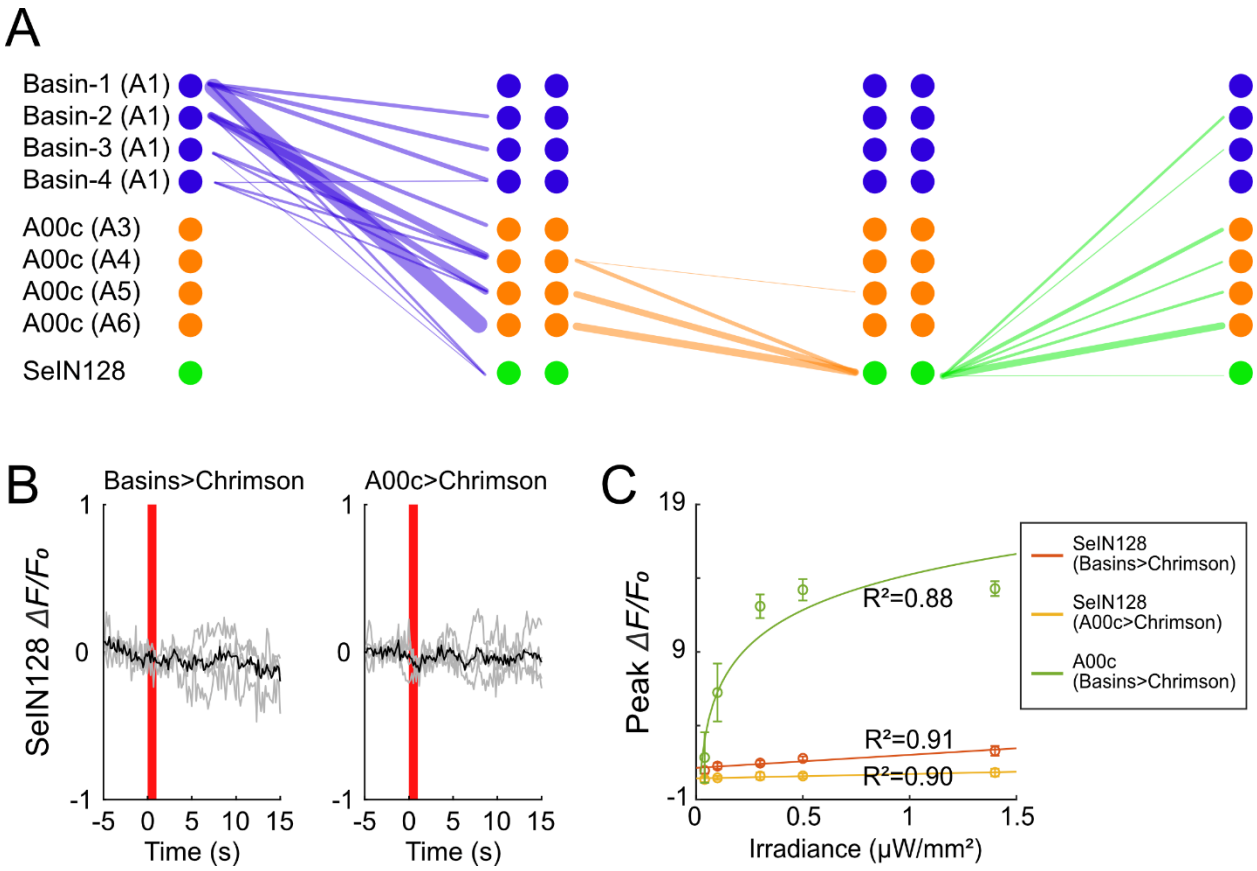


**Figure S4-1. SeIN128 is downstream of Basin and A00c neurons**

(A) Connectivity among Basin, A00c, and SeIN128. Each line represents synaptic connections from the pre-synaptic neurons (left) to the post-synaptic neurons (right). Line widths are proportional to the counts of the synapses.

(B) SeIN128 does not respond to light stimulation when all-trans retinal is not fed. Calcium transients, $\Delta F/F_0$ traces of GCaMP6s in SeIN128 axons (black line, mean; gray line, single larva) during 610-nm optogenetic activation of Basins at various intensities. Vertical gray line represents optogenetic activation. The shaded gray area indicates the period of optogenetic activation (0 to 1 s). Irradiance, 1.4 μW/mm$^2$. n=4. Genotype: *w; R72F11-LexA (left panel) or R71A10-LexA (right panel) /R54B01-Gal4.AD; 13xLexAop2-IVS-CsChrimson::tdTomato, 20xUAS-IVS-GCaMP6s/R46E07-Gal4.DBD.*

(C) Peak $\Delta F/F_0$ increased with increasing irradiance in both SeIN128 and A00c neurons. The orange line corresponds with Figure 4B; yellow line corresponds with Figure 4C; and green line corresponds with Figure 4D.

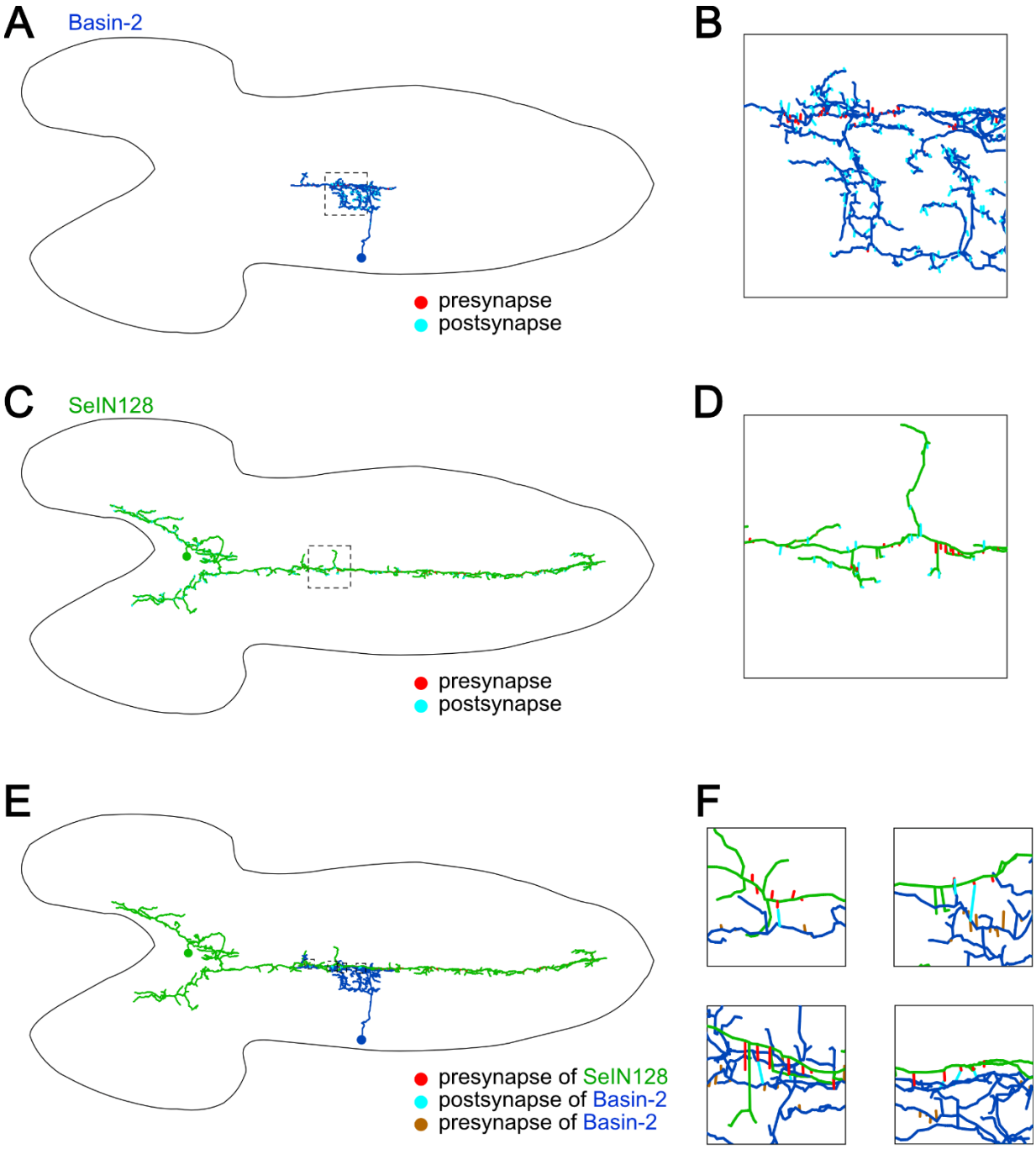
A
Basin-2
presynapse
postsynapse
B
C
SeIN128
presynapse
postsynapse
D
E
presynapse of SeIN128
postsynapse of Basin-2
presynapse of Basin-2
F
G
0.5μm

**Figure S4-2. Synapses from SeIN128 to Basin-2 are located near Basin-2 outputs**

(A) Basin-2 morphology and cell body location reported in EM reconstruction dataset (A1, left hemi-segment). Dorsal view. Red lines, presynaptic sites; cyan lines, postsynaptic sites.

(B) A zoomed-in view of the square in (A).

(C) SeIN128 morphology and cell body location reported in EM reconstruction dataset (right). Dorsal view. Red lines, presynaptic sites; cyan lines, postsynaptic sites.

(D) A zoomed-in view of the square in (C).

(E) Connections between SeIN128 and Basin-2. Dorsal view. Red lines, presynaptic sites of SeIN128; cyan lines, postsynaptic sites of Basin-2; brown lines, presynaptic sites of Basin-2.

(F) Zoomed-in views of squares in (E).

(G) EM view of left top panel in (F). Green, SeIN128. Blue, Basin-2. White arrows show SeIN128 presynaptic sites adjacent to Basin-2. Yellow arrows are two presynaptic sites of Basin-2.

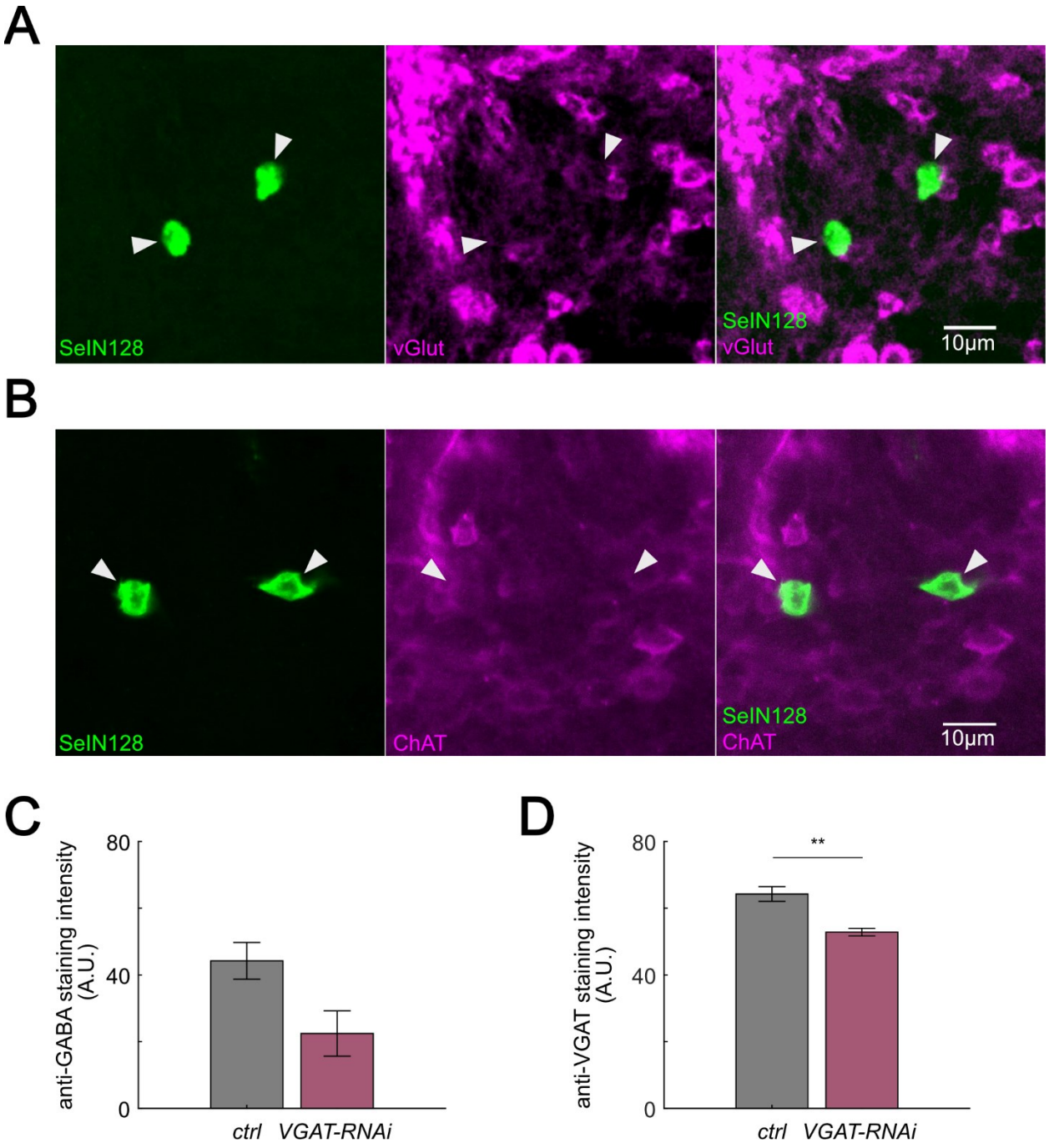


**Figure S5. SeIN128 is GABAergic**

(A) Immunostaining of SeIN128 cell body (green) and glutamatergic neuron (magenta). Genotype: *10xUAS-IVS-myr::GFP/+; R54B01-Gal4.AD/+; R46E07-Gal4.DBD/+*.

(B) Immunostaining of SeIN128 cell body (green) and cholinergic neuron (magenta). Genotype: *10xUAS- IVS-myr::GFP/+; R54B01-Gal4.AD/+; R46E07-Gal4.DBD/+*.

In (A)-(B), white triangles indicate locations of SeIN128 cell bodies. Anterior, up; dorsal view; scale bar, 10 μm.

(C) Anti-GABA fluorescence intensities in the neuropil in A4-A6 segments. A.U., arbitrary unit. Genotype: *w; ; R57C10-Gal4 /+* (black) and *w; ; R57C10-Gal4 /UAS-HMS02355* (red). Statistics: Student's t test, $p = 0.040$, n = 5, 4.

(D) Anti-VGAT fluorescence intensities in the neuropil in A4-A6 segments. A.U., arbitrary unit. Genotype: *w; ; R57C10-Gal4 /+* (black) and *w; ; R57C10-Gal4 /UAS-HMS02355* (red). Statistics: Student's t test, $p = 0.0031$, n = 6, 5.

**$p < 0.01$.

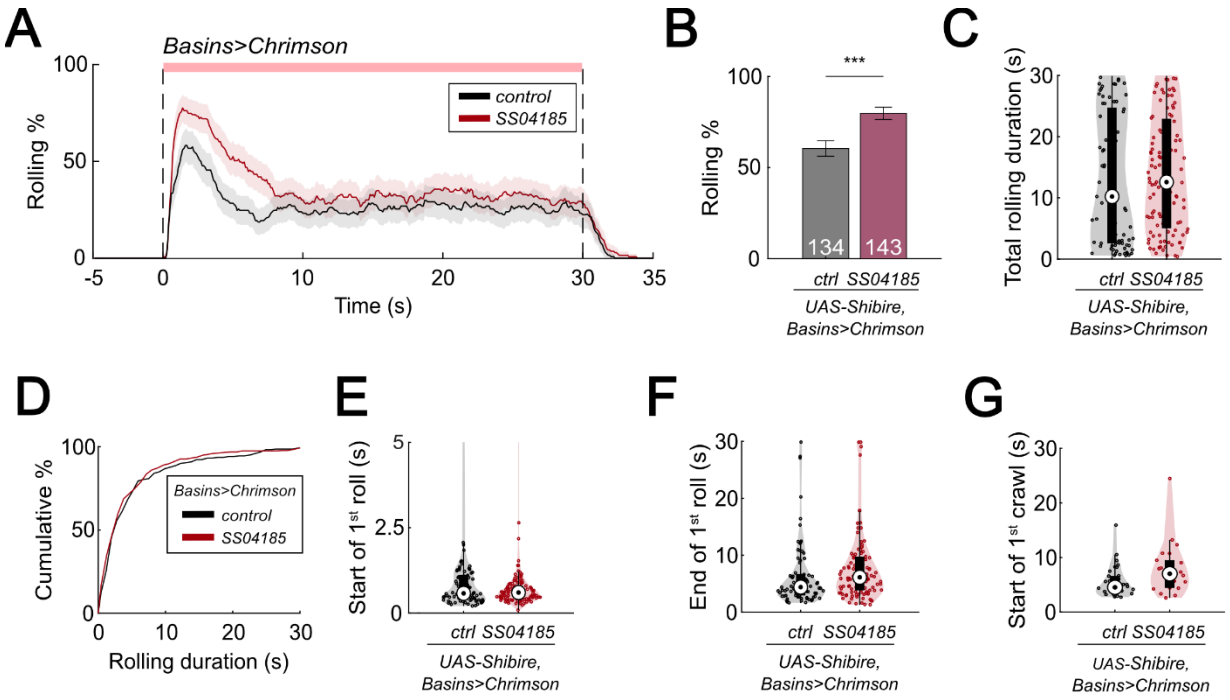


**Figure S6. SeIN128 inhibition enhances rolling**

(A) Time series of rolling probabilities of larvae with Basin activation (black), or SS04185 inhibition and Basin activation (red). Larvae were incubated with heat to trigger the effect of shibire$^{ts1}$. The red bar and dashed lines display the window of optogenetic stimulation eliciting larval escape responses. Shaded areas show 95% confidential intervals of rolling probabilities. Genotypes: *13xLexAop2-IVS-CsChrimson::mVenus;R72F11-LexA/+; 20xUAS-TTS-Shibire/+* (black); *13xLexAop2-IVS-CsChrimson::mVenus; R72F11-LexA/R54B01-Gal4.AD; 20xUAS-TTS-Shibire/R46E07-Gal4.DBD* (red). Genotypes in (B-G) are the same as mentioned here.

(B) Binned larval rolling probabilities during first 5 s of stimulation in (A). Error bars, 95% confidence interval. n = 134, 143. Statistics: Chi-square test, $\chi^2 = 12.33$, $p < 0.001$.

(C) A violin plot of total time spent rolling for each individual larva during stimulation. Statistics: Mann-Whitney test, $p > 0.05$, n = 85, 115.

(D) Cumulative plot of rolling duration. Statistics: Mann-Whitney test, $p > 0.05$, n = 219, 352.

(E) A violin plot of start of first rolling bout for each larva during stimulation. Statistics: Mann-Whitney test, $p > 0.05$, n = 85, 115.

(F) A violin plot of end of first rolling bout for each larva during stimulation. Statistics: Mann-Whitney test, $p = 0.013$, n = 85, 115.

(G) A violin plot of start of first crawling bout for each larva during stimulation. Statistics: Mann-Whitney test, $p = 0.034$, n = 32, 22.

$^{**}p < 0.01$, $^{***}p < 0.001$.

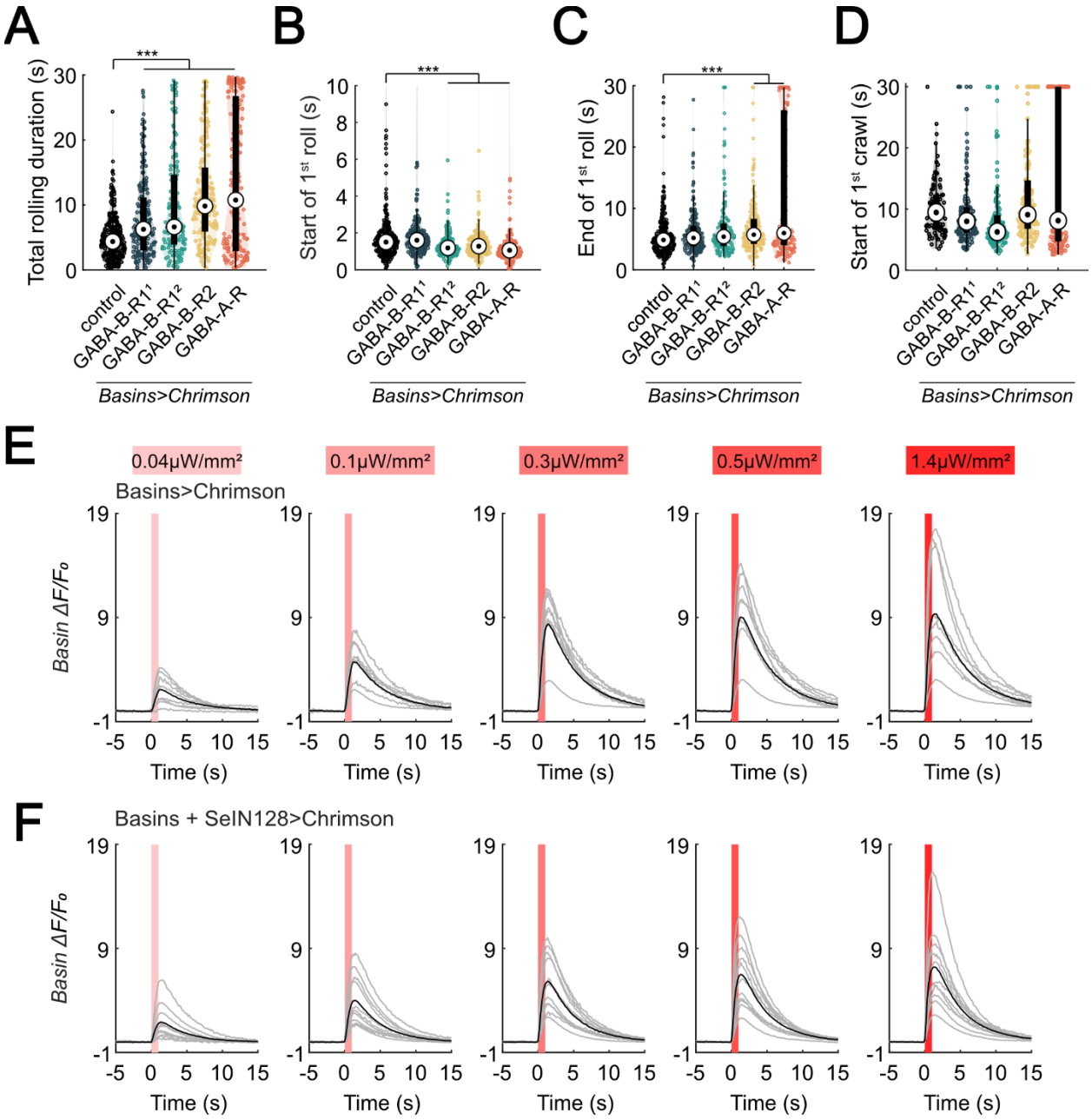


**Figure S7. SeIN128 sends feedback inhibition to Basins**

(A) A violin plot of total time spent rolling for each individual larva with GABAR-RNAi in their Basin neurons during stimulation. Statistics: Kruskal-Wallis test: H = 110.86, $p < 0.001$; Bonferroni-corrected Mann-Whitney test, $p < 0.001$ for all RNAi groups, n = 271, 194, 154, 178, 174 from left to right. The genotypes are *20xUAS-IVS-CsChrimson::mVenus/+; ; R72F11-Gal4/+* (black), *20xUAS—IVS-CsChrimson::mVenus/+; ; R72F11-Gal4/UAS-HMC03388* (blue),

*20xUAS-IVS-CsChrimson::mVenus/+; ; R72F11-Gal4/UAS-JF02989* (green), *20xUAS-IVS-CsChrimson::mVenus/+; ; R72F11-Gal4/UAS-HMC02975* (yellow), and *20xUAS-IVS-CsChrimson::mVenus/+; ; R72F11-Gal4/UAS-HMC03643* (orange). Genotypes in (B-D) are the same as mentioned here.

(B) A violin plot of start of first rolling bout for each larva during stimulation. Statistics: Kruskal-Wallis test: H = 86.50, $p < 0.001$; Bonferroni-corrected Mann-Whitney test, $p < 0.001$ for GABA-B-R1$^2$, GABA-B-R2, and GABA-A-R groups, n = 271, 194, 154, 178, 174 from left to right.

(C) A violin plot of end of first rolling bout for each larva during stimulation. Statistics: Kruskal-Wallis test: H=36.01, $p < 0.001$; Bonferroni-corrected Mann-Whitney test, $p < 0.001$ for GABA-B-R2 and GABA-A-R groups, n = 271, 194, 154, 178, 174 from left to right.

(D) A violin plot of start of first crawling bout for each larva during stimulation. Statistics: Kruskal-Wallis test: H = 53.07, $p < 0.001$; Bonferroni-corrected Mann-Whitney test, $p < 0.001$ for GABA-B-R1$^2$ group, n = 89, 119, 139, 135, 137 from left to right.

(E) Calcium transients (mean ± s.e.m.) represented by $\Delta F/F_0$ are evoked in Basin axons by optogenetic activation of Basin neurons various intensities. N = 9. Genotype: *20xUAS-Syn21-opGCaMP6s,10XUAS-Syn21-CsChrimson88::tdTomato/+;CyO/+;TM6/R72F11-Gal4*.

(F) Calcium transients (mean ± s.e.m.) in Basin axons represented by $\Delta F/F_0$ are decreased by optogenetic activation of SeIN128 neurons at various intensities. N = 10. Genotype: *20xUAS-Syn21-opGCaMP6s,10XUAS-Syn21-CsChrimson88::tdTomato/+;CyO/R54B01-Gal4.AD;R72F11-Gal4/R46E07-Gal4.DBD*.

For (E) to (F), irradiances from left to right are 0.04, 0.1, 0.3, 0.5, and 1.4 μW/mm$^2$. For each irradiance, individual traces are shown with gray lines, whereas the average of individuals is shown in black. Shaded gray area denotes period of optogenetic activation (0 to 1 s).

$^{**}p < 0.01$, $^{***}p < 0.001$.

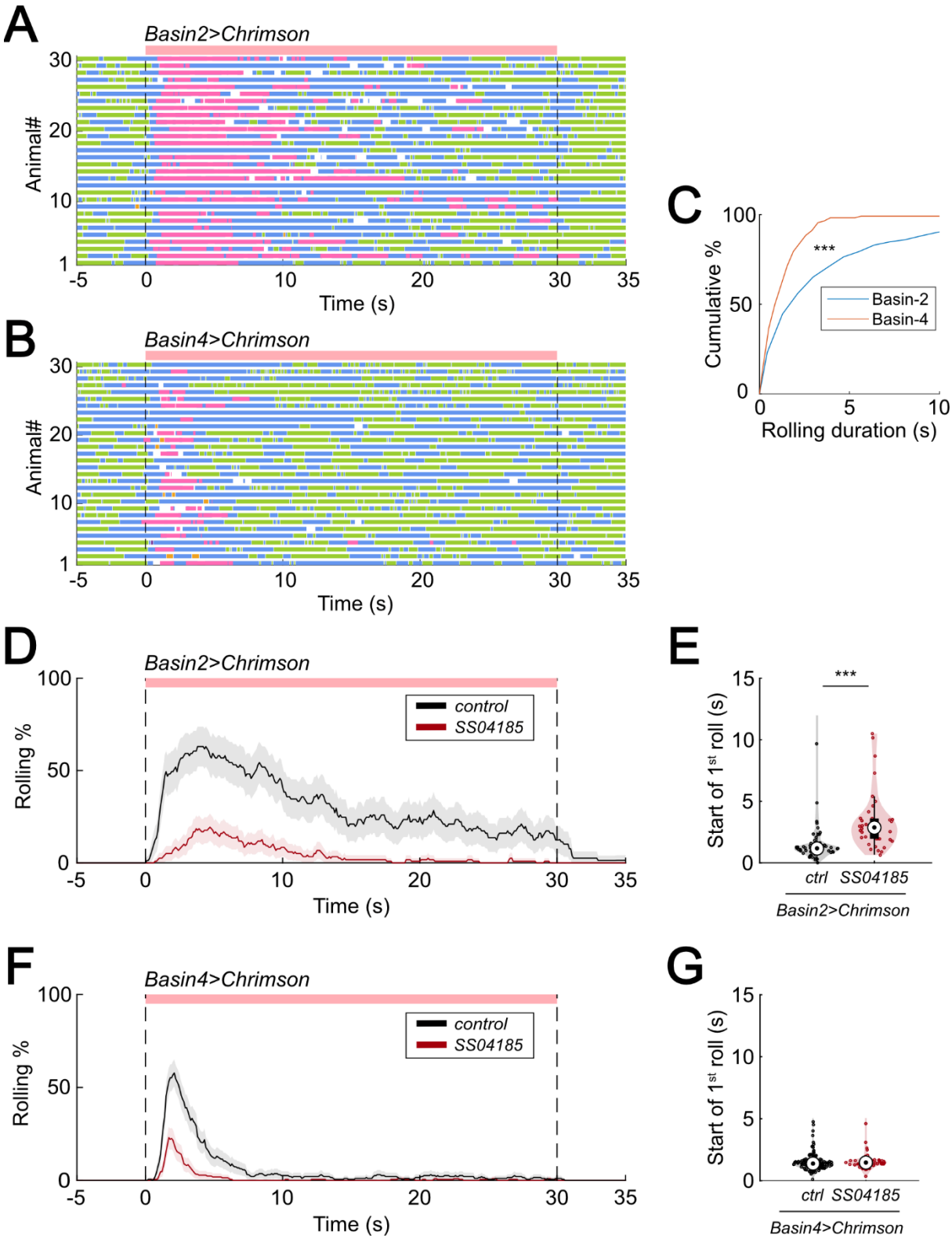


**Figure S8. SeIN128 inhibits rolling elicited by both Basin-2 and Basin-4 activation.**

(A) and (B) show ethograms of Basin-2 activation (A) and Basin-4 activation (B). Each row represents an individual larva. Pink, blue, green, orange, and purple lines represent bouts of rolling, turning, crawling, backward crawling, and hunching. The red bar and dashed lines denote the time window during the period of neural activation. Genotypes: *20xUAS-IVS-CsChrimson::mVenus/+; R72F11-Gal4.AD/+; R38H09-Gal4.DBD/+* (A); *20xUAS-IVS-CsChrimson::mVenus/+; R72F11-Gal4.AD/+; R57F07-Gal4.DBD/+* (B). Genotypes in (C) are the same as mentioned here.

(C) Cumulative plot of rolling duration. Statistics: Mann-Whitney test, $p < 0.001$, n = 681, 141.

(D) Time series of rolling probabilities of larvae with Basin-2 activation (black), or SS04185 and Basin-2 coactivation (red). The red bar and dashed lines display the window of optogenetic stimulation eliciting larval escape responses. Shaded areas show 95% confidential intervals of rolling probabilities. Genotypes: *20xUAS-IVS-CsChrimson::mVenus/+; R72F11-Gal4.AD/+; R38H09-Gal4.DBD/+* (black); *20xUAS-IVS-CsChrimson::mVenus/+; R72F11-Gal4.AD/R54B01-Gal4.AD; R38H09-Gal4.DBD/R46E07-Gal4.DBD* (red). Genotypes in (E) are the same as mentioned here.

(E) A violin plot of start of first rolling bout for each larva during stimulation. Statistics: Mann-Whitney test, $p < 0.001$, n = 57, 38.

(F) Time series of rolling probabilities of larvae with Basin-4 activation (black), or SS04185 and Basin-4 coactivation (red). The red bar and dashed lines display the window of optogenetic stimulation eliciting larval escape responses. Shaded areas show 95% confidential intervals of rolling probabilities. Genotypes: *20xUAS-IVS-CsChrimson::mVenus/+; R72F11-Gal4.AD/+; R57F07-Gal4.DBD/+* (black); *20xUAS-IVS-CsChrimson::mVenus/+; R72F11-Gal4.AD/R54B01-Gal4.AD; R57F07-Gal4.DBD/R46E07-Gal4.DBD* (red). Genotypes in (G) are the same as mentioned here.

(G) A violin plot of start of first rolling bout for each larva during stimulation. Statistics: Mann-Whitney test, $p > 0.05$, n = 129, 61.

$^{**}p < 0.01$, $^{***}p < 0.001$.

**References**


Burgos, A., Honjo, K., Ohyama, T., Qian, C. S., Shin, G. J., Gohl, D. M., Silies, M., Tracey, W. D., Zlatic, M., Cardona, A., & Grueber, W. B. (2018). Nociceptive interneurons control modular motor pathways to promote escape behavior in Drosophila. *Elife*, *7*. https://doi.org/10.7554/eLife.26016

Burrell, B. D. (2017). Comparative biology of pain: What invertebrates can tell us about how nociception works. *J Neurophysiol*, *117*(4), 1461-1473. https://doi.org/10.1152/jn.00600.2016

Campagner, D., Vale, R., Tan, Y. L., Iordanidou, P., Pavon Arocas, O., Claudi, F., Stempel, A. V., Keshavarzi, S., Petersen, R. S., Margrie, T. W., & Branco, T. (2023). A cortico-collicular circuit for orienting to shelter during escape. *Nature*, *613*(7942), 111-119. https://doi.org/10.1038/s41586-022-05553-9

Cattaert, D., & El Manira, A. (1999). Shunting versus inactivation: analysis of presynaptic inhibitory mechanisms in primary afferents of the crayfish. *J Neurosci*, *19*(14), 6079-6089. https://doi.org/10.1523/JNEUROSCI.19-14-06079.1999

Chalfie, M., & Sulston, J. (1981). Developmental genetics of the mechanosensory neurons of Caenorhabditis elegans. *Dev Biol*, *82*(2), 358-370. https://doi.org/10.1016/0012-1606(81)90459-0

Chalfie, M., Sulston, J. E., White, J. G., Southgate, E., Thomson, J. N., & Brenner, S. (1985). The neural circuit for touch sensitivity in Caenorhabditis elegans. *J Neurosci*, *5*(4), 956-964. https://doi.org/10.1523/JNEUROSCI.05-04-00956.1985

Chin, M. R., & Tracey, W. D., Jr. (2017). Nociceptive Circuits: Can't Escape Detection. *Curr Biol*, *27*(16), R796-R798. https://doi.org/10.1016/j.cub.2017.07.031

Dason, J. S., Cheung, A., Anreiter, I., Montemurri, V. A., Allen, A. M., & Sokolowski, M. B. (2020). Drosophila melanogaster foraging regulates a nociceptive-like escape behavior through a developmentally plastic sensory circuit. *Proc Natl Acad Sci U S A*, *117*(38), 23286-23291. https://doi.org/10.1073/pnas.1820840116

Dolan, M. J., Luan, H., Shropshire, W. C., Sutcliffe, B., Cocanougher, B., Scott, R. L., Frechter, S., Zlatic, M., Jefferis, G., & White, B. H. (2017). Facilitating Neuron-Specific Genetic Manipulations in Drosophila melanogaster Using a Split GAL4 Repressor. *Genetics*, *206*(2), 775-784. https://doi.org/10.1534/genetics.116.199687

Guo, D., & Hu, J. (2014). Spinal presynaptic inhibition in pain control. *Neuroscience*, *283*, 95-106. https://doi.org/10.1016/j.neuroscience.2014.09.032

Hu, C., Petersen, M., Hoyer, N., Spitzweck, B., Tenedini, F., Wang, D., Gruschka, A., Burchardt, L. S., Szpotowicz, E., Schweizer, M., Guntur, A. R., Yang, C. H., & Soba, P. (2017). Sensory integration and neuromodulatory feedback facilitate Drosophila

mechanonociceptive behavior. *Nat Neurosci*, *20*(8), 1085-1095. https://doi.org/10.1038/nn.4580

Hu, Y., Wang, C., Yang, L., Pan, G., Liu, H., Yu, G., & Ye, B. (2020). A Neural Basis for Categorizing Sensory Stimuli to Enhance Decision Accuracy. *Curr Biol*, *30*(24), 4896-4909 e4896. https://doi.org/10.1016/j.cub.2020.09.045

Hwang, R. Y., Zhong, L., Xu, Y., Johnson, T., Zhang, F., Deisseroth, K., & Tracey, W. D. (2007). Nociceptive neurons protect Drosophila larvae from parasitoid wasps. *Curr Biol*, *17*(24), 2105-2116. https://doi.org/10.1016/j.cub.2007.11.029

Im, S. H., & Galko, M. J. (2012). Pokes, sunburn, and hot sauce: Drosophila as an emerging model for the biology of nociception. *Dev Dyn*, *241*(1), 16-26. https://doi.org/10.1002/dvdy.22737

Imambocus, B. N., Zhou, F., Formozov, A., Wittich, A., Tenedini, F. M., Hu, C., Sauter, K., Macarenhas Varela, E., Heredia, F., Casimiro, A. P., Macedo, A., Schlegel, P., Yang, C. H., Miguel-Aliaga, I., Wiegert, J. S., Pankratz, M. J., Gontijo, A. M., Cardona, A., & Soba, P. (2022). A neuropeptidergic circuit gates selective escape behavior of Drosophila larvae. *Curr Biol*, *32*(1), 149-163 e148. https://doi.org/10.1016/j.cub.2021.10.069

Isaacson, J. S., & Scanziani, M. (2011). How inhibition shapes cortical activity. *Neuron*, *72*(2), 231-243. https://doi.org/10.1016/j.neuron.2011.09.027

Kabra, M., Robie, A. A., Rivera-Alba, M., Branson, S., & Branson, K. (2013). JAABA: interactive machine learning for automatic annotation of animal behavior. *Nat Methods*, *10*(1), 64-67. https://doi.org/10.1038/nmeth.2281

Kaneko, T., Macara, A. M., Li, R., Hu, Y., Iwasaki, K., Dunnings, Z., Firestone, E., Horvatic, S., Guntur, A., Shafer, O. T., Yang, C. H., Zhou, J., & Ye, B. (2017). Serotonergic Modulation Enables Pathway-Specific Plasticity in a Developing Sensory Circuit in Drosophila. *Neuron*, *95*(3), 722. https://doi.org/10.1016/j.neuron.2017.07.023

Kapfer, C., Glickfeld, L. L., Atallah, B. V., & Scanziani, M. (2007). Supralinear increase of recurrent inhibition during sparse activity in the somatosensory cortex. *Nat Neurosci*, *10*(6), 743-753. https://doi.org/10.1038/nn1909

Manoim, J. E., Davidson, A. M., Weiss, S., Hige, T., & Parnas, M. (2022). Lateral axonal modulation is required for stimulus-specific olfactory conditioning in Drosophila. *Curr Biol*, *32*(20), 4438-4450 e4435. https://doi.org/10.1016/j.cub.2022.09.007

Masson, J. B., Laurent, F., Cardona, A., Barre, C., Skatchkovsky, N., Zlatic, M., & Jovanic, T. (2020). Identifying neural substrates of competitive interactions and sequence transitions during mechanosensory responses in Drosophila. *PLoS Genet*, *16*(2), e1008589. https://doi.org/10.1371/journal.pgen.1008589

McGann, J. P. (2013). Presynaptic inhibition of olfactory sensory neurons: new mechanisms and potential functions. *Chem Senses*, *38*(6), 459-474. https://doi.org/10.1093/chemse/bjt018

Nakamizo-Dojo, M., Ishii, K., Yoshino, J., Tsuji, M., & Emoto, K. (2023). Descending GABAergic pathway links brain sugar-sensing to peripheral nociceptive gating in Drosophila. *Nat Commun*, *14*(1), 6515. https://doi.org/10.1038/s41467-023-42202-9

Nern, A., Pfeiffer, B. D., & Rubin, G. M. (2015). Optimized tools for multicolor stochastic labeling reveal diverse stereotyped cell arrangements in the fly visual system. *Proc Natl Acad Sci U S A*, *112*(22), E2967-2976. https://doi.org/10.1073/pnas.1506763112

Ohyama, T., Jovanic, T., Denisov, G., Dang, T. C., Hoffmann, D., Kerr, R. A., & Zlatic, M. (2013). High-throughput analysis of stimulus-evoked behaviors in Drosophila larva reveals multiple modality-specific escape strategies. *PLoS One*, *8*(8), e71706. https://doi.org/10.1371/journal.pone.0071706

Ohyama, T., Schneider-Mizell, C. M., Fetter, R. D., Aleman, J. V., Franconville, R., Rivera-Alba, M., Mensh, B. D., Branson, K. M., Simpson, J. H., Truman, J. W., Cardona, A., & Zlatic, M. (2015). A multilevel multimodal circuit enhances action selection in Drosophila. *Nature*, *520*(7549), 633-639. https://doi.org/10.1038/nature14297

Oikawa, I., Kondo, S., Hashimoto, K., Yoshida, A., Hamajima, M., Tanimoto, H., Furukubo-Tokunaga, K., & Honjo, K. (2023). A descending inhibitory mechanism of nociception mediated by an evolutionarily conserved neuropeptide system in Drosophila. *Elife*, *12*. https://doi.org/10.7554/eLife.85760

Oleson, E. B., Beckert, M. V., Morra, J. T., Lansink, C. S., Cachope, R., Abdullah, R. A., Loriaux, A. L., Schetters, D., Pattij, T., Roitman, M. F., Lichtman, A. H., & Cheer, J. F. (2012). Endocannabinoids shape accumbal encoding of cue-motivated behavior via CB1 receptor activation in the ventral tegmentum. *Neuron*, *73*(2), 360-373. https://doi.org/10.1016/j.neuron.2011.11.018

Onodera, K., Baba, S., Murakami, A., Uemura, T., & Usui, T. (2017). Small conductance Ca(2+)-activated K(+) channels induce the firing pause periods during the activation of Drosophila nociceptive neurons. *Elife*, *6*. https://doi.org/10.7554/eLife.29754

Palay, S. L. (1956). Synapses in the central nervous system. *J Biophys Biochem Cytol*, *2*(4 Suppl), 193-202. https://doi.org/10.1083/jcb.2.4.193

Pan-Vazquez, A., Wefelmeyer, W., Gonzalez Sabater, V., Neves, G., & Burrone, J. (2020). Activity-Dependent Plasticity of Axo-axonic Synapses at the Axon Initial Segment. *Neuron*, *106*(2), 265-276 e266. https://doi.org/10.1016/j.neuron.2020.01.037

Papadopoulou, M., Cassenaer, S., Nowotny, T., & Laurent, G. (2011). Normalization for sparse encoding of odors by a wide-field interneuron. *Science*, *332*(6030), 721-725. https://doi.org/10.1126/science.1201835

Patel, N. H. (1994). Imaging neuronal subsets and other cell types in whole-mount Drosophila embryos and larvae using antibody probes. *Methods Cell Biol*, *44*, 445-487. https://doi.org/10.1016/s0091-679x(08)60927-9

Peirs, C., & Seal, R. P. (2016). Neural circuits for pain: Recent advances and current views. *Science*, *354*(6312), 578-584. https://doi.org/10.1126/science.aaf8933

Pinault, D., Smith, Y., & Deschenes, M. (1997). Dendrodendritic and axoaxonic synapses in the thalamic reticular nucleus of the adult rat. *J Neurosci*, *17*(9), 3215-3233. https://doi.org/10.1523/JNEUROSCI.17-09-03215.1997

Ray, S., Aldworth, Z. N., & Stopfer, M. A. (2020). Feedback inhibition and its control in an insect olfactory circuit. *Elife*, *9*. https://doi.org/10.7554/eLife.53281

Schneider-Mizell, C. M., Bodor, A. L., Collman, F., Brittain, D., Bleckert, A., Dorkenwald, S., Turner, N. L., Macrina, T., Lee, K., Lu, R., Wu, J., Zhuang, J., Nandi, A., Hu, B., Buchanan, J., Takeno, M. M., Torres, R., Mahalingam, G., Bumbarger, D. J., . . . Costa, N. M. D. (2021). Structure and function of axo-axonic inhibition. *Elife*, *10*. https://doi.org/10.7554/eLife.73783

Stokes, C. C., & Isaacson, J. S. (2010). From dendrite to soma: dynamic routing of inhibition by complementary interneuron microcircuits in olfactory cortex. *Neuron*, *67*(3), 452-465. https://doi.org/10.1016/j.neuron.2010.06.029

Swierczek, N. A., Giles, A. C., Rankin, C. H., & Kerr, R. A. (2011). High-throughput behavioral analysis in C. elegans. *Nat Methods*, *8*(7), 592-598. https://doi.org/10.1038/nmeth.1625

Takagi, S., Cocanougher, B. T., Niki, S., Miyamoto, D., Kohsaka, H., Kazama, H., Fetter, R. D., Truman, J. W., Zlatic, M., Cardona, A., & Nose, A. (2017). Divergent Connectivity of Homologous Command-like Neurons Mediates Segment-Specific Touch Responses in Drosophila. *Neuron*, *96*(6), 1373-1387 e1376. https://doi.org/10.1016/j.neuron.2017.10.030

Tracey, W. D., Jr., Wilson, R. I., Laurent, G., & Benzer, S. (2003). painless, a Drosophila gene essential for nociception. *Cell*, *113*(2), 261-273. https://doi.org/10.1016/s0092-8674(03)00272-1

Veres, J. M., Fekete, Z., Muller, K., Andrasi, T., Rovira-Esteban, L., Barabas, B., Papp, O. I., & Hajos, N. (2023). Fear learning and aversive stimuli differentially change excitatory synaptic transmission in perisomatic inhibitory cells of the basal amygdala. *Front Cell Neurosci*, *17*, 1120338. https://doi.org/10.3389/fncel.2023.1120338

Vogt, K., Aso, Y., Hige, T., Knapek, S., Ichinose, T., Friedrich, A. B., Turner, G. C., Rubin, G. M., & Tanimoto, H. (2016). Direct neural pathways convey distinct visual information to Drosophila mushroom bodies. *Elife*, *5*. https://doi.org/10.7554/eLife.14009

Winding, M., Pedigo, B. D., Barnes, C. L., Patsolic, H. G., Park, Y., Kazimiers, T., Fushiki, A., Andrade, I. V., Khandelwal, A., Valdes-Aleman, J., Li, F., Randel, N., Barsotti, E., Correia, A., Fetter, R. D., Hartenstein, V., Priebe, C. E., Vogelstein, J. T., Cardona, A., & Zlatic, M. (2023). The connectome of an insect brain. *Science*, *379*(6636), eadd9330. https://doi.org/10.1126/science.add9330

Yoshimura, Y., & Callaway, E. M. (2005). Fine-scale specificity of cortical networks depends on inhibitory cell type and connectivity. *Nat Neurosci*, *8*(11), 1552-1559. https://doi.org/10.1038/nn1565

Yoshino, J., Morikawa, R. K., Hasegawa, E., & Emoto, K. (2017). Neural Circuitry that Evokes Escape Behavior upon Activation of Nociceptive Sensory Neurons in Drosophila Larvae. *Curr Biol*, *27*(16), 2499-2504 e2493. https://doi.org/10.1016/j.cub.2017.06.068

Zheng, Z., Lauritzen, J. S., Perlman, E., Robinson, C. G., Nichols, M., Milkie, D., Torrens, O., Price, J., Fisher, C. B., Sharifi, N., Calle-Schuler, S. A., Kmecova, L., Ali, I. J., Karsh, B., Trautman, E. T., Bogovic, J. A., Hanslovsky, P., Jefferis, G., Kazhdan, M., . . . Bock, D. D. (2018). A Complete Electron Microscopy Volume of the Brain of Adult Drosophila melanogaster. *Cell*, *174*(3), 730-743 e722. https://doi.org/10.1016/j.cell.2018.06.019

## CHAPTER 3 Comparative connectomics and escape behavior in larvae of closely related *Drosophila* species

Chapter 3 showcases how evolutionary comparative studies benefit behavioral neuroscience research in the animal model, *Drosophila* larval escape behavior. This manuscript investigated the escape rolling behavior in 12 *drosophilid* species. *D. santomea* was thus identified with an increased rolling response compared to *D. melanogaster*. By comparing their connectomes, this upregulated rolling might be attributed to enhanced nociceptive inputs projecting to Basin-1 and A27n. This phenotype was recapitulated with additional Basin-1 activation in *D. melanogaster*. Moreover, the crawling speed increased with extra Basin-1 activation, suggesting that this enhanced sensory input elevated the response level for both rolling and fast crawling in this rigid action sequence. This finding indicates that increased sensory input influences the overall escape sequence together, but it might not bias the balance between more specific escape responses (i.e., rolling vs. fast crawling).

**Title: Comparative connectomics and escape behavior in larvae of closely related *Drosophila* species**

**Authors:** Jiayi Zhu[1,2,7], Jean-Christophe Boivin[1,2,7], Song Pang[4,5], C. Shan Xu[4,6], Zhiyuan Lu[4], Stephan Saalfeld[4], Harald F. Hess[4], Tomoko Ohyama[1,3*]

[1] Department of Biology, McGill University, Docteur penfield, Montreal, QC, H3A 1B1, Canada

[2] Integrated Program of Neuroscience, Pine Ave. W., McGill University, Montreal, QC, H3A 1A1, Canada

[3]Alan Edwards Center for Research on Pain, McGill University, Unversity st., Montreal, QC, H3A 2B4, Canada

[4] Janelia Research Campus, Howard Hughes Medical Institute, Helix Drive, Ashburn, VA, 20147, USA

[5] Current address: Yale School of Medicine, Cedar St., New Haven, CT, 06510 USA

[6] Current address: Department of Cellular and Molecular Physiology, Yale School of Medicine, Cedar St., New Haven, CT, 06510 USA

[7] Equal contributions

*Correspondence: tomoko.ohyama@mcgill.ca

Lead Contact: Tomoko Ohyama (tomoko.ohyama@mcgill.ca)

**Summary**

Evolution has generated an enormous variety of morphological, physiological, and behavioral traits in animals. How do behaviors evolve in different directions in species equipped with similar neurons and molecular components? Here we adopted a comparative approach to investigate the similarities and differences of escape behaviors in response to noxious stimuli and their underlying neural circuits between closely related drosophilid species. Drosophilids show a wide range of escape behaviors in response to noxious cues, including escape crawling, stopping, head casting, and rolling. Here we find that *D. santomea*, compared with its close relative *D. melanogaster*, shows a higher probability of rolling in response to noxious stimulation. To assess whether this behavioral difference could be attributed to differences in neural circuitry, we generated focused ion beam–scanning electron microscope volumes of the ventral nerve cord of *D. santomea* to reconstruct the downstream partners of mdIV, a nociceptive sensory neuron in *D. melanogaster*. Along with partner interneurons of mdVI (including Basin-2, a multisensory integration neuron necessary for rolling) previously identified in *D. melanogaster*, we identified two additional partners of mdVI in *D. santomea*. Finally, we showed that joint activation of one of the partners (Basin-1) and a common partner (Basin-2) in *D. melanogaster* increased rolling probability, suggesting that the high rolling probability in *D. santomea* is mediated by the additional activation of Basin-1 by mdIV. These results provide a plausible mechanistic explanation for how closely related species exhibit quantitative differences in the likelihood of expressing the same behavior.

**Keywords**

Drosophila larvae, comparative analysis, escape behavior, connectome, nociception, neural circuits, evolution

## Introduction

Systems neuroscientists have made great strides toward understanding the mechanistic basis of behavioral change in model organisms by identifying the neural circuits that underlie specific behaviors and the mechanisms that allow for behavioral plasticity (e.g., alterations in cells and neural circuits). Evolutionary and comparative biologists, on the other hand, in seeking to understand how nervous systems evolve, have revealed the great diversity of neuroanatomy, brain function, and behavior across a wide range of species, from invertebrates to mammals (including humans) [1-6]. Behavioral changes that occur ontogenetically (i.e., during the lifetime of an individual organism) may be mediated by the same mechanisms as those that occur phylogenetically (i.e., mediating the behavioral changes that occur across generations, for example, via natural selection operating on behaviors that optimize survival, and in turn, on the neural circuits that underlie them). However, testing this hypothesis remains a major challenge, given the difficulty of identifying the core circuitry for any behavior because of the complexity of most nervous systems.

Behaviors are produced by neural circuits, whose structural and functional properties are determined during development by genetic and environmental factors. For behavioral outputs to be adaptive, neurons and neural circuits must be able to select the proper outputs. Understanding how a neural circuit functions to produce a particular behavior requires a relatively complete knowledge of its connectome or wiring diagram. Recent advances in electron microscopy have led to an explosion of large-scale and dense connectomics studies of the nervous systems of numerous species, including, among others, adult [7-9] and larval *Drosophila* [10], zebrafish [11,12] the roundworm *C. elegans* [13], tadpole larvae of the sea squirt *Ciona* [14], *Platynereis* [15], and mice (e.g., retina [16], taste buds [17]). More recently, comparative connectome studies have identified sex differences in *C.*

*elegans* [18], as well as developmental differences in both *Drosophila* larvae [19] and *C. elegans* at different stages of development [20]. A recent connectome study comparing *C. elegans* and *P. pacificus* has also demonstrated that the positions of neuronal somata and processes, as well as divergence in their fine structural morphology and synaptic connectivity, are generally conserved [21].

Behaviors that help an organism escape from predators are essential for survival, and hence, are likely to be under strong selective pressure. *Drosophila* larvae exhibit a characteristic rolling response when attacked by a parasitic wasp [22]. This nocifensive behavior relies on multi-dendritic nociceptive neurons (MdIV) [22]. Depending on the type of threat, larvae can respond to tactile stimulation by accelerating forward, crawling backwards [23,24], or rolling perpendicularly to the body axis [22,25,26]. Specifically, it is thought that rolling reduces the likelihood of penetration by the wasp's ovipositor [22]. Neural activation and inactivation studies have revealed that activation of MdIV is necessary and sufficient for rolling in *D. melanogaster* larvae [22,25,26]. Subsequent studies, by combining genetic modification of specific neurons with reconstruction of neural circuitry from transmission electron microscopy (TEM) images, identified the core circuitry mediating this nocifensive behavior [10,27-30]. This work set the stage for detailed comparative analyses of neural circuits and behavior in closely related species.

Here, we characterized the differences and similarities in an escape behavior commonly seen in drosophilids, rolling, and its underlying circuitry between *D. melanogaster* and its close relative, *D. santomea*. We found that while rolling occurs in both species, its likelihood of occurrence differs markedly, with *D. santomea* showing a much higher rolling probability than *D. melanogaster*. To determine whether differences in the rolling circuits might explain this behavioral difference, we compared the connectomes between the two species by generating

focused ion beam–scanning electron microscope (FIB–SEM) images in *D. santomea* and reconstructing the neural circuits downstream of the nociceptive sensory neurons. We identified a distinct difference in a particular neural circuit motif, namely, an additional functional connection (present only in *D. santomea* but not in *D. melanogaster*) between Basin-1 and Basin-2, two downstream partner interneurons of mdIV (a key nociceptive sensory neuron critical for rolling). An experimental test in *D. melanogaster* by jointly activating Basin-1 and Basin-2 increased rolling, suggesting that the additional functional connection in *D. santomea* is a plausible mechanism underlying the behavioral change.

## Results

### Diversity of escape behaviors in response to noxious heat

To investigate the diversity of larval escape behavior in drosophilids, we examined the reactions of 12 species to application of noxious thermal stimulation (Figure 1A and Table S1): eight species of the *melanogaster* group, including *D. simulans, D. sechellia, D. melanogaster* (two independent lines, Canton-S and w1118)*, D. yakuba, D. santome*a, *D. erecta*, *D. biarmipes* (a member of the suzuki subgroup), and *D. ananassae* (a member of the ananassae subgroup); *D. persimilis and D. pseudoobscura*, which form the obscura group; *D. willistoni*, a member of the willistoni group; and *D. virilis*, a member of the virilis group, which diverged around 7–11 million years ago (MYA) [31].

To compare the relationship between phylogenetic status and behavior, we first examined the locomotion of each species. Prior to noxious heat stimulation, larval behavior generally consisted of peristaltic crawling interrupted by exploratory head casts. To examine the baseline level of locomotion, we quantified the average speed before stimulation (Figure S1A). *D. willistoni*

showed the highest speed, whereas *D. yakuba* showed the lowest speed. We also calculated the baseline level of body curvature from the average body spine angle (Figure S1B). Curvature was highest for *D. virilis* and lowest for *D. sechellia*.

Next, to compare the responses of different species to noxious heat stimulation, we computed the average normalized speed (the speed after stimulation normalized by that before stimulation) and crabspeed (i.e., the speed of the body perpendicular to the body axis after stimulation, a measure positively correlated with rolling) and body curvature (Figure 1B, and C, respectively; Figure S1C). In a previous study of *D. melanogaster*, we showed that noxious heat stimulation evoked head bending and rolling, followed by fast escape crawling [10,32]. We found that heat stimulation increased the speed of escape crawling in most species, and most prominently in *D. melanogaster* (w1118). In contrast, heat stimulation did not increase speed in *D. virilis*, *D. pseudoobscura*, or *D. sechellia*. Interestingly, *D. biarmipes* showed the lowest normalized speed (Figure 1B), which was even lower than that before heat stimulation. Instead, *D. biarmipes* exhibited stopping and head casting after heat stimulation (Video S1). We also found that crabspeed was lowest in *D. biarmipes* and highest in *D. persimilis,* being strongly correlated with normalized speed after stimulation (Figure 1C). Third, body curvature in response to heat stimulation was highest in *D. virilis* and lowest in *D. yakuba* (Figure S1C). These data show that upon heat stimulation, *D. virilis* bends its body vigorously but does not exhibit rolling or escape crawling (Figure 1C and S1C; Video S2). In contrast, post-stimulation crabspeed was higher in *D. persimilis* than in *D. melanogaster*, indicating that *D. persimilis* rolls more than *D. melanogaster* (Video S3).

### ***D. santomea*** **shows more rolling than** ***D. melanogaster***

Parasitoid wasps are natural predators of drosophilids [33,34]. The adults inject eggs into the body of *Drosophila* larvae, after which the hatched wasp larvae proceed to eat the fly larva from the inside [35]. As mentioned above, rolling is an escape response that *Drosophila* larvae exhibit when they are attacked [22]. This behavior is also evoked by other noxious cues, such as thermal [25], mechanical [25], and chemical stimuli [36]. To address how such nocifensive rolling varies across species, we analyzed the probability of rolling in response to noxious heat. Using a machine learning method previously developed to automatically detect larval behaviors [10,37], we found that *D. santomea* showed significantly more rolling than either *D. melanogaster* or *D. yakuba* (which is phylogenetically closest to *D. santomea*) (Figure 1D and E; Chi-square test: $p < 0.05$, *D. santomea* vs *D. melanogaster or D. yakuba*; Video S4 and S5). To further confirm this behavioral difference between *D. santomea* and *D. melangaster*, we used a heat probe to apply noxious heat stimulation to 3 different lines of *D. santomea* and 3 members of the *D. melanogaster* group (Canton-S, w1118, and an additional member, Oregon-R). All 3 lines of *D. santomea* exhibited rolling upon heat stimulation (Figure 1F).

To test whether the high rolling probability of *D. santomea* was specific to noxious heat, we applied other modes of stimulation to 3 different lines of *D. santomea* and 3 members of the *D. melanogaster* group. All 3 lines of *D. santomea* responded earlier (Figure 1G) upon stimulation with 9% HCl, and with greater rolling probability than members of the *D. melanogaster* group in response to mechanical stimulation (Figure 1H).

Next, we varied the strength of noxious mechanical stimulation to examine whether the difference in rolling probability between *D. santomea* and *D. melanogaster* was dependent on stimulation intensity. At an intensity of 20 mN, we found a significant increase in rolling probability compared to baseline in both species, indicating that the sensitivity of mechanical

nociceptive stimulation between *D. melanogaster* and *D. santomea* is similar. At 40 mN, the proportion of animals showing rolling increased in both species, but to a greater extent in *D. santomea* (Figure 1I). This difference was consistently maintained up to an intensity of 150 mN (Figure 1I). These data suggest that the difference in rolling probability is not merely a result of differences in sensory processes, but possibly due to differences downstream of sensory neurons.

The results from population analyses of rolling in response to noxious thermal (Figure 1D-F), chemical (Figure 1G), and mechanical stimulation (Figure H and I), which all show a higher probability of rolling in *D. santomea* than in *D. melanogaster*, might be explained by differences in the proportions of rollers and non-rollers within each population. Therefore, we also examined rolling probability at the individual level by applying 5 bouts of noxious mechanical stimulation every 30 seconds. On average, *D. santomea* rolled 3.1 out of 5 times, whereas *D. melanogaster* rolled 2.3 out of 5 times (Figure 1J). These data indicate that even at the individual level, *D. santomea* are more likely to roll than *D. melanogaster* in response to noxious stimulation. Collectively, these results suggest a genuine species difference in the likelihood of a naturalistic escape behavior.

### ***D. santomea, D. persimilis, D. biarmipes, D. virilis*** **and** ***D. melanogaster*** **have similar peripheral nervous systems**

Where does this difference in the likelihood of rolling come from? *Drosophila* larvae detect noxious stimulation primarily when multi-dendritic Class IV (mdIV) neurons are activated [38,39]. To examine the anatomy of peripheral sensory neurons in *D. santomea, D. persimilis, D. biarmipes,* and *D. virilis,* which show high or low probabilities of rolling compared to *D. melanogaster*, we utilized antibodies commonly employed to visualize the morphology of the corresponding sensory

neurons in *D. melanogaster*: anti-Futch/22C10, which labels axons/dendrites [40,41], and anti-Elav, which labels neuronal nucleoli [42]. In *D. santomea*, we found that anti-Futsch and anti-Elav also stained sensory neurons (Figure 2A). When we counted cell numbers and identified the positions of these neurons within the hemi-segments of 6 different animals, we found that their numbers and positions were the same as those in *D. melanogaster* (Figure 2B and Table S2). Specifically, we found that dorsal, lateral, ventral prime (v′), and ventral neurons clustered in the same peripheral positions as those in *D. melanogaster*. Furthermore, we identified the same numbers of chordotonal neurons lch1-5, vchA, vchB, and v′ch in *D. santomea* (Figure 2A and B) based on the position and shape of dendrites with cap cells. We could not confirm the identity of each type of sensory neuron in this study. Nonetheless, the morphological data indicate that the overall structure of the sensory system in *D. santomea* is similar to that in *D. melanogaster*. Similarly, in *D. persimilis* (high rolling probability), *D. biarmipes* (low rolling probability), and *D. virilis* (low rolling probability), we found comparable numbers of dorsal, lateral, v′, and ventral neurons clustered in similar peripheral positions as those in *D. melanogaster* (Figure 2B-E, Table S2).

These data are consistent with previous comparative studies, which showed that the peripheral nervous systems of most drosophilids exhibit the same structural pattern as that of *D. melanogaste*r [43]. To our knowledge, the only documented structural difference, the absence of a specific external sensory organ, has been reported in the subgenus *D. busckii*, which diverged about 40 MYA from *D. melanogaster* [43]. These data suggest that the observed differences in rolling between drosophilids is not due to differences in the structural organization of sensory neurons.

**Reconstruction of mdIV and chordotonal sensory neurons from volume electron microscope images of *D. santomea***

To characterize the connectivity of the nociceptive neural circuit in *D. santomea*, we generated FIB–SEM images of L1-stage larvae between the second abdominal and second thoracic segments (70 µm × 55 µm × 105 µm, 10-nm resolution; see Methods for details). FIB–SEM images, which have isotropic resolution, make it possible to generate X-Y, Y-Z, and X-Z views [44]. By uploading these 3 views into the CATMAID platform [45], we reconstructed neurons manually and identified their synaptic partners.

A previous study in *D. melanogaster* showed that mdIV and chordotonal neurons are important for the rolling exhibited by a larva when attacked by a parasitoid wasp [10,22,46] (Figure 3A). In *D. melanogaster*, each hemi-segment contains 3 mdIV neurons and 8 chordotonal neurons with dendrites that tile the body wall [47] (Figure 3A). We first reconstructed the mdIV and chordotonal neurons from the lateral and ventral sensory bundles in the second abdominal segment of *D. santomea*. We identified mdIV neurons (ddaC, v′ada, and vdaB) and the chordotonal neurons (lch1-5, vchA/B, v′ch), based on the shape of their axon terminals in the FIB–SEM images of *D. santomea*. We found that mdIV neurons were located in the most medial and ventral regions of the ventral nerve cord (VNC) and chordotonal neurons were positioned laterally to the mdIV neurons (Figure 3B-E).

We then measured the cable length of each mdIV neuron using CATMAID tools, and found that this was similar between each pair of corresponding neurons on the left and right sides and was not very different from that of *D. melanogaster* [19] (Figure 3F). We were also able to identify synapses at the axon terminals of neurons in our FIB–SEM images from their thick, dense terminals and vesicles (Figure 3G), although their T-bars were not as obvious as those observed in TEM images of *D. melanogaster* synapses [19].

Finally, we identified all synapses on mdIV neurons the total numbers of which are shown in Figure 3H. For each mdIV neuron, the synapses were concentrated at the axon terminals, forming a "rung of the ladder" within the VNC (Figure 3I). Insect neurons are polysynaptic, meaning that one T-bar provides inputs to several partner neurons [19]. The average number of targets per synapse is 3; we observed 1 to 11 targets in *D. santomea*, which is similar to the range reported for synapses in *D. melanogaster* [10, 48]. These synapses were concentrated in the medial part of each VNC segment (Figure 3I and J). Overall, we found highly stereotyped morphological features similar to those in *D. melanogaster*, including anterior-posterior dendrite projection, dorso-ventral position, and midline crossing of mdIV neurons in *D. santomea* FIB–SEM image data [10,48,49] (Figure 3B–J).

**Identification of the main local target of mdIV sensory neurons in *D. santomea*, and differences in connectivity between *D. santomea* and *D. melanogaster***

To compare the connectivity of mdIV neurons and first-order interneurons between *D. melanogaster* and *D. santomea*, we reconstructed the synaptic partners of mdIV neurons (a total of 352 neuronal arbors, Figure 4A) in our *D. santomea* FIB–SEM volumes. A previous *D. melanogaster* reconstruction revealed that nociceptive neurons reproducibly make numerically strong connections (i.e., >10 synapses) with homologous neurons in the left and right hemi-segments, across different segments in the same individual, at different developmental stages in the same individual, and in different individuals of the same species [10,48,50,51]. Furthermore, other studies indicate that in contrast to numerically strong connections, numerically weak connections are not conserved between the left and right sides of the same individual [10,19,48]. We therefore focused our analysis on 36 strongly connected neurons (Figure 4B, Table S3; >10 synapses from

all mdIV neurons), which we grouped into 20 local neurons (i.e., those within the same segment) and 16 intersegmental neurons (i.e., ascending or descending neurons) (Figure 4B, Table S3). Among the 20 local neurons, 16 were located in the second abdominal segment and 4 in the first or third abdominal segment. Among the 16 intersegmental neurons, based on the shape of neuronal arbors, we identified 6 neurons as candidate ascending or descending neurons (A08n, TePn19 and SeIN138) and 4 as candidate A02o neurons (Table S3) [48]. The remaining 6 could not be identified because they exited the 3-segment EM volumes and their shapes were unclear.

We identified Down and Back [29,48], Chair-1 (A10a) [48], A02n and m [48], Basin-2 [10,48], and Basin-4 [10,48] as strongly preferred partners of mdIV neurons in *D. santomea* (Figure 4C) based on the shape of the neuronal arbor and the position of the cell body [10,19,48]. These same neurons have previously been identified as preferred partners of mdIV neurons in *D. melanogaster* [48]. In addition to these partners, we identified two other preferred partners, Basin-1 and A27n, in our *D. santomea* FIB–SEM volumes. Specifically, we found that Basin-1 broadened its dendritic coverage towards more medial-ventral regions of the neuropil than in *D. melanogaster* (Figure 4D).

To compare the connectivity between nociceptive neurons and first-order interneurons in the two species, we normalized synapse numbers by the total number of synaptic contacts between the preferred interneurons and nociceptive sensory neurons (36 neurons [993 synapses in total] receiving >10 synapses from mdIV in *D. santomea*, and 33 neurons [780 synapses in total] receiving >10 synapses from mdIV in *D. melanogaster*; Figure 4E), using previously published *D. melanogaster* connectome data . We examined 16 local interneurons (12 partners common to *D. santomea* and *D. melanogaster*; 4 novel partners unique to *D. santomea*) and candidate intersegmental neurons (A08n, TePN19, SeIN138, and A02o). Down and Back neurons and Basin-4 received slightly fewer synaptic inputs from nociceptive neurons in *D. santomea* than in *D.*

*melanogaster* (Figure 4D). Chair-1, Basin-2, and A02n/m neurons received similar levels of synaptic input from mdIV in both species. In *D. santomea*, A27n received 2.8% and 2.1% of all mdIV inputs from the left and right, respectively, with the corresponding percentages being 4.2% and 3.8% for Basin-1. In *D. melanogaster*, A27n received 0.3% and 0.0% of all mdIV inputs from the left and right, respectively, with the corresponding percentages being 0.1% and 0.0 % for Basin-1 (Figure 1E). These data indicate that the preferred partners of mdIV are largely similar between *D. melanogaster* and *D. santomea*, although mdIV neurons in the latter species have a few additional partners.

**Connectivity between sensory neurons and Basin cells**

Basin neurons process multisensory information from mechanosensory and nociceptive neurons [10]. Specifically, in *D. melanogaster*, there are four independent Basin cells, with only Basin-2 and Basin-4 receiving both mechanosensory and nociceptive inputs [10]. A previous study showed that integration of chordotonal and nociceptive sensory inputs mediated by Basin neurons could facilitate rolling [10]. To examine whether this integration motif was similar in *D. santomea*, we reconstructed all Basin neurons and identified the synapses between them. We first looked the synapses between the Basins and mdIV or chordotonal neurons and found that, as in *D. melanogaster*, Basin-2 and Basin-4 receive inputs from both mdIV (nociceptive sensory) and chordotonal (mechanosensory) neurons (Figure 5A, Table S4). However, in contrast to *D. melanogaster*, in which Basin-1 receives inputs from chordotonal neurons but not from mdIV neurons, we found that in *D. santomea*, Basin-1 receives inputs from both chordotonal and mdIV neurons. These data suggest that the additional source of nociceptive input to Basin-1 in *D.*

*santomea*, which is not available in *D. melanogaster*, might account for higher likelihood of nociception-induced rolling in *D. santomea*.

To identify any other differences in connectivity that might underlie the differences in rolling, we also analyzed the local circuitry between the mdIV and Basin neurons, and found that in both species, Basin-1 makes synaptic contacts with Basin-2 and Basin-4, which are essential for rolling and multisensory integration in *D. melanogaster* [10] (Figure 5B). These results suggest that local connections among the Basins are comparable between the two species, and that the lower probability of rolling in *D. melanogaster* is due to the lack of Basin-1 activation.

To test this conjecture, we jointly activated Basin-1 and Basin-2 to see whether the probability of rolling in *D. melanogaster* would increase. We found that whereas activation of Basin-1 alone evoked little rolling, joint activation of Basin-1 and Basin-2 significantly increased the probability of rolling compared to activation of Basin-2 alone (Figure 5C). Interestingly, joint activation of Basin-1 and Basin-2 also significantly increased crawling speed compared to activation of Basin-1 or Basin-2 alone (Mann-Whitney *U* test: $p < 0.01$ or $p < 0.001$ respectively, with corresponding rank biserial correlations of r = -0.19 or r = -0.343) (Figure 5D). These data demonstrate that activation of Basin-1 in *D. melanogaster* can modify rolling probability, and to a lesser extent crawling speed after rolling. To further examine the effect of Basin-1 activation in rolling, we activated neurons five consecutive times and counted the number of rolls. We found that co-activation of Basin-1 and Basin-2 significantly increased the number of rolls compared to activation of Basin-1 or Basin-2 alone (Figure 5E). These results are consistent with the view that, the additional nociceptive inputs onto Basin-1 from mdIV neurons in *D. santomea* increases the probability of rolling in this species relative to that of *D. melanogaster.*

**Discussion**

A major unresolved question in evolutionary biology is how behavior evolves through the alteration of genes, molecules, cells, and circuits. Here, taking advantage of larval *Drosophila*, a model organism for studying behavioral neurogenetics, we adopted a comparative approach to investigate the similarities and differences in rolling, a characteristic escape behavior whose core circuitry has been identified in *D. melanogaster*, in several additional drosophilid species. Although all showed rolling in response to noxious heat stimulation, they differed widely in their probability of rolling (~6% to ~65%). In particular, *D. santomea* larvae were much more likely to roll in response to noxious stimulation (thermal, chemical, and mechanical) than were *D. melanogaster* larvae. To explore the biological basis of this difference, we reconstructed the downstream partners of nociceptive sensory neurons in *D. santomea* using FIB-SEM volumes and identified those previously identified as partners in *D. melanogaster*, as well as two additional interneurons, Basin-1 and A27n, in *D. santomea*. In contrast to our previous work, which showed that only Basins-2 and Basin-4 receive inputs from mdIV in *D. melanogaster*, here we discovered that in *D. santomea*, Basin-1 also receives inputs from mdIV and chordotonal neurons, and in addition, forms synaptic connections with Basin-2. Finally, joint activation of Basin-1 and Basin-2 increased rolling probability in *D. melanogaster*, suggesting that the identified differences in circuitry among the nociceptive sensory neurons and their downstream partner interneurons could account for the difference in rolling between the two species.

In insects, neuronal morphology, such as the branching pattern of a neuron, is stereotyped [51-53]. Morphologically homologous neurons can be identified between segments within an animal, between animals, and between species. For example, during development, stereotypic connectivity between mdIV and interneurons is observed in both *Drosophila* larvae [48] and *C. elegans* [20], as well

as in different L1-stage *Drosophila* larvae [10,48]. Similarly, in the present study, the overall connectivity between mdIV neurons and interneurons was also similar between *D. melanogaster* and *D. santomea*. These data support the idea that stereotypic morphology and connectivity are conserved during evolution. Although such examples of conservation may indicate that these neuronal branching patterns are functionally important [51], particular branching morphologies might also be shaped by influences that are not obviously adaptive, such as developmental or physical constraints that limit the shape or organization of neurons [54]. Thus, in determining the functional significance of a particular branching morphology, examples in which a specific alteration in branching is correlated with a novel function or behavior are more informative, such as the differences in fine connectivity that have been demonstrated between species (i.e., *C. elegans* and *P. pacificus*) [21], as well as within species depending on sex [18] and developmental stage (*C. elegans*) [20]. In our study, the connectivity between nociceptive neurons and their downstream partners, Basin-1, Basin-2, and Basin-4, slightly differed between *D. melanogaster* and *D. santomea*, in that only Basins-2 and Basin-4 received nociceptive inputs in the former, whereas all three Basins received nociceptive inputs in the latter. That this difference was of functional significance is strongly suggested by our finding that joint activation of Basin-1 and Basin-2 in *D. melanogaster* facilitated rolling.

Our findings build upon those of a previous study of *D. melanogaster* larvae, which showed that integration of chordotonal and nociceptive inputs could enhance rolling in a supralinear manner[10]. In that study, we found that although activation of chordotonal neurons alone by a mechanical stimulus did not trigger rolling, the same stimulus applied coincidently with optogenetic activation of nociceptive sensory neurons triggered rolling more frequently than when only nociceptive stimulation was applied [10]. A previous study showed that Basin-2 and Basin-4

integrate inputs from chordotonal and nociceptive neurons, and that this process likely plays a key role in multisensory integration [10]. The present study shows that Basin-1 also integrates inputs from these sensory neurons in *D. santomea*. That Basin-2 was found to be a downstream partner of Basin-1, not only in *D. melanogaster* but in *D. santomea* as well, prompted us to test whether joint activation of Basin-1 and Basin-2 would enhance rolling in *D. melanogaster*, which was indeed the case. It should be noted that nociceptive neurons in both species share other interneurons as downstream partners, including Down & Back, A02m/n, and Chair-1 cells. Although the extent to which these interneurons contribute to multisensory integration remains to be determined, it is possible that a diverse population of multisensory neurons could contribute to the varying degrees of rolling probabilities observed among the drosophilids tested here.

Our study has a number of potential limitations. First, the conclusions regarding the species difference in rolling circuitry depend on EM reconstruction data from three *D. melanogaster* larvae [10,48] and a single *D. santomea* larva. Admittedly, additional samples for *D. santomea* going forward would strengthen our conclusions, although it is noteworthy that none of the three *D. melanogaster* samples showed evidence of the additional functional partners of nociceptive neurons (i.e., Basin-1 and A27n) seen in our *D. santomea* sample. Second, it may be argued that the differences in rolling probability between the drosophilids we tested merely reflect differences in motor thresholds (e.g., due to differences in cuticle thickness, body size, body weight). We consider this unlikely, however, as shown by the lack of a strong correlation between body size and rolling probability (Figure S1D). In addition, although the dose-response curves obtained using noxious mechanical stimulation (Figure 1I) suggest that the sensory thresholds for *D. santomea* and *D. melanogaster* are comparable, the possibility that the consistent differences in rolling probability observed are mediated by differences at the level of sensory neuron cannot be ruled out, unless the

activity of nociceptive sensory neurons in response to different noxious cues is directly measured. Third, as we only examined local feedforward excitatory circuits and did not investigate the inhibitory neurons between the Basins and chordotonal microcircuits, the functional roles of such neurons in circuit dynamics and behavior remain to be investigated. Inhibitory inputs have been proposed to contribute importantly to the sequencing of behaviors [55]. In this context, we have observed that heat-induced noxious stimulation can also trigger the rolling–escape crawling sequence [32]. Our experimental preparation, which identified various behaviors evoked by noxious stimulation, could reveal how inhibitory neurons contribute to such behavioral sequences [55]. Finally, our study does not address the issue of how the differences in rolling probability relate to evolutionary fitness. Field studies will be required to answer, for example, whether the differences indicate that species with low rolling probabilities live in areas with low levels of parasitization by wasps, or that species differ in terms of their most successful escape behavior in evading parasitzation.

Previous comparative studies have provided insight into the ultimate causes of, and constraints on, behavioral diversity [3,56-58]. To date, however, few studies have illuminated the mechanisms by which behavior evolves, in part due to the polygenetic nature of behavior, as well as the lack of tools to identify the circuits that underlie behaviors and to manipulate individual genes, neurons, and circuits to test specific hypotheses regarding the mechanisms involved at different levels of analysis (e.g., changes in neural circuits, molecules within neurons [e.g., sensory receptors, neuromodulators], number of neurons, muscle physiology [59,60]). In recent years, the emergence of new tools has revitalized studies on the evolution of neuronal circuits underlying species-specific behaviors, such as feeding [61] and courtship [56,62] in fruit flies, swimming in sea slugs [63], and escape behavior in zebrafish [57]. Our findings add to this work, demonstrating the

utility of high-throughput EM imaging technology in advancing comparative neuroscience. We identified a difference in circuit motif between the rolling circuits of closely related fruit fly larvae (*D. melanogaster* and *D. santomea*), which was associated with a marked difference in the likelihood of larvae rolling in response to noxious heat stimulation. We then showed that by "equating" the motifs via optogenetic activation of a specific multisensory interneuron (Basin-1) we could reduce the difference in rolling probability. These results demonstrate the potential of our approach in systematically identifying the mechanisms that contribute to the evolution of an escape behavior and its underlying brain circuit.

**Acknowledgements**

We thank A. Cardona and C. Michel for suggestions on neuron tracing methodology; T. Kazimiers for CATMAID server maintenance; M. Zlatic for constructive inputs on the project; R. Tabano and undergraduate students for their assistance in neuron tracing; and D. Stern for sharing drosophid stocks. Confocal images were collected at the McGill University Advanced Bio Imaging Facility (ABIF), RRID:SCR_017697. This work was funded by McGill University, the National Sciences and Engineering Research Council (NSERC, RGPIN/04781-2017), the Canadian Institute of Health Research (CIHR, PTJ-376836), the Fonds de recherche du Quebéc - Nature et technologies (FRQNT, 2019-N-25523), the Canada Foundation for Innovation (CFI, CFI365333), and the Janelia Research Campus Visiting Program. J-C.B was supported by Fonds de recherche du Quebéc-Santé (FRQS) graduate training award.

**Author contributions**

Conceptualization, J.Z., J-C.B., and T.O. Writing – Original Draft, J.Z. and T.O, Writing – Review & Editing, J.Z., J-C.B., S.P., Z.L, C.S.X., and H.F.H. Formal Analysis, J.Z., J-C.B., and T.O. Methodology, H.F.H., C.S.X, S.P and Z.L., Resources, H.F.H., C.S.X and S.P. Supervision, T.O.

**Declaration of Interests**

Portions of the technology described here are covered by U.S. Patent 10,600,615 titled 'Enhanced FIB-SEM systems for large-volume 3D imaging', which was issued to C.S.X., K.J.H. and H.F.H. and assigned to Howard Hughes Medical Institute on 24 March 2020. The other authors declare no competing interests.

**Inclusion and Diversity**

One or more of authors of this paper self-identifies as a member of the LGBTYQ+ community.

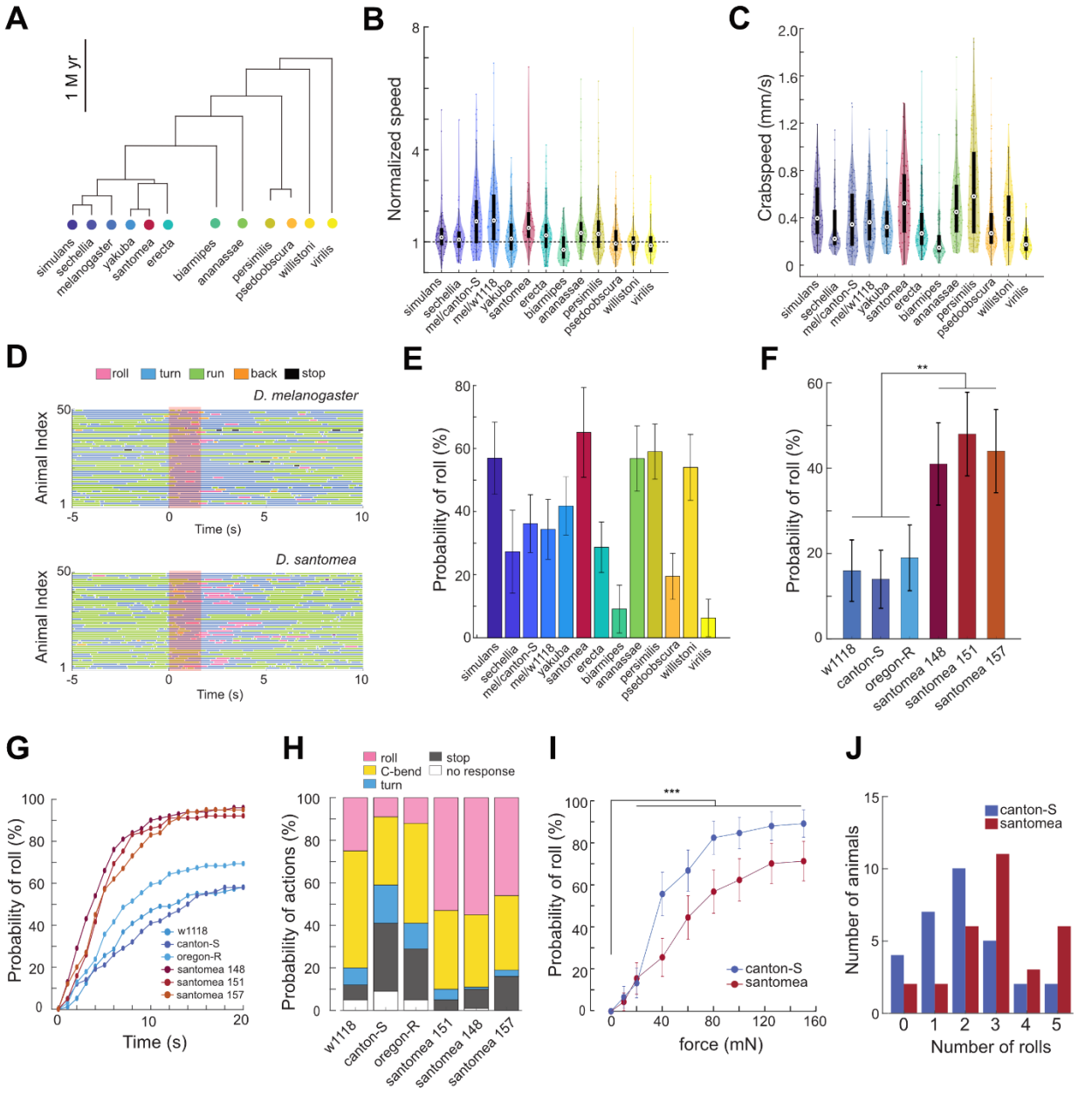


**Figure 1. *Drosophila* species show a wide range of escape responses to noxious stimulation**

(A) Consensus phylogenetic tree showing species used in this study. (See also Table S1)

(B) Violin plot of normalized speed after noxious heat by speed before stimulation in each species. Circles with filled inner dots show the median values. Upper and lower edges of filled bars show 25$^{th}$ and 75$^{th}$ percentiles, respectively. (See also Figure S1.)

(C) Violin plot of crabspeed after noxious heat application. Circles with filled inner dots show the median values. Upper and lower edges of filled bars show 25$^{th}$ and 75$^{th}$ percentiles, respectively.

(D) Behavioral raster plots showing periods during which individual larva rolled, turned, ran, moved backward, or stopped during the 5-s period before stimulation (i.e., red shaded area, showing application of an 808-nm laser for 2 s starting at time 0) and the 10-s period following stimulation. Top and bottom panels show results for *D. santomea* and *D. melanogaster*, respectively. Each row represents data for a single larva (from among 50 randomly selected animals) tracked continuously throughout the interval.

(E) Bar charts showing rolling probability within a 5-s time window after infrared laser stimulation. Error bars indicate 95% confidence interval. (N = 71, 44, 104, 96, 90, 42, 103, 54, 39, 122, 111, 87, 63: from left to right) (See also Video S1-5)

(F) Bar charts showing rolling probability after applying a heat probe for 5 s. Error bars indicate 95% confidence interval in 3 different lines of *D. melanogaster* (w1118, Canton-S, and Oregon-R) and 3 independent lines of *D. santomea* (148, 151, and 157). N = 100 per genotype. Chi-square test: ** $p < 0.01$.

(G) Cumulative frequency of rolling as a function of time following application of a 1.5 ml of 7% HCl in 3 different lines of *D. melanogaster* (w1118, Canton-S, and Oregon-R) and 3 independent lines of *D. santomea* (148, 151, and 157). N = 100 per line.

(H) Distribution of larval behaviors observed upon presentation of a mechanical nociceptive stimulus (50 mN) in 3 different lines of *D. melanogaster* (w1118, Canton-S, and oregon-R) and 3 independent lines of *D. santomea* (148, 151, and 157). The behaviors were categorized into nociceptive (roll, bend) and non-nociceptive actions (stop and turn, stop, no response). N = 100 per line.

(I) Dose response curves showing rolling probability in response to a mechanical nociceptive stimulus applied at various intensities (10, 20, 40, 60, 80,100, 125, and 150 mN) in *D. melanogaster* (Canton-S) and 3 independent lines of *D. santomea* (151). N = 90 per condition. Probability of rolling was higher at stimulation intensity ≥ 20 mN vs. no stimulation; Chi-square test: *** $p < 0.001$. Probability of rolling was higher in *D. santomea* vs. *D. melanogaster*; Chi-square test: ** $p < 0.01$

(J) Number of rolls observed across 5 consecutive presentations of a mechanical nociceptive stimulus (50 mN) in *D. melanogaster* (Canton-S) and *D. santomea* (line 151). Mann-whitney U test: $p<0.001$

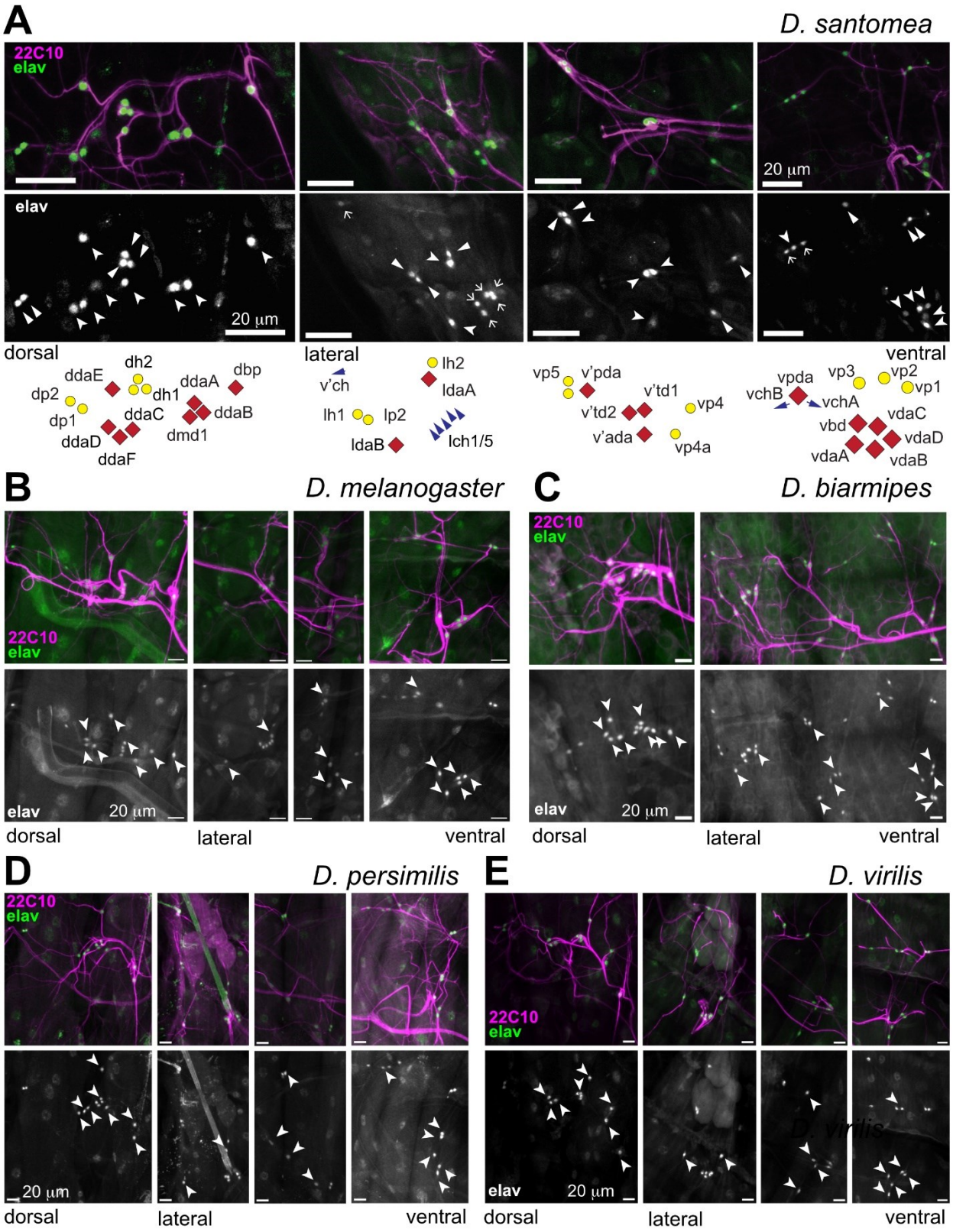


**Figure 2. Anatomy of *D. santomea, D. melanogaster, D. biarmipes, D. persimilis, and D. virilis***

**sensory neurons in the peripheral nervous system**

Expression patterns of antibodies in confocal microscope images of an abdominal hemi-segment in *D. santomea* (A)*, D. melanogaster* (B), *D. biarmipes* (C), *D. persimilis* (D), and *D. virilis* (E) third instar larvae. Images show transverse sections with anterior and posterior regions at the top and bottom, respectively. Larvae were co-immunostained with antibodies against Elav (9F8A9; green in top panel), a marker of nucleoli, and Futsch (22C10; magenta in top panel, white in middle panel), a marker of all peripheral sensory neurons. Left, middle, and right panels show dorsal, lateral, and ventral clusters, respectively. Scale bar: 20 μm. Triangular arrowheads (middle panel) and yellow circles (bottom panel): external sensory neurons; notched arrowheads (middle panel) and red squares (bottom panel): multi-dendritic neurons; arrows (middle panel) and blue triangles (bottom panel): chordotonal sensory neurons. (See also Table S2)

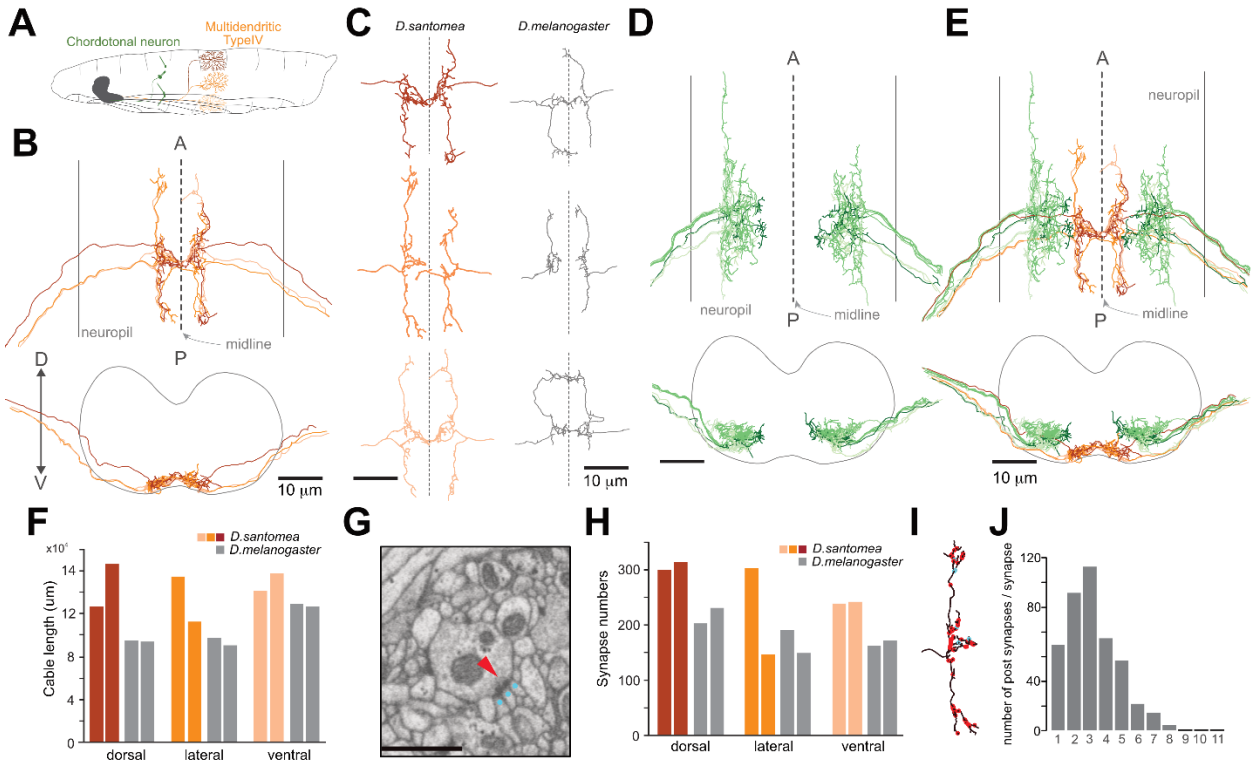


**Figure 3. Structure of mdIV and chordotonal neuron terminals in *D. santomea***

(A) Schematic representations showing the organization of the chordotonal neurons (green) and the dendritic fields of three nociceptive mdIV sensory neurons (ddaC: red, v′ada:orange, and vdaB:light orange) within the nerve cord (sagittal view). The central nervous system is shown in black to the left.

(B) Dorsal (top: transverse plane) and ventral (bottom: coronal plane) views of all EM-reconstructed mdIV terminals from the second abdominal segment in *D. santomea*. Colors are as shown in A. The area between the two outer solid gray vertical lines (top) and the gray outline of the ventral nerve cord (bottom) demarcates the 3-dimensional area constituting the neuropil. The dashed line indicates the midline. A, anterior; P, posterior; D, dorsal; V, ventral. Scale bar: 10 µm.

(C) Morphology of the terminals of each mdIV subtype of *D. sanotmea*, as shown in B, and that of corresponding mdIV subtypes from the first abdominal segment in *D. melanogaster*. The dashed line indicates the midline. Scale bar: 10 μm.

(D) and (E) Dorsal (top: transverse plane) and ventral (bottom: coronal plane) views of all EM-reconstructed chordotonal (D) and mdIV and chordotonal (E) terminals from the second abdominal segment in *D. santomea*. Colors are as shown in A. The outer gray vertical lines (top) and the gray outline of the ventral nerve cord (bottom) demarcate the area of the neuropil. The dashed line indicates the midline. Scale bar: 10 μm.

(F) Total dendritic cable lengths of all mdIV sensory neurons. Red, orange, and light orange bars represent cable lengths of A2-segment mdIV neurons of *D. santomea* whose dendritic fields are localized within the dorsal, lateral, and ventral regions of the nerve cord. For each pair of bars, the bars on the left and right indicate the cable lengths on the left and right sides of the larva, respectively. Gray bars represent cable lengths of A1-segment mdIV neurons in *D. melanogaster*.

(G) Representative image of a polyadic synapse from a *D. santomea* FIB-SEM volume. Scale bar: 1 μm.

(H) Number of synaptic outputs on the terminals of the three A2-segment mdIV neurons in *D. santomea* and *D. melanogaster*. Bar colors are as shown in F, as are the relationships between the left and right bars for each mdIV neuron.

(I) Dorsal view of a single v′ada terminal from *D. santomea*, shown with synapses (outputs, red; inputs, cyan).

(J) Histogram of the number of postsynaptic contacts per presynaptic site on mdIV terminals in *D. santomea*.

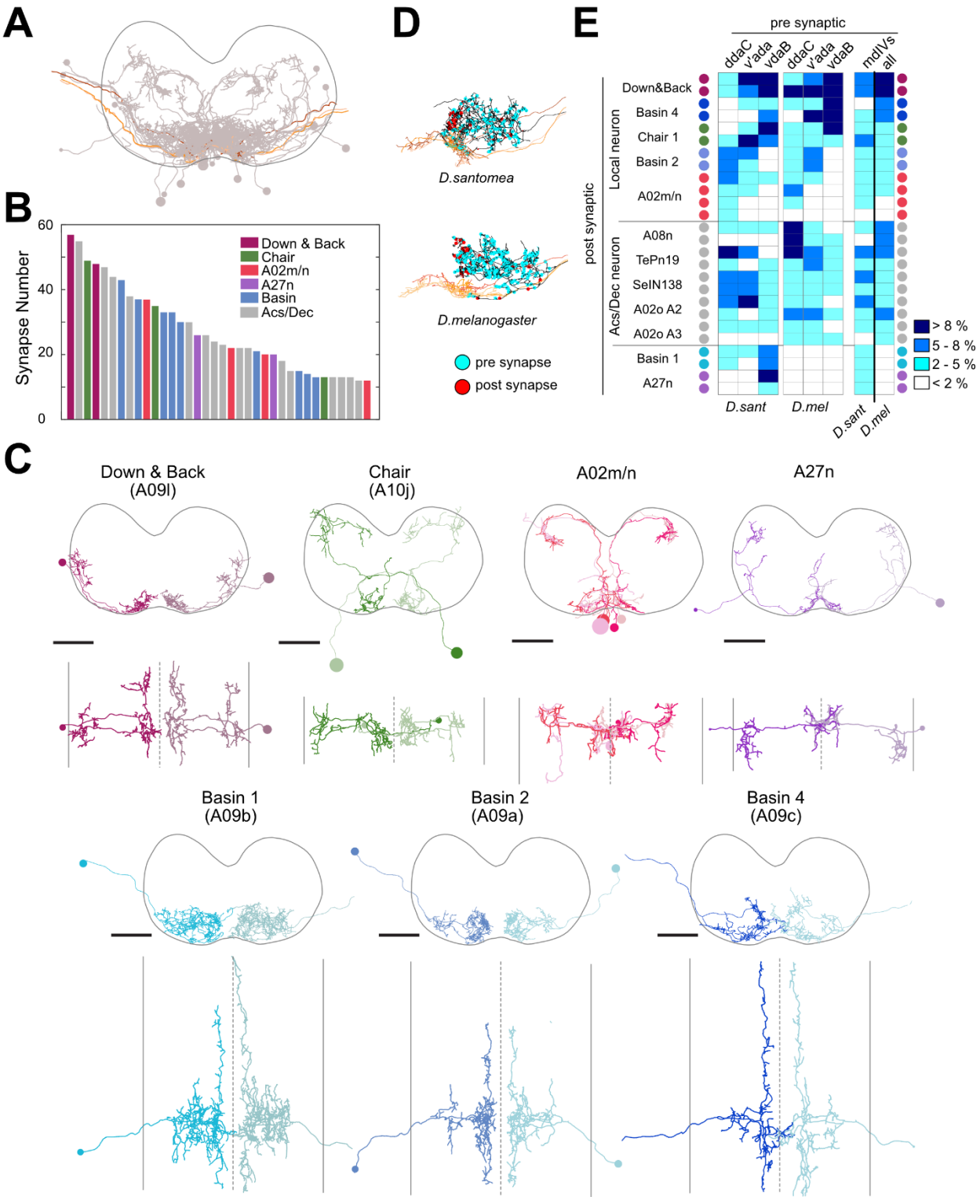


**Figure 4. Morphology and properties of second-order nociceptive local interneurons**

(A) Electron microscopy reconstruction of all direct synaptic targets (reconstructed neurons shown in gray) of the mdIV neurons (three each on the left and right) in abdominal segment A2.

(B) Connectivity ranking plots of postsynaptic partners of mdIV neurons in *D. santomea* abdominal segment A2. Each bar represents an individual neuron. Synapse numbers represent the sum of all synaptic contacts made by the axon terminals of the six mdIV neurons onto single neurons. Only neurons with ≥10 synapses from mdIV neurons in each segment and were identifiable in the A2 segment EM volume were fully reconstructed. Gray bars denote intersegmental neurons spanning multiple segments. (See also Table S3)

(C) Dorsal (upper panel) and coronal (lower panel) views of reconstructed axons of mdIV partners in *D. santomea*. Scale bar: 10 μm.

(D) Electron microscopy reconstruction showing all synaptic inputs (light blue dots) of Basin-1 (black line) in *D. santomea* and *D. melanogaster*. MdIV neurons are shown in orange lines. The dendritic branches of Basin-1 in *D. santomea* innervate areas nearer to the ventral midline than those of Basin-1 in *D. melanogaster*. The output synapses of Basin-1 are shown as red dots.

(E) Connectivity matrix of presynaptic and postsynaptic neuronal connections between mdVI (presynaptic: ddaC, v′ada, vdaB, or all mdIVs) and local neurons (postsynaptic: left or right side of Down & Back, Chair, A02n/m, Basin-1, Basin-2, Basin-4, or A27n neurons), or ascending/descending neurons (postsynaptic: candidate neurons A08n, TePn19, SeIN138, and A02os) in *D. santomea* and *D. melanogaster*. Color-coded by percentage of inputs from output neurons.

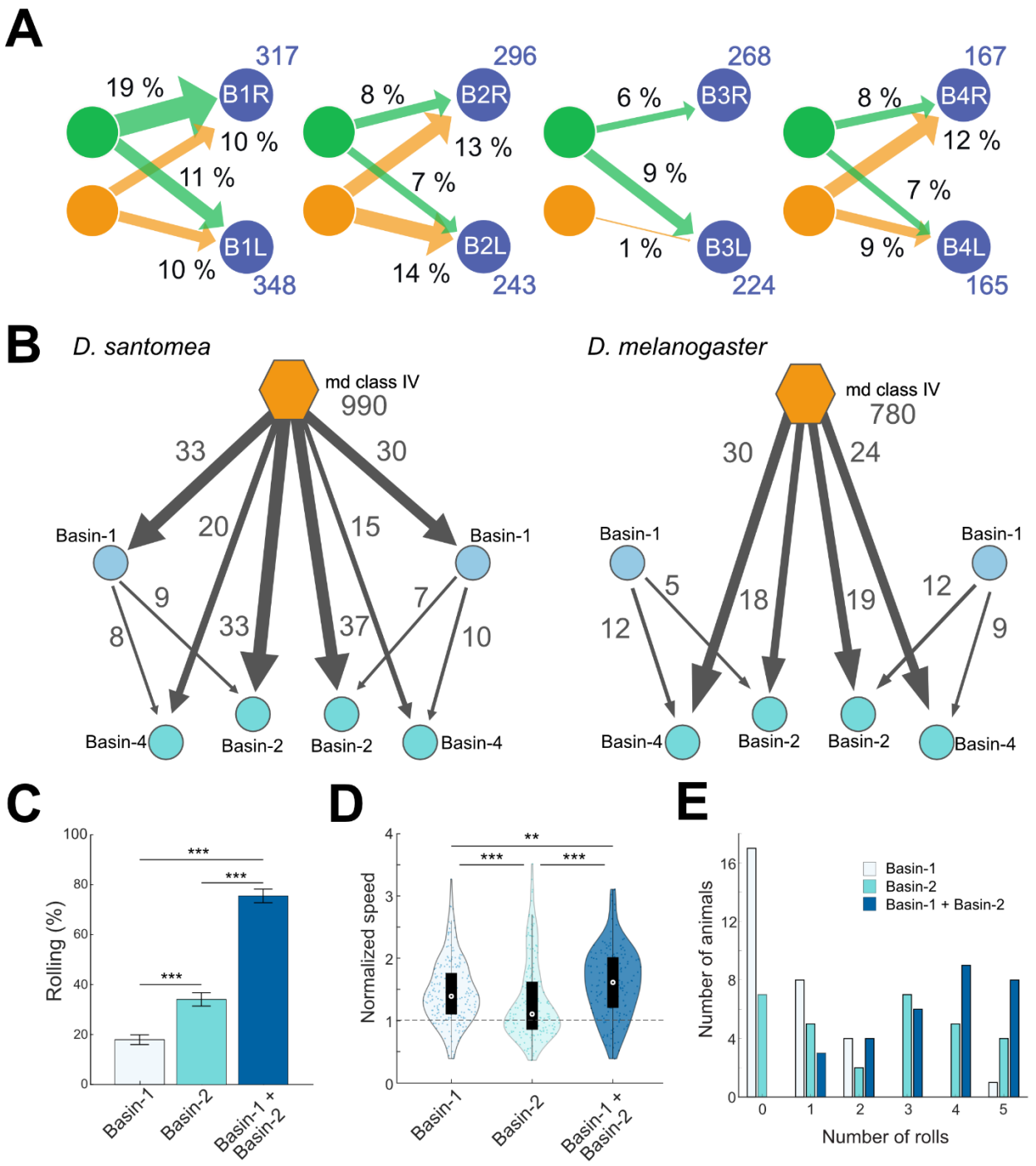


**Figure 5. Basin-1, Basin-2, and Basin-4 receive inputs from mdIV neurons and chordotonal neurons in *D. santomea***

(A) The proportions of synaptic inputs onto Basins originating from chordotonal (green) or mdIV (orange) terminals. The thickness of an arrow represents the proportion of input from a specific

sensory neuron. The number of synapses for each Basin neuron is shown in blue. (See also Table S4)

(B) Connectivity between mdIV neurons and Basins in *D. santomea* and *D. melanogaster*. Each node represents a cell type. Basin-2 receives direct inputs from mdIV and indirect inputs from mdIV via Basin-1.

(C) Bar charts showing rolling probability within a 15-s time window after 610-nm LED stimulation. In *D. melanogaster,* activation of Basin-2 evokes rolling, whereas activation of Basin-1 does not. Nonetheless, coactivation of Basin-2 and Basin-1 enhances the probability of rolling compared to activation of Basin-2 alone. Error bars indicate 95% confidence interval (N = 390, 320, and 253). Chi-square test: *** $p < 0.001$

(D) Violin plot of normalized crawling speed after optogenetic activation of Basin-1 alone, Basin-2 alone, or both Basin-1 and Basin-2. Circles with filled inner dots show the median values. Upper and lower edges of filled bars show 25$^{th}$ and 75$^{th}$ percentiles, respectively. (N = 229, N = 185, N = 158). Mann-Whitney U test: ** $p < 0.001$, *** $p < 0.001$. Rank-biserial correlation between Basin-1 and Basin-2, r = 0.246; between Basin-1 and co-activation of Basin-1 and Basin-2, r = -0.19; and between Basin 1 and co-activation of Basin-1 and Basin-2, r = -0.343.

(E) Number of rolls observed across 5 consecutive bouts of optogenetic activation (5 s / 30 s × 5 times) of Basin-1 alone, Basin-2 alone, or Basin-1 and Basin-2 (N = 30 per genotype). Basin-2 activation alone differed significantly from co-activation of Basin-1 and Basin-2. Mann-Whitney U test: $p = 0.010$

**STAR Methods:**

**Resource Availability**

**Lead contact**

Further information and requests for resources and reagents should be directed to and will be filled by the lead contact, Tomoko Ohyama (tomoko.ohyama@mcgill.ca)

**Materials Availability**

This study did not generate any new unique reagents.

**Data and Code Availability**

The EM volume data are available at https://ohyamalab.cs.mcgill.ca. Both the login name and password are "readonly".

All other data and analyses reported in this paper will be provided by the lead contact upon request.

This study did not generate any original code.

Any additional information required to reanalyse the data reported in this paper is available from the lead contact upon request.

**Experimental Model and Subject Details**

**Fly stocks and maintenance**

Drosophilds and *D. melanogaster* stock lines used in this study were raised on BDSC cornmeal food. Flies were maintained humidity-controlled chambers kept at 18°C and set to a 12-hour light/dark cycle. All crosses for experiments are reared at 25 °C.

**Methodological Details**

**Behavioral experiments**

Embryos grown on normal cornmeal food were collected for 24 hours at 25°C and 60% humidity. Nociceptive behavior experiments were performed on 3rd instar larvae in the wandering stage (see Table 1 for number of days). Optogenetic experiments were performed on wandering-stage 3rd instar larvae (for 4 days at 25°C). For optogenetic activation experiments, larvae containing the UAS-*CsChrimson* transgene were grown in the dark at 25°C for 4 days on fly food containing trans-retinal (SIGMA R2500) at a final concentration of 200 μM.

Before the experiments, the larvae were separated from the food using 15% sucrose, scooped with a paint brush into a sieve, and washed with water. The larvae were then dried and used for behavior experiments (using mechanical, thermal, or chemical nociceptive stimuli or optogenetic stimulation).

- **Thermal heat nociception assay**

The apparatus for the high-throughput nociceptive behavior assay has been described previously [32]. The setup consisted of a ring light illuminator; a computer to control stimulus presentation and record neural activity; and a camera to monitor and record larval behavior. Right before the behavior experiment, a black dot was painted with a permanent marker (Sharpie, Rub a Dub) on the dorsal midline of each individual larva at segments A4-6. Thermal nociceptive stimulation was applied by a 40 $mW/mm^2$, 808 nm laser light in the arena. All experiments were done with dots on the top. We tested approximately 20 larvae at once for the nociceptive behavior assay and 100 larvae at once for the optogenetic assay. The dot itself did not alter baseline behavior significantly without the 808 nm laser light. Snapshots of the arena were taken on the first frame of each recording to monitor the size and initial position of the dot. We selected dots ranging in size from 10 $mm^2$ to 150 $mm^2$ to minimize the effect of dot size on larval responses.

- **Thermal heat probe nociception assay**

Third instar larvae were subjected to a previously described thermal probe stimulation assay [38]. Animals were placed on moisturized petri dishes, and then stimulated with a heat probe on the dorsal side of the A4-6 segments until they started rolling or 5 seconds had elapsed. For each species, 100 animals were tested in a blinded fashion.

- **Mechanical nociception assay**

Third instar larvae were subjected to a previously described mechanical stimulation assay [28], but with a slight modification. They were placed on moisturized petri dishes, and then stimulated twice on the dorsal side of the A4-6 segments within 2 s, using Von Frey filaments (calibrated to 10–150 mN) adapted from Omniflex monofilament fishing line (6 lb test, 0.009 in [0.23 mm] in diameter) and attached to wooden handles. The corresponding responses were manually scored as no response, stop, stop and turn, bend, and roll. For each species, 100 animals were tested multiple times on different days in a blinded fashion.

- **Chemical nociception assay**

Third instar larvae were collected as in the mechanical nociception assay and placed on moisturized petri dishes. Subsequently, 1.5 ml of 7% HCl was pipetted gently on the posterior end of an individual larva, and simultaneously, the delay between the application of HCl and the start of first rolling was recorded. For each species, total of 100 animals were tested on different days in a blinded fashion.

- **Optogenetic behavior experiments**

The behavior apparatus was the similar as described previously [10], with modifications. The larvae were dried and placed in the center of the arena. The substrate for the behavioral experiments was 2% Bacto agar gel in a 25×25 $cm^2$ square plastic dishes. Larvae were washed with water at room

temperature in dim light room. The apparatus consisted of an infrared (IR) 850 nm light illuminator (Waveform Lighting), a computer controlling 627 LED (Waveform Lighting) stimulation, and a C-MOS camera (FLIR Grasshopper3; GS-U3-51S5M-C: Sony IMX250, Mono, 75 frames/s maximum, 2,448 × 2048 pixels) equipped with a fixed 25-mm lens (Edmund) and IR filter (750 nm M25.5 × 0.5 long-pass filter, Edmund) to monitor and record larvae. More than 100 animals were tested per genotype.

**Behavioral data analysis**

For the thermal heat nociception and optogenetic assay, larvae were tracked in real-time using MWT software https://github.com/Ichoran/choreography. We rejected objects that were tracked for less than 5 s or moved less than one body length of a larva. For each larva, MWT returns a contour, spine, and center of mass as a function of time [65]. From these tracking data we computed the key parameters of larval motion, using specific Choreography (a component of the MWT software package) variables that we tailored for larvae (as opposed to *C. elegans*) as described previously [10,32].

For further details of the software implementations for the above calculations, we refer the reader to the open-source package. The exact Choreography commands used to obtain each of the variables for all animals from one run were as follows (see documentation on Choreography [64] for definitions of all the parameters):

java -Xincgc -Xms8000m -Xmx8000m -jar/Users/Applications/Chore.jar -t 5 -s 0.1 -p 0.095 -M 1–shadowless –segment –nanless -o Dts1234 -O speed -N all.

java -Xincgc -Xms8000m -Xmx8000m -jar/Users/Applications/Chore.jar -t 5 -s 0.1 -p 0.095 -M 1–shadowless –segment –nanless -o Dtr1234 -O crabspeed -N all.

java -Xincgc -Xms8000m -Xmx8000m -jar/Users/Applications/Chore.jar -t 5 -s 0.1 -p 0.095 -M 1–shadowless –segment –nanless –plugin SpinesForward::rebias –plugin Reoutline::exp –plugin Respine::0.23::tapered=0.28,1,2 -o Dtm1234 -O length -N all.

java -Xincgc -Xms8000m -Xmx8000m -jar/Users/Applications/Chore.jar -t 5 -s 0.1 -p 0.095 -M 1–shadowless –segment –nanless –plugin Reoutline::exp –plugin Respine::0.23::tapered=0.28,1,2–plugin SpinesForward::rebias –minimum-biased 3mm -o DtC1234 -O cast -N all.

Depending on the follow-up analysis, these features were processed differently. To compare the same feature among all species as shown in Figure 1A, the feature of interest was averaged in a pre-determined time window for each individual and plotted as a violin plot. The time window for crabspeed and curvature was between 0 and 5 s after the onset of stimulation. The time window for calculating the speed before stimulation was the 5-s period immediately before the onset of stimulation, whereas that for calculating the speed after stimulation was the 5-s period beginning 5 s after the onset of stimulation. The time window for calculating the speed after stimulation was 5 s later than crabspeed and curvature because the first 5 s was mostly composed of crabspeed but not the speed along the body axis. The normalised speed was equal to the speed after stimulation divided by the speed before stimulation.

- **Behavior/action detection**

For the optogenetic assay, after extracting features from Choreography, we used a previously developed behavior classification method [10,37] to detect and quantify the following behaviors: hunching (Hunch), head-Bending (Bend), backwards crawling (Back-up), stopping (Stop), peristaltic crawling (Crawl), and escape rolling (Roll).

For the thermal (heat probe or IR stimulation), mechanical, and chemical nociception experiments, observers scored the behaviors manually. Rolling was defined as a 360-degree rotation around the body axis. The experimentalist was blind to the genotype. The behaviors tested by at least 2 independent observers were combined.

**Larval dissections and immunocytochemistry**

To analyze the location of sensory neurons in peripheral, we performed immunostaining for *D. melanogaster*, *D. santomea*, *D. virilis, D. persimilis*, and *D. biarmipes* larvae. Third instar progeny larvae were placed in phosphate-buffered saline (PBS; pH 7.4) in a Sylgard-coated dish and cut along the dorsal midline, after which its body wall was pinned. Filleted larvae were fixed with 4.0% paraformaldehyde for 30 min at room temperature, and then rinsed several times in PBS with 0.4% Triton X-100 (PBS-X). Primary antibodies were used at a concentration of 1:50 for rat mAb Elav-9F8A9 [42] and 1:25 for mouse mAb Futsch-22C10 [41] and then incubated overnight at 4°C. Secondary antibodies were anti-mouse Alexa488 (diluted 1:250; Invitrogen) and anti-rat Alexa568 (diluted 1:250; Invitrogen). After overnight incubation in secondary antibodies, the tissue was rinsed for several hours in PBS-X, and mounted in PRoLong Gold Antifade (Invitrogen). Immunofluorescence images were acquired by a Zeiss LSM 710 confocal microscope with 20×/NA0.8 and Zen digital imaging software (Zeiss). Optical sections or maximum intensity

projections were adjusted, cropped, and exported for presentation using Fiji software (ImageJ, NIH Bethesda).

**FIB-SEM sample preparation**

CNS of 1st instar larva of *D. santomea* were directly dissected out in fixative of 2.5 % folmaldehyde and 2.5% glutaraldehyde in 0.06 M phosphate buffer at pH 7.4, and fixed for 2 hours at 22 °C. After washing, the CNS were post-fixed in 0.5% osmium tetroxide in 0.05M sodium cacodylate buffer for 40 min then treaded with 0.8% potassium ferricyanide in buffer for 2 hours at 4 °C. After thoroughly washing, CNSs were incubated in 1% thiocarbohydrazide (TCH) in $H_2O$ for 15 min at 22°C, then thoroughly washed and followed by 2% osmium tetroxide in $H_2O$ for 30 min, After then tissue was incubated with 0.5% aqueous uranyl acetate for 30 min at 4 °C then followed by lead aspartate *en bloc* staining at 4 °C for overnight. A Progressive Lowering Temperature (PLT) procedure started from 0 °C when the tissues were transferred into 10% acetone. The temperature was progressively decreased to −25 °C while the acetone concentration was gradually increased to 97%. The tissue was incubated in 1% osmium tetroxide and 0.3% uranyl acetate in acetone for 32 hours at −25 °C. After PLT and low temperature incubation, the temperature was increased to 22 °C, and tissues were rinsed in pure acetone then infiltrated and embedded in Durcupan (ACM Fluka) [44]. One Durcupan embedded 1st instar larva of *D. santomea* sample, Santomea11172016_04, was chosen to prepare the high-resolution large volume images of the central nervous system (CNS) from the A3 to T1 region. This sample was first mounted to the top of a 1 mm copper post that was in contact with the metal-stained sample for better charge dissipation, as previously described [45]. A small vertical sample post was trimmed to the region of interest (ROI) with a width of 130 μm and a depth of 100 μm in the direction of the ion beam for each sample. The trimming was guided by X-ray tomography data obtained by a Zeiss Versa XRM-510 and optical inspection under a

microtome. Thin layers of conductive material of 10-nm gold followed by 100-nm carbon were coated on the trimmed samples using a Gatan PECS 682 High-Resolution Ion Beam Coater. The coating parameters were as follows: 6 keV, 200 nA on both argon gas plasma sources, and 10 rpm sample rotation with 45-degree tilt.

**FIB-SEM 3D large volume imaging**

The FIB-SEM prepared sample was imaged by a customized Zeiss NVision40 FIB-SEM system as previously described [44,65,66]. The block face was imaged by a 3 nA electron beam with 1.5 keV landing energy at 1.25 MHz scanning rate. A sample bias voltage of +400V was applied to filter out the secondary electrons. The x-y pixel resolution was set at 10 nm. A subsequently applied focused Ga+ beam of 27 nA at 30 keV strafed across the top surface and ablated away 5 nm of the surface. The newly exposed surface was then imaged again. The ablation – imaging cycle continued about once every minute for 13 days to complete the FIB-SEM imaging. The sequence of acquired images formed a raw imaged volume, followed by post processing of image registration and alignment using a Scale Invariant Feature Transform (SIFT) based algorithm. Every two consecutive images were finally binned and averaged down to one, forming a 10 nm × 10 nm × 10 nm isotropic voxel size throughout entire volume. The aligned dataset consists of CNS A3 to T1 region with a final volume of 70 μm × 55 μm × 105 μm, which can be viewed in any arbitrary orientation.

**Neuron reconstruction and analysis**

We performed neuron reconstruction in a CATMAID [45] to obtain the skeletonized structure and connectivity of the cells of interest. The process of reconstructing neurons in CATMAID involves

starting with a specified neurite in a section of the electron microscopy data, and manually building a 3-D skeleton representation of the neuronal morphology and the location of synaptic active zones and synaptic partners. The synaptic connections mapped and reported in this study all represent fast, chemical synapses. Synapses must match several criteria over multiple adjacent sections: a thick, black, active zone; vesicles; presynaptic specializations (e.g., a T-bar on the presynaptic side); and evidence of postsynaptic membrane specializations.

The neuronal reconstruction process has been previously described in detail [10,19]. Briefly, to identify sensory axons, reconstruction was initiated at the entry point of the nerves into the neuropil. Because sensory neurons project ventrally in the nerve cord and motor neurons project dorsally [67,68] the sensory axons were readily identified in the ventral portion of the nerve root. After reconstructing the main cables of all sensory neurons, we characterized the axonal arbors to identify mdIV neurons. For the annotation of mdIV targets in *D. santomea* FIB-SEM volumes, we manually reconstructed neurons postsynaptic to the mdIV terminals. As our imaging data were obtained from segments A3 to T2, we only reconstructed neurons that were located within segments A3 to A1s (i.e., local interneurons). After an experienced staff member first reconstructed and annotated the synapses and their partner neurons, a second experienced staff member independently reviewed the reconstruction and synapse annotation. We comprehensively reviewed and fully reconstructed only neurons that received a total of at least 10 synaptic inputs from mdIV neurons. In *Drosophila*, as in other insects, many neurons exhibit a stereotyped gross morphology, which makes it possible to identify individual neurons. Furthermore, insect nervous systems are largely bilaterally symmetric, with homologous neurons on the left and the right sides. In this study, therefore, we validated the wiring diagram by *1*) independently reconstructing partners of homologous neurons on the left and right sides of the nervous system, and *2*) identifying the

reconstructed homologous neurons from EM volumes of *D. melanogaster* data (https://l1em.catmaid.virtualflybrain.org/) based on the shapes of the neurons and the locations of their cell bodies.

Cable length and synapse numbers for each neuron, as well as dorsal and coronal views of neurons, were obtained from CATMAID software. All connectome data for *D. melanogaster* were obtained from *D. melanogaster* EM connectome data (https://l1em.catmaid.virtualflybrain.org/).

The EM volume data are available at https://ohyamalab.cs.mcgill.ca. Both the login name and password are "readonly".

**Quantification and statistical analysis**

Matlab was used for statistical analysis. The type of statistical test used in each experiment is indicated in figure legends. Sample numbers are indicated in figure legends. P values are represented by asterisks: **: $p < 0.01$, ***: $p < 0.001$

**Supplemental Video Title:**

**Video S1: Example of response to noxious heat in *D. biarmipes*, related to Figure 1**

**Video S2: Example of response to noxious heat in *D. virilis*, related to Figure 1**

**Video S3: Example of response to noxious heat in *D. persimilis*, related to Figure 1**

**Video S4: Example of response to noxious heat in *D. santomea*, related to Figure 1**

**Video S5: Example of response to noxious heat in *D. melanogaster*, related to Figure 1**

**Reference**


1. Finlay, B.L., Hinz, F., and Darlington, R.B. (2011). Mapping behavioural evolution onto brain evolution: the strategic roles of conserved organization in individuals and species. Philos Trans R Soc Lond B Biol Sci *366*, 2111-2123. 10.1098/rstb.2010.0344.

2. Striedter, G.F., Avise, J.C., and Ayala, F.J. (2012). In the light of evolution VI: brain and behavior. Proc Natl Acad Sci U S A *109 Suppl 1*, 10607-10611. 10.1073/pnas.1206166109.

3. Hale, M.E., Long, J.H., Jr., McHenry, M.J., and Westneat, M.W. (2002). Evolution of behavior and neural control of the fast-start escape response. Evolution *56*, 993-1007. 10.1111/j.0014-3820.2002.tb01411.x.

4. Godfrey, R.K., and Gronenberg, W. (2019). Brain evolution in social insects: advocating for the comparative approach. J Comp Physiol A Neuroethol Sens Neural Behav Physiol *205*, 13-32. 10.1007/s00359-019-01315-7.

5. Fischer, E.K., and O'Connell, L.A. (2017). Modification of feeding circuits in the evolution of social behavior. J Exp Biol *220*, 92-102. 10.1242/jeb.143859.

6. Katz, P.S. (2016). Evolution of central pattern generators and rhythmic behaviours. Philos Trans R Soc Lond B Biol Sci *371*, 20150057. 10.1098/rstb.2015.0057.

7. Scheffer, L.K., Xu, C.S., Januszewski, M., Lu, Z., Takemura, S.Y., Hayworth, K.J., Huang, G.B., Shinomiya, K., Maitlin-Shepard, J., Berg, S., et al. (2020). A connectome and analysis of the adult Drosophila central brain. Elife *9*. 10.7554/eLife.57443.

8. Takemura, S.Y., Bharioke, A., Lu, Z., Nern, A., Vitaladevuni, S., Rivlin, P.K., Katz, W.T., Olbris, D.J., Plaza, S.M., Winston, P., et al. (2013). A visual motion detection circuit suggested by Drosophila connectomics. Nature *500*, 175-181. 10.1038/nature12450.

9. Takemura, S.Y., Karuppudurai, T., Ting, C.Y., Lu, Z., Lee, C.H., and Meinertzhagen, I.A. (2011). Cholinergic circuits integrate neighboring visual signals in a Drosophila motion detection pathway. Curr Biol *21*, 2077-2084. 10.1016/j.cub.2011.10.053.

10. Ohyama, T., Schneider-Mizell, C.M., Fetter, R.D., Aleman, J.V., Franconville, R., Rivera-Alba, M., Mensh, B.D., Branson, K.M., Simpson, J.H., Truman, J.W., et al. (2015). A multilevel multimodal circuit enhances action selection in Drosophila. Nature *520*, 633-639. 10.1038/nature14297.

11. Dow, E., Jacobo, A., Hossain, S., Siletti, K., and Hudspeth, A.J. (2018). Connectomics of the zebrafish's lateral-line neuromast reveals wiring and miswiring in a simple microcircuit. Elife *7*. 10.7554/eLife.33988.

12. Wanner, A.A., Genoud, C., Masudi, T., Siksou, L., and Friedrich, R.W. (2016). Dense EM-based reconstruction of the interglomerular projectome in the zebrafish olfactory bulb. Nat Neurosci *19*, 816-825. 10.1038/nn.4290.

13. White, J.G., Southgate, E., Thomson, J.N., and Brenner, S. (1986). The structure of the nervous system of the nematode Caenorhabditis elegans. Philosophical transactions of the Royal Society of London. Series B, Biological sciences *314*, 1-340.

14. Ryan, K., Lu, Z., and Meinertzhagen, I.A. (2017). Circuit Homology between Decussating Pathways in the Ciona Larval CNS and the Vertebrate Startle-Response Pathway. Curr Biol *27*, 721-728. 10.1016/j.cub.2017.01.026.

15. Randel, N., Asadulina, A., Bezares-Calderon, L.A., Veraszto, C., Williams, E.A., Conzelmann, M., Shahidi, R., and Jekely, G. (2014). Neuronal connectome of a sensory-motor circuit for visual navigation. eLife, e02730. 10.7554/eLife.02730.

16. Berning, M., Boergens, K.M., and Helmstaedter, M. (2015). SegEM: Efficient Image Analysis for High-Resolution Connectomics. Neuron *87*, 1193-1206. 10.1016/j.neuron.2015.09.003.

17. Wilson, C.E., Lasher, R.S., Yang, R., Dzowo, Y., Kinnamon, J.C., and Finger, T.E. (2022). Taste Bud Connectome: Implications for Taste Information Processing. J Neurosci *42*, 804-816. 10.1523/JNEUROSCI.0838-21.2021.

18. Cook, S.J., Jarrell, T.A., Brittin, C.A., Wang, Y., Bloniarz, A.E., Yakovlev, M.A., Nguyen, K.C.Q., Tang, L.T., Bayer, E.A., Duerr, J.S., et al. (2019). Whole-animal connectomes of both Caenorhabditis elegans sexes. Nature *571*, 63-71. 10.1038/s41586-019-1352-7.

19. Schneider-Mizell, C.M., Gerhard, S., Longair, M., Kazimiers, T., Li, F., Zwart, M.F., Champion, A., Midgley, F.M., Fetter, R.D., Saalfeld, S., and Cardona, A. (2016). Quantitative neuroanatomy for connectomics in Drosophila. Elife *5*. 10.7554/eLife.12059.

20. Witvliet, D., Mulcahy, B., Mitchell, J.K., Meirovitch, Y., Berger, D.R., Wu, Y., Liu, Y., Koh, W.X., Parvathala, R., Holmyard, D., et al. (2021). Connectomes across development reveal principles of brain maturation. Nature *596*, 257-261. 10.1038/s41586-021-03778-8.

21. Hong, R.L., Riebesell, M., Bumbarger, D.J., Cook, S.J., Carstensen, H.R., Sarpolaki, T., Cochella, L., Castrejon, J., Moreno, E., Sieriebriennikov, B., et al. (2019). Evolution of neuronal anatomy and circuitry in two highly divergent nematode species. Elife *8*. 10.7554/eLife.47155.

22. Hwang, R.Y., Zhong, L., Xu, Y., Johnson, T., Zhang, F., Deisseroth, K., and Tracey, W.D. (2007). Nociceptive neurons protect Drosophila larvae from parasitoid wasps. Curr Biol *17*, 2105-2116. S0960-9822(07)02268-3 [pii] 10.1016/j.cub.2007.11.029.

23. Tsubouchi, A., Caldwell, J.C., and Tracey, W.D. (2012). Dendritic filopodia, Ripped Pocket, NOMPC, and NMDARs contribute to the sense of touch in Drosophila larvae. Curr Biol *22*, 2124-2134. 10.1016/j.cub.2012.09.019.

24. Takagi, S., Cocanougher, B.T., Niki, S., Miyamoto, D., Kohsaka, H., Kazama, H., Fetter, R.D., Truman, J.W., Zlatic, M., Cardona, A., and Nose, A. (2017). Divergent Connectivity

of Homologous Command-like Neurons Mediates Segment-Specific Touch Responses in Drosophila. Neuron *96*, 1373-1387 e1376. 10.1016/j.neuron.2017.10.030.

25. Tracey, W.D., Jr., Wilson, R.I., Laurent, G., and Benzer, S. (2003). painless, a Drosophila gene essential for nociception. Cell *113*, 261-273. S0092867403002721 [pii].

26. Honjo, K., Hwang, R.Y., and Tracey, W.D., Jr. (2012). Optogenetic manipulation of neural circuits and behavior in Drosophila larvae. Nat Protoc *7*, 1470-1478. 10.1038/nprot.2012.079.

27. Yoshino, J., Morikawa, R.K., Hasegawa, E., and Emoto, K. (2017). Neural Circuitry that Evokes Escape Behavior upon Activation of Nociceptive Sensory Neurons in Drosophila Larvae. Curr Biol *27*, 2499-2504 e2493. 10.1016/j.cub.2017.06.068.

28. Hu, C., Petersen, M., Hoyer, N., Spitzweck, B., Tenedini, F., Wang, D., Gruschka, A., Burchardt, L.S., Szpotowicz, E., Schweizer, M., et al. (2017). Sensory integration and neuromodulatory feedback facilitate Drosophila mechanonociceptive behavior. Nat Neurosci *20*, 1085-1095. 10.1038/nn.4580.

29. Burgos, A., Honjo, K., Ohyama, T., Qian, C.S., Shin, G.J., Gohl, D.M., Silies, M., Tracey, W.D., Zlatic, M., Cardona, A., and Grueber, W.B. (2018). Nociceptive interneurons control modular motor pathways to promote escape behavior in Drosophila. Elife *7*. 10.7554/eLife.26016.

30. Dason, J.S., Cheung, A., Anreiter, I., Montemurri, V.A., Allen, A.M., and Sokolowski, M.B. (2020). Drosophila melanogaster foraging regulates a nociceptive-like escape behavior through a developmentally plastic sensory circuit. Proc Natl Acad Sci U S A *117*, 23286-23291. 10.1073/pnas.1820840116.

31. Russo, C.A., Takezaki, N., and Nei, M. (1995). Molecular phylogeny and divergence times of drosophilid species. Mol Biol Evol *12*, 391-404. 10.1093/oxfordjournals.molbev.a040214.

32. Ohyama, T., Jovanic, T., Denisov, G., Dang, T.C., Hoffmann, D., Kerr, R.A., and Zlatic, M. (2013). High-throughput analysis of stimulus-evoked behaviors in Drosophila larva reveals multiple modality-specific escape strategies. PloS one *8*, e71706. 10.1371/journal.pone.0071706.

33. Fleury, F., Ris, N., Allemand, R., Fouillet, P., Carton, Y., and Bouletreau, M. (2004). Ecological and genetic interactions in Drosophila-parasitoids communities: a case study with D. melanogaster, D. simulans and their common Leptopilina parasitoids in south-eastern France. Genetica *120*, 181-194.

34. Carton Y, B.M., van Alphen JJM, van Lenteren JC (1986). The Drosophila parasitic waps (London Academic Press).

35. Carton, Y., and David, J.R. (1985). Relation between the genetic variability of digging behavior of Drosophila larvae and their susceptibility to a parasitic wasp. Behav Genet *15*, 143-154.

36. Lopez-Bellido, R., Himmel, N.J., Gutstein, H.B., Cox, D.N., and Galko, M.J. (2019). An assay for chemical nociception in Drosophila larvae. Philos Trans R Soc Lond B Biol Sci *374*, 20190282. 10.1098/rstb.2019.0282.

37. Masson, J.B., Laurent, F., Cardona, A., Barre, C., Skatchkovsky, N., Zlatic, M., and Jovanic, T. (2020). Identifying neural substrates of competitive interactions and sequence transitions during mechanosensory responses in Drosophila. PLoS Genet *16*, e1008589. 10.1371/journal.pgen.1008589.

38. Zhong, L., Hwang, R.Y., and Tracey, W.D. (2010). Pickpocket is a DEG/ENaC protein required for mechanical nociception in Drosophila larvae. Curr Biol *20*, 429-434. 10.1016/j.cub.2009.12.057.

39. Kim, S.E., Coste, B., Chadha, A., Cook, B., and Patapoutian, A. (2012). The role of Drosophila Piezo in mechanical nociception. Nature *483*, 209-212. 10.1038/nature10801.

40. Fujita, S.C., Zipursky, S.L., Benzer, S., Ferrus, A., and Shotwell, S.L. (1982). Monoclonal antibodies against the Drosophila nervous system. Proc Natl Acad Sci U S A *79*, 7929-7933. 10.1073/pnas.79.24.7929.

41. Zipursky, S.L., Venkatesh, T.R., Teplow, D.B., and Benzer, S. (1984). Neuronal development in the Drosophila retina: monoclonal antibodies as molecular probes. Cell *36*, 15-26. 10.1016/0092-8674(84)90069-2.

42. O'Neill, E.M., Rebay, I., Tjian, R., and Rubin, G.M. (1994). The activities of two Ets-related transcription factors required for Drosophila eye development are modulated by the Ras/MAPK pathway. Cell *78*, 137-147. 10.1016/0092-8674(94)90580-0.

43. Orgogozo, V., and Schweisguth, F. (2004). Evolution of the larval peripheral nervous system in Drosophila species has involved a change in sensory cell lineage. Dev Genes Evol *214*, 442-452. 10.1007/s00427-004-0422-4.

44. Xu, C.S., Hayworth, K.J., Lu, Z., Grob, P., Hassan, A.M., Garcia-Cerdan, J.G., Niyogi, K.K., Nogales, E., Weinberg, R.J., and Hess, H.F. (2017). Enhanced FIB-SEM systems for large-volume 3D imaging. Elife *6*. 10.7554/eLife.25916.

45. Saalfeld, S., Cardona, A., Hartenstein, V., and Tomancak, P. (2009). CATMAID: collaborative annotation toolkit for massive amounts of image data. Bioinformatics *25*, 1984-1986. 10.1093/bioinformatics/btp266.

46. Robertson, J.L., Tsubouchi, A., and Tracey, W.D. (2013). Larval defense against attack from parasitoid wasps requires nociceptive neurons. PloS one *8*, e78704. 10.1371/journal.pone.0078704.

47. Grueber, W.B., Jan, L.Y., and Jan, Y.N. (2002). Tiling of the Drosophila epidermis by multidendritic sensory neurons. Development *129*, 2867-2878.

48. Gerhard, S., Andrade, I., Fetter, R.D., Cardona, A., and Schneider-Mizell, C.M. (2017). Conserved neural circuit structure across Drosophila larval development revealed by comparative connectomics. Elife *6*. 10.7554/eLife.29089.

49. Merritt, D.J., and Whitington, P.M. (1995). Central projections of sensory neurons in the Drosophila embryo correlate with sensory modality, soma position, and proneural gene function. J Neurosci *15*, 1755-1767.

50. Valdes-Aleman, J., Fetter, R.D., Sales, E.C., Heckman, E.L., Venkatasubramanian, L., Doe, C.Q., Landgraf, M., Cardona, A., and Zlatic, M. (2021). Comparative Connectomics Reveals How Partner Identity, Location, and Activity Specify Synaptic Connectivity in Drosophila. Neuron *109*, 105-122 e107. 10.1016/j.neuron.2020.10.004.

51. Grueber, W.B., Yang, C.H., Ye, B., and Jan, Y.N. (2005). The development of neuronal morphology in insects. Curr Biol *15*, R730-738. 10.1016/j.cub.2005.08.023.

52. de Bruyne, M., Foster, K., and Carlson, J.R. (2001). Odor coding in the Drosophila antenna. Neuron *30*, 537-552. 10.1016/s0896-6273(01)00289-6.

53. Lu, T., Qiu, Y.T., Wang, G., Kwon, J.Y., Rutzler, M., Kwon, H.W., Pitts, R.J., van Loon, J.J., Takken, W., Carlson, J.R., and Zwiebel, L.J. (2007). Odor coding in the maxillary palp of the malaria vector mosquito Anopheles gambiae. Curr Biol *17*, 1533-1544. 10.1016/j.cub.2007.07.062.

54. Dumont, J.P., and Robertson, R.M. (1986). Neuronal circuits: an evolutionary perspective. Science *233*, 849-853. 10.1126/science.233.4766.849.

55. Jovanic, T., Schneider-Mizell, C., Shao, M., Masson, J-B., Denisov, G., Fetter, R. G., Mensh, B. D., Truman, J. W., Cardona, A., Zlatic, M. (2016). Competitive disinhibition mediates behavioral choice and sequences in Drosophila. Cell *in press*.

56. Ding, Y., Berrocal, A., Morita, T., Longden, K.D., and Stern, D.L. (2016). Natural courtship song variation caused by an intronic retroelement in an ion channel gene. Nature *536*, 329-332. 10.1038/nature19093.

57. Aiello, B.R., Westneat, M.W., and Hale, M.E. (2017). Mechanosensation is evolutionarily tuned to locomotor mechanics. Proc Natl Acad Sci U S A *114*, 4459-4464. 10.1073/pnas.1616839114.

58. Jourjine, N., and Hoekstra, H.E. (2021). Expanding evolutionary neuroscience: insights from comparing variation in behavior. Neuron *109*, 1084-1099. 10.1016/j.neuron.2021.02.002.

59. Baker, B.S., Taylor, B.J., and Hall, J.C. (2001). Are complex behaviors specified by dedicated regulatory genes? Reasoning from Drosophila. Cell *105*, 13-24. 10.1016/s0092-8674(01)00293-8.

60. Massey, J.H., Chung, D., Siwanowicz, I., Stern, D.L., and Wittkopp, P.J. (2019). The yellow gene influences Drosophila male mating success through sex comb melanization. Elife *8*. 10.7554/eLife.49388.

61. Auer, T.O., Shahandeh, M.P., and Benton, R. (2021). Drosophila sechellia: A Genetic Model for Behavioral Evolution and Neuroecology. Annu Rev Genet *55*, 527-554. 10.1146/annurev-genet-071719-020719.

62. Ding, Y., Lillvis, J.L., Cande, J., Berman, G.J., Arthur, B.J., Long, X., Xu, M., Dickson, B.J., and Stern, D.L. (2019). Neural Evolution of Context-Dependent Fly Song. Curr Biol *29*, 1089-1099 e1087. 10.1016/j.cub.2019.02.019.

63. Katz, P.S. (2011). Neural mechanisms underlying the evolvability of behaviour. Philos Trans R Soc Lond B Biol Sci *366*, 2086-2099. 10.1098/rstb.2010.0336.

64. Swierczek, N.A., Giles, A.C., Rankin, C.H., and Kerr, R.A. (2011). High-throughput behavioral analysis in C. elegans. Nat Methods *8*, 592-598. nmeth.1625 [pii] 10.1038/nmeth.1625.

65. Xu. C. S., H., K. J. & Hess, H. F (2020) Enhanced FIB-SEM systems for large-volume 3D imaging. USA.

66. Xu, C.S., Pang, S., Hayworth, K. J. & Hess, H. F. (2020). Transforming FIB-SEM Systems for Large-Volume Connectomics and Cell Biology. (Springer Protocols). https://doi.org/10.1007/978-1-0716-0691-9_12.

67. Landgraf, M., Jeffrey, V., Fujioka, M., Jaynes, J.B., and Bate, M. (2003). Embryonic origins of a motor system: motor dendrites form a myotopic map in Drosophila. PLoS biology *1*, E41. 10.1371/journal.pbio.0000041.

68. Kohsaka, H., Okusawa, S., Itakura, Y., Fushiki, A., and Nose, A. (2012). Development of larval motor circuits in Drosophila. Dev Growth Differ *54*, 408-419. 10.1111/j.1440-169X.2012.01347.x.

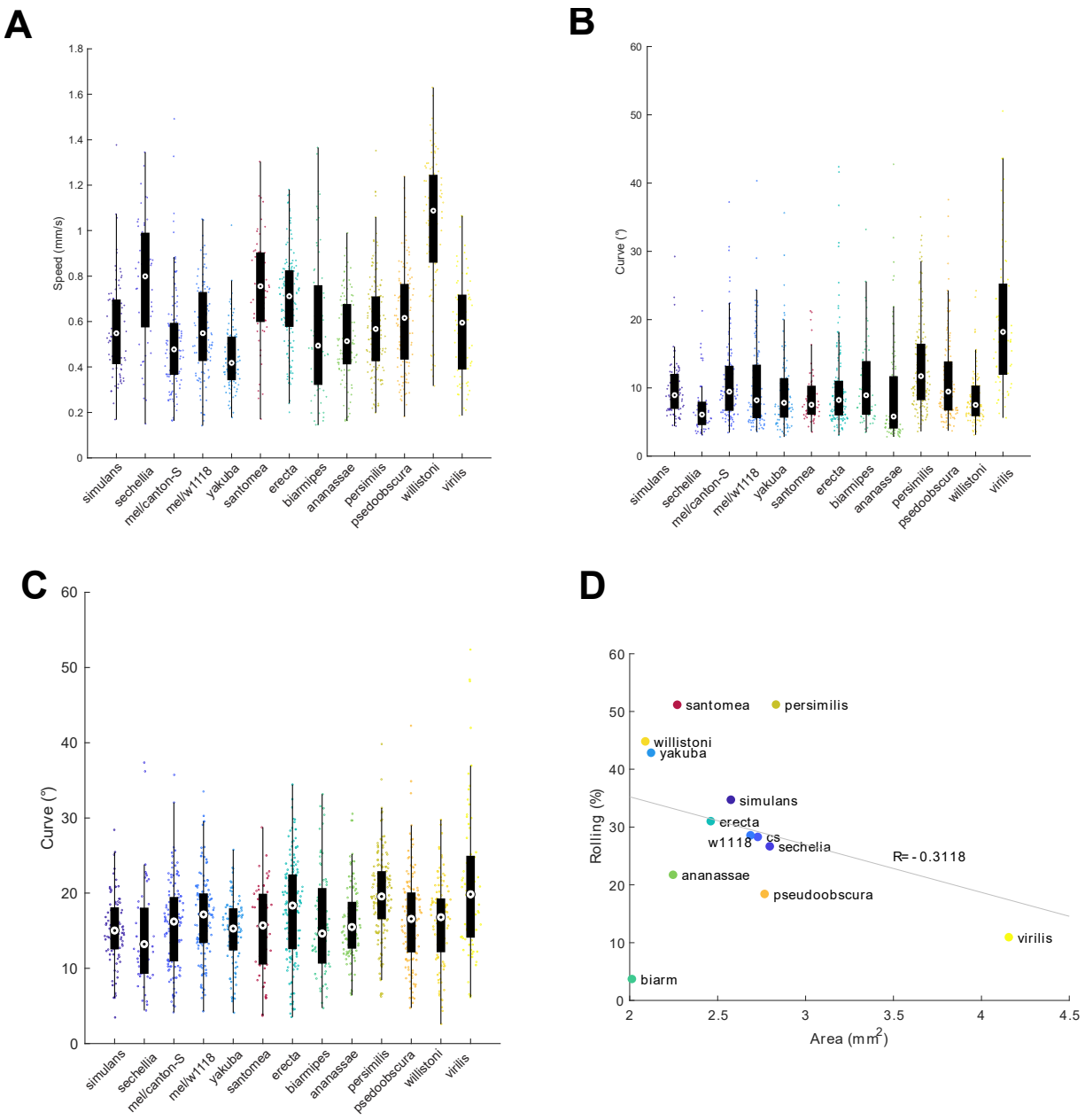


**Figure S1. Drosophila species show a wide range of escape responses to noxious heat stimulation. Related to Figure 1**

(A) Violin plot of crawling speed before noxious heat in each species. Circles with filled inner dots show the median values. Upper and lower edges of filled bars show 25$^{th}$ and 75$^{th}$ percentiles, respectively.

(B) Violin plot of curvature of body before noxious heat application. Circles with filled inner dots show the median values. Upper and lower edges of filled bars show $25^{th}$ and $75^{th}$ percentiles, respectively.

(C) Violin plot of curvature of body after noxious heat application. Circles with filled inner dots show the median values. Upper and lower edges of filled bars show $25^{th}$ and $75^{th}$ percentiles, respectively.

(D) Correlation analysis between probability of rolling and area of larvae.

| species name | habitat | land | subgroup | group | 3rd instar |
|---|---|---|---|---|---|
| *D. simulans* | generalist | mainland | melanogaster | melanogaster | 4 days |
| *D. sechellia* | specialist | island | melanogaster | melanogaster | 4 days |
| *D. melanogaster* | generalist | mainland | melanogaster | melanogaster | 4 days |
| *D. yakuba* | generalist | mainland | melanogaster | melanogaster | 4 days |
| *D. santomea* | generalist | island | melanogaster | melanogaster | 4 days |
| *D. erecta* | specialist | mainland | melanogaster | melanogaster | 4 days |
| *D. biarmipes* | generalist | mainland | suzuki/takahashii | melanogaster | 4 days |
| *D. ananassae* | generalist | mainland | ananassae | melanogaster | 4 days |
| *D. persimilis* | generalist | mainland | | obscura | 4 days |
| *D. pseudoobscura* | generalist | mainland | | obscura | 7 days |
| *D. willistoni* | generalist | mainland | | willistoni | 4 days |
| *D. virilis* | generalist | mainland | | virilis | 7 days |

**Table S1: Drosophid species used in this study. Related to Figure 1**

| | | *D.melanogaster* | | *D. santomea* | | | | | | *D. biampes* | | | *D. virilis* | | | *D. persimilis* | | |
|---|---|---|---|---|---|---|---|---|---|---|---|---|---|---|---|---|---|---|
| | | 1 | 2 | 1 | 2 | 3 | 4 | 5 | 6 | 1 | 2 | 3 | 1 | 2 | 3 | 1 | 2 | 3 |
| Dorsal cluster | | | | | | | | | | | | | | | | | | |
| md | **8** | 8 | 8 | 8 | 8 | 8 | 7 | 8 | 8 | 8 | 8 | 7 | 8 | 8 | 8 | 8 | 7 | 8 |
| es | **5** | 5 | 5 | 5 | 5 | 5 | 4 | 5 | 5 | 5 | 5 | 5 | 5 | 5 | 5 | 5 | 5 | 5 |
| subtotal | **13** | 13 | 13 | 13 | 13 | 13 | 12 | 14 | 13 | 13 | 13 | 12 | 13 | 13 | 13 | 13 | 12 | 13 |
| Lateral cluster | | | | | | | | | | | | | | | | | | |
| md | **2** | 2 | 2 | 2 | 2 | 2 | 2 | 3 | 2 | 2 | 2 | 2 | 2 | 2 | 2 | 2 | 2 | 2 |
| vch | **1** | 1 | 1 | 1 | 1 | 1 | 1 | 1 | 1 | 1 | 1 | 1 | 1 | 1 | 1 | 1 | 1 | 1 |
| lch | **5** | 5 | 5 | 5 | 5 | 5 | 5 | 5 | 5 | 5 | 5 | 4 | 5 | 5 | 5 | 5 | 5 | 5 |
| es | **3** | 3 | 3 | 3 | 3 | 3 | 2 | 2 | 3 | 3 | 2 | 3 | 3 | 3 | 2 | 3 | 2 | 3 |
| subtotal | **11** | 11 | 11 | 11 | 11 | 11 | 10 | 11 | 11 | 11 | 10 | 10 | 11 | 11 | 10 | 11 | 10 | 11 |
| v'cluster | | | | | | | | | | | | | | | | | | |
| md | **4** | 4 | 4 | 4 | 4 | 4 | 4 | 4 | 4 | 4 | 4 | 4 | 4 | 4 | 4 | 4 | 4 | 4 |
| es | **4** | 4 | 4 | 4 | 4 | 4 | 4 | 4 | 4 | 4 | 4 | 4 | 4 | 4 | 4 | 4 | 4 | 4 |
| subtotal | **8** | 8 | 8 | 8 | 8 | 8 | 8 | 8 | 8 | 8 | 8 | 8 | 8 | 8 | 8 | 8 | 8 | 8 |
| Ventral cluster | | | | | | | | | | | | | | | | | | |
| md | **6** | 6 | 6 | 6 | 6 | 6 | 6 | 6 | 6 | 6 | 6 | 6 | 6 | 6 | 6 | 6 | 6 | 6 |
| ch | **2** | 2 | 2 | 2 | 2 | 2 | 2 | 2 | 2 | 2 | 2 | 2 | 2 | 2 | 2 | 2 | 2 | 2 |
| es | **3** | 3 | 3 | 3 | 3 | 3 | 3 | 3 | 3 | 3 | 4 | 3 | 3 | 3 | 2 | 3 | 3 | 3 |
| subtotal | **11** | 11 | 11 | 11 | 11 | 11 | 11 | 11 | 11 | 11 | 12 | 11 | 11 | 11 | 11 | 11 | 11 | 11 |

**Table S2. Number of sensory neurons in *D. melanogasterD. santomea, D. biampes, D. virilis* and *D. persimilis.* Related to Figure 2**

Notes: The leftmost column lists the types of sensory neurons, grouped into four clusters from top to bottom, by location within the larval body: dorsal, lateral, ventral prime, and ventral. The second column from the left shows the numbers (in bold) of each sensory neuron type identifiable in an individual larva, as reported in the literature [S1]. The columns to the right show the corresponding numbers of neurons we identified from dissections performed in two *D. melanogaster*, six *D. santomaea, three D.biampes, three D.virilis and three D. persimilis* larvae. ch, chordotonal neurons; d, dorsal; es, external sensory neurons; md, multidendritic neurons, v', ventral prime.

| Neuron Name | Neuron Type | Cell body position | Number of Synapse | left dorsal | left medial | Left ventral | right dorsal | right medial | right ventral |
|---|---|---|---|---|---|---|---|---|---|
| Neuron 292196_A2L_D&B | D&B | A2 | 57 | 15 | 20 | 18 | 2 | 2 | 0 |
| neuron 199926 | Ace/Dec | Inter | 55 | 22 | 9 | 18 | 3 | 3 | 0 |
| A2_R_Chair | Chair-1 | A2 | 50 | 0 | 2 | 0 | 11 | 17 | 20 |
| Neuron 219265_A2R_D&B | D&B | A2 | 48 | 0 | 2 | 0 | 10 | 25 | 11 |
| neuron 3977 | Ace/Dec | Inter | 47 | 27 | 5 | 10 | 5 | 0 | 0 |
| Neuron 214395 | Cand SeIN138 Dec | Inter | 44 | 15 | 8 | 9 | 9 | 3 | 0 |
| neuron 3967 | Basin | A3 | 44 | 9 | 12 | 18 | 1 | 3 | 1 |
| neuron 45666 | Cand SeIN138 Dec | Inter | 38 | 3 | 2 | 11 | 17 | 5 | 0 |
| Neuron 69015 putative basin 2 R | Basin | A2 | 37 | 0 | 0 | 0 | 28 | 4 | 5 |
| Neuron 203347 A2R_pseudolooper3/4 | A02n/m | A2 | 37 | 17 | 2 | 5 | 9 | 4 | 0 |
| A2_L_Chair | Chair-1 | A2 | 35 | 3 | 21 | 7 | 0 | 3 | 1 |
| neuron 72844 putative basin 2 L | Basin | A2 | 33 | 22 | 1 | 9 | 1 | 0 | 0 |
| Neuron 219773 putative basin 1L | Basin | A2 | 33 | 12 | 10 | 5 | 3 | 3 | 0 |
| neuron 54415 putative basin 1 R | Basin | A2 | 30 | 0 | 3 | 0 | 13 | 14 | 0 |
| neuron 197062 | Cand A02o | Inter | 30 | 14 | 4 | 7 | 2 | 3 | 0 |
| A2_R_A27n | A27n | A2 | 26 | 0 | 7 | 1 | 2 | 14 | 2 |
| neuron 133032 | Unknown | Inter | 26 | 0 | 0 | 0 | 16 | 10 | 0 |
| Neuron 284599 | Cand A08n Asc | Inter | 24 | 2 | 4 | 4 | 11 | 3 | 0 |
| neuron 126189 | Ace/Dec | Inter | 24 | 3 | 11 | 5 | 0 | 5 | 0 |
| Neuron 282631 | Cand A02o | A2 | 23 | 0 | 1 | 1 | 12 | 9 | 0 |

| | | | | | | | | | |
|---|---|---|---|---|---|---|---|---|---|
| neuron 4601 | | | | | | | | | |
| A2R_pseudolooper3/4 | A02n/m | Inter | 22 | 5 | 0 | 0 | 11 | 0 | 6 |
| Neuron 284030 | Ace/Dec | Inter | 22 | 0 | 0 | 0 | 14 | 8 | 0 |
| neuron 65240 putative | | | | | | | | | |
| basin 4 R | Ace/Dec | A2 | 20 | 0 | 3 | 0 | 2 | 12 | 3 |
| neuron 258300 | | | | | | | | | |
| A2L_pseudolooper3/4 | A02n/m | A2 | 20 | 10 | 2 | 2 | 6 | 0 | 0 |
| A2_L_A27n | A27n | A2 | 18 | 4 | 8 | 3 | 1 | 2 | 0 |
| neuron 218890 | Ace/Dec | Inter | 18 | 5 | 6 | 0 | 5 | 1 | 1 |
| Neuron 284476 | | | | | | | | | |
| putative basin 4L | Basin | A2 | 15 | 1 | 7 | 4 | 2 | 1 | 0 |
| neuron 218606 | Ace/Dec | Inter | 15 | 2 | 0 | 2 | 7 | 3 | 1 |
| neuron 26482 | Basin | A3 | 14 | 0 | 0 | 0 | 10 | 4 | 0 |
| neuron 186890 | Cand A08n | Inter | 13 | 0 | 0 | 3 | 6 | 4 | 0 |
| neuron 38703 | Ace/Dec | Inter | 13 | 0 | 0 | 0 | 0 | 2 | 11 |
| neuron 8158 | Basin | A3 | 13 | 0 | 0 | 0 | 1 | 9 | 3 |
| neuron 29388 | Chair | A1 | 13 | 0 | 0 | 0 | 0 | 3 | 10 |
| Neuron 171223 | | | | | | | | | |
| A2L_pseudolooper3/4 | A02n/m | A2 | 12 | 10 | 0 | 0 | 2 | 0 | 0 |
| neuron 123536 | Ace/Dec | Inter | 12 | 0 | 0 | 0 | 5 | 7 | 0 |
| neuron 163036 | Ace/Dec | Inter | 11 | 0 | 0 | 0 | 0 | 0 | 11 |

**Table S3 Strong partners (>10 synapses from downstream of mdIV neurons) of mdIV neurons and synapse number with each mdIV neurons. Related to Figure 4**

| ***D.santomea*** | **Basin1** | **Basin1** | **Basin2** | **Basin2** | **Basin3** | **Basin3** | **Basin4** | **Basin4** |
|---|---|---|---|---|---|---|---|---|
| Total Synapse number of Basin | 337 | 317 | 235 | 291 | 222 | 263 | 168 | 165 |
| Upstream neuron | | | | | | | | |
| mdiivA2 left dorsal | 10 | 0 | 21 | 0 | 1 | 0 | 2 | 0 |
| mdivA2 right dorsal | 2 | 13 | 1 | 25 | 1 | 0 | 3 | 2 |
| mdiv A2 left medial | 10 | 3 | 1 | 0 | 0 | 0 | 5 | 3 |
| mdiv A2 right medial | 3 | 12 | 0 | 4 | 0 | 0 | 1 | 13 |
| mdivA2 left ventral | 5 | 0 | 8 | 0 | 1 | 0 | 4 | 0 |
| mdivA2 right ventral | 0 | 0 | 0 | 6 | 0 | 0 | 0 | 3 |
| | **30** | **28** | **31** | **35** | **3** | **0** | **15** | **21** |
| **Fraction input from MdIV** | **8.90%** | **8.83%** | **13.19%** | **12.03%** | **1.35%** | **0.00%** | **8.93%** | **12.73%** |
| A2l_lch5-1 | 6 | 0 | 2 | 0 | 1 | 0 | 0 | 0 |
| A2l_lch5-24-1 | 0 | 0 | 1 | 0 | 0 | 0 | 0 | 0 |
| A2l_lch5-24-2 | 1 | 0 | 1 | 0 | 0 | 0 | 0 | 0 |
| A2l_lch5-3 | 5 | 0 | 0 | 0 | 5 | 0 | 3 | 0 |
| A2l_lch5-5 | 3 | 0 | 2 | 0 | 1 | 0 | 0 | 0 |
| A2r_lch5_24-1 | 0 | 4 | 0 | 2 | 0 | 0 | 0 | 0 |
| A2r_lch5_24-2 | 0 | 3 | 0 | 0 | 0 | 0 | 0 | 0 |
| A2r_lch5-1 | 0 | 11 | 0 | 5 | 0 | 0 | 0 | 0 |
| A2r_lch5-3 | 0 | 8 | 0 | 2 | 0 | 4 | 0 | 2 |
| A2l_v'ch1 | 13 | 0 | 8 | 0 | 2 | 0 | 0 | 0 |
| A2l_vchA/B_1 | 6 | 0 | 2 | 0 | 4 | 0 | 5 | 0 |
| A2l_vchA/B_2 | 1 | 0 | 1 | 0 | 8 | 0 | 1 | 0 |
| A2r_v'ch1 | 0 | 17 | 0 | 9 | 0 | 0 | 0 | 0 |
| A2r_vchA/B_1 | 0 | 5 | 0 | 2 | 0 | 7 | 0 | 6 |
| A2r_vchA/B_2 | 0 | 13 | 0 | 5 | 0 | 5 | 0 | 4 |
| | **35** | **61** | **17** | **25** | **21** | **16** | **9** | **12** |
| **Fraction input from mechano-ch** | **10.39%** | **19.24%** | **7.23%** | **8.59%** | **9.46%** | **6.08%** | **5.36%** | **7.27%** |

| ***D.melanogaster*** | **Basin1** | **Basin1** | **Babsin2** | **Basin2** | **Basin3** | **Basin3** | **Basin4** | **Basin4** |
|---|---|---|---|---|---|---|---|---|
| Total Synapse number of Basin | 360 | 393 | 301 | 337 | 249 | 172 | 198 | 206 |
| Upstream neuron | | | | | | | | |
| ppk_ddaC_a1 | 0 | 0 | 0 | 7 | 0 | 0 | 3 | 0 |
| ppk_ddaC_a1 | 0 | 0 | 4 | 0 | 0 | 0 | 0 | 5 |
| ppk_v'ada_a1 | 0 | 0 | 0 | 12 | 0 | 0 | 19 | 0 |
| ppk_v'ada_a1 | 0 | 0 | 12 | 0 | 0 | 0 | 0 | 10 |

| | | | | | | | | |
|---|---|---|---|---|---|---|---|---|
| ppk_vdaB_a1 | 2 | 0 | 2 | 0 | 0 | 1 | 2 | 15 |
| ppk_vdaB_a1 | 0 | 1 | 0 | 1 | 0 | 0 | 14 | 5 |
| | **2** | **1** | **18** | **20** | **0** | **1** | **38** | **35** |
| **Fraction input from MdIV** | **0.56%** | **0.25%** | **5.98%** | **5.93%** | **0.00%** | **0.58%** | **19.19%** | **16.99%** |
| chos_lch5-1_a1 | 0 | 9 | 0 | 1 | 13 | 0 | 4 | 0 |
| chos_lch5-1_a1 | 4 | 0 | 3 | 0 | 0 | 4 | 0 | 3 |
| chos_lch5-24-1_a1 | 0 | 9 | 0 | 0 | 0 | 0 | 0 | 0 |
| chos_lch5-24-1_a1 | 4 | 0 | 0 | 0 | 0 | 0 | 0 | 0 |
| chos_lch5-24-2_a1 | 0 | 5 | 0 | 1 | 0 | 0 | 0 | 0 |
| chos_lch5-24-2_a1 | 3 | 0 | 0 | 0 | 0 | 0 | 0 | 0 |
| chos_lch5-3_a1 | 2 | 0 | 2 | 0 | 0 | 3 | 0 | 0 |
| chos_lch5-3_a1 | 0 | 5 | 0 | 0 | 0 | 0 | 0 | 0 |
| chos_lch5-5_a1 | 0 | 0 | 0 | 1 | 0 | 0 | 0 | 0 |
| chos_v'ch_a1 | 0 | 11 | 0 | 13 | 4 | 0 | 0 | 0 |
| chos_v'ch_a1 | 11 | 0 | 6 | 0 | 0 | 0 | 0 | 0 |
| chos_vchAB1_a1 | 5 | 0 | 0 | 0 | 0 | 10 | 0 | 8 |
| chos_vchAB1_a1 | 0 | 4 | 0 | 0 | 9 | 0 | 0 | 0 |
| chos_vchAB2_a1 | 0 | 9 | 0 | 0 | 12 | 0 | 3 | 0 |
| chos_vchAB2_a1 | 1 | 0 | 1 | 0 | 0 | 11 | 0 | 9 |
| | **30** | **52** | **12** | **16** | **38** | **28** | **7** | **20** |
| **Fraction input from mechano-ch** | **8.33%** | **13.23%** | **3.99%** | **4.75%** | **15.26%** | **16.28%** | **3.54%** | **9.71%** |

**Table S4 Connectivity between Basins and mdIV or chordotonal neurons in *D. santomea* and *D. melanogaster.* Related to Figure 5**

## Supplemental Reference

S1. Orgogozo V, Grueber WB. FlyPNS, a database of the Drosophila embryonic and larval peripheral nervous system. BMC Dev Biol. 2005;5:4.

## CHAPTER 4 Discussion

1. Subtypes of Basin neurons have different functions in escape-rolling

Basin-1 and -2 have been found to favor different responses to vibratory mechanosensory stimuli and to compete through various inhibition motifs (Jovanic et al., 2016). This finding supports the idea that although Basin-1 to Basin-4 are all Basin neurons with similar morphologies, they might perform different tasks under different scenarios.

Previous studies have revealed that Basin neurons receive sensory inputs from different neurons: Basin-2 and Basin-4 receive both nociceptive inputs from mdIV neurons and mechanosensory inputs from chordotonal neurons, while Basin-1 and Basin-3 only receive mechanosensory inputs from chordotonal neurons (Ohyama et al., 2015). Varied inputs from the sensory system suggest that they may function differently in the escape rolling circuit. Ohyama et al. (2015) explored their functions and reported that Basin-2 and Basin-4 trigger rolling while Basin-1 or Basin-3 do not. However, Basin-1 activation facilitated Basin-4-evoked rolling in a supra-linear manner. This facilitation is also examined in Figure 5C-E of Chapter 3, where the activation of Basin-1 and Basin-2 increased not only the rolling percentage at the population level, but also the total rolling events of individual larvae in a repeated stimulation protocol. The connectome comparison in Chapter 3 illustrates that this Basin-1-mediated facilitation might be enhanced in *D. santomea* due to strengthened nociceptive inputs onto Basin-1 neurons, which results in an increased level of rolling. As mentioned above, Basin-3, like Basin-1, is not reported to trigger rolling. Although evidence on their functional roles in escape rolling has yet to be published, connectome data shows that Basin-3 is directly upstream of A00c (i.e., a group of ascending neurons facilitating rolling in a supralinear way) and indirectly upstream of Goro (via

both the VNC and the brain pathway. This connectivity suggests that similar to Basin-1, Basin-3 may also facilitate *Drosophila* larval escape rolling.

It should be noted that although rolling is triggered by activating either Basin-2 or Basin-4, the rolling patterns differ, as indicated by the single activation data shown in Figure 8 – supplement 1A-C of Chapter 2. Whereas Basin-4 activation elicits a short burst of rolling exclusively at the onset of the stimulation, Basin-2 activation triggers continuous rolling throughout the period of stimulation. This finding suggests that distinct mechanisms may modulate their firing patterns and functions. On the one hand, Basin-4 neurons seem to be in charge of rolling initiation and possess mechanisms that suppress their prolongation. On the other hand, Basin-2 could be activated continuously to maintain the state of rolling and prevent automatic termination of rolling. The elongated rolling events during Basin-2 activation suggest the existence of neural mechanisms ensuring that Basin-2 rarely habituates to long periods of activation. In order to examine such a mechanism, it would be helpful to record Basin-2 and Basin-4 firing with sensory stimuli and simultaneously observe whether they fire for different durations. With the same stimuli given to intact larvae, latencies of larval behavioral responses could also be recorded to compare with the timing of Basin-2 and Basin-4 firing to test the association. Selective inhibition of either Basin-2 or Basin-4 could provide more precise insights into whether or not they play different roles within the escape circuit.

2. *Drosophila* larvae as an animal model for elucidating the neural bases of the hierarchical suppression model of behavioral sequences

Ohyama et al. (2015) reported that *Drosophila* larval escape behavior triggered by Basin neurons is a sequential behavior where rolling is followed by escape crawling (i.e., a locomotion

faster than its standard form). This escape sequence was investigated in this thesis, and the results supported the hierarchical suppression model better than other theories of action sequences.

The hierarchical suppression model was first introduced in a seminal work discussing human typing behavior, demonstrating that mistakenly typed letters did not happen randomly (Lashley, 1951). Rather, these letters were expected to be typed within the same word or the immediate neighboring word in a sentence. Thus, Lashley (1951) posited that once the action modules of typing different letters were activated simultaneously, they inhibited each other to form an inhibition hierarchy. This mutual inhibition would establish the correct typing sequence, whereby letters with a higher hierarchy were typed earlier. To summarize, the hierarchical suppression model posits that in an action sequence: a) action modules are activated in parallel and mutually inhibited; b) an inhibition hierarchy encodes the action sequence; and c) each action terminates itself to allow the execution of other actions. To date, we have accumulated a good amount of behavior-level evidence, although we still lack evidence at the level of neural circuits.

*Drosophila* larval escape behavior has the potential to serve as an animal model to provide evidence for the hierarchical suppression model of behavioral sequences at both the behavioral and neural circuit levels. With this strict sequence of rolling and the subsequent fast crawling, previous research reported that when activated by Goro, rolling could be triggered without the following fast crawling. This finding suggests the separate activation of rolling and fast crawling, refuting a possible synfire chain explanation. The ramp-to-threshold model does not comply with the *Drosophila* escape sequence either. According to the ramp-to-threshold model, the earlier action in the sequence (i.e., rolling) would be activated with a lower threshold. In contrast, the data (not present here) seemed to show the opposite (i.e., fast crawling being activated with a lower threshold).

The current evidence on the *Drosophila* larval escape sequence points to the hierarchical suppression model. SeIN128 neurons supported this model since this feedback motif might function in the self-termination of rolling and promote the consequential execution of fast crawling. Notably, this finding implied inhibition from rolling to fast crawling because SeIN128 caused rolling suppression and disinhibited fast crawling, leading to the earlier onset of fast crawling shown in Chapter 2. Without rolling inhibiting fast crawling, the onset of fast crawling would not be shifted. Although direct evidence of mutual inhibition has yet to be identified, given the current *Drosophila* larval connectome data and powerful toolkit, this question will likely be resolved soon. To the extent that the results support the hierarchical suppression model, the insights into mechanisms at the circuit level could potentially be generalized to behavioral sequences observed in other animal models.

3. *Drosophila* larval escape behavior serves as a model for action selection

At the transition from rolling to escape crawling, the *Drosophila* larval CNS performs selection between these two options, meaning that *Drosophila* larval escape behavior might also shine light on neural networks of action selection.

According to Redgrave, Prescott, and Gurney (1999), to be considered an animal model of action selection, a system shall receive both internal and external information, calculate the salience of each action, resolve the conflicts between the actions, allow the winning action to be expressed, and disallow the losing actions. In *Drosophila* larval escape behavior, rolling and escape crawling are mutually exclusive, and this conflict is resolved to display either of these behaviors. This selection is driven by integrating multisensory information, possibly including internal cues. Therefore, *Drosophila* larval escape behavior could serve as an animal model for action selection. Especially when Basin-1 and Basin-2 have been investigated in the selection between hunching

and turning, it is plausible that similar action selection motifs exist in this escape circuitry involving Basin neurons. Besides, a recent report on the neural mechanisms of the competition between feeding and escaping in *Drosophila* larvae showcased the integration of internal cues into action selection, whose principles could be transferable to the selection between the two components of escape behaviors (Nakamizo-Dojo et al., 2023).

For example, in the previous discussion on the functions of Basin-2 and Basin-4, the elongated C-shape phenotype when Basin-2 is activated could be potential evidence where Basin-2 favored escape rolling but not crawling by maintaining the C-shape and thus forbidding crawling. The inhibition of Basin-2 by SeIN128 could thus be explained by these neurons' role in inhibiting rolling and promoting escape crawling. Since SeIN128 does not trigger crawling, it might be an integrator that modulates the rolling and escape crawling circuits. To explore this possibility, researchers would need further information on the circuit of escape crawling and how SeIN128 interacts with it. With a detailed understanding of both rolling and fast crawling circuits and their interaction with potential integrators such as SeIN128, the puzzle of how *Drosophila* larvae encode the action selection between these two responses could be solved.

4. Descending neurons play various roles in *Drosophila* behaviors

Descending neurons project from the brain to either the VNC in invertebrates or the spinal cord in vertebrates. Based on their anatomy, it is reasonable to assume that they significantly convey higher-level information from the brain to local circuits. It has been reported that descending neurons initiate, maintain, modulate, and terminate behaviors (Capelli et al., 2017; Cregg et al., 2020; Severi et al., 2014).

In *Drosophila*, previous research has shown that descending neurons mainly induce modular behaviors and has discussed their function in initiating various behaviors, including

courtship, grooming, and backward-walking behaviors (Bidaye et al., 2014; Guo et al., 2022; Nakamizo-Dojo et al., 2023). Besides, descending neurons also regulate the speed or direction of adult flying and walking (Bidaye et al., 2014; Schnell et al., 2017). Notably, descending neurons trigger different behaviors in female courtship behavior depending on their activation intensities. This result has been a useful animal model for ramp-to-threshold model of action sequences (McKellar et al., 2019). In Chapter 2, we reported that a pair of descending neurons, SeIN128, inhibits *Drosophila* larval escape behavior, implying their role in terminating this behavior. Similarly, with sugar intake after starvation, descending neurons inhibit escape behavior (Nakamizo-Dojo et al., 2023). Although the evidence of descending control of behavior persistence in *Drosophila* is lacking thus far, there are reports on this function of descending neurons in cricket walking behaviors (Naniwa & Aonuma, 2021). Given the similar walking patterns in crickets and adult *Drosophila*, *Drosophila* might also possess descending neurons with such a function.

In conclusion, *Drosophila* descending neurons conduct numerous functions in regulating behaviors, including behavior initiation and modulation. The similarity in the roles played by descending neurons in descending controls of behaviors between *Drosophila* and other animal models calls for more future studies using descending neurons in *Drosophila* as a model to depict their neural characteristics and significance in behavioral control.

5. Motor motifs are involved in the escape rolling sequence

Previous studies have focused on illustrating the sensory neurons and integration neurons in the escape rolling circuit but have left the motor control segments less explored (Burgos et al., 2018; Dason et al., 2020; Hu et al., 2017; Hu et al., 2020; Im & Galko, 2012; Imambocus et al., 2022; Kaneko et al., 2017; Ohyama et al., 2015; Oikawa et al., 2023; Takagi et al., 2017; Tracey

et al., 2003; Yoshino et al., 2017). Although the connectome has been available for a while, the functions of motor and premotor neurons in this circuit still need to be discovered. Only Goro, the command-like neuron, and SNa, the motor neuron, have been reported to activate rolling (Ohyama et al., 2015; Yoshino et al., 2017).

In Chapter 3, however, we reported that A27n received more sensory input from mdIV neurons in *D. santomea*. The fact that A27n innervates MN22/23-1b, the same muscle as innervated by SNa motor neurons, suggests that the enhanced nociceptive input onto A27n could be relayed to the muscle necessary for rolling with only one synapse and thus contribute to the increased rolling in *D. santomea* (Kim et al., 2009; Zarin et al., 2019). In addition, Basin-2 targets a group of neurons not downstream of Basin-4. In this group, A02m and A02n are inhibitory neurons downstream of SeIN128 and upstream of RP2, the motor neuron activating dorsal muscles to trigger the C-shape (Masson et al., 2020; Zarin et al., 2019). This connectivity indicates that SeIN128 activation can disinhibit RP2 to promote the C-shape, which may suppress perpendicular sliding, an essential action in rolling.

As discussed above, being the execution part of this escape-rolling neural circuit, motor motifs have the potential to be involved in modulating behavior outcomes. A more in-depth motor circuit analysis would significantly benefit our understanding of *Drosophila* larval escape behavior.

6. Evolutionary studies shine a light on the encoding of escape sequences

Developmental studies have provided insights into evolutionary research since the seminal report of the homeotic gene expressed in multiple metazoans to regulate their axis patterning (Lewis, 1978; McGinnis et al., 1984). Conversely, evolutionary comparisons reveal the development of differences between closely related species. Due to the similarity in the anatomy of nervous systems across phyla, differences in nervous systems and their behavioral outcomes

could originate in more subtle alterations at a micro level, for example, at the cellular or molecular level (Katz, 2011; Katz & Harris-Warrick, 1999). This perspective allows researchers to investigate the neural mechanisms of given behaviors if they could identify species that differ in the behaviors of interest, such as the role of *pdf* in *Drosophila* circadian rhythm (Bahn et al., 2009).

*Drosophila* larval escape behavior can be investigated in this way, too. In Chapter 3, we compared the larval escape behavior in *drosophilids* and targeted *D. santomea* as a super-roller. By investigating the connectomic differences between *D. santomea* and *D. melanogaster*, the synaptic connection between multidendritic class IV neurons and Basin-1 was targeted to cause the increased escape rolling behavior in *D. santomea*. To examine this possibility, Basin-1 was activated in *D. melanogaster* to simulate the neural activities in *D. santomea,* which recapitulated the increase in escape rolling. What was found in Chapter 3 indicates that comparing *Drosophilid* species provides researchers with a fresh perspective to identify the subtle yet influential differences in the neural mechanisms and their corresponding effects on *Drosophila* larval escape behavior. All these significant motifs lead to a more thorough understanding of the functional encoding of this escape sequence in this larval escape behavior.

7. Action sequences are likely compatible with several mechanisms

Three major hypotheses have been proposed in the field of action sequences to decode their neural circuits - synfire chain, ramp-to-threshold, and hierarchical suppression hypothesis (Abeles, 1982; Lashley, 1951; Manning, 1960). Numerous pieces of evidence have been reported to support each hypothesis, which may be responsible for different action sequences in various animal models (Averbeck et al., 2002; Diesmann et al., 1999; Geddes et al., 2018; Henry & Rogers, 1960; Long et al., 2010; McKellar et al., 2019; Seeds et al., 2014; Vijayan et al., 2023). However, since different frameworks were found to function within the same animal but in different behaviors, these

frameworks may coexist with each other. To take a further step, we cannot even eliminate the chance that these frameworks coexist in the same action sequence, and combining various frameworks allows the CNS to encode action sequences with fewer mistakes. In this *Drosophila* larval escape sequence, Goro-activated rolling events were not followed by fast crawling events, refuting the synfire chain hypothesis. However, the inhibition of Goro activation reduced the percentage of larvae performing fast crawling when the entire escape sequence was triggered by Basin activation (data not shown). This observation suggested that Goro activation or downstream events could send feedback signals to integrators to inform them of the activation of the action module of rolling, which facilitates the command of fast crawling. This hypothesis implies the existence of a plausible partial synfire chain that is necessary but insufficient to evoke fast crawling behavior. If true, this encoding mechanism could prevent fast crawling from occurring before rolling, thus ensuring that the optimal escape sequence is performed. In addition, SeIN128 fires in a gradual manner, which is an essential feature of the ramp-to-threshold hypothesis. Although SeIN128 does not initiate rolling or fast crawling, other neurons may encode the larval escape sequence following the ramp-to-threshold model. The *Drosophila* larval escape sequence may employ several paradigms with different motifs to encode the complete functional sequence.

## 8. Limitations

There are several limitations to the studies mentioned in this thesis. First, it would be ideal to activate SeIN128 only to conclude that these neurons are the rolling-inhibiting neurons in SS04185-expressing neurons. However, there is no single genetic line that manipulates only SeIN128. In the effort to express sporadic neurons in SS04185-expressing neurons, the expression of MB neurons was never eliminated due to the approximate ratio of 1:80 of the neuronal counts between SeIN128 and SS04185-MB neurons. Second, when testing whether activation of SeIN128

inhibits the firing of Basin, Basin was activated with CsChrimson to achieve baseline activation so that inhibition could be observed. Due to the limitations of genetic tools, Basin and SeIN128 neurons both express CsChrimson and GCaMP6s, causing differential levels of baseline activation of the Basin with different activation irradiances. Ideally, the conclusions would have been more evident if Basin and SeIN128 were driven by different binary systems and activated by different wavelengths of light to accomplish individual neural control between these two groups of neurons.

## 9. Concluding remarks

Overall, this thesis explored the stereotyped escape sequence of *Drosophila* larvae from diverse perspectives and identified essential motifs in this sequence. These findings enable us to discuss the specific encoding mechanisms and general underlying models for action sequences. GABAergic SeIN128 neurons and their relevant feedback motif allow the self-termination of rolling and promote fast crawling. Therefore, SeIN128 identification and investigation have supported the hierarchical suppression model in action sequences and strengthened the significance of descending neurons in behavior control. Chapter 3 has highlighted the importance of the mdIV-to-Basin-1 connection in escape-rolling and encourages similar comparative studies in closely related species to elucidate the neural mechanism of behaviors. Both Chapter 2 and Chapter 3 showcase the different functions of subtypes of basin neurons in this escape sequence. Basin-2 and Basin-4 neurons both trigger rolling, but Basin-2 neurons promote the prolongation and suppress other escape behaviors, while Basin-4 neurons elicit shorter rolling bursts and continue with fast crawling behavior. Basin-1 neurons do not trigger rolling but facilitate both rolling and fast crawling in this sequence. In addition, the difference between the functions of Basin neurons and the enhanced rolling behaviors in *D. santomea* may be explained by premotor and motor neuron networks, motivating further research on this topic.

**References**


Abeles, M. (1982). *Local Cortical Circuits: An Electrophysiological Study*. Springer-Verlag. https://books.google.ca/books?id=s25lwwEACAAJ

Abeles, M. (1991). *Corticonics : neural circuits of the cerebral cortex*. Cambridge University Press. https://books.google.ca/books?id=v46SDOLJrLcC

Adams, J. A. (1984). Learning of movement sequences. *Psychological Bulletin*, *96*(1), 3-28. https://doi.org/10.1037/0033-2909.96.1.3

Anthony, J. L., & Fernando, N. (2000). Age at Deafening Affects the Stability of Learned Song in Adult Male Zebra Finches. *The Journal of Neuroscience*, *20*(13), 5054. https://doi.org/10.1523/JNEUROSCI.20-13-05054.2000

Auer, T. O., Khallaf, M. A., Silbering, A. F., Zappia, G., Ellis, K., Alvarez-Ocana, R., Arguello, J. R., Hansson, B. S., Jefferis, G., Caron, S. J. C., Knaden, M., & Benton, R. (2020). Olfactory receptor and circuit evolution promote host specialization. *Nature*, *579*(7799), 402-408. https://doi.org/10.1038/s41586-020-2073-7

Averbeck, B. B., Chafee, M. V., Crowe, D. A., & Georgopoulos, A. P. (2002). Parallel processing of serial movements in prefrontal cortex. *Proc Natl Acad Sci U S A*, *99*(20), 13172-13177. https://doi.org/10.1073/pnas.162485599

Bahn, J. H., Lee, G., & Park, J. H. (2009). Comparative analysis of Pdf-mediated circadian behaviors between Drosophila melanogaster and D. virilis. *Genetics*, *181*(3), 965-975. https://doi.org/10.1534/genetics.108.099069

Berck, M. E., Khandelwal, A., Claus, L., Hernandez-Nunez, L., Si, G., Tabone, C. J., Li, F., Truman, J. W., Fetter, R. D., Louis, M., Samuel, A. D., & Cardona, A. (2016). The wiring diagram of a glomerular olfactory system. *Elife*, *5*. https://doi.org/10.7554/eLife.14859

Bertet, C., Rauzi, M., & Lecuit, T. (2009). Repression of Wasp by JAK/STAT signalling inhibits medial actomyosin network assembly and apical cell constriction in intercalating epithelial cells. *Development*, *136*(24), 4199-4212. https://doi.org/10.1242/dev.040402

Bidaye, S. S., Machacek, C., Wu, Y., & Dickson, B. J. (2014). Neuronal control of Drosophila walking direction. *Science*, *344*(6179), 97-101. https://doi.org/10.1126/science.1249964

Boivin, J. C., Zhu, J., & Ohyama, T. (2023). Nociception in fruit fly larvae. *Front Pain Res (Lausanne)*, *4*, 1076017. https://doi.org/10.3389/fpain.2023.1076017

Brand, A. H., & Perrimon, N. (1993). Targeted gene expression as a means of altering cell fates and generating dominant phenotypes. *Development*, *118*(2), 401-415. https://doi.org/10.1242/dev.118.2.401

Brian, K. S., & William, B. K., Jr. (1997). The Neuronal Basis of the Behavioral Choice between Swimming and Shortening in the Leech: Control Is Not Selectively Exercised at Higher Circuit Levels. *The Journal of Neuroscience*, *17*(2), 786. https://doi.org/10.1523/JNEUROSCI.17-02-00786.1997

Burgos, A., Honjo, K., Ohyama, T., Qian, C. S., Shin, G. J., Gohl, D. M., Silies, M., Tracey, W. D., Zlatic, M., Cardona, A., & Grueber, W. B. (2018). Nociceptive interneurons control modular motor pathways to promote escape behavior in Drosophila. *Elife*, *7*. https://doi.org/10.7554/eLife.26016

Burrell, B. D. (2017). Comparative biology of pain: What invertebrates can tell us about how nociception works. *J Neurophysiol*, *117*(4), 1461-1473. https://doi.org/10.1152/jn.00600.2016

Campagner, D., Vale, R., Tan, Y. L., Iordanidou, P., Pavon Arocas, O., Claudi, F., Stempel, A. V., Keshavarzi, S., Petersen, R. S., Margrie, T. W., & Branco, T. (2023). A cortico-collicular circuit for orienting to shelter during escape. *Nature*, *613*(7942), 111-119. https://doi.org/10.1038/s41586-022-05553-9

Cao, G., Platisa, J., Pieribone, V. A., Raccuglia, D., Kunst, M., & Nitabach, M. N. (2013). Genetically targeted optical electrophysiology in intact neural circuits. *Cell*, *154*(4), 904-913. https://doi.org/10.1016/j.cell.2013.07.027

Capelli, P., Pivetta, C., Soledad Esposito, M., & Arber, S. (2017). Locomotor speed control circuits in the caudal brainstem. *Nature*, *551*(7680), 373-377. https://doi.org/10.1038/nature24064

Cartmill, M., Hylander, W. L., & Shafland, J. (1987). *Human structure*. Harvard University Press.

Cattaert, D., & El Manira, A. (1999). Shunting versus inactivation: analysis of presynaptic inhibitory mechanisms in primary afferents of the crayfish. *J Neurosci*, *19*(14), 6079-6089. https://doi.org/10.1523/JNEUROSCI.19-14-06079.1999

Chalfie, M., & Sulston, J. (1981). Developmental genetics of the mechanosensory neurons of Caenorhabditis elegans. *Dev Biol*, *82*(2), 358-370. https://doi.org/10.1016/0012-1606(81)90459-0

Chalfie, M., Sulston, J. E., White, J. G., Southgate, E., Thomson, J. N., & Brenner, S. (1985). The neural circuit for touch sensitivity in Caenorhabditis elegans. *J Neurosci*, *5*(4), 956-964. https://doi.org/10.1523/JNEUROSCI.05-04-00956.1985

Chin, M. R., & Tracey, W. D., Jr. (2017). Nociceptive Circuits: Can't Escape Detection. *Curr Biol*, *27*(16), R796-R798. https://doi.org/10.1016/j.cub.2017.07.031

Cohen, R. G., & Rosenbaum, D. A. (2004). Where grasps are made reveals how grasps are planned: generation and recall of motor plans. *Experimental Brain Research*, *157*(4), 486-495. https://doi.org/10.1007/s00221-004-1862-9

Colquitt, B. M., Merullo, D. P., Konopka, G., Roberts, T. F., & Brainard, M. S. (2021). Cellular transcriptomics reveals evolutionary identities of songbird vocal circuits. *Science*, *371*(6530). https://doi.org/10.1126/science.abd9704

Cregg, J. M., Leiras, R., Montalant, A., Wanken, P., Wickersham, I. R., & Kiehn, O. (2020). Brainstem neurons that command mammalian locomotor asymmetries. *Nat Neurosci*, *23*(6), 730-740. https://doi.org/10.1038/s41593-020-0633-7

Dason, J. S., Cheung, A., Anreiter, I., Montemurri, V. A., Allen, A. M., & Sokolowski, M. B. (2020). Drosophila melanogaster foraging regulates a nociceptive-like escape behavior through a developmentally plastic sensory circuit. *Proc Natl Acad Sci U S A*, *117*(38), 23286-23291. https://doi.org/10.1073/pnas.1820840116

Dawkins, R. (1976). Hierarchical organisation: A candidate principle for ethology. In *Growing points in ethology.* Cambridge U Press.

Diesmann, M., Gewaltig, M. O., & Aertsen, A. (1999). Stable propagation of synchronous spiking in cortical neural networks. *Nature*, *402*(6761), 529-533. https://doi.org/10.1038/990101

Ding, Y., Lillvis, J. L., Cande, J., Berman, G. J., Arthur, B. J., Long, X., Xu, M., Dickson, B. J., & Stern, D. L. (2019). Neural Evolution of Context-Dependent Fly Song. *Curr Biol*, *29*(7), 1089-1099 e1087. https://doi.org/10.1016/j.cub.2019.02.019

Dolan, M. J., Luan, H., Shropshire, W. C., Sutcliffe, B., Cocanougher, B., Scott, R. L., Frechter, S., Zlatic, M., Jefferis, G., & White, B. H. (2017). Facilitating Neuron-Specific Genetic Manipulations in Drosophila melanogaster Using a Split GAL4 Repressor. *Genetics*, *206*(2), 775-784. https://doi.org/10.1534/genetics.116.199687

Doring, F., Wischmeyer, E., Kuhnlein, R. P., Jackle, H., & Karschin, A. (2002). Inwardly rectifying K+ (Kir) channels in Drosophila. A crucial role of cellular milieu factors Kir

channel function. *J Biol Chem*, *277*(28), 25554-25561. https://doi.org/10.1074/jbc.M202385200

Drosophila 12 Genomes, C., Clark, A. G., Eisen, M. B., Smith, D. R., Bergman, C. M., Oliver, B., Markow, T. A., Kaufman, T. C., Kellis, M., Gelbart, W., Iyer, V. N., Pollard, D. A., Sackton, T. B., Larracuente, A. M., Singh, N. D., Abad, J. P., Abt, D. N., Adryan, B., Aguade, M., . . . MacCallum, I. (2007). Evolution of genes and genomes on the Drosophila phylogeny. *Nature*, *450*(7167), 203-218. https://doi.org/10.1038/nature06341

Eichler, K., Li, F., Litwin-Kumar, A., Park, Y., Andrade, I., Schneider-Mizell, C. M., Saumweber, T., Huser, A., Eschbach, C., Gerber, B., Fetter, R. D., Truman, J. W., Priebe, C. E., Abbott, L. F., Thum, A. S., Zlatic, M., & Cardona, A. (2017). The complete connectome of a learning and memory centre in an insect brain. *Nature*, *548*(7666), 175-182. https://doi.org/10.1038/nature23455

Fleury, F., Ris, N., Allemand, R., Fouillet, P., Carton, Y., & Boulétreau, M. (2004). Ecological and Genetic Interactions in Drosophila–parasitoids Communities: A Case Study with D. Melanogaster, D. Simulans and their Common Leptopilina Parasitoids in South-eastern France. *Genetica*, *120*(1), 181-194. https://doi.org/10.1023/B:GENE.0000017640.78087.9e

Geddes, C. E., Li, H., & Jin, X. (2018). Optogenetic Editing Reveals the Hierarchical Organization of Learned Action Sequences. *Cell*, *174*(1), 32-43 e15. https://doi.org/10.1016/j.cell.2018.06.012

Gerhard, S., Andrade, I., Fetter, R. D., Cardona, A., & Schneider-Mizell, C. M. (2017). Conserved neural circuit structure across Drosophila larval development revealed by comparative connectomics. *Elife*, *6*. https://doi.org/10.7554/eLife.29089

Govorunova, E. G., Cunha, S. R., Sineshchekov, O. A., & Spudich, J. L. (2016). Anion channelrhodopsins for inhibitory cardiac optogenetics. *Sci Rep*, *6*, 33530. https://doi.org/10.1038/srep33530

Guo, D., & Hu, J. (2014). Spinal presynaptic inhibition in pain control. *Neuroscience*, *283*, 95-106. https://doi.org/10.1016/j.neuroscience.2014.09.032

Guo, L., Zhang, N., & Simpson, J. H. (2022). Descending neurons coordinate anterior grooming behavior in Drosophila. *Curr Biol*, *32*(4), 823-833 e824. https://doi.org/10.1016/j.cub.2021.12.055

Henry, F. M., & Rogers, D. E. (1960). Increased response latency for complicated movements and a "memory drum" theory of neuromotor reaction. *Research Quarterly of the American Association for Health, Physical Education, & Recreation*, *31*, 448-458. https://doi.org/10.1080/10671188.1960.10762052

Herberholz, J., Issa, F. A., & Edwards, D. H. (2001). Patterns of neural circuit activation and behavior during dominance hierarchy formation in freely behaving crayfish. *J Neurosci*, *21*(8), 2759-2767. https://doi.org/10.1523/jneurosci.21-08-02759.2001

Himmel, N. J., Letcher, J. M., Sakurai, A., Gray, T. R., Benson, M. N., & Cox, D. N. (2019). Drosophila menthol sensitivity and the Precambrian origins of transient receptor potential-dependent chemosensation. *Philos Trans R Soc Lond B Biol Sci*, *374*(1785), 20190369. https://doi.org/10.1098/rstb.2019.0369

Himmel, N. J., Letcher, J. M., Sakurai, A., Gray, T. R., Benson, M. N., Donaldson, K. J., & Cox, D. N. (2021). Identification of a neural basis for cold acclimation in Drosophila larvae. *iScience*, *24*(6), 102657. https://doi.org/10.1016/j.isci.2021.102657

Houghton, G., & Hartley, T. (1995). Parallel models of serial behavior: Lashley revisited. *Psyche*, *2*(25), 1-25.

Hoy, R. R., Hahn, J., & Paul, R. C. (1977). Hybrid cricket auditory behavior: evidence for genetic coupling in animal communication. *Science*, *195*(4273), 82-84. https://doi.org/10.1126/science.831260

Hu, C., Petersen, M., Hoyer, N., Spitzweck, B., Tenedini, F., Wang, D., Gruschka, A., Burchardt, L. S., Szpotowicz, E., Schweizer, M., Guntur, A. R., Yang, C. H., & Soba, P. (2017). Sensory integration and neuromodulatory feedback facilitate Drosophila mechanonociceptive behavior. *Nat Neurosci*, *20*(8), 1085-1095. https://doi.org/10.1038/nn.4580

Hu, Y., Wang, C., Yang, L., Pan, G., Liu, H., Yu, G., & Ye, B. (2020). A Neural Basis for Categorizing Sensory Stimuli to Enhance Decision Accuracy. *Curr Biol*, *30*(24), 4896-4909 e4896. https://doi.org/10.1016/j.cub.2020.09.045

Huckesfeld, S., Schlegel, P., Miroschnikow, A., Schoofs, A., Zinke, I., Haubrich, A. N., Schneider-Mizell, C. M., Truman, J. W., Fetter, R. D., Cardona, A., & Pankratz, M. J. (2021). Unveiling the sensory and interneuronal pathways of the neuroendocrine connectome in Drosophila. *Elife*, *10*. https://doi.org/10.7554/eLife.65745

Hwang, R. Y., Zhong, L., Xu, Y., Johnson, T., Zhang, F., Deisseroth, K., & Tracey, W. D. (2007). Nociceptive neurons protect Drosophila larvae from parasitoid wasps. *Curr Biol*, *17*(24), 2105-2116. https://doi.org/10.1016/j.cub.2007.11.029

Ikegaya, Y., Aaron, G., Cossart, R., Aronov, D., Lampl, I., Ferster, D., & Yuste, R. (2004). Synfire chains and cortical songs: temporal modules of cortical activity. *Science*, *304*(5670), 559-564. https://doi.org/10.1126/science.1093173

Im, S. H., & Galko, M. J. (2012). Pokes, sunburn, and hot sauce: Drosophila as an emerging model for the biology of nociception. *Dev Dyn*, *241*(1), 16-26. https://doi.org/10.1002/dvdy.22737

Imambocus, B. N., Zhou, F., Formozov, A., Wittich, A., Tenedini, F. M., Hu, C., Sauter, K., Macarenhas Varela, E., Heredia, F., Casimiro, A. P., Macedo, A., Schlegel, P., Yang, C. H., Miguel-Aliaga, I., Wiegert, J. S., Pankratz, M. J., Gontijo, A. M., Cardona, A., & Soba, P. (2022). A neuropeptidergic circuit gates selective escape behavior of Drosophila larvae. *Curr Biol*, *32*(1), 149-163 e148. https://doi.org/10.1016/j.cub.2021.10.069

Isaacson, J. S., & Scanziani, M. (2011). How inhibition shapes cortical activity. *Neuron*, *72*(2), 231-243. https://doi.org/10.1016/j.neuron.2011.09.027

Jing, J., & Gillette, R. (1995). Neuronal elements that mediate escape swimming and suppress feeding behavior in the predatory sea slug Pleurobranchaea. *Journal of Neurophysiology*, *74*(5), 1900-1910. https://doi.org/10.1152/jn.1995.74.5.1900

Jovanic, T., Schneider-Mizell, C. M., Shao, M., Masson, J. B., Denisov, G., Fetter, R. D., Mensh, B. D., Truman, J. W., Cardona, A., & Zlatic, M. (2016). Competitive Disinhibition Mediates Behavioral Choice and Sequences in Drosophila. *Cell*, *167*(3), 858-870 e819. https://doi.org/10.1016/j.cell.2016.09.009

Kabra, M., Robie, A. A., Rivera-Alba, M., Branson, S., & Branson, K. (2013). JAABA: interactive machine learning for automatic annotation of animal behavior. *Nat Methods*, *10*(1), 64-67. https://doi.org/10.1038/nmeth.2281

Kachergis, G., Wyatte, D., O'Reilly, R. C., de Kleijn, R., & Hommel, B. (2014). A continuous-time neural model for sequential action. *Philos Trans R Soc Lond B Biol Sci*, *369*(1655). https://doi.org/10.1098/rstb.2013.0623

Kaneko, T., Macara, A. M., Li, R., Hu, Y., Iwasaki, K., Dunnings, Z., Firestone, E., Horvatic, S., Guntur, A., Shafer, O. T., Yang, C. H., Zhou, J., & Ye, B. (2017). Serotonergic Modulation Enables Pathway-Specific Plasticity in a Developing Sensory Circuit in Drosophila. *Neuron*, *95*(3), 722. https://doi.org/10.1016/j.neuron.2017.07.023

Kang Derwent, J. J., Qtaishat, N. M., & Pepperberg, D. R. (2002). Excitation and desensitization of mouse rod photoreceptors in vivo following bright adapting light. *J Physiol*, *541*(Pt 1), 201-218. https://doi.org/10.1113/jphysiol.2001.013227

Kapfer, C., Glickfeld, L. L., Atallah, B. V., & Scanziani, M. (2007). Supralinear increase of recurrent inhibition during sparse activity in the somatosensory cortex. *Nat Neurosci*, *10*(6), 743-753. https://doi.org/10.1038/nn1909

Kaplan, H. S., Salazar Thula, O., Khoss, N., & Zimmer, M. (2020). Nested Neuronal Dynamics Orchestrate a Behavioral Hierarchy across Timescales. *Neuron*, *105*(3), 562-576.e569. https://doi.org/https://doi.org/10.1016/j.neuron.2019.10.037

Karaiskos, N., Wahle, P., Alles, J., Boltengagen, A., Ayoub, S., Kipar, C., Kocks, C., Rajewsky, N., & Zinzen, R. P. (2017). The Drosophila embryo at single-cell transcriptome resolution. *Science*, *358*(6360), 194-199. https://doi.org/10.1126/science.aan3235

Katz, P. S. (2011). Neural mechanisms underlying the evolvability of behaviour. *Philos Trans R Soc Lond B Biol Sci*, *366*(1574), 2086-2099. https://doi.org/10.1098/rstb.2010.0336

Katz, P. S., & Harris-Warrick, R. M. (1999). The evolution of neuronal circuits underlying species-specific behavior. *Curr Opin Neurobiol*, *9*(5), 628-633. https://doi.org/10.1016/S0959-4388(99)00012-4

Kent, R. D. (1983). The Segmental Organization of Speech. In P. F. MacNeilage (Ed.), *The Production of Speech* (pp. 57-89). Springer New York. https://doi.org/10.1007/978-1-4613-8202-7_4

Khakh, B. S., Gittermann, D., Cockayne, D. A., & Jones, A. (2003). ATP modulation of excitatory synapses onto interneurons. *J Neurosci*, *23*(19), 7426-7437. https://doi.org/10.1523/JNEUROSCI.23-19-07426.2003

Kim, D., Alvarez, M., Lechuga, L. M., & Louis, M. (2017). Species-specific modulation of food-search behavior by respiration and chemosensation in Drosophila larvae. *Elife*, *6*. https://doi.org/10.7554/eLife.27057

Kim, M. D., Wen, Y., & Jan, Y. N. (2009). Patterning and organization of motor neuron dendrites in the Drosophila larva. *Dev Biol*, *336*(2), 213-221. https://doi.org/10.1016/j.ydbio.2009.09.041

Klapoetke, N. C., Murata, Y., Kim, S. S., Pulver, S. R., Birdsey-Benson, A., Cho, Y. K., Morimoto, T. K., Chuong, A. S., Carpenter, E. J., Tian, Z., Wang, J., Xie, Y., Yan, Z., Zhang, Y., Chow, B. Y., Surek, B., Melkonian, M., Jayaraman, V., Constantine-Paton, M., . . . Boyden, E. S. (2014). Independent optical excitation of distinct neural populations. *Nat Methods*, *11*(3), 338-346. https://doi.org/10.1038/nmeth.2836

Lai, S. L., & Lee, T. (2006). Genetic mosaic with dual binary transcriptional systems in Drosophila. *Nat Neurosci*, *9*(5), 703-709. https://doi.org/10.1038/nn1681

Lashley, K. S. (1951). The problem of serial order in behavior. In *Cerebral mechanisms in behavior; the Hixon Symposium.* (pp. 112-146). Wiley.

Lewis, E. B. (1978). A gene complex controlling segmentation in Drosophila. *Nature*, *276*(5688), 565-570. https://doi.org/10.1038/276565a0

Li, X., Gutierrez, D. V., Hanson, M. G., Han, J., Mark, M. D., Chiel, H., Hegemann, P., Landmesser, L. T., & Herlitze, S. (2005). Fast noninvasive activation and inhibition of neural and network activity by vertebrate rhodopsin and green algae channelrhodopsin. *Proc Natl Acad Sci U S A*, *102*(49), 17816-17821. https://doi.org/10.1073/pnas.0509030102

Lim, M. M., Wang, Z., Olazabal, D. E., Ren, X., Terwilliger, E. F., & Young, L. J. (2004). Enhanced partner preference in a promiscuous species by manipulating the expression of a single gene. *Nature*, *429*(6993), 754-757. https://doi.org/10.1038/nature02539

Lin, M. F., Carlson, J. W., Crosby, M. A., Matthews, B. B., Yu, C., Park, S., Wan, K. H., Schroeder, A. J., Gramates, L. S., St Pierre, S. E., Roark, M., Wiley, K. L., Jr., Kulathinal, R. J., Zhang, P., Myrick, K. V., Antone, J. V., Celniker, S. E., Gelbart, W. M., & Kellis, M. (2007). Revisiting the protein-coding gene catalog of Drosophila melanogaster using 12 fly genomes. *Genome Res*, *17*(12), 1823-1836. https://doi.org/10.1101/gr.6679507

Liu, Q., Yang, X., Luo, M., Su, J., Zhong, J., Li, X., Chan, R. H. M., & Wang, L. (2023). An iterative neural processing sequence orchestrates feeding. *Neuron*, *111*(10), 1651-1665 e1655. https://doi.org/10.1016/j.neuron.2023.02.025

Long, M. A., Jin, D. Z., & Fee, M. S. (2010). Support for a synaptic chain model of neuronal sequence generation. *Nature*, *468*(7322), 394-399. https://doi.org/10.1038/nature09514

Lorenz, K., & Tinbergen, N. (1938). Taxis und Instinkthandlung in der Eirollbewegung der Graugans. [Directed and instinctive behavior in the egg rolling movements of the gray goose.]. *Zeitschrift für Tierpsychologie*, *2*, 1-29. https://doi.org/10.1111/j.1439-0310.1939.tb01558.x

Louradour, I., Sharma, A., Morin-Poulard, I., Letourneau, M., Vincent, A., Crozatier, M., & Vanzo, N. (2017). Reactive oxygen species-dependent Toll/NF-kappaB activation in the Drosophila hematopoietic niche confers resistance to wasp parasitism. *Elife*, *6*. https://doi.org/10.7554/eLife.25496

Luan, H., Diao, F., Scott, R. L., & White, B. H. (2020). The Drosophila Split Gal4 System for Neural Circuit Mapping. *Front Neural Circuits*, *14*, 603397. https://doi.org/10.3389/fncir.2020.603397

Luan, H., Peabody, N. C., Vinson, C. R., & White, B. H. (2006). Refined spatial manipulation of neuronal function by combinatorial restriction of transgene expression. *Neuron*, *52*(3), 425-436. https://doi.org/10.1016/j.neuron.2006.08.028

Manning, A. (1960). The Sexual Behaviour of Two Sibling Drosophila Species. *Behaviour*, *15*(1-2), 123-145. https://doi.org/https://doi.org/10.1163/156853960X00133

Manoim, J. E., Davidson, A. M., Weiss, S., Hige, T., & Parnas, M. (2022). Lateral axonal modulation is required for stimulus-specific olfactory conditioning in Drosophila. *Curr Biol*, *32*(20), 4438-4450 e4435. https://doi.org/10.1016/j.cub.2022.09.007

Marler, P. (1970). A comparative approach to vocal learning: Song development in white-crowned sparrows. *Journal of Comparative and Physiological Psychology*, *71*(2, Pt.2), 1-25. https://doi.org/10.1037/h0029144

Masson, J. B., Laurent, F., Cardona, A., Barre, C., Skatchkovsky, N., Zlatic, M., & Jovanic, T. (2020). Identifying neural substrates of competitive interactions and sequence transitions during mechanosensory responses in Drosophila. *PLoS Genet*, *16*(2), e1008589. https://doi.org/10.1371/journal.pgen.1008589

Mazzucato, L. (2022). Neural mechanisms underlying the temporal organization of naturalistic animal behavior. *Elife*, *11*. https://doi.org/10.7554/eLife.76577

McGann, J. P. (2013). Presynaptic inhibition of olfactory sensory neurons: new mechanisms and potential functions. *Chem Senses*, *38*(6), 459-474. https://doi.org/10.1093/chemse/bjt018

McGinnis, W., Garber, R. L., Wirz, J., Kuroiwa, A., & Gehring, W. J. (1984). A homologous protein-coding sequence in Drosophila homeotic genes and its conservation in other metazoans. *Cell*, *37*(2), 403-408. https://doi.org/10.1016/0092-8674(84)90370-2

McKellar, C. E., Lillvis, J. L., Bath, D. E., Fitzgerald, J. E., Cannon, J. G., Simpson, J. H., & Dickson, B. J. (2019). Threshold-Based Ordering of Sequential Actions during Drosophila Courtship. *Curr Biol*, *29*(3), 426-434 e426. https://doi.org/10.1016/j.cub.2018.12.019

Murakami, M., & Mainen, Z. F. (2015). Preparing and selecting actions with neural populations: toward cortical circuit mechanisms. *Curr Opin Neurobiol*, *33*, 40-46. https://doi.org/10.1016/j.conb.2015.01.005

Nakai, J., Ohkura, M., & Imoto, K. (2001). A high signal-to-noise Ca(2+) probe composed of a single green fluorescent protein. *Nat Biotechnol*, *19*(2), 137-141. https://doi.org/10.1038/84397

Nakamizo-Dojo, M., Ishii, K., Yoshino, J., Tsuji, M., & Emoto, K. (2023). Descending GABAergic pathway links brain sugar-sensing to peripheral nociceptive gating in Drosophila. *Nat Commun*, *14*(1), 6515. https://doi.org/10.1038/s41467-023-42202-9

Naniwa, K., & Aonuma, H. (2021). Descending and Ascending Signals That Maintain Rhythmic Walking Pattern in Crickets. *Front Robot AI*, *8*, 625094. https://doi.org/10.3389/frobt.2021.625094

Neely, G. G., Keene, A. C., Duchek, P., Chang, E. C., Wang, Q. P., Aksoy, Y. A., Rosenzweig, M., Costigan, M., Woolf, C. J., Garrity, P. A., & Penninger, J. M. (2011). TrpA1 regulates thermal nociception in Drosophila. *PLoS One*, *6*(8), e24343. https://doi.org/10.1371/journal.pone.0024343

Newcomb, J. M., Sakurai, A., Lillvis, J. L., Gunaratne, C. A., & Katz, P. S. (2012). Homology and homoplasy of swimming behaviors and neural circuits in the Nudipleura (Mollusca, Gastropoda, Opisthobranchia). *Proc Natl Acad Sci U S A*, *109 Suppl 1*(Suppl 1), 10669-10676. https://doi.org/10.1073/pnas.1201877109

Ohyama, T., Jovanic, T., Denisov, G., Dang, T. C., Hoffmann, D., Kerr, R. A., & Zlatic, M. (2013). High-throughput analysis of stimulus-evoked behaviors in Drosophila larva reveals multiple modality-specific escape strategies. *PLoS One*, *8*(8), e71706. https://doi.org/10.1371/journal.pone.0071706

Ohyama, T., Schneider-Mizell, C. M., Fetter, R. D., Aleman, J. V., Franconville, R., Rivera-Alba, M., Mensh, B. D., Branson, K. M., Simpson, J. H., Truman, J. W., Cardona, A., & Zlatic, M. (2015). A multilevel multimodal circuit enhances action selection in Drosophila. *Nature*, *520*(7549), 633-639. https://doi.org/10.1038/nature14297

Oikawa, I., Kondo, S., Hashimoto, K., Yoshida, A., Hamajima, M., Tanimoto, H., Furukubo-Tokunaga, K., & Honjo, K. (2023). A descending inhibitory mechanism of nociception mediated by an evolutionarily conserved neuropeptide system in Drosophila. *Elife*, *12*. https://doi.org/10.7554/eLife.85760

Oleson, E. B., Beckert, M. V., Morra, J. T., Lansink, C. S., Cachope, R., Abdullah, R. A., Loriaux, A. L., Schetters, D., Pattij, T., Roitman, M. F., Lichtman, A. H., & Cheer, J. F. (2012). Endocannabinoids shape accumbal encoding of cue-motivated behavior via CB1 receptor activation in the ventral tegmentum. *Neuron*, *73*(2), 360-373. https://doi.org/10.1016/j.neuron.2011.11.018

Onodera, K., Baba, S., Murakami, A., Uemura, T., & Usui, T. (2017). Small conductance Ca(2+)-activated K(+) channels induce the firing pause periods during the activation of Drosophila nociceptive neurons. *Elife*, *6*. https://doi.org/10.7554/eLife.29754

Palay, S. L. (1956). Synapses in the central nervous system. *J Biophys Biochem Cytol*, *2*(4 Suppl), 193-202. https://doi.org/10.1083/jcb.2.4.193

Pan-Vazquez, A., Wefelmeyer, W., Gonzalez Sabater, V., Neves, G., & Burrone, J. (2020). Activity-Dependent Plasticity of Axo-axonic Synapses at the Axon Initial Segment. *Neuron*, *106*(2), 265-276 e266. https://doi.org/10.1016/j.neuron.2020.01.037

Papadopoulou, M., Cassenaer, S., Nowotny, T., & Laurent, G. (2011). Normalization for sparse encoding of odors by a wide-field interneuron. *Science*, *332*(6030), 721-725. https://doi.org/10.1126/science.1201835

Pastalkova, E., Itskov, V., Amarasingham, A., & Buzsaki, G. (2008). Internally generated cell assembly sequences in the rat hippocampus. *Science*, *321*(5894), 1322-1327. https://doi.org/10.1126/science.1159775

Peirs, C., & Seal, R. P. (2016). Neural circuits for pain: Recent advances and current views. *Science*, *354*(6312), 578-584. https://doi.org/10.1126/science.aaf8933

Pepperberg, D. R. (2003). Bleaching desensitization: background and current challenges. *Vision Res*, *43*(28), 3011-3019. https://doi.org/10.1016/s0042-6989(03)00484-x

Pfeiffer, B. D., Ngo, T. T., Hibbard, K. L., Murphy, C., Jenett, A., Truman, J. W., & Rubin, G. M. (2010). Refinement of tools for targeted gene expression in Drosophila. *Genetics*, *186*(2), 735-755. https://doi.org/10.1534/genetics.110.119917

Pinault, D., Smith, Y., & Deschenes, M. (1997). Dendrodendritic and axoaxonic synapses in the thalamic reticular nucleus of the adult rat. *J Neurosci*, *17*(9), 3215-3233. https://doi.org/10.1523/JNEUROSCI.17-09-03215.1997

Potter, C. J., Tasic, B., Russler, E. V., Liang, L., & Luo, L. (2010). The Q system: a repressible binary system for transgene expression, lineage tracing, and mosaic analysis. *Cell*, *141*(3), 536-548. https://doi.org/10.1016/j.cell.2010.02.025

Prieto-Godino, L. L., Rytz, R., Cruchet, S., Bargeton, B., Abuin, L., Silbering, A. F., Ruta, V., Dal Peraro, M., & Benton, R. (2017). Evolution of Acid-Sensing Olfactory Circuits in Drosophilids. *Neuron*, *93*(3), 661-676 e666. https://doi.org/10.1016/j.neuron.2016.12.024

Ray, S., Aldworth, Z. N., & Stopfer, M. A. (2020). Feedback inhibition and its control in an insect olfactory circuit. *Elife*, *9*. https://doi.org/10.7554/eLife.53281

Rizki, T. M., & Rizki, R. M. (1992). Lamellocyte differentiation in Drosophila larvae parasitized by Leptopilina. *Dev Comp Immunol*, *16*(2-3), 103-110. https://doi.org/10.1016/0145-305x(92)90011-z

Rosenbaum, D. A. (1988). Successive Approximations to a Model of Human Motor Programming. In G. H. Bower (Ed.), *Psychology of Learning and Motivation* (Vol. 21,

pp. 153-182). Academic Press. https://doi.org/https://doi.org/10.1016/S0079-7421(08)60028-6

Rosenbaum, D. A., Cohen, R. G., Jax, S. A., Weiss, D. J., & van der Wel, R. (2007). The problem of serial order in behavior: Lashley's legacy. *Hum Mov Sci*, *26*(4), 525-554. https://doi.org/10.1016/j.humov.2007.04.001

Sakurai, A., & Katz, P. S. (2017). Artificial Synaptic Rewiring Demonstrates that Distinct Neural Circuit Configurations Underlie Homologous Behaviors. *Curr Biol*, *27*(12), 1721-1734 e1723. https://doi.org/10.1016/j.cub.2017.05.016

Salazar-Jaramillo, L., & Wertheim, B. (2021). Does Drosophila sechellia escape parasitoid attack by feeding on a toxic resource? *PeerJ*, *9*, e10528.

Scheffer, L. K., Xu, C. S., Januszewski, M., Lu, Z., Takemura, S. Y., Hayworth, K. J., Huang, G. B., Shinomiya, K., Maitlin-Shepard, J., Berg, S., Clements, J., Hubbard, P. M., Katz, W. T., Umayam, L., Zhao, T., Ackerman, D., Blakely, T., Bogovic, J., Dolafi, T., . . . Plaza, S. M. (2020). A connectome and analysis of the adult Drosophila central brain. *Elife*, *9*. https://doi.org/10.7554/eLife.57443

Schneider-Mizell, C. M., Bodor, A. L., Collman, F., Brittain, D., Bleckert, A., Dorkenwald, S., Turner, N. L., Macrina, T., Lee, K., Lu, R., Wu, J., Zhuang, J., Nandi, A., Hu, B., Buchanan, J., Takeno, M. M., Torres, R., Mahalingam, G., Bumbarger, D. J., . . . Costa, N. M. D. (2021). Structure and function of axo-axonic inhibition. *Elife*, *10*. https://doi.org/10.7554/eLife.73783

Schnell, B., Ros, I. G., & Dickinson, M. H. (2017). A Descending Neuron Correlated with the Rapid Steering Maneuvers of Flying Drosophila. *Curr Biol*, *27*(8), 1200-1205. https://doi.org/10.1016/j.cub.2017.03.004

Seeds, A. M., Ravbar, P., Chung, P., Hampel, S., Midgley, F. M., Jr., Mensh, B. D., & Simpson, J. H. (2014). A suppression hierarchy among competing motor programs drives sequential grooming in Drosophila. *Elife*, *3*, e02951. https://doi.org/10.7554/eLife.02951

Severi, K. E., Portugues, R., Marques, J. C., O'Malley, D. M., Orger, M. B., & Engert, F. (2014). Neural control and modulation of swimming speed in the larval zebrafish. *Neuron*, *83*(3), 692-707. https://doi.org/10.1016/j.neuron.2014.06.032

Sherrington, C. S. (1906). *The Integrative Action of the Nervous System*. Yale University Press. https://books.google.ca/books?id=f69LAAAAMAAJ

Siegel, M. S., & Isacoff, E. Y. (1997). A genetically encoded optical probe of membrane voltage. *Neuron*, *19*(4), 735-741. https://doi.org/10.1016/s0896-6273(00)80955-1

Sineshchekov, O. A., Jung, K. H., & Spudich, J. L. (2002). Two rhodopsins mediate phototaxis to low- and high-intensity light in Chlamydomonas reinhardtii. *Proc Natl Acad Sci U S A*, *99*(13), 8689-8694. https://doi.org/10.1073/pnas.122243399

Stark, A., Lin, M. F., Kheradpour, P., Pedersen, J. S., Parts, L., Carlson, J. W., Crosby, M. A., Rasmussen, M. D., Roy, S., Deoras, A. N., Ruby, J. G., Brennecke, J., Harvard FlyBase, c., Berkeley Drosophila Genome, P., Hodges, E., Hinrichs, A. S., Caspi, A., Paten, B., Park, S. W., . . . Kellis, M. (2007). Discovery of functional elements in 12 Drosophila genomes using evolutionary signatures. *Nature*, *450*(7167), 219-232. https://doi.org/10.1038/nature06340

Sternberg, S., Monsell, S., Knoll, R. L., & Wright, C. E. (1978). 6 - The Latency and Duration of Rapid Movement Sequences: Comparisons of Speech and Typewriting. In G. E. Stelmach (Ed.), *Information Processing in Motor Control and Learning* (pp. 117-152). Academic Press. https://doi.org/https://doi.org/10.1016/B978-0-12-665960-3.50011-6

Stokes, C. C., & Isaacson, J. S. (2010). From dendrite to soma: dynamic routing of inhibition by complementary interneuron microcircuits in olfactory cortex. *Neuron*, *67*(3), 452-465. https://doi.org/10.1016/j.neuron.2010.06.029

Sweeney, S. T., Broadie, K., Keane, J., Niemann, H., & O'Kane, C. J. (1995). Targeted expression of tetanus toxin light chain in Drosophila specifically eliminates synaptic transmission and causes behavioral defects. *Neuron*, *14*(2), 341-351. https://doi.org/10.1016/0896-6273(95)90290-2

Swierczek, N. A., Giles, A. C., Rankin, C. H., & Kerr, R. A. (2011). High-throughput behavioral analysis in C. elegans. *Nat Methods*, *8*(7), 592-598. https://doi.org/10.1038/nmeth.1625

Takagi, S., Cocanougher, B. T., Niki, S., Miyamoto, D., Kohsaka, H., Kazama, H., Fetter, R. D., Truman, J. W., Zlatic, M., Cardona, A., & Nose, A. (2017). Divergent Connectivity of Homologous Command-like Neurons Mediates Segment-Specific Touch Responses in Drosophila. *Neuron*, *96*(6), 1373-1387 e1376. https://doi.org/10.1016/j.neuron.2017.10.030

Tinbergen, N. (1952). The Curious Behavior of the Stickleback. *Scientific American*, *187*(6), 22-27. http://www.jstor.org.proxy3.library.mcgill.ca/stable/24944080

Tosches, M. A., Yamawaki, T. M., Naumann, R. K., Jacobi, A. A., Tushev, G., & Laurent, G. (2018). Evolution of pallium, hippocampus, and cortical cell types revealed by single-cell transcriptomics in reptiles. *Science*, *360*(6391), 881-888. https://doi.org/10.1126/science.aar4237

Tracey, W. D., Jr., Wilson, R. I., Laurent, G., & Benzer, S. (2003). painless, a Drosophila gene essential for nociception. *Cell*, *113*(2), 261-273. https://doi.org/10.1016/s0092-8674(03)00272-1

van de Goor, J., Ramaswami, M., & Kelly, R. (1995). Redistribution of synaptic vesicles and their proteins in temperature-sensitive shibire(ts1) mutant Drosophila. *Proc Natl Acad Sci U S A*, *92*(12), 5739-5743. https://doi.org/10.1073/pnas.92.12.5739

van der Wel, R. P. R. D., & Rosenbaum, D. A. (2007). Coordination of locomotion and prehension. *Experimental Brain Research*, *176*(2), 281-287. https://doi.org/10.1007/s00221-006-0618-0

Veres, J. M., Fekete, Z., Muller, K., Andrasi, T., Rovira-Esteban, L., Barabas, B., Papp, O. I., & Hajos, N. (2023). Fear learning and aversive stimuli differentially change excitatory synaptic transmission in perisomatic inhibitory cells of the basal amygdala. *Front Cell Neurosci*, *17*, 1120338. https://doi.org/10.3389/fncel.2023.1120338

Vijayan, V., Wang, F., Wang, K., Chakravorty, A., Adachi, A., Akhlaghpour, H., Dickson, B. J., & Maimon, G. (2023). A rise-to-threshold process for a relative-value decision. *Nature*, *619*(7970), 563-571. https://doi.org/10.1038/s41586-023-06271-6

Vogt, K., Aso, Y., Hige, T., Knapek, S., Ichinose, T., Friedrich, A. B., Turner, G. C., Rubin, G. M., & Tanimoto, H. (2016). Direct neural pathways convey distinct visual information to Drosophila mushroom bodies. *Elife*, *5*. https://doi.org/10.7554/eLife.14009

Winding, M., Pedigo, B. D., Barnes, C. L., Patsolic, H. G., Park, Y., Kazimiers, T., Fushiki, A., Andrade, I. V., Khandelwal, A., Valdes-Aleman, J., Li, F., Randel, N., Barsotti, E., Correia, A., Fetter, R. D., Hartenstein, V., Priebe, C. E., Vogelstein, J. T., Cardona, A., & Zlatic, M. (2023). The connectome of an insect brain. *Science*, *379*(6636), eadd9330. https://doi.org/10.1126/science.add9330

Wu, J., Abdelfattah, A. S., Zhou, H., Ruangkittisakul, A., Qian, Y., Ballanyi, K., & Campbell, R. E. (2018). Genetically Encoded Glutamate Indicators with Altered Color and Topology. *ACS Chem Biol*, *13*(7), 1832-1837. https://doi.org/10.1021/acschembio.7b01085

Yang, H., & Hultmark, D. (2017). Drosophila muscles regulate the immune response against wasp infection via carbohydrate metabolism. *Sci Rep*, *7*(1), 15713. https://doi.org/10.1038/s41598-017-15940-2

Yoshimura, Y., & Callaway, E. M. (2005). Fine-scale specificity of cortical networks depends on inhibitory cell type and connectivity. *Nat Neurosci*, *8*(11), 1552-1559. https://doi.org/10.1038/nn1565

Yoshino, J., Morikawa, R. K., Hasegawa, E., & Emoto, K. (2017). Neural Circuitry that Evokes Escape Behavior upon Activation of Nociceptive Sensory Neurons in Drosophila Larvae. *Curr Biol*, *27*(16), 2499-2504 e2493. https://doi.org/10.1016/j.cub.2017.06.068

Zarin, A. A., Mark, B., Cardona, A., Litwin-Kumar, A., & Doe, C. Q. (2019). A multilayer circuit architecture for the generation of distinct locomotor behaviors in Drosophila. *Elife*, *8*. https://doi.org/10.7554/eLife.51781

Zheng, Z., Lauritzen, J. S., Perlman, E., Robinson, C. G., Nichols, M., Milkie, D., Torrens, O., Price, J., Fisher, C. B., Sharifi, N., Calle-Schuler, S. A., Kmecova, L., Ali, I. J., Karsh, B., Trautman, E. T., Bogovic, J. A., Hanslovsky, P., Jefferis, G., Kazhdan, M., . . . Bock, D. D. (2018). A Complete Electron Microscopy Volume of the Brain of Adult Drosophila melanogaster. *Cell*, *174*(3), 730-743 e722. https://doi.org/10.1016/j.cell.2018.06.019